Mitophagy and Mitochondrial DNA Disease

Louise King

UCL PhD Thesis

I, Louise King, confirm that the work presented in this thesis is my own. Where information has been derived from other sources, I confirm that this has been indicated in the thesis.

Acknowledgements

There are a number of people that I am incredibly grateful to for their support throughout the duration of my PhD.

Firstly I would like to thank my supervisors Dr Hélène Plun-Favreau and Professor Michael Hanna. It was nearly 5 years ago that I applied for a studentship at the Centre for Neuromuscular Diseases and to this day I am so appreciative that Professor Hanna and colleagues offered me a place at Queen Square. I would like to thank Hélène for inviting me to join her lab after my rotation, I could not have asked for a better mentor throughout my PhD. Your passion for science is inspiring and infectious, and I truly appreciate all the opportunities and advice you have given me throughout this time.

I feel incredibly lucky to have worked in an environment where everyone is so willing to help and offer advice, but in particular I would like to thank Marc Soutar, Zhi Yao and Monika Madej. Between the three of you, you have taught me nearly everything I know and I will forever be grateful for the patience and kindness you have shown me since day one.

I have learnt over the past few years that keeping going when experiments aren't working is much easier with good friends around you. I would like to thank my desk partners David Lynch and Chris Lovejoy who were there through all the highs and lows, and made me laugh along the way. I would also like to thank Martha Foiani, Jasmine Harley and Lisa Kiani for their support, I feel lucky to have had such lovely people around me during these years.

Finally I would like to thank John and my family for everything they have done for me. Unfortunately, the writing of this thesis came at a particularly hard time for all of us and I wasn't expecting so many of my 'writing breaks' to be spent in hospital waiting rooms. I am so grateful to have such a strong family around me and I can't thank my parents enough for giving me quiet space when I needed it to keep writing throughout all this. The main person who has bore the brunt of all my PhD woes is John; you have been an absolute rock throughout everything, and even though I'm sure you still have no idea what mitochondria are, I really appreciate you pretending to listen!

Abstract

This thesis focuses on the mechanism of mitophagy and the initiation of mitophagy in various cell models derived from patients harbouring pathogenic mutations in the mitochondrial genome. Mitochondrial DNA mutations are maternally inherited and present with considerable clinical heterogeneity. Pathogenic cases can be homoplasmic or heteroplasmic; the latter of which means that wild-type and mutant mitochondria coexist. Particularly in cases of heteroplasmy, it is unclear how critical levels of mutant load can be reached, despite the presence of mitochondrial quality control pathways such as mitophagy. Mitophagy is a quality control process which facilitates the complete elimination of dysfunctional mitochondria.

Mitophagy is known to be stimulated by a loss of mitochondrial membrane potential, however other triggers of the process are well less characterised. Here, the compound Rhodamine 6G was used to demonstrate the triggering of mitophagy independently of membrane potential in a Parkin-overexpressing neuroblastoma cell line model. Further analysis suggested that this compound generates mild oxidative stress and deep-sequencing of mitochondrial genome revealed the presence of mtDNA mutations upon exposure to Rhodamine 6G.

The role of mitophagy in primary mitochondrial DNA disease is poorly understood. Using several patient fibroblast lines containing different mutations, significant impairments were identified in the ubiquitination of mitofusins upon stimulation of the mitophagy pathway and a considerable activation of mitochondrial biogenesis was observed, which did not occur in control fibroblasts. Further

experiments were performed focusing on the m.7472insC mutation, in which similarities in morphology and function were identified between these and PINK1 mutant fibroblasts. The m.7472insC fibroblasts were reprogrammed to induced pluripotent stem cells and differentiated to cortical neurons and myoblasts. Using a mitochondrial uncoupler, significant reductions in the accumulation of PINK1 and degradation of mitofusin 1 were observed in mutant myoblasts, however this was not seen in the mutant neurons.

Contents

Table of Contents

Table of Figures

Table of Tables

Abbreviations

ADP	Adenosine diphosphate
ANT	Adenine nucleotide translocase
ATP	Adenosine triphosphate
BER	Base excision repair
CCCP	Carbonyl cyanide *m*-chlorophenyl hydrazine
cDNA	Complementary DNA
CMT	Charcot-Marie-Tooth
COX	Cytochrome c oxidase
COXICA65	Cytochrome *c* oxidase subunit I gene
D-loop	Displacement loop
dHMN	Distal hereditary motor neuropathy
DMEM	Dulbecco's Modified Eagle Serum
DNA	Deoxyribonucleic Acid
dNTPs	Deoxynucleotide triphosphates
Drp1	Dynamin-related protein
dsDNA	Double-stranded DNA
DTT	Dithiothreitol
ECL	Enhanced chemiluminescence
EM	Electromagnetic
ER	Endoplasmic reticulum
ETC	Electron transport chain
FA	Folic acid
FAC	Fluorescence-activated cell sorting
FADH2	Reduced flavin adenine dinucleotide
FBS	Fetal Bovine Serum
FCCP	Carbonyl cyanide-p-trifluoromethoxyphenylhydrazone
FDA	Food and Drug Administration
FGF	Fibroblast growth factor
Fis1	Mitochondrial fission 1 protein

GFP	Green Fluorescent protein
GSH	Reduced glutathione
HBSS	Hank's Balanced Salt Solution
HGF	Hepatocyte growth factor
HRP	Horseradish peroxide
HSP	Heavy strand promoter
IGF	Insulin-like growth factor
IMM	Inner mitochondrial membrane
iPSC	Induced pluripotent stem cell
ITS	Insulin-transferrin-selenium
KD	Knockdown
KLF4	Kruppel-like factor 4
KO	Knockout
LAMP1	Lysosomal-associated membrane protein 1
LHON	Leber hereditary optic neuropathy
LSP	Light strand promoter
MCB	Monochlorobimane
MDVs	Mitochondrial-derived vesicles
MEF	Mouse embryonic fibroblast
MELAS	Mitochondrial encephalopathy with lactic acidosis and stroke-like episodes
MERFF	Myoclonic epilepsy with ragged-red fibers
Mff	Mitochondrial fission factor
Mfn1	Mitofusin 1
Mfn2	Mitofusin 2
MRGs	Mitochondrial RNA granules
mRNA	Messenger RNA
mtDNA	Mitochondrial DNA
NAC	N-acetyl-L-cysteine
NADH	Reduced nicotinamide adenine dinucleotide
NGS	Next generation sequencing
Oct 4	Octamer-binding transcription factor 4
OMM	Outer mitochondrial membrane

OPTN	Optineurin
OSCP	Oligomycin-sensitivity conferring protein
OXPHOS	Oxidative phosphorylation
PAGE	Polyacrylamide gel electrophoresis
PARL	Presenilin-associated rhomboid-like protein
PBS	Phosphate-buffered saline
PCR	Polymerase Chain Reaction
PD	Parkinson's disease
PFA	Paraformaldehyde
PGC	Peroxisome proliferator-activated receptor-gamma coactivator
PINK1	Phosphatase and tensin homolog-induced putative kinase 1
R6G	Rhodamine 6G
Rho7	Rhomboid-7
RING	Really interesting new gene
RNA	Ribonucleic Acid
ROCK	Rho-associated protein kinase
ROS	Reactive oxygen species
rRNA	Ribosomal RNA
RT	Room temperature
SEM	Standard error of mean
shRNA	Short hairpin RNA
ssDNA	Single-stranded DNA
TALENs	Transcription activator-like effector nucleases
TFAM	Mitochondrial transcription factor A
TIM	Translocase of the inner membrane
TMRM	Tetramethylrhodamine methyl ester
TOM	Translocase of the outer membrane
tRNA	Transfer RNA
UV	Ultraviolet
WT	Wild-type
$\Delta\Psi_m$	Mitochondrial membrane potential

Introduction

Mitochondria

Structure and Function of Mitochondria

Mitochondrial Structure

Mitochondria are double-membrane bound organelles that have essential roles in several cellular processes, such as energy production through oxidative phosphorylation (OXPHOS). The mitochondrion comprises of an outer (OMM) and inner membrane (IMM), and between these membranes are the matrix (within the IMM) and the intermembrane space between the IMM and OMM (Figure 1).

The two membranes are structurally and functionally distinct, with the IMM forming cristae structures and the OMM having a more homogeneous structure. The IMM is the site of oxidative phosphorylation, and contains the electron transport chain and numerous channels, such as the mitochondrial Ca^{2+} uniporter and the inner membrane anion channel (Zoratti et al. 2009). The OMM contains fewer proteins, all of which are encoded for in the nucleus, including pore forming proteins, enzymes and proteins involved in fission and fusion processes (Walther & Rapaport 2009; Zahedi et al. 2005; Burri et al. 2006; Schmitt et al. 2006). The OMM is porous and therefore unlike the IMM, there is no membrane potential across the outer membrane. The translocase of the outer mitochondrial membrane (TOM) and the equivalent on the inner mitochondrial membrane (TIM) form a large conductance channel, with partial cation selectivity through which large molecules can be

imported (Grigoriev et al. 2004). For molecules to pass the IMM, selective membrane transport proteins are required to cross the tight diffusion barrier. Consequently, a membrane potential is formed across the IMM due to the ion selectivity and electrochemical gradient that forms.

The matrix of mitochondria maintains a high pH, which contributes to the electrochemical gradient across the IMM required for oxidative phosphorylation, and is the area that houses mitochondrial DNA (mtDNA) and where mtDNA replication and transcription occurs. In addition it is the site of many biosynthetic reaction, catalysed by numerous enzymes. The intermembrane space is a gap of approximately 20nm between the inner and outer mitochondrial membranes, through which all molecules pass to reach the IMM and matrix. The TOM/TIM complexes span across the intermembrane space.

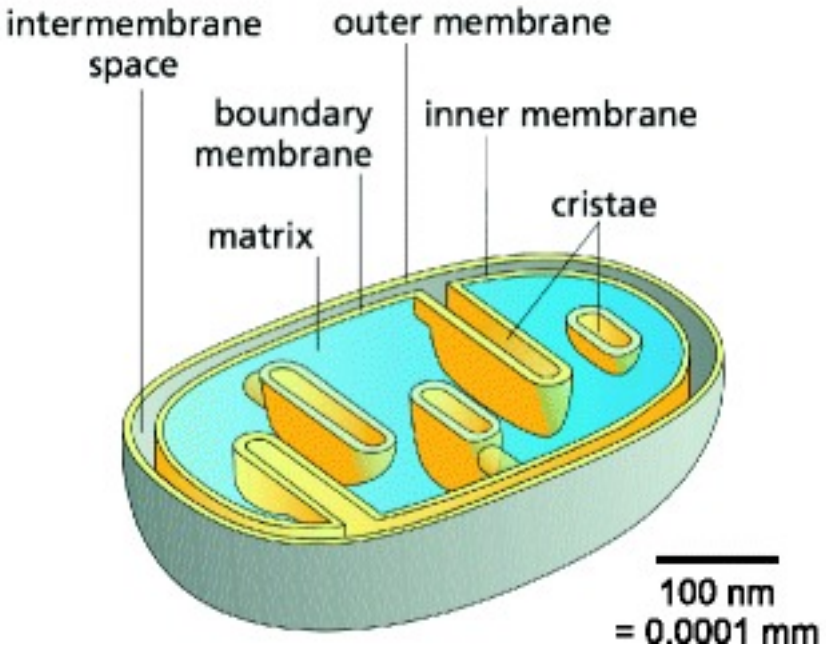

Figure 1: Structure of the Mitochondrion

Diagram depicts the size and structure of a mitochondrion, showing the position of the major structural features, such as the inner membrane which is the site of oxidative phosphorylation. Diagram obtained from BMC Biology (Kühlbrandt 2015). **Creative Commons License: http://creativecommons.org/licenses/by/4.0/**

Functions of mitochondria

Mitochondria generate adenosine triphosphate (ATP) in eukaryotic cells via the process of oxidative phosphorylation (OXPHOS) at the IMM and in the matrix. An electrochemical gradient is established across IMM via the transfer of electrons across respiratory complexes fixed within the inner membrane and the movement of protons out of the matrix. This gradient facilitates the passive movement of protons through the ATP synthase into the matrix for the conversion of adenosine diphosphate (ADP) to ATP, as well as enabling buffering of Ca^{2+}, another essential function of mitochondria.

Mitochondria import Ca^{2+} into the mitochondrial matrix via a mitochondrial calcium uniporter from the plasma membrane and endoplasmic reticulum, a finding first established in 1992 (Rizzuto et al. 1992; De Stefani et al. 2011; Baughman et al. 2011). The process of calcium buffering by mitochondria is critical for the release of neurotransmitters and the generation and plasticity of neurons, as well as the Ca^{2+} signalling that facilitates muscle contraction. These processes cause a rise in intramitochondrial Ca^{2+} via the mitochondrial calcium uniporter, which is then released back to the cytosol via a sodium/calcium exchanger (Cai & Lytton 2004). The concentration of calcium in the matrix subsequently affects the rate of ATP generation, with higher intramitochondrial calcium concentrations causing an up-regulation of oxidative phosphorylation to supply the energy-demanding activities that stimulate the uptake of calcium.

Mitochondria also play a crucial role in the activation of apoptosis, through the release of cytotoxic proteins, such as cytochrome c.

Soluble proteins are released from the intermembrane space of the mitochondria to the cytosol, initiating caspase activation.

Glycolysis and Oxidative Phosphorylation

Glycolysis

Glycolysis is a series of reactions that converts glucose into pyruvate, forming two ATP molecules and two NADH molecules. This pathway occurs in both prokaryotic and eukaryotic cells. In eukaryotes, glycolysis occurs in the cytosol of the cell and can be divided into three stages (Figure 2).

The first stage involves the phosphorylation of glucose by ATP, which is catalysed by hexokinase. This is followed by an isomerisation and a second phosphorylation to produce fructose 1,6-bisphosphate. The glucose 6-phosphate ring structure is opened before isomerisation can occur, and needs to be returned to its cyclic form before the next phosphorylation. Isomerisation converts aldoses to ketones, and is catalysed by phosphoglucose isomerase, producing fructose 6-phosphate. Fructose 6-phosphate subsequently undergoes phosphorylation by ATP to form fructose 1,6-bisphosphate, catalysed by phosphofructokinase.

The second stage involves the cleavage of fructose 1,6-bisphosphate into glyceraldehyde 3-phosphate and dihydroxyacetone phosphate, the former of which consists of three-carbon units. Dihydroxyacetone is converted to glyeraldehyde 3-phosphate, as the remaining reactions in glycolysis require a three-carbon unit. This conversion occurs via isomerisation, catalysed by triose phosphate isomerase in a quick and reversible reaction.

The third stage of glycolysis involves the oxidation of the three-carbon units, and the generation of ATP. Glyceraldehyde 3-phosphate is converted into 1,3-bisphosphoglycerate, catalysed by glyceraldehyde 3-phosphate dehydrogenase, which reduces NAD^+ to produce NADH. Following this, ATP is generated in the donation of the phosphoryl group of 1,3-bisphosphoglycerate to ADP, catalysed by phosphoglycerate kinase. Due to the conversion of dihydroxyacetone by triose phosphate isomerase, two ATP molecules are generated in this process, which balances the two ATP molecules that were used in the two phosphorylation reactions that occur in stage 1.

The generation of extra ATP occurs during the conversion of 3-phosphoglycerate, formed by the loss of the phosphate group of 1,3- bisphosphoglycerate in the previous step. The 3-phosphoglycerate is first rearranged, so that a dehydration reaction can occur to produce phosphenolpyruvate, catalysed by enolase. The phosphoryl group can then be transferred to ADP, forming ATP and pyruvate. Overall this results in a net formation of two ATP molecules and two pyruvate molecules per glucose molecule.

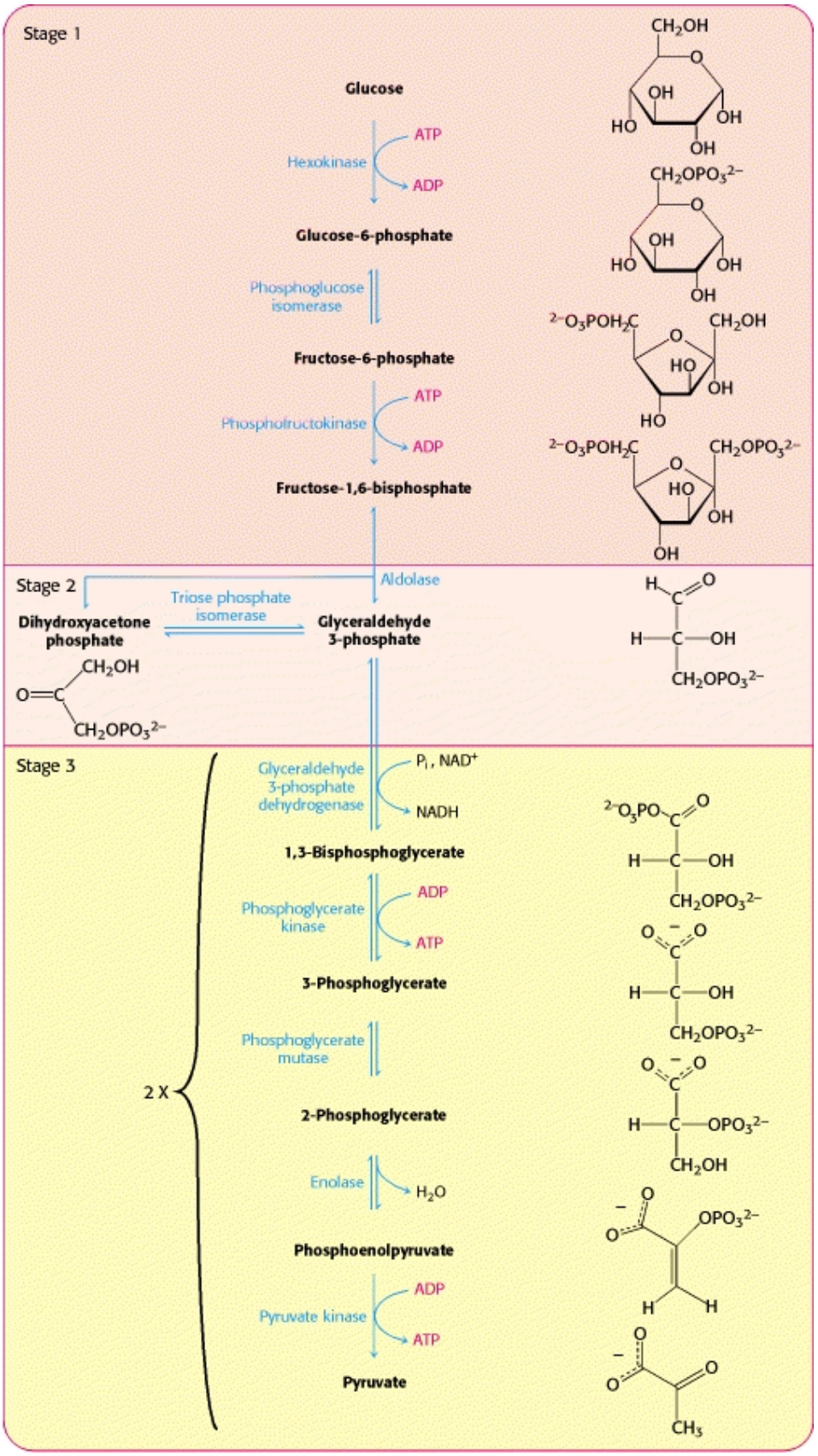

Figure 2: Pathway of glycolysis, divided into three stages

Diagram obtained from Biochemistry 5th Edition, Berg JM, Tymoczko JL, Stryer L; 2002.

Krebs Cycle

The process of glycolysis results in a net generation of two pyruvate molecules, two ATP molecules and two NADH molecules in the cytoplasm of the cell. The Krebs cycle, or citric acid cycle, occurs in the matrix of mitochondria. Pyruvate is oxidised to acetyl CoA whilst NAD+ is reduced, in preparation for the Krebs cycle. The aim of the Krebs cycle is to generate the inputs for oxidative phosphorylation: NADH and $FADH_2$. To do this, acetyl CoA, a 2-carbon molecule, combines with oxaloacetate, a 4-carbon molecule, to form citric acid, a 6-carbon molecule. Citric acid is oxidatively decarboxylated twice, with the two carbon atoms leaving the cycle as carbon dioxide. The electrons lost from citric acid through oxidation are used to form NADH and $FADH_2$ through reduction.

Oxidative Phosphorylation

Oxidative phosphorylation is the generation of ATP culminating from a series of energy transformations. The IMM contains protein complexes embedded within it that constitute the electron transport chain (Figure 3). Electrons from NADH and $FADH_2$ combine with O_2 in oxidation/reduction reactions, which release energy for the synthesis of ATP. The electron transport chain comprises four protein complexes and a final fifth complex, termed the ATP synthase, which facilitates the generation of ATP.

The process begins at complex I, where electrons from NADH are transferred to flavin mononucleotide in the complex, then to an iron-sulfur protein and subsequently to coenzyme Q, otherwise known as ubiquinone. Coenzyme Q is situated in the membrane as complex II, and carries electrons from complex I through the membrane. The electrons are then passed to complex III, from

cytochrome *b* to cytochrome *c*, which is a peripheral membrane protein, and onto complex IV.

As electrons pass along the complexes, energy is released which facilitates the movement of protons out of the matrix into the intermembrane space. This creates an electrochemical gradient across the IMM due to the movement of protons against their pH and charge gradient. The gradient that is created enables an influx of protons into the matrix, however since the phospholipid bilayer is impermeable to ions, protons must enter via the ATP synthase. The influx of protons facilitates the conversion of ADP to ATP.

The amount of ATP generated from oxidative phosphorylation is considerably greater than that from glycolysis. Movement of electrons from NADH across the electron transport chain supports the generation of between 30 and 36 ATP molecules.

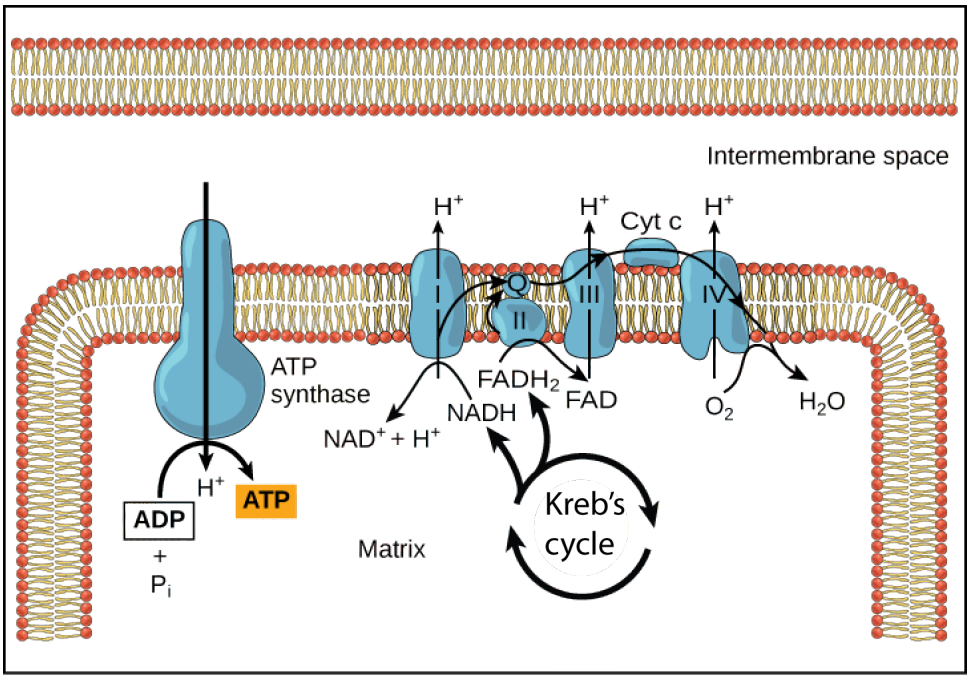

Figure 3 Oxidative Phosphorylation at the inner mitochondrial membrane

Electron carrier complexes I-IV generate an electrochemical gradient across the IMM through a series of oxidation/reduction reactions, which cause protons to enter the intermembrane space. This gradient then enables the

movement of protons through the ATP synthase which converts ADP to ATP. Diagram obtained from CNX.org

Mitochondrial DNA

Mitochondria are unique organelles in that they house a small amount of their own DNA, separate to the majority present in cell nuclei. The expression of mitochondrial DNA (mtDNA) has been shown to be essential for the process of oxidative phosphorylation (Larsson et al. 1998).

The mitochondrial nucleoid

MtDNA encodes 37 genes and is organised along with various proteins into nucleoids contained in the matrix of the mitochondrion. The nucleoid containing DNA does not have a classical membrane and it remains unknown how it separates itself from the mitochondrial matrix (Kolesnikov 2016). The nucleoids in human mitochondria appear to be of a spherical or ellipsoid shape, measuring up to 100 nm in diameter (Kukat et al. 2011). It has been shown that nucleoids in mammalian mitochondria each contain 1 or 2 molecules of mtDNA, however this can be up to 4 times greater in embryonic cells compared to somatic (Kukat et al. 2011). Since mitochondria exist in dynamic networks, it is not estimated how many nucleoids there are per mitochondrion, however it is known that depending on the cell type, there can be 500-12900 nucleoids per human cell (Bogenhagen 2012).

Proteins also present in the mitochondrial nucleoid are required for functions such as compressing mtDNA at least 20 times within the nucleoid, for replication and transcription of mDNA, and also for protection of mtDNA from nucleases. Mitochondrial transcription factor A (TFAM) is one such ‘packaging’ protein, which enables the

formation of loops by bending the mitochondrial genome in short stretches, termed U-turns (Rubio-Cosials et al. 2011; Ngo et al. 2011).

It remains unclear however how the mitochondrial nucleoid is organised and whether it has an internal structure (Kolesnikov 2016).

The mitochondrial genome

The mitochondrial genome is 16,569 base pairs in length and contains 37 genes, which encode for 13 mitochondrial peptide subunits, 2 ribosomal RNAs and 22 transfer RNAs. Mitochondrial DNA forms a small closed-circular structure, which is double stranded. The two strands have different densities due to their GT base composition and are labelled ‘heavy’ and ‘light’ (Kasamatsu & Vinograd 1974).

The outer heavy chain contains the genes for the ribosomal RNAs, 14 of the transfer RNAs and 12 of the polypeptides, with the remainder being coded for on the inner light chain. The mitochondrial genome is spatially efficient, with coding regions accounting for approximately 93% of the genome, no introns being present and even regions of overlap between two genes (Turnbull et al. 1999). The non-coding areas of genome are mainly confined to the displacement loop (D-loop), termed as such due to the presence of a third strand which holds apart one strand of the double-stranded DNA and contains a complimentary sequence to it, thus displacing the other main strand. Whilst it appears that at least a quarter of this area is dispensable, the D-loop contains the origins of strand replication and the major promoters for transcription (Behar et al. 2008).

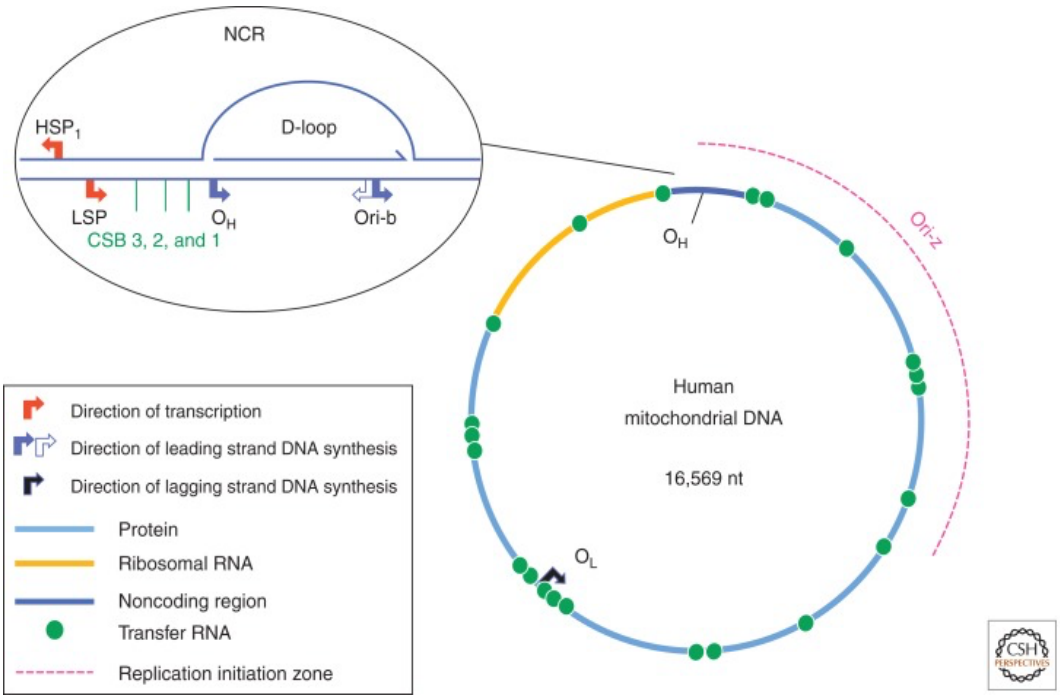

Figure 4: Mitochondrial genome structure

A schematic of the mitochondrial genome showing the distribution of the coding regions and the non-coding region. NCR, noncoding region; HSP, heavy strand promoter; LSP, light strand promoter; O_H, initiation site for heavy strand synthesis; O_L, initiation site for light strand synthesis. Diagram obtained from (Holt & Reyes 2012)**, © 2012 Cold Spring Harbor Laboratory Press.**

Mitochondrial DNA inheritance and processing

Mitochondrial DNA is maternally inherited (Giles et al. 1980). After fertilisation, the oocyte contains both paternal and maternal mitochondria however paternal mitochondria are not transmitted to offspring, therefore it is thought that the paternal mitochondria is either diluted out by maternal mitochondria, or that the paternal mitochondria is specifically degraded. Studies in numerous animal models have put forward several potential mechanisms and time-points for degradation, including ubiquitin-mediated degradation

after fertilisation or degradation by endonuclease G during spermatogenesis (DeLuca & O'Farrell 2012; Schatten et al. 1999; Sutovsky et al. 2000).

MtDNA replication is in general poorly understood however it is thought that replication is initiated at the D-loop region beginning with the leading strand (heavy strand) and then subsequently starting the lagging strand (light strand) once the leading strand replication is about one third from finishing (Clayton 1982). At this point, a stem-loop structure is formed from the single stranded DNA molecule at O_L (initiation site for light strand synthesis) to which mitochondrial RNA polymerase binds to in order to start the replication of the lagging strand (Wanrooij et al. 2008; Wanrooij et al. 2012).

Transcription involves the mitochondrial RNA polymerase, TFAM and mitochondrial transcription factor B2. Two polycistronic transcripts are generated from transcription by mitochondrial RNA polymerase, originating from H strand promoter (HSP) and L strand promoter (LSP), which are then processed to separate the individual mRNAs, rRNAs and tRNAs (Ojala et al. 1981). Transcript processing has been hypothesised to occur in mitochondrial RNA granules (MRGs) which house the mitochondrial 5'-processing machinery; this is thought to occur before a second round of processing elsewhere in the mitochondrial matrix (Antonicka et al. 2013; Jourdain et al. 2013).

Mitochondrial DNA damage and repair mechanisms

Mitochondrial DNA is more vulnerable to damage than nuclear DNA for several reasons. Reactive oxygen species (ROS) are formed as a by-product of oxidative phosphorylation due to side reactions between electrons and oxygen directly generating the hydroxyl radical. Therefore the close proximity of mtDNA to a site of ROS production makes it at greater risk of damage. Furthermore, the nature of the gradient across the IMM means that lipophilic positively charged toxic chemicals, such as 8-oxoguanine, more readily accumulate in mtDNA compared to nuclear DNA (Beckman & Ames 1996). Mutations in mtDNA can also occur due to mistakes in DNA replication, or from the amplification of age-related mtDNA rearrangements (Hayakawa et al. 1996; Kajander et al. 2000).

For a long time it was thought that mitochondria did not have DNA repair mechanisms, due to a study showing the lack of repair of pyrimidine dimers caused by UV-irradiation (Clayton et al. 1974). However, it is now known that several mtDNA repair pathways exist. One of which is known as base excision repair (BER), which involves a series of reactions and is the mechanism most commonly used to repair oxidative damage (Lan et al. 2004). The steps of BER include base excision, DNA end processing, base replacement and end-ligation. The damaged base is removed by DNA glycosylases and DNA cleaved by apurinic/apyrimidinic endonuclease 1. DNA polymerase replaces the removed base and the ends are ligated by DNA ligase.

Mitochondrial Quality Control Processes

Mitochondria exist in large networks within cells, and due to their vulnerability to oxidative damage, require quality control processes to maintain efficient functioning. Extensive mitochondrial damage will trigger apoptosis, however in attempt to combat this, several mechanisms of repair and damage control occur within mitochondria, which will be discussed in this section.

Fission and Fusion

It is well known that mitochondria are highly dynamic organelles, which constantly undergo two opposing processes of fission and fusion (Figure 5). Together these processes enable the movement of mitochondrial contents between mitochondria to preserve a homogenous population.

During the process of fusion, the OMM and IMM of two mitochondria merge simultaneously, which facilitates the mixing of the intermembrane space and mitochondrial matrix. In human cells, proteins OPA1 and mitofusins 1and 2 (Mfn1 and Mfn2) are essential mediators for this process. The Mfn1 and Mfn2 are transmembrane GTPases embedded in the OMM and therefore mediate outer membrane fusion. OPA1 is a dynamin-related GTPase embedded in the IMM, which mediates inner membrane fusion. OPA1 heterozygous mutations have been associated with the autosomal dominant disease optic atrophy, in which degeneration occurs of retinal ganglion cells. Missense mutations in Mfn2 cause the peripheral neuropathy Charcot-Marie-Tooth disease type 2A (Züchner et al. 2004).

Studies using mouse embryonic fibroblasts (MEFs) carrying null alleles of mitofusins show that fusion of both the outer and inner

mitochondrial membranes is lost, however OPA1-null MEFs continue to exhibit outer mitochondrial membrane fusion (Song et al. 2009). This finding indicated that there is a sequential process of fusion in mammalian cells, which are readily uncoupled (Song et al. 2009). For outer mitochondrial membrane fusion, mitofusins are required on both mitochondria that are fusing, however inner membrane fusion only requires OPA1 to be present on one mitochondrion, i.e. a wild-type mitochondrion can fuse with an OPA1 deficient mitochondrion (Koshiba et al. 2004; Meeusen et al. 2004; Song et al. 2009).

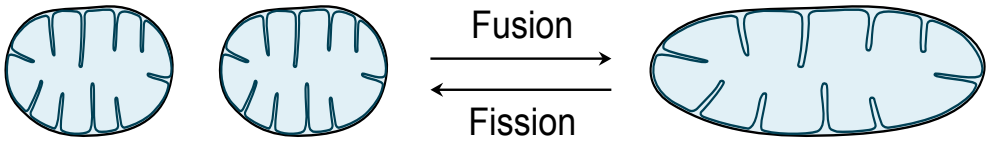

Figure 5: Schematic diagram to show the processes of fusion and fission

The process of two adjacent mitochondria joining to enable mixing of mitochondrial contents is known as fusion. The separation of one mitochondrion into two daughter mitochondria is known as fission.

An extended antiparallel coiled coil on the C-terminal of mitofusin 1 enables mitochondria to be brought together with a gap of only 100 Å. Oligomerisation is then mediated by mitofusin 1 and it is thought that GTP hydrolysis facilitates conformational changes that enable membrane fusion (Koshiba et al. 2004; Chan 2012).

Fission is the opposite process of fusion, in which daughter mitochondria are created from the division of one mitochondrion. This process involves dynamin-related protein (Drp1), a protein that resides in the cytosol, and mitochondrial proteins including mitochondrial fission 1 protein (Fis1) and mitochondrial fission factor (Mff). The mechanism of fission is less well understood and studies have shown that some types of mitochondrial fission do not require the presence of Drp1 (Ishihara et al. 2009; Wakabayashi et al.

2009). Cytosolic Drp1 is recruited to mitochondria, thought to be caused by Fis1 although that has also been disputed, after the initial mitochondrial constriction (Stojanovski et al. 2004; Yoon et al. 2003; Yu et al. 2005; Otera et al. 2010). Mff is a well established Drp1 receptor, separate from Fis1, which mediates recruitment of Drp1 to mitochondria (Otera et al. 2010).

Importantly for maintenance of a healthy mitochondrial network, fission and fusion enable the segregation of damaged mitochondria for complete removal, and sharing of healthy mitochondrial contents. Healthy mitochondria can be fused to the existing network or eliminated if the organelle is damaged. The mitochondrial membrane potential of the mitochondria is considered the determining factor by which fusion or fission occurs; it has been shown previously that a hyperpolarised mitochondrion is more likely to undergo fusion than a depolarised mitochondrion (Twig, Elorza, Anthony J. A. Molina, et al. 2008; Horbay & Bilyy 2016). The process by which damaged mitochondria are eliminated is known as mitophagy.

Proteolytic and Proteasomal degradation

Mitochondria have a proteolytic system, which consists of AAA protease complexes embedded in the inner mitochondrial membrane, whose catalytic sites face outwards on either side of the inner membrane (Langer et al. 2001). AAA protease complexes are present to degrade unfolded membrane proteins in order to prevent their toxic accumulation. Molecular chaperones in mitochondria also participate in the degradation of mitochondrial proteins by resolubilising aggregated polypeptides (Voos 2013). The degradation of unfolded proteins normally occurs in the mitochondria, however the removal of damaged outer mitochondrial

membrane proteins is achieved using the cytoplasmic ubiquitin proteasome system.

Mitochondrial-derived vesicles

It has been shown that defective mitochondrial components can be directly passed on to the lysosome for elimination via mitochondrial-derived vesicles (Soubannier, G. L. McLelland, et al. 2012). These vesicles bud from mitochondrial tubules and sequester mitochondrial cargos under basal conditions. This mechanism of quality control is known also to be upregulated in the presence of oxidative stress, and enables the organelle to remain intact whilst oxidised mitochondrial proteins are eliminated. Importantly, the generation of mitochondrial-derived vesicles has been found to be dependent upon the presence of PINK1 and Parkin, two key proteins involved in the process of mitophagy, which is described in detail in the following section (McLelland et al. 2014). It has been suggested that MDVs provide an initial mechanism of defence before the process of mitophagy is activated (Sugiura et al. 2014).

Mitophagy

When damage to mitochondria is beyond the removal of a subset of mitochondrial proteins, mitophagy is employed to eliminate an entire organelle. Mitophagy ensures optimal cellular energy production through the selective degradation of damaged mitochondria in order to avoid toxic accumulation. This process will be discussed in detail in the following section.

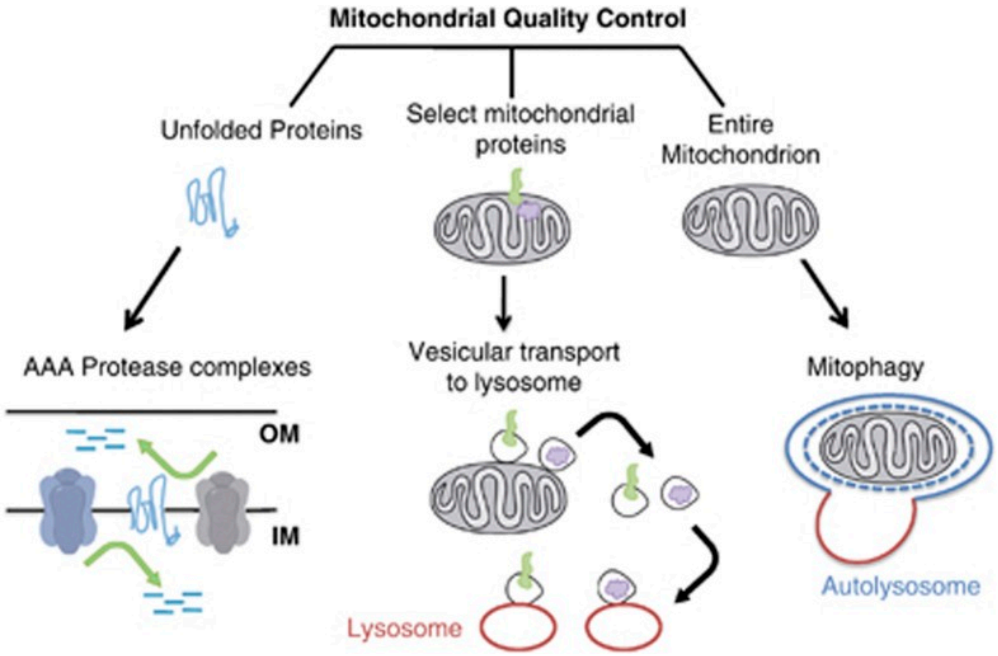

Figure 6: Mechanisms of mitochondrial quality control

Subsets of mitochondrial proteins can be removed by protease degradation or the budding of vesicles from mitochondrial tubules to deliver damaged contents to the lysosomes. Alternatively entire damaged mitochondrial organelles can be removed by mitophagy. (Ashrafi & Schwarz 2013) © 2013 Macmillan Publishers Limited

The Mechanism of Mitophagy

The current model of the mitophagy pathway involves two essential mediators: phosphatase and tensin homolog-induced putative kinase 1 (PINK1) and Parkin.

PINK1

The *PINK1* gene contains 8 exons and encodes for a 581-amino acid protein. Mutations in the *PINK1* gene cause autosomal recessive early-onset Parkinson's disease, and over 50 mutation sites having been identified in the kinase and carboxyl-terminal regulatory domains (the former of which are shown in Figure 7).

PINK1 is synthesised in the cytosol and imported through TOM into the mitochondria due to its mitochondrial targeting sequence at its N-terminus. PINK1 is ubiquitously expressed and maintained at a low level under physiological conditions through degradation by Rhomboid-7/Presenilin-associated rhomboid-like protein (Rho-7/PARL) processing and also degradation in the mitochondrial matrix by protease Lon ((Thomas et al. 2014; Whitworth et al. 2008; Jin et al. 2010).

In the mitochondria, whilst at very low levels, expression of PINK1 under basal conditions can be detected in the outer and inner mitochondrial membranes (Gandhi et al. 2006; Silvestri et al. 2005). PINK1 can also be detected in the cytosol and the endoplasmic reticulum (Fedorowicz et al. 2014; Weihofen et al. 2008).

PINK1 knockout mice have a phenotype of decreased oxidative phosphorylation and reduced mitochondrial respiration, suggesting that PINK1 has a protective function against oxidative stress (Gautier et al. 2008).

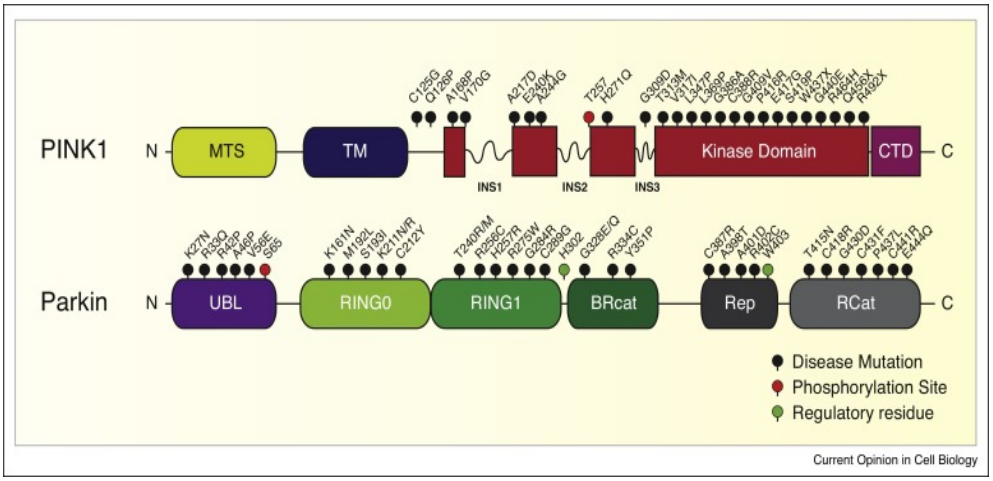

Figure 7: PINK1 and Parkin domain architecture

Schematic diagram showing the regions of PINK1 and Parkin, MTS: mitochondrial targeting sequence, TM: transmembrane domain, INS: insertion, CTD: C-terminal domain, UBL: ubiquitin-like domain, RING: really interesting new gene domain, BRcat: benign-catalytic domain, Rep: repressor element, Rcat: required for catalysis domain. (McWilliams & Muqit 2017)

Parkin

Parkin is a cytosolic E3 ubiquitin ligase and under basal conditions it's activity is repressed as it resides in the cytosol (Lazarou et al. 2012). The Parkin structure includes an ubiquitin-like domain at the N-terminus, and belongs to the RING-between-RING group of E3 ubiquitin ligases (Figure 7). Parkin is folded into an auto-inhibited conformation under physiological conditions. Autosomal recessive Parkinson's disease is most often caused by loss of function mutations in the *Parkin* gene, and more than 120 different mutations in this gene have been identified and linked to the disease (Durcan & Fon 2015).

The process of ubiquitination involves three enzymes. First E1 ubiquitin-activating enzymes use ATP to enable ubiquitin to conjugate, before being delivered to E2 ubiquitin conjugating

enzymes, which interact with E3 ubiquitin ligases. E3 ubiquitin ligases transfer ubiquitin to the amino groups of substrates, which can then be the start of the formation of ubiquitin chains.

PINK1/Parkin-dependent mitophagy

As previously described, under basal conditions PINK1 is imported into mitochondria, cleaved and degraded. However, upon loss of mitochondrial membrane potential, which can be induced through the use of mitochondrial uncouplers such as carbonyl cyanide *m*-chlorophenyl hydrazine (CCCP), PINK1 is not imported through the TIM complex but becomes stabilised on the OMM. The presence of full-length PINK1 on the outer surface of damaged mitochondria enables these to be marked for degradation, separated from the healthy unmarked mitochondria. PINK1 at the OMM is positioned so that the kinase domain remains accessible to cytosolic substrates, however the mechanism by which is occurs is not fully understood (Pickrell & Youle 2015; Zhou et al. 2008).

Parkin was first associated with mitophagy from experiments in immortalised cell lines, which showed that cytosolic Parkin could be recruited to depolarised mitochondria after stimulation with CCCP (Narendra et al. 2008; Narendra et al. 2010; Vives-Bauza, Zhou, Huang, Cui, Rosa L. A. de Vries, et al. 2010).

PINK1 and Parkin functioning in a common pathway

The involvement of PINK1 and Parkin in a common mitochondrial quality control process was implicated through several observations and experiments. Autosomal recessive Parkinson's disease (PD) is known to be caused by mutations in PINK1 and Parkin, and post-mortem analysis of PD patient brains revealed an accumulation of damaged mitochondria (Keeney et al. 2006; Perier & Vila 2012).

Studies using *Drosophila* with loss of PINK1 or Parkin showed flies to have a strong mitochondrial dysfunction phenotype, male sterility and mitochondrial morphology defects, which could be ameliorated in PINK1-KO *Drosophila* with the overexpression of human PINK1 or Parkin (Clark et al. 2006; Park et al. 2006; Yang et al. 2006). Interestingly, the phenotype seen in Parkin-KO *Drosophila* could not be reversed with the overexpression of PINK1, only human Parkin, suggesting that in the mechanistic pathway Parkin acted down-stream of PINK1.

PINK1 activation of Parkin

Recent studies have shown that upon translocation of cytosolic Parkin to damaged mitochondria, PINK1 phosphorylates Parkin and ubiquitin at their serine 65 residues (Kane et al. 2014; Kazlauskaite et al. 2014; Koyano et al. 2014) (Figure 8). The phosphorylation of both Parkin and ubiquitin by PINK1 is necessary for the activation of Parkin's E3 ubiquitin ligase activity.

The kinase activity of PINK1 is activated by self-phosphorylation, however the precise mechanism by which this occurs is unknown (Okatsu et al. 2012; Aerts et al. 2015). The involvement of other PINK1 substrates in the activation of Parkin was indicated when mutation of Parkin serine (including Ser65) and threonine sites did not completely block Parkin translocation (Kane et al. 2014). Phosphorylation of ubiquitin by PINK1 was identified using mass spectrometry, and phospho-ubiquitin was shown to directly activate Parkin, revealing a feed-forward mechanism of activation (Kane et al. 2014).

Activated Parkin ubiquitinates numerous mitochondrial proteins, in particular proteins residing in the outer mitochondrial membrane and in addition is thought to elongate pre-existing ubiquitin chains

creating, among others, K48 and K63 ubiquitin linkages (Sarraf et al. 2013; Chan et al. 2011; Ordureau et al. 2014). These polyubiquitin chains can then be phosphorylated by PINK1, amplifying the activation of Parkin and driving the removal of dysfunctional mitochondria in a feed-forward amplification mechanism. If there is a particular role of each type of linked ubiquitin chain (Lys 6, 11, 48 and 63) it remains unknown.

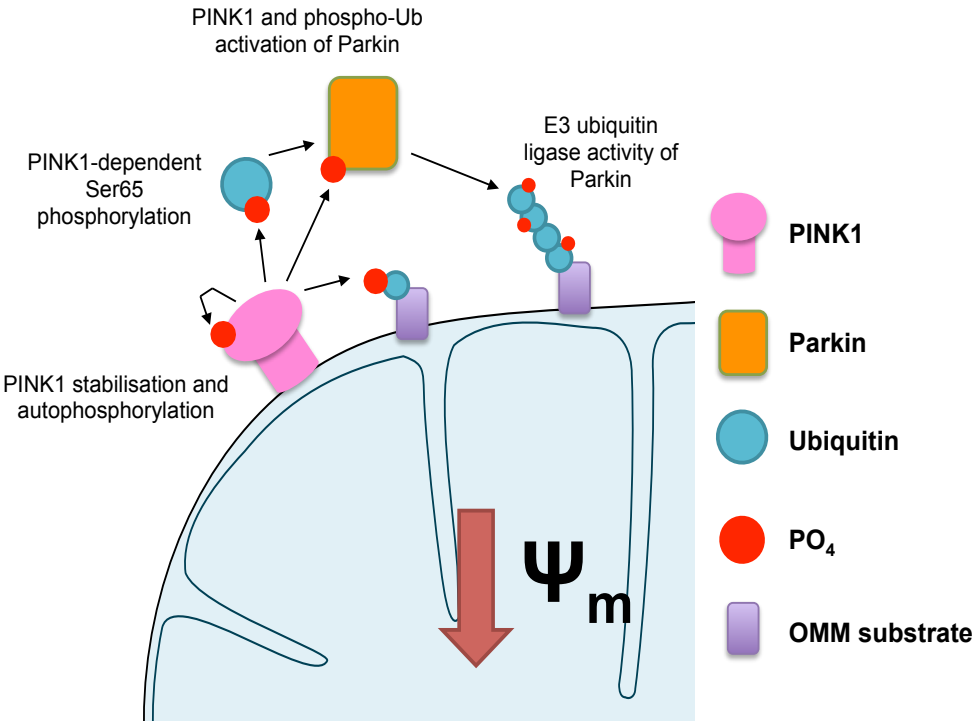

Figure 8: PINK1 stabilisation and phosphorylation

Schematic diagram to show the stabilization of PINK1 upon loss of mitochondrial membrane potential. PINK1 kinase activity is stimulated following autophosphorylation, which in turn causes the phosphorylation of ubiquitin and Parkin at Ser65. Phosphorylation and the activity of phospho-ubiquitin cause activation of Parkin's E3 ubiquitin ligase activity which leads to the formation of polyubiquitin chains on mitochondrial substrates. Diagram adapted from (McWilliams & Muqit 2017).

Recruitment of autophagic machinery

Ubiquitin-binding autophagy receptor proteins are recruited to the damaged mitochondria and are directly responsible for the ultimate clearance of mitochondria. These include p62/SQSTM1, optineurin (OPTN), NDP52 and AMBRA1 (Geisler et al. 2010; Lazarou et al. 2015; Strappazzon et al. 2015). Recently it has been shown that PINK1 can recruit OPTN and NDP52 via phosphorylated ubiquitin independently of Parkin (Lazarou et al. 2015). Mutations in OPTN have been associated with amyotrophic lateral sclerosis (ALS), a neurodegenerative disease (Maruyama et al. 2010).

PINK1 and/or Parkin-independent mitophagy

As described above, a recent study showed the recruitment of OPTN and NDP52 caused by PINK1, that occurs independently of Parkin (Lazarou et al. 2015). This finding called to question whether Parkin is completely necessary for mitophagy or rather an amplifier of the process in mammalian cells. Interestingly in PINK1 KO flies, overexpression of human Parkin was found to restore mitochondrial function, suggesting that in this system it is PINK1 that is dispensable (Clark et al. 2006).

Whilst PINK1 and Parkin mutations are a known cause of early-onset Parkinson's disease, targeting dopaminergic neurons, iPSC-derived dopaminergic neurons show mitochondrial dysfunction but not an increase in mitochondrial mass as would be expected with the involvement of these proteins in mitophagy (Rakovic et al. 2015; Shaltouki et al. 2015). This strongly suggests that alternative PINK1 and Parkin independent mechanisms of mitochondrial clearance exist.

In the dissection of the mitophagy pathway, many experiments have made use of Parkin-overexpression systems to enable easier identification of the process. Using the hypothesis that Parkin is an amplifier of mitophagy, these systems create predictable timeframes for conducting experiments; the workings of the mitophagy pathway can be easily detected after 1.5 hours of stimulation by CCCP. Moreover, Parkin-overexpression in immortalised cell lines enables the development of convenient biochemical assays, which can be used to detect inhibitors of mitophagy, as a result of the significant response induced by mitochondrial uncouplers. Detecting increased mitophagy is more difficult in these assays since, for example, 10 μM CCCP can cause the complete loss of mitochondrial proteins in Parkin-overexpressing SH-SY5Y cells within 24 hours; therefore a maximal response may already have been reached. In a study aiming to avoid any problems that may occur with using overexpressed Parkin, or to prevent this masking any so far unknown processes, a mitophagy assay was developed which utilised fluorescently tagged mitochondria, which changed colour once delivered to the acidic environment of the lysosome (Allen et al. 2013). This was achieved by using a tandem mCherry-GFP tag, which under basal conditions would fluoresce red and green, but under acidic condition only red since the low pH would quench the GFP signal only (Figure 9). Using this non Parkin-overexpressing system, the authors showed that the iron chelator deferiprone caused a significant increase in the percentage of cells undergoing mitophagy, seemingly independent of PINK1 or Parkin (Allen et al. 2013). Whilst the signalling pathway by which this occurs remains unknown, this observation has been of great interest since deferiprone is an FDA-approved drug for treating blood disorders known as thalassemias, therefore a phase 3 clinical trial is currently recruiting PD patients to assess tolerability. The study involves 17 centres across the world and is expected to be completed in 2020.

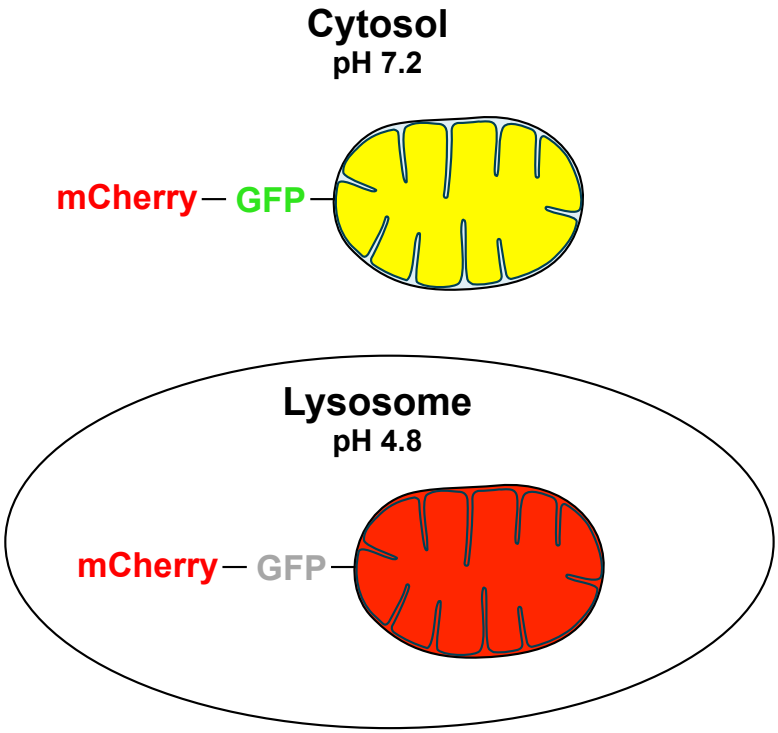

Figure 9: Fluorescence assay based on the pH change from cytosol to lysosome for detecting mitophagy

Schematic to show the red and green fluorescence from the tandem mCherry-GFP tag in the cytosol, and the red fluorescence caused by the quenching of the GFP signal in the acidic environment of the lysosome. Diagram adapted from (Allen et al. 2013).

Another mitochondrial clearance mechanism not dependent on PINK1 and Parkin is the activation of NIX and BNIP3 in response to hypoxia, during erythrocyte maturation and more recently during cell differentiation (Ney 2015; Esteban-Martínez & Boya 2017). These proteins function as autophagy receptors and cause the opening of the mitochondrial permeability transition pore, which triggers depolarisation of the mitochondrial membrane potential and stimulates envelopment of mitochondrial within autophagosomes.

Mitochondrial DNA disease

Prevalence of mitochondrial DNA mutations

The first pathogenic mutations in the mitochondrial genome were reported in 1988, and since then numerous other mutations in mitochondrial DNA have been associated with disease (Holt et al. 1988; Wallace et al. 1988). Despite early assumptions, diseases caused by mitochondrial DNA mutations are not exceptionally rare and instead affect approximately 1 in 4,300 of the population (Gorman et al. 2015; Chinnery et al. 2000). A study of just adults in the North East of England found mtDNA mutations in occur with a prevalence of 6.57/100,000, of which around half of those presented with Leber hereditary optic neuropathy (LHON) (Schaefer et al. 2008). This study highlighted the prevalence of mtDNA diseases, revealing them to be among the most common genetic disorders and also a substantial burden on medical and social services.

Presentation of mitochondrial DNA diseases

Mutations in the mitochondrial genome have the potential to affect all organs in the body, however they most often present as neuromuscular or neurodegenerative diseases as the tissues affected in these disorders rely heavily on an efficiently functioning mitochondrial network. Not only do mitochondrial diseases present with great clinical heterogeneity, they also have a variable age of onset. In general, the age of onset is relative to the severity of the mitochondrial defect.

Mitochondrial diseases can be divided into primary and secondary diseases; of which the former are caused by mutations in the mitochondrial genome and the latter caused by mutations in the

nuclear genome. As can be seen in Figure 10, all complexes in the respiratory chain except for complex II have subunits encoded for by both mitochondrial and nuclear DNA; therefore mutation in nuclear genes can affect the functioning of oxidative phosphorylation.

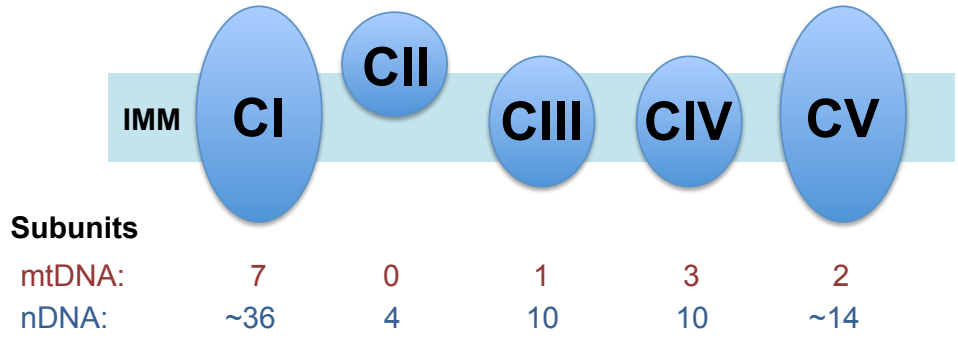

Figure 10: The origin of genomic encoding of the respiratory chain complex subunits

Schematic showing the number of subunits encoded for by the mitochondrial genome and the nuclear genome for each respiratory chain enzyme complex. Adapted from (DiMauro & Davidzon 2005).

Heteroplasmy in Primary mtDNA disease

As there are numerous copies of the mitochondrial genome within cells, compared to the single copy of the nuclear genome, in the vast majority of primary mitochondrial DNA disease cases the pathogenic mutation is not present in all copies of the genome.

Primary mitochondrial diseases can be homoplasmic, where the mtDNA mutation is present in all copies of the genome, or heteroplasmic, where mutated mtDNA coexists with wild-type mtDNA.

In cases of heteroplasmy, there is a threshold at which a certain number of genomes must contain the mutation for there to be a biochemical effect. Whilst this threshold level is typically between 60-90% mutant load, in reality it varies considerably depending on both the mutation itself and the tissue in which the mitochondria are found. In theory, the threshold is predicted to be lower in cell types more reliant on oxidative phosphorylation for energy production, compared to those which can be maintained using glycolysis. Although a greater mutant load would suggest a more severe biochemical defect, there is not consistently a direct correlation between level of heteroplasmy and clinical severity (Wong 2007).

Despite there being exceptions, in general heteroplasmic mtDNA mutations cause biochemical dysfunction in several different organ systems at a time, such as the muscle, endocrine organs and the brain, and homoplasmic mtDNA point mutations have a milder effect in a single tissue (Stewart & Chinnery 2015). Furthermore, deletions of the mitochondrial genome are always heteroplasmic (Chinnery et al. 2004).

The mutant load level in cells can both decrease and increase overtime, as a result of vegetative segregation. This process is the mechanism by which daughter cells gain differing amounts of wild-type and mutant mitochondrial DNA during cell division (Figure 11). The selection is random, except however if the effect of the mutation has a negative impact on replication, for example, in which case there will be a natural selection against the mutation. In post mitotic cells, which are not dividing, changes in heteroplasmy level can occur due to uneven replication of mtDNA.

The direction of mutant load change may not be the same in all tissues. In rapidly dividing cells, such as blood cells, mutations are likely to be lost overtime, however in postmitotic tissues such as

skeletal muscle, mutant load is more likely to increase, even from very low starting levels (Payne et al. 2013).

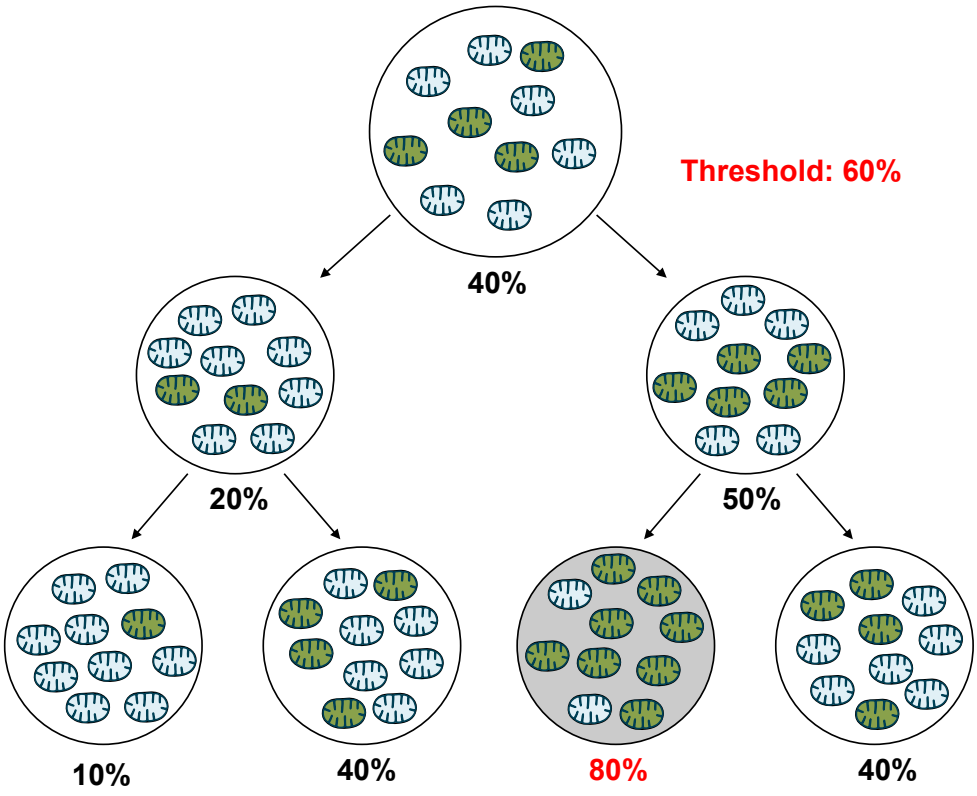

Figure 11: Vegetative Segregation of mtDNA in dividing cells

Vegetative segregation is the mechanism by which daughter cells receive a proportion of mutant (depicted in green) and wild-type mtDNA (depicted in blue) that may differ from the dividing cell, and cause the increase or decrease of heteroplasmy levels. The presence of mutant mtDNA must reach a threshold level before it has a damaging biochemical effect. Diagram adapted from (Stewart & Chinnery 2015).

Molecular mechanisms of mitochondrial DNA disease

Mutations in the mitochondrial genome typically cause reduced cellular respiration and ATP synthesis, as well as inefficient respiratory chain complex activity. Since the mitochondrial genome contains no introns, mutations will most often affect a coding region.

Although tRNA genes account for only 9% of the genome, it has been reported that two thirds of pathogenic mtDNA mutations are found in these genes, of which they are most often heteroplasmic (Wittenhagen & Kelley 2003; Scaglia & Wong 2008). Mutations in tRNA genes are more likely to be inherited than protein-coding gene mutations, since a purifying selection has been shown to select against mtDNA protein-coding genes (Stewart et al. 2008). Mitochondrial transfer RNAs are required for translation and they fold into a characteristic cloverleaf shape structure, which forms four domains; the correct formation of this structure is essential for its function. One of the most common tRNA mutations, m.3243A>G, which most often presents as mitochondrial encephalopathy with lactic acidosis and stroke-like episodes (MELAS) has been found to interfere at the transcription termination site leading to unprocessed RNA intermediates (Hess et al. 1991; King et al. 1992).

Other consequences of mitochondrial DNA mutations are transcriptional responses to the biochemical dysfunction. It has been found that in response to mitochondrial impairments, ubiquitin-mediated protein degradation is inhibited in addition to mitochondrial and nuclear ribosomal protein synthesis (Jahangir Tafrechi et al. 2005; Alemi et al. 2007).

Clinical manifestations of mitochondrial DNA diseases

The variable clinical features of mitochondrial DNA diseases make initial diagnosis sometimes difficult, however the involvement of multiple systems and a maternal family history are key clues. Diagnosis is usually confirmed with histochemical and biochemical analysis to identify common features such as cytochrome *c* oxidase deficiency and ragged red fibres, as well as dysfunction in

respiratory chain complex activity. Sequencing of the mitochondrial genome is used to confirm the mutation and gauge mutant load.

Common features of paediatric mitochondrial DNA diseases include optic atrophy, failure to thrive, hepatic failure, renal tubular defects, adrenal failure, biventricular hypertrophic cardiomyopathy, anaemia, psychomotor retardation, spasticity and epilepsy (Taylor & Turnbull 2005). Common features of mitochondrial DNA diseases in adults include migraine, strokes, sensorineural deafness, epilepsy, irritable bowel, heart failure, respiratory failure, thyroid disease, ovarian failure, optic atrophy and cataracts (Taylor & Turnbull 2005).

Objectives of thesis

Mitochondrial DNA diseases have several unique features and are particularly complex to understand. In this thesis, the objective is to provide data which helps to better understand two such unique features of mitochondrial DNA disease.

The first characteristic of mtDNA diseases is that mutant mtDNA can coexist with wild-type mtDNA, above a certain threshold of which will result in the patient presenting with a phenotype. As described in the introduction, mitophagy is a quality control process, which aims to selectively remove defective mitochondria. Therefore, I hypothesise that the process of mitophagy may be impaired in mtDNA disease patients, which enables high ratios of mutant to wild-type mtDNA to persist. To explore this, chapter one focuses on triggers of the mitophagy pathway. Since a lot of what is known about mitophagy has been discovered using the mitochondrial uncoupler CCCP, an alternative compound was used in this chapter to highlight potential misconceptions on the requirements of mitophagy induction, such as the loss of mitochondrial membrane potential, mitochondrial DNA mutations and oxidative stress. Moreover, in chapter two, the induction of the mitophagy pathway is studied in a wide range of patient fibroblasts. The patient fibroblasts used had various clinical phenotypes, a range of mutant loads and different locations of the mutation in the mitochondrial genome. The aim was to use mitochondrial uncoupling to assess the recruitment and response of mitophagy related proteins, in comparison to both wild-type fibroblasts and PINK1 and Parkin mutant fibroblasts.

The second unique feature of mitochondrial DNA diseases is that within a patient, the presence of mutant mtDNA can cause a phenotype in some tissues but not others. I hypothesise that iPSCs derived from patient fibroblasts can be differentiated into various cell

types with differing phenotypes, thus creating a valid disease model which can be used to better understand this phenomenon. Taking the results from chapter two, a patient fibroblast line and a control fibroblast line were reprogrammed into iPSCs in chapter 3. IPSCs were then differentiated into both cortical neurons and myotubes and the same experiments performed in both to compare phenotypes.

Methods

Cell culture

Human neuroblastoma cell line SH-SY5Y was cultured in Dulbecco's Modified Eagle Serum (DMEM; Gibco) media, supplemented with 10% Fetal Bovine Serum (FBS; Gibco) and maintained at 37°C, 5% CO_2. Cell media was changed on average every 3 days and cells grown to 90% confluency before splitting. Cells were split by trypsinising to collect adherent cells and plating into T175 tissue culture flasks at a 1:5 ratio.

Fibroblasts were cultured in DMEM media supplemented with 10% FBS and 200 µM uridine (Sigma) and maintained at 37°C, 5% CO_2. The production of uridine is dependent upon the functioning of the respiratory chain, and since uridine is a precursor of nucleic acids, it is essential that uridine is supplemented in cells which may have a deficient respiratory chain. Mitochondrial DNA mutations can be lost in cells that are not supplemented with uridine. Cells were maintained in T75 tissue culture flasks and media changed on average twice a week. Cells were grown to 90% confluency before splitting by trypsinising and plating at a 1:2 ratio.

Molecular Biology techniques

Mitochondrial isolation

In order to identify the presence of proteins in the mitochondria or to improve the signal of low-expressed mitochondrial proteins by

Western blot, isolation of mitochondria can be performed prior to immunoblotting. The method of mitochondrial isolation used in these experiments involved gentle disruption of the cell membrane followed by centrifugal fractionation.

Cells were plated onto 10 cm tissue culture plates and incubated overnight to reach full confluency. After treatments, if relevant, media was aspirated and cells were washed briefly with ice-cold phosphate-buffered saline (PBS; Sigma). PBS was completely removed before cells were harvested in mitochondrial isolation buffer (10 mM Tris-HCl (pH 7.4), 1 mM sodium EDTA (Ethylenediaminetetraacetic acid), 250 mM sucrose, supplemented with protease and phosphatase inhibitors (Roche)).

Tris-HCl is present in the buffer to maintain a pH of 7.4, under which our target proteins are most stable. EDTA is a chelator of divalent cations and since many DNases and proteases require magnesium ions (Mg^{2+}) to function, EDTA along with additional protease and phosphatase inhibitors are present in the buffer to protect extracted proteins. Sucrose is added to the buffer to stabilise lysosomal membranes and reduce protease release into the lysate.

To each 10 cm plate, 400 µl of mitochondrial isolation buffer was added and then frozen at -80°C overnight. The following day the plates were thawed on ice and cells collected into eppendorf tubes using plastic cell scrappers. The plates were washed with another 400 µl of isolation buffer and added to the eppendorf to ensure complete collection. Next, the eppendorfs were frozen at -80°C for 1 hour then thawed again on ice. Ice crystals are formed during freeze-thawing, which rupture cell membranes and cause cell lysis.

Cell lysates were centrifuged at 1,500 *g* for 20 minutes at 4°C to pellet cell debris. The supernatant was transferred to a clean eppendorf and centrifuged at 12,500 *g* for 20 minutes (4°C) to pellet

the mitochondria. The cytoplasmic fraction was collected in a different eppendorf and the mitochondrial pellet washed twice in mitochondrial isolation buffer (centrifugation at 16,100 *g* for 10 minutes at 4°C) to remove any contaminating cytoplasmic proteins.

Protein levels of the cytoplasmic fraction were measured using the DC protein assay (Bio-Rad), and these measurements used to infer relative differences between mitochondria enriched samples. The cytoplasmic fraction was diluted in 4X LDS buffer (10 mM Dithiothreitol; DTT; Sigma), and the mitochondrial pellet resuspended in 1X LDS buffer (10 mM DTT). DTT is used to reduce protein disulfide bonds prior to SDS-PAGE, and is less toxic than 2-mercaptoethanol. Mitochondria enriched samples were sonicated for 20 seconds at a power amplitude of 10 microns.

Cell lysate preparation

For analysis of proteins in whole cell lysates, cells were plated in one well of a 6-well plate and incubated overnight at 37°C. The following day cells were treated if applicable (16 or 24 hours for mitophagy experiments, 1.5 hours for PINK1 accumulation) then harvested. To harvest cells, on ice, the media was aspirated and cells washed briefly in cold PBS, then once all the residual PBS had been removed, 100 µl of lysis buffer was added to each well. The lysis buffer used in these experiments was NP-40 buffer, containing 150 mM NaCl, 50 mM Tris-Cl (pH8.0) and 1% NP-40 (abcam cat# ab142227). NP-40 is a non-ionic detergent comprising a water-soluble hydrophilic head and a hydrophobic tail, which allows it to enter and disrupt membranes. In addition, protease and phosphatase inhibitors were added to the NP-40 lysis buffer to protect extracted proteins. To ensure complete lysis, the samples were frozen to -80°C for at least 1 hour. Once thawed on ice, cells were collected into clean eppendorfs using cell scrappers and

centrifuged at 12,000 *g* for 10 minutes at 4°C to pellet cell debris and the supernatant collected in a new eppendorf. Protein quantification was performed using DC protein assay and samples were diluted to approximately 1 µg/µl in 4 x LDS buffer (10 mM DTT). When analysing proteins extracted from SH-SY5Y cells, approximately 10 µg of protein would be loaded onto a gel for Western blotting. When analysing proteins extracted from fibroblasts, approximately 20 µg of protein would be loaded onto a gel for Western blotting.

Western blotting

After sample preparation, proteins are separated using gel electrophoresis. This separation technique utilises the mobility of charged proteins through a porous matrix when a voltage is applied. The speed at which a molecule will move through the matrix depends upon the size and shape of the protein. In these experiments, precast polyacrylamide gels were used for protein separation (NuPAGE® 4-12% Bis-Tris gel; Novex). Polyacrylamide gels contain pores similar in size to many proteins, formed by crosslinked structures of bisacrylamide between acrylamide polymer strands.

Proteins can be positively or negatively charged; therefore in order to separate proteins only by size and not charge, gels are run in the presence of the detergent SDS. As described above, SDS was added to the sample proteins, and this coats proteins in a negative charge, as well as being present in the buffer. In these experiments, a continuous buffer system was used, which means that the same buffer is in the gel and tanks, which are generally less susceptible to problems than discontinuous systems. Due to the size of proteins being detected, the NuPAGE® MES SDS running buffer (ThermoFisher) was used, since it is recommended for separating

small to medium protein sizes. The buffer was diluted in deionized water before adding to the electrophoresis tank.

In the electrophoresis unit, the gel is placed within a buffer chamber so that movement from the cathode to anode can only occur through the porous gel. Once voltage is applied, samples loaded in the wells of the gel (formed using a gel comb) will first enter a lower density stacking gel, which is approximately twice the length of the sample wells. The purpose of this is to concentrate the proteins before reaching the higher density area of the gel, known as the resolving gel (created using a higher concentration solution of bisacrylamide and acrylamide), so proteins separate dependent on size.

Alongside the samples, a molecular weight marker was loaded on the gel (Novex Sharp Pre-stained Protein Standard; Life Technologies) to enable size estimation of the proteins. On average, samples were run through the stacking gel at 100 V, and then resolved at a voltage of 180V for 1.5 hours.

Following separation by size, proteins must be immobilised onto an inert membrane to enable detection using antibodies. The process used in these experiments was electrotransfer onto PVDF Immobilon-P membrane (Merck Millipore). The most common membranes used in Western blotting are nitrocellulose and PVDF membranes, which are both porous materials. The pore size of the material affects the binding capacity; many small pores increases the binding surface compared to fewer bigger pores. PVDF membranes have a higher binding capacity, however this also means that the background signal is greater compared to nitrocellulose membranes. PVDF membranes are hydrophobic, so before use membranes were cut to size and soaked in methanol for 1 minute, then rinsed in distilled water and soaked for 20 minutes in transfer buffer.

The transfer buffer used in electrotransfer contains Tris/glycine diluted in distilled water and 20% methanol (V/V). This buffer enables movement of the negatively charged proteins towards the anode, and the methanol is required for efficient binding to the PVDF membrane.

In these experiments a ‘wet transfer’ method was used, which means that the gel containing separated proteins and membrane are positioned in an electrotransfer tank submerged in transfer buffer. As in polyacrylamide gel electrophoresis (PAGE), electrotransfer utilises current to move charged proteins, in this case from the gel to the membrane, perpendicular to the direction of movement in PAGE so that the migration positions remain intact.

Within the tank, the ‘transfer sandwich’ is assembled as follows, starting from the cathode side of the tank:
Sponge
Filter paper
Gel
PVDF membrane
Filter paper
Sponge

Sponges are added as required outside of the sandwich to enable a close fit in the tank. This avoids movement or bubbles to form between the layers. Since the buffer can become hot during transfer, this process is run at a low voltage (35 V) over a long period of 2-3 hours.

In these experiments, the transfer of proteins was checked before membranes were blocked and incubated with antibody. For this, Ponceau S (Sigma) was used, as it is quick and gentle on the membrane. To do this, the transfer sandwich was removed from the

tank and, using forceps, the membrane was placed in distilled water (keeping the proteins facing up, i.e. the side that was in contact with the gel). The membrane was then transferred to Ponceau S for 1 minute and back into distilled water so the excess Ponceau S was removed and protein bands clearly visible. If membranes were to be cut (for detection of multiple proteins) this was done after visualisation with Ponceau S. Membranes were then washed with PBS 2% Tween-20 (Sigma) (PBST) to remove Ponceau S before blocking.

Membranes were blocked in 5% milk in PBST for 1 hour at RT, placed in 50 ml falcons on a laboratory roller. Primary antibodies were diluted in 1% milk PBST and membranes incubated overnight at 4 °C. The following day, at RT, membranes were washed 3 times in PBST (10 minutes for each wash) then incubated for 1 hour with secondary antibody diluted in 1% milk PBST. Finally, the membranes were washed again 3 times in PBST and visualised using chemiluminescence.

Primary antibodies bind to the protein target and secondary antibodies conjugated to horseradish peroxidase (HRP) will bind to primary antibody. Enhanced chemiluminescence (ECL) reagent added to HRP causes the HRP enzyme to catalyse the oxidation of luminol, which generates the emission of light (enhanced by the ECL). The intensity of light emission is proportional to the amount of antibody, and therefore the amount of protein. The light emission signal was detected using X-ray film and developed using a Konica Minolta SRX-101A processor.

The densitometry of the bands obtained from Western blotting were analysed using ImageJ software. The densitometry of the protein of interest was always normalised to a loading control, such as β-actin or GAPDH. All Western blots were performed at least 3 times.

Immunocytochemistry

Cells were plated on 13 mm glass coverslips at a confluency of 50-60% if experiments involved long treatment times, or 70-80% for characterisation or short treatment times. Cells were incubated overnight at 37°C.

If applicable, treatments were added with fresh media to the cells the following day. Once timepoints had been reached or cells were suitably confluent, the coverslips were fixed using 4% paraformaldehyde (PFA; Sigma). Cells are fixed to stabilise cell morphology and enable cellular processes to be 'frozen' in time for analysis these processes, since proteolytic enzymes will be inactivated. Furthermore, fixation of cells strengthens the layer of cells so they are not damaged by further processing and protected from contamination. PFA is a chemical fixative which reacts with primary amines, forming methylene bridges.

To fix cells, media was aspirated from the coverslips and cells were washed briefly in PBS. Coverslips were just covered in fresh 4% PFA (diluted in PBS), around 150 µl in a 24-well plate, and incubated at RT, covered, for 20 minutes.

Fixed cells were then permeabilised with 0.5% Triton X-100 (Sigma) in PBS for 30 minutes at RT. Triton X-100 is a detergent that dissolves lipids from cell membranes, enabling improved penetration of antibody if target proteins are intracellular.

Following permeabilisation, cells were blocked to reduce background fluorescence of staining. Blocking buffer comprised of 10% fetal bovine serum (FBS) in PBS + 0.5% Triton X-100. Serum contains antibodies which will bind to non-specific sites so that there is less non-specific binding to antibody, causing background

fluorescence. Coverslips were incubated with blocking buffer for 40 minutes at RT.

Primary antibodies were diluted in blocking buffer and well mixed. Coverslips were washed three times in PBS then incubated with primary antibody for 2 hours at RT. Primary antibody will bind to the antigen of interest and the signal is then amplified by the use of a fluorophore-conjugated secondary antibody. The secondary antibody needs to be raised *against* the species in which the primary was raised.

Following primary antibody incubation, coverslips were washed 3 times in fresh PBS to remove excess primary antibody. Secondary antibody was diluted in blocking buffer and protected from light exposure. Cells were then incubated with secondary antibody for 1 hour at RT, also protected from light exposure. After incubation, coverslips were washed three times with PBS to remove excess antibody and then mounted on microscope slides using ProLong Gold antifade reagent with DAPI (ThermoFisher). DAPI is a blue-fluorescent DNA stain, used for identifying cell nuclei. Microscope slides were dried at RT overnight to enable mountant to hard-set.

Images were collected using a Zeiss LSM 700 upright confocal microscope, 63x oil-immersion lens and 1.4 numerical aperture; and digitally captured using ZEN 2009 software. Laser power was adjusted to prevent saturation and reduce background signal for each fluorescent channel. Settings were kept the same throughout image capture for each experiment. DAPI nuclei staining was used for cell counting and ImageJ FIJI software was used for all image analysis.

Antibodies

Primary antibodies for Western blotting:

Mouse anti-β-Actin (1:10,000; Sigma-Aldrich A2228 cat# 123m4887v)

Rabbit anti-FLAG (1:5000; Sigma-Aldrich F7425)

Mouse anti-Mitofusin 1 (1:1000; Abcam cat# ab57602)

Mouse anti-Mitofusin 2 (1:1000; Abcam cat# ab50838)

Mouse anti-ATPβ (1:5000; Abcam cat# ab14730)

Mouse anti-PINK1 (1:1000; University of Dundee; Novis)

Rabbit anti-PINK1 (1:1000; Takeda)

Mouse anti-Parkin (Prk8) (1:700; Cell Signaling Technology #4211)

Rabbit anti-TOM20 (1:5000; Santa Cruz Biotechnology cat# G2304)

Mouse anti-Tim23 (1:1000; BD Biosciences cat# 611223)

Goat anti-Hsp60 (N-20) (1:1000; Santa Cruz Biotechnology cat#SC1052)

Mouse anti-GAPDH (6C5) (1:5000; Abcam cat# ab8245)

Primary antibodies for immunocytochemistry:

Rabbit anti-FLAG (1:2000; Sigma-Aldrich F7425)

Mouse anti-ATPβ (1:2000; Abcam cat# ab14730)

Rabbit anti-TOM20 (1:500; Santa Cruz Biotechnology cat# G2304)

Mouse anti-SQSTM1/p62 (1:2000; Abcam cat# ab56416)

Mouse anti-Tim23 (1:100; BD Biosciences cat# 611223)

Goat anti-Hsp60 (N-20) (1:100; Santa Cruz Biotechnology cat#SC1052)

Goat anti-hNanog (1:100; R&D Systems AF1997-SP)

Goat anti-hSox2 (1:200; R&D Systems AF2018-SP)

Mouse anti-Oct4 (1:500; Abcam cat# ab59545)

Rabbit anti-TBR1 (1:300; Abcam cat# ab31940)

Rat anti-Ctip2 (25B6) (1:300; Abcam cat# ab18465)

Mouse anti-Satb2 (1:100; Abcam cat# ab51502)

Mouse anti-MF20 MYH1 (MIgG2b) (1:100; DSHB)

Rabbit anti-MyoD (C-20) (1:100; Santa Cruz)

Secondary antibodies for Western blotting:

Goat anti-rabbit IgG-HRP (1:5000; Santa Cruz Biotechnology cat# K1010)

Goat anti-mouse IgG-HRP (1:5000; Santa Cruz Biotechnology cat# K1710)

Secondary antibodies for immunocytochemistry:

Alexa Fluor 568 goat anti-mouse (1:2000; Invitrogen cat# A11004)

Alexa Fluor 488 goat anti-rabbit (1:2000; Invitrogen cat# A11008)

Alexa Fluor 488 donkey anti-goat (1:2000; Invitrogen cat# A11055)

Alexa Fluor 488 goat anti-rat (1:2000; Invitrogen cat# A11006)

DNA extraction

DNA was extracted from cells using the Wizard® Genomic DNA Purification Kit (Promega, cat# A1125). Cells were plated in 10cm tissue culture plates and incubated at 37°C overnight. The following day, cells were treated if applicable, then media was aspirated, cells washed in PBS and trypsinised to collect a cell pellet. Cell pellets were lysed in Nuclei Lysis Solution and mixed with RNase Solution for RNase digestion. This mixture was incubated for 15-30 minutes at 37°C, then the sample was left to cool at room temperature for 5 minutes before proceeding. The cellular proteins were removed by salt precipitation, by adding the kit's protein precipitation solution and vortexing vigorously at high speed for at least 20 seconds. The sample was chilled on ice for 5 minutes and then centrifuged for 4 minutes at 16,000 *g*. The precipitated protein forms a tight pellet and the supernatant containing the high molecular weight genomic DNA was then transferred to a new eppendorf containing room temperature isopropanol. The genomic DNA was desalted by isopropanol precipitation and DNA pelleted by centrifugation. The DNA was then rehydrated in DNA Rehydration Solution overnight at 4°C.

DNA was quantified on the Nanodrop Spectrophotometer (ThermoFisher Scientific). To identify the 'purity' of DNA, the ratio of absorbance at 260 nm and 280 nm is used, and a 260/280 ratio of ~1.8 is expected.

Long-range PCR and quantification

DNA was extracted using the Wizard® Genomic DNA Purification kit (Promega) and two large PCR products covering the mitochondrial genome generated using the Expand™ Long Template PCR kit (Roche) according to manufacturer's instructions using the primer

sequences: L16331 (5'-ACATAGCACATTACAGTCAAATCCCTTCTCGTCCC-3') and H9068 (5'-ATTGCTAGGGTGGCGCTTCCAATTAGGTGC-3'); and L8753 (5'-TCATTTTTATTGCCACAACTAACCTCCTCGGACTC-3') and H16566 (5'-CGTGATGTCTTATTTAAGGGGAACGTGTGGGCTAT-3'). The amplified products were quantified using the Qubit dsDNA BR Quantification Kit and pooled to a final working stock of 0.2 ng/µl. Libraries were prepared according to manufacturer's instructions using the Nextera XT DNA Sample Preparation Kit and sequencing reactions carried out using the MiSeq or HiSeq platforms.

Nextera library preparation

Sequencing of the mitochondrial genome was performed on the Illumina MiSeq platform, and samples were prepared using the Nextera XT DNA Sample Preparation Kit.

The Nextera XT transposome simultaneously fragments and adds adapter sequences to the ends of template DNA. Tagment DNA buffer and Amplicon Tagment mix buffer were added to 1 µg of template DNA and heated to 55°C for 5 minutes. Once cooled to 10°C, Neutralise Tagment buffer was added.

The tagmented samples were then indexed with oligos to allow pooling of the samples, using index primers and full adapter sequences. The Nextera PCR Mastermix and primers (making a note of which indexes were used for each sample, as this is required for cluster formation) were added to the tagmented samples, then cycled as follows: 72°C for 3 minutes, 95°C for 30 s, then 12 cycles of 95°C for 10 s, 55°C for 10 s and 72°C for 10 s. Finally the plate was held at 72°C for a further 5 minutes before cooled to 10°C.

The samples underwent PCR clean up using Agencourt AMPure XP beads. In this process, the PCR products bind to the magnetic beads and can therefore be separated from contaminants using a magnetic stand. The contaminants can then be removed and whilst still in the magnetic stand, washed with 80% freshly prepared ethanol. Finally the PCR amplicons can be eluted from the magnetic particles and transferred to a clean plate for library normalisation. For clean up, AMPure XP beads were added to each well of PCR product and incubated with shaking (1800 rpm) for 2 minutes, then incubated without shaking for 5 minutes. The plate was then placed on a magnetic stand and once the supernatant was clear (approximately 2 minutes after placing on stand), the supernatant was discarded. The beads were washed twice with 80% EtOH, using the magnetic stand to collect the beads before discarding the supernatant. The beads were air-dried on the magnetic stand for 15 minutes before adding resuspension buffer, shaking for 2 minutes then incubating without shaking for a further 2 minutes. The plate was then put back on the magnetic stand and the clear supernatant transferred to a new plate.

Library normalisation aims to ensure equal representation in the final pooled sample, using magnetic beads. The Nextera beads can only ‘hold’ a limited about of material; therefore excess sample can be easily removed by discarding the supernatant when the plate is on the magnet. The Nextera beads were added to the cleaned PCR products and once thoroughly mixed and then separated using a magnetic stand, the supernatant containing excess product was removed, and the beads then washed twice with wash buffer. The bound PCR products were eluted from the beads for library pooling before loading onto the MiSeq by taking 5 µl of each library.

The MiSeq run was conducted by Deborah Hughes and Cathy Woodward (UCL), and data analysed by Dr A. Pittman and Dr M. Athanasopoulou (UCL).

Sanger Sequencing

DNA was extracted using the Wizard® Genomic DNA Purification Kit and quantified as described above. Sanger Sequencing utilises DNA polymerase enzymes, which copy single-stranded DNA templates.

After DNA extraction, polymerase chain reaction (PCR) was used to amplify the gene of interest for the sequencing reaction, using primers designed to flank the region of interest. DNA is separated into single strands by exposure to high temperature on a PCR cycler, then the temperature is lowered, which enables the single-stranded primers to find and anneal to their complementary sequences. The Taq polymerase, a heat stable catalyst isolated from *Thermis aquaticus* bacterium, can withstand the high denaturing temperature and then begin DNA synthesis once the primers are annealed and the temperature has reached the optimum activity temperature for the particular enzyme (approximately 72°C). The Taq polymerase uses deoxynucleotide triphosphates (dNTPs) to synthesise the new DNA strand complementary to the DNA template strand in the 5' to 3' direction. In these experiments, the FastStart™ High Fidelity PCR System (Roche) was used for the PCR reaction at a total volume of 25 µl and a reaction of 35 cycles.

PCR products were cleaned to remove the reagents from the PCR reaction before sequencing, such as excess primers and unincorporated nucleotides. In these experiments enzymatic purification was used by incubation of 5 µl PCR product with 2 µl

ExoSAP-IT™ (Affymetrix USB) for 15 minutes at 37°C followed by 15 minutes at 80°C. The PCR product was run on a 1% agarose gel to ensure a single band was present, indicating specific amplification of target by the primers.

The sequencing reaction requires the cleaned PCR product, primers, DNA polymerase, four nucleotides (A, T, C, G) and four dideoxynucleotides containing fluorescent tags. The sequencing reaction works similarly to a PCR reaction, whereby the sample is heated to separate the double strands of the template DNA, then the temperature lowered for the primers to anneal at the complementary sequences on the template DNA. The temperature is then raised again so the enzyme can bind to the DNA, from which new nucleotides are used to extend the chain, complementary to the template strand. When a fluorescently tagged dideoxynucleotide is incorporated however, the reaction is terminated, as these lack a 3'-hydroxyl group with which another nucleotide can join. The random incorporation of dideoxynucleotides results in a mixture containing thousands of differing length strands.

For these experiments, the BigDye™ Terminator Cycle Sequencing Kit (Applied Biosystems) was used to a total volume of 20 µl:

Component	Volume/reaction (µL)	RT conditions
BigDye™ Terminator Ready Reaction Mix	8	96°C – 1 min 25 cycles of: 96°C – 10 s 50°C – 5 s 60°C – 4 mins
Forward Primer (3.2 µM)	1	
Reverse Primer (3.2 µM)		
Deionized water	9	
Template	2	

Table 1: BigDye Terminator Cycle Sequencing reaction

The reaction was then purified using the BigDye XTerminator® Purification Kit (Applied Biosystems) by adding the SAM™ Solution and XTerminator ™ Solution directly to the plate, sealing the plate and vortexing for 30 minutes. The plate was then centrifuged briefly and loaded onto the 3730 DNA Analyser (Applied Biosystems) for capillary electrophoresis.

The capillaries in DNA analysers are filled with polymer and a voltage is applied, so that the negatively charged DNA products of the sequencing reaction move through the polymer, separating by size, towards the anode. A laser beam is applied near the anode that causes the DNA fragments to fluoresce in the correct order of sequence due to the separation by size.

Mitochondrial membrane potential

Cells were plated on 25 mm glass coverslips at a confluency of 60-70% and incubated overnight at 37°C. For each treatment or cell line, at least 2 coverslips were prepared per experiment, and experiments were performed on 3 independent occasions. The following day the cells were loaded with dye 40 minutes prior to imaging.

The dye most commonly used for mitochondrial membrane potential is tetramethylrhodamine methyl ester (TMRM), which is a cell-permeant cationic dye. TMRM is a single-wavelength indicator or membrane potential ($\Delta\Psi_m$) and accumulates electrophoretically in cells in proportion to $\Delta\Psi_m$ without inhibiting mitochondrial function (Chazotte 2011; Scaduto & Grotyohann 1999). In cells with intact membrane potentials, TMRM loaded at low concentrations will accumulate in the negatively charged mitochondrial matrix, due to the charge properties of the compound, without inducing

aggregation and fluorescence quenching. Upon loss of membrane potential, the TMRM dye will disperse throughout the cell cytosol, causing a substantial reduction in fluorescence.

TMRM (Life Technologies T-668) was diluted to 25 nM in Hank's Balanced Salt Solution (HBSS) (156 mM NaCl, 3 mM KCl, 2 mM $MgSO_4$, 1.25 mM KH_2PO_4, 2 mM $CaCl_2$, 10 mM glucose and 10 mM HEPES, pH 7.35), a buffer used to maintain physiological pH when imaging. Cell media was aspirated then cells were washed once in HBSS, before 1 ml of 25 nM TMRM in HBSS was added to each coverslip. The cells were left to load for 40 minutes at RT, covered from light. Attofluor cell chambers (ThermoFisher Scientific A-7816) were used to hold the coverslips whilst imaging, which were thoroughly cleaned with ethanol and distilled water before use to remove any toxins from previous experiments. After 40 minutes of loading, one coverslip at a time was secured in a chamber and 500 µl of fresh diluted TMRM was added.

Images were taken using a Zeiss LSM 700 upright confocal, 63 x oil-immersion lens, 1.4 numerical aperture and captured using Zen 2009 software. In order to assess $\Delta\Psi_m$, we used untreated healthy controls to determine the laser power settings, which were to be kept the same throughout all data collection on that day. It is of vital importance to not image using a high laser power, as the heat of the laser can cause stress in the live cells and give misleading results. Furthermore, saturation of images causes unusable data, since the correlation between fluorescence and $\Delta\Psi_m$ will not be linear, so it is important to determine settings so that hyperpolarised cells can be accurately quantified.

Once TMRM settings were determined, Z-stacks images of the cells were captured and approximately 5 images were taken per coverslip. If several lines (for example in the patient fibroblast experiments) were being imaged, addition of TMRM was staggered

so cells were always loaded for 40 minutes before imaging. Addition of compounds was recorded using the ZEN time-lapse feature, whereby basal TMRM signal was recorded, then recording paused whilst compound was added into the 500 µl of solution in the chamber as quickly and carefully as possible before starting recording again. It is important when adding small volumes to mix the solution well in order to be able to identify the given effect when visualising only a small subset of cells.

In cases where use of TMRM was not appropriate, e.g. when pretreating with Rhodamine 6G, Rhodamine 123 was used to measure $\Delta\Psi_m$ using the same protocol as above, but loaded with 1 mM Rhodamine 123. For large numbers of cell lines, TMRM data was acquired using the ImageXpress® (Molecular Devices) for which cells were plated in BD Falcon 96 well clear bottom tissue culture imaging plates (SLS). Cells were loaded with 25 nM TMRM as described above.

Images were analysed using FIJI software, where the maximal intensity projection was used to threshold the red channel (in order to eliminate background) and measure mean intensity across the field using ROI (region of interest) manager. In each experiment the mean for each treatment or cell line was calculated, and the means were then averaged across three independent experiments.

Mitochondrial network analysis

Cells were plated on 25 mm glass coverslips at a confluency of 60-70% and incubated overnight at 37°C. For each treatment or cell line, at least 2 coverslips were prepared per experiment, and experiments were performed on 3 independent occasions.

The following day, cells were loaded with 200 nM MitoTracker® Green FM (ThermoFisher) in HBSS for 40 minutes at RT. MitoTracker® Green FM is a carbocyanide-based probe which is fluorescent in lipid environments and therefore exhibits minimal background fluorescence. Unlike other MitoTracker® probes, MitoTracker® Green FM accumulates in mitochondria independently of membrane potential, making it suitable for mitochondrial quantification and network analysis.

Cells were imaged by taking z-stacks at several sites on each coverslip, in order to analyse the entire depth of cells on the coverslips. Images were analysed using ImageJ FIJI software, where mitochondrial staining was thresholded to remove background signal and enabled quantification. Mitochondrial content was quantified per field: on each Z-stack slice, the area of MitoTracker signal was calculated, then summed across all Z-stacks (i.e. the depth of the cell) and divided by the number of cells in that field (obtained by counting nuclei). This gave a measurement referred to in these experiments as mitochondrial volume per cell. Ideally, a volume of the cell would be used to obtain mitochondrial volume per cell volume, however it was found during experimental optimisation that Calcein Blue (Thermofisher) (a commonly used dye for cell volume measurements) was not retained by the fibroblasts for the duration of the experiment. Therefore, the cell volume would appear to reduce over time and consequently was deemed unreliable for these experiments. Several fields of view were obtained and the mean mitochondrial volume per cell was calculated across three independent experiments.

For analysis of mitochondrial network, images taken from cells loaded with MitoTracker® Green FM were used. ImageJ FIJI software was used to threshold the MitoTracker® Green FM signal and the mitochondrial network was convolved using the following kernel:

-10 -5 -2 -1 -2 -5 -10
-5 0 3 4 3 0 -5
-2 3 6 7 6 3 -2
-5 0 3 4 3 0 -5
-10 -5 -2 -1 -2 -5 -10

A kernel is a matrix whereby the center represents the source pixel and the outer numbers correspond to pixels neighbouring the source pixel. This enables the analysis software to interpret the network and allow measurement of area, perimeter and aspect ratio. Form factor could be determined using the following formula: $(perimeter)^2/(area \times 4\pi)$. These data were collected for images from each cell line and the mean value calculated. Data across three independent experiments were then averaged and the standard error or mean calculated.

GSH levels by live imaging

Intracellular reduced glutathione (GSH) is detected using monochlorobimane (MCB), a lipophilic GSH specific probe. MCB can passively diffuse across cellular membranes and is only fluorescent upon conjugation to low molecular weight thiols, due to quenching by its chorine group when unbound. GSH levels were assessed in live cells, which had been incubated on 25 mm glass coverslips overnight at 37°C. Cells were loaded with 1 mM MCB in HBSS for 40 minutes at RT and Z-stack images captured. Images were analysed using ImageJ FIJI software. The MCB fluorescent signal was thresholded and mean intensity across the field analysed. The data was averaged across all coverslips imaged, and then this was averaged across three independent experiments.

EM imaging

Fibroblasts were cultured in T75 flasks and fixed overnight in 0.1 M sodium cacodylate buffer (pH 7.4) containing 2% paraformaldehyde and 2.5% glutaraldehyde. Samples were post-fixed for 1 h at room temperature in a solution containing 1% osmium tetroxide and 1% potassium ferrocyanide.

After fixation, samples were stained en bloc with 5% aqueous uranyl acetate overnight at 4^{o}C; the samples were then dehydrated via a series of ethanol washes and embedded in TAAB epoxy resin (TAAB Laboratories Equipment Ltd., Aldermaston, UK). Semi-thin sections were stained with toluidine blue, and areas of the sections were selected for ultramicrotomy. Ultrathin sections were stained with lead citrate and imaged using a MegaView 3 digital camera and iTEM software (Olympus Soft Imaging Solutions GmbH, Münster, Germany) in a Jeol JEM-1400 electron microscope (Jeol UK Ltd., Welwyn Garden City, UK) at an accelerating voltage of 100kV. Sample preparation, electron microscopy and image analysis was performed by Dr Samantha Loh at the University of Leicester. The fibroblasts send for preparation and analysis had each been allocated a code, so Dr Loh was unaware of the genotype of each fibroblast line. Using the images obtained, two parameters were analysed: mitochondrial-ER contacts and mitochondrial length. Mitochondrial-ER contact was counted by eye, and only a physical contact between organelles was considered as contact. If any distance between organelles could be measured, then these were considered not in contact. A minimum of 120 mitochondria were identified for each sample, and the number of those in contact with ER was counted. The data was then presented as the percentage of mitochondria in contact with ER. Mitochondrial length was measured as the longest straight length for each mitochondria, and each data point (measured in micrometers) was plotted on a scatter

graph for each sample. The mean mitochondrial length was calculated and analysed using a Bonferroni's multiple comparison test.

RNA extraction

RNA was extracted from either one confluent well of a 6-well plate or a 10 cm plate. Cells were plated, incubated overnight and, if applicable, treated the following day. Cells were pelleted and disrupted using lysis buffer from the RNeasy® Mini Kit (Qiagen cat# 74104). The RNeasy® Mini Kit enables the purification of RNA molecules longer than 200 nucleotides, consequently enriching for mRNA molecules. Cells were lysed and homogenised to disrupt the cell walls and plasma membranes then reduce the viscosity of the resulting lysates. Before loading sample to the RNeasy Mini spin column, ethanol was added to promote selective binding of the RNA to the column membrane. Once lysates had been passed through the column using centrifugation (16,000 *g*), wash buffer was applied to remove contaminants from the membrane-bound RNA. To ensure complete removal of remaining DNA, which is essential for RT-PCR analysis, on-column DNase digestion was subsequently performed (Qiagen cat# 79254). RNA was treated with DNase incubation mix directly onto the membrane and incubated at RT for 15 min. Finally the membrane was washed again with the provided buffers and eluted in RNase-free water.

RNA was quantified on the Nanodrop Spectrophotometer (ThermoFisher Scientific). Absorbance measurements include the absorbance of all molecules present in the sample, including RNA, ssDNA and dsDNA, therefore the ratio of absorbance at 260 nm and 280 nm is used to identify the purity of the extracted RNA sample. For 'pure' RNA, a 260/280 ratio of ~2.0 is expected.

cDNA synthesis

An RNA template can be used to produce complementary DNA (cDNA) using a process known as reverse transcription. Random primers anneal to the RNA template, providing a starting point for the reverse transcriptase enzyme. This ensures first strand synthesis occurs efficiently with all RNA molecules in the sample. Reverse transcriptases are RNA-dependent DNA polymerases, isolated from retroviral sources, such as the Moloney murine leukemia virus.

Total RNA was reverse transcribed to single-stranded cDNA using the High Capacity cDNA Reverse Transcription Kit (Applied Biosystems) and the following reaction (prepared on ice):

Component	Volume/reaction (µL)	RT conditions
10X RT Buffer	2.0	25°C - 10 mins 37°C - 120 mins 85°C - 5 mins 4°C - ∞
25X dNTP Mix (100 mM)	0.8	
10X RT Random Primers	2.0	
MultiScribe™ Reverse Transcriptase	1.0	
Nuclease-free H_2O	4.2	
RNA sample	10	

Table 2: High Capacity cDNA Reverse Transcriptase reaction

Q-PCR reaction

Quantitative-PCR, or real-time PCR, is used to quantify gene expression whereby amplified DNA is detected by fluorescence during each cycle of PCR. SYBRgreen is an intercalating

fluorescent dye, which fluoresces more greatly when intercalated within the DNA double helix as this alters the structure of the dye. Therefore, as the PCR cycles amplify more DNA, SYBRgreen can intercalate with more DNA and more fluorescence is generated. This can be quantified and used to identify relative gene expression to controls.

Forward and reverse primers approximately 20 nucleotides in length were designed for each gene of interest and housekeeping gene, and ordered from Sigma at a concentration of 100 μM.

To identify the fold change in mRNA expression between patients and controls or untreated and treated cells, the C_t value needs to be used. This is the PCR cycle at which the fluorescent signal crosses a threshold within the exponential phase of amplification. The lower the C_t the greater the amount of amplicon, since fewer rounds of PCR cycle would be required to generate the same amount of amplicon. Therefore, to ensure that the exponential phase is reached within the total number of cycles, the amount of starting template needs to be determined for each primer set, as these will have differing efficiencies. To do this, a standard curve needs to be generated for each primer set. In order to represent the expression of the gene of interest across all samples, 4 μl of neat cDNA from 5 reactions were combined to make the dilutions for the standard curve. Serial dilutions 1:5, 1:50, 1:500, 1:5000 and 1:50000 were made (thoroughly mixing between dilutions) and a blank prepared with RNase-free water. These were used with each primer pair (diluted to 3.3 μM in RNase-free water) in triplicate using the following reaction:

Component	**Volume/reaction (μL)**	**qPCR conditions**
2X Fast SYBR green	10	95°C – 20 s

Master Mix		45 cycles of:
Forward primer (3.3 µM)	1	95°C – 3 s
Reverse primer (3.3 µM)	1	60°C – 20 s
H_2O	3	
cDNA	5	

Table 3: Fast SYBR green QPCR reaction

Reactions were prepared on ice and the 384-well plate sealed and loaded onto the QuantStudio 7 Flex Real-Time PCR System (Applied Biosystems®). At the end of the run, triplicates were checked and wells with errors attached were removed and re-analysed. The dissociation curves were checked for each primer set, for which all products should appear at the same temperature, without any 'shoulders' indicating a second product, which would require redesigning of primers. To identify the suitable amount of template to use with each primer set, the lowest dilution for which the exponential phase occurred within the 45 cycles was selected.

With this information, the experiment was performed as above but with the 5 µl cDNA from single reactions at the appropriate dilution for each primer set. After removal of unsuccessful reactions, the average C_t from the triplicate (or duplicate if one removed) was obtained for the gene of interest and housekeeping gene, for each sample. Then, for each sample the C_t from the housekeeping gene was subtracted from the C_t for the gene of interest, to normalise for starting amounts of amplicon across the samples. The fold change in mRNA expression between patients and controls was calculated using the formula:

$2^{-((Ct\ gene\ of\ interest - Ct\ housekeeping\ gene)\ patient - (Ct\ gene\ of\ interest - Ct\ housekeeping\ gene)\ control)}$

Each experiment was performed three times and the average fold change in expression calculated.

MtDNA copy number

Mitochondrial DNA copy number was determined using quantitative real-time PCR. As described above, quantitative-PCR is used to quantify gene expression whereby amplified DNA is detected by fluorescence during each cycle of PCR. To identify the relative amount of mitochondrial DNA present in cells from different patients, genomic DNA is used as a control from which the number of mitochondrial DNA copies can be normalised.

DNA was extracted from fibroblast cell pellets as described above, and primers designed to a house-keeping genomic DNA gene and a mitochondrial gene (one which did not contain a mutation in any of the patient lines). Primers used were for the quantification of the *ND1* gene in mtDNA and for the amplification of the single-copy nuclear gene human globulin (*HGB*).

ND1-F: 5'-CCCTAAAACCCGCCACATCT-3'
ND1-R: 5'-GAGCGATGGTGAGAGCTAAGGT-3'

HGB-F: 5'-GCTTCTGACACAACTGTGTTCACTAGC-3'
HGB-R: 5'-CACCAACTTCATCCACGTTCACC-3'

DNA was diluted to 3 ng/µl in TE buffer. TE buffer consists of Tris, a pH buffer, and EDTA, a cation chelator, and is used to solubilise DNA, preventing it from degradation.

Preparation for the PCR reaction was performed on ice, as follows:

Component	Volume/reaction (µL)	qPCR conditions
SYBR Green PCR Mastermix	12.5	95°C – 10 mins 40 cycles of: 95°C – 5 s 60°C –60 s
Forward primer (0.4 µM)	2	
Reverse primer (0.4 µM)	2	
H_2O	2	
Template DNA	8.5	

Table 4: SYBR Green PCR reaction

For each cell line, a PCR reaction was performed using the *ND1* primers and another using the *HGB* primers. On the plate, each reaction was performed in triplicate and overall the experiment was performed on 3 independent occasions from new cell pellets.

Using the triplicate reactions, the mean C_t was found for each cell line for *ND1* and *HGB*. The delta C_t (ΔC_t) was calculated: gDNA C_t – mtDNA C_t , and relative mtDNA content calculated: $2^{-\Delta Ct}$

The mean $2^{-\Delta Ct}$ was calculated from the three independent experiments and SEM determined.

Primer Sequences

PGC1α -F: 5'-GTCACCACCCAAATCCTTAT-3'
PGC1α-R: 5'-ATCTACTGCCTGGAGACCTT-3'

PINK1-F: 5'-GCCTCATCGAGGAAAAACAGG-3'
PINK1-R: 5'-GTCTCGTGTCCAACGGGTC-3'

GAPDH-F: 5'-GGAGCGAGATCCCTCCAAAAT-3'
GAPDH-R: 5'-GGCTGTTGTCATACTTCTCATGG-3'

ND1-F: 5’-CCCTAAAACCCGCCACATCT-3’
ND1-R: 5’-GAGCGATGGTGAGAGCTAAGGT-3’

HGB-F: 5’-GCTTCTGACACAACTGTGTTCACTAGC-3’
HGB-R: 5’-CACCAACTTCATCCACGTTCACC-3’

DNMT3B-F: 5’-ATAAGTCGAAGGTGCGTCGC-3’
DNMT3B-R: 5’-GGCAACATCTGAAGCCATTT-3’

KLF4-F: 5’-GGTCGGACCACCTCGCCTTACAC-3’
KLF4-R: 5’-CTCAGTTGGGAACTTGACCA-3’

Rex-F: 5’-CCGAGACCACGTCTGTGCGG-3’
Rex-R: 5’-AGCGCTTTCCGCACCCTTCA-3’

Myc-F: 5’-CTGAAGAGGACTTGTTGCGGAAAC-3’
Myc-R: 5’-TCTCAAGACTCAGCCAAGGTTGTG-3’

Complex I activity assay

The enzyme activity of mitochondrial OXPHOS Complex I was analysed using the Complex I Enzyme Activity Microplate Assay Kit from Abcam (ab109721). This assay measures the NADH-dependent activity of Complex I and is not dependent on the presence of ubiquinone. The microplate wells are pre-coated with capture antibodies specific for Complex I and the samples are immobilised in the wells. As NADH is oxidised to NAD^+, simultaneously the dye in the well (ε = 25.9/mM/well) is reduced which causes an increase in absorbance at OD 450 nm.

Fibroblasts plated in a 10 cm tissue culture plate were harvested and the cell pellet washed twice with PBS. The cell pellet was

resuspended in PBS to a concentration of 5.5 mg/ml and the proteins extracted by adding detergent and incubating on ice for 30 minutes to allow solubilisation. The samples were then centrifuged at 16,000 *g* for 20 minutes at 4°C and the supernatants collected in a new eppendorf. For the assay, 200 µg of sample was loaded onto the plate in duplicate with background wells (containing only buffer) and background control sample wells (containing sample but no assay solution to be added after incubation), and the microplate was incubated for 3 hours at room temperature. The wells were then emptied, washed twice with buffer (all wells except the background control sample wells) and emptied again. The assay solution, containing buffer, NADH and dye, was then added to all wells except the background control sample wells, avoiding bubbles, and loaded onto the plate reader with the following program:

Mode	**Kinetic**
Wavelength:	450 nm
Time:	30 minutes
Interval:	20 sec – 1 min
Shaking:	Shake between readings
Temperature:	Room temperature

Table 5: Complex I activity assay program settings

Complex I activity is proportional to the increase in absorbance at OD 450 nm. To analyse the data, the duplicates of each sample were averaged and the background control was subtracted from the sample reading. Then the linear rate of increase calculated for each sample and expressed as mOD/min. This experiment was repeated three times.

IPSC and Differentiation techniques

Stemgent microRNA-Enhanced mRNA Reprogramming System

Reprogramming of human fibroblasts to induced pluripotent stem cells (iPS) was achieved using the Stemgent mRNA Reprogramming Kit, the Stemgent microRNA Booster Kit and Stemgent Stemfect RNA Transfection Kit. This method of reprogramming has a high efficiency, is fast and avoids the use of genome-integrating viruses. This process utilises the daily transfection of synthetic mRNAs, together with interferon inhibitor B18R, as first described by Warren *et al.* (Warren et al. 2010). In total, the protocol takes 16 days to produce iPS cell cultures, in which there are 2 microRNA transfections and 11 mRNA transfections.

Before beginning reprogramming, NuFF-Conditioned Pluriton Medium must be prepared, which is used to supplement cultures when reprogramming in feeder-free conditions. The generation and maintenance of culture systems traditionally uses animal product-based components (e.g. 'feeder cells'), however these can cause problems with contamination of the culture, limiting their use in many important applications, such as drug development. In this protocol inactivated newborn human foreskin fibroblasts (NuFF cells) are incubated with Pluriton Medium (Stemgent) for 24 hours. This medium becomes 'conditioned' and can be frozen (for up to 3 months) before use in the reprogramming experiment. In addition, before reprogramming, single-use aliquots were prepared of the Pluriton supplement and B18R Recombinant protein (stored at -80°C), and the mRNA and microRNA cocktails prepared.

The mRNA Reprogramming cocktail consisted of:

Oct4 mRNA	400.0 µl
Sox2 mRNA	123.8 µl
Klf4 mRNA	162.0 µl
c-Myc mRNA	153.5 µl
Lin28 mRNA	85.7 µl
nGFP mRNA	115.0 µl
Total cocktail	**1040 µl**

Table 6: mRNA reprogramming cocktail components

The cocktail was mixed thoroughly, aliquoted into single-use volumes and stored at -80°C.

The tissue-culture plates used in these experiments were coated with Corning® Matrigel® Matrix (hESC-qualified) a day before use. Matrigel is a solubilised basement membrane preparation used to improve attachment and differentiation of iPSCs.

On day 0, Fibroblasts were plated by removing culture medium, washing cells briefly with PBS and adding 0.05% Trypsin/EDTA to the culture surface of the flask. The flask was incubated for at least 3 minutes at 37°C until detached. Conditioned Pluriton medium was added to the flask to neutralise the trypsin/EDTA and transferred to a 15ml falcon. Cells were centrifuged at 200 *g* for 5 minutes, supernatant removed and cell pellet resuspended in 5 ml media. Cells were counted using a counting chamber and 5 x 10^4 cells were plated per well into the Matrigel® coated 6-well tissue culture plates. Plates were incubated at 37°C and 5% CO_2 overnight.

On day 1, cells were to be pre-treated with B18R protein and then transfected with microRNA cocktail. Conditioned media was warmed to 37°C in the incubator and Pluriton supplement and B18R protein thawed on ice; these were then combined and mixed well.

The media was aspirated from the cell culture plate and the freshly made media containing B18R added to the cells for 2 hours at 37°C and 5% CO_2. The microRNA cocktail aliquot was thawed on ice, and the Stemfect Buffer and Stemfect Transfection Reagent allowed to equilibriate to RT for 30 minutes. The Stemfect Buffer was combined with the microRNA cocktail in one tube (tube 1), and the Stemfect Buffer combined with the Stemfect Transfection Reagent in another tube (tube 2). The contents from tube 2 was combined with tube 1 and pipetted gently 3-5 times. This complex was incubated at RT for 15 minutes, then aliquoted into the wells of the cell culture plate in a dropwise fashion. The plate was gently rocked from side to side, front to back, and incubated at 37°C and 5% CO_2 overnight.

On days 2-4, cells were again pre-treated with B18R, as described above, then transfected with the mRNA cocktail. Where possible, transfections was performed at the same time each day in order to maintain sufficient levels of factors. As described previously, the Stemfect Buffer and Stemfect Transfection Reagent were allowed to equilibriate to RT for 30 minutes, and the mRNA reprogramming cocktail was thawed on ice. The Stemfect Buffer and mRNA cocktail was combined in tube 1 and the Stemfect Buffer and Stemfect Transfection Reagent combined in tube 2. The contents of tube 2 was then transferred to tube 1, gently mixed 3-5 times and incubated at RT for 15 minutes. The complex was added to the wells of the cell culture plate in a dropwise fashion and gently mixed, then the plate was incubated at 37°C and 5% CO_2 overnight.

On day 5, the cell culture was co-transfected with both the mRNA reprogramming cocktail and the microRNA cocktail. As described previously, the cells were pre-treated with B18R protein, and the mRNA and microRNA complexes prepared as before. The two complexes were added to the wells in a dropwise fashion, mRNA

just before the microRNA, and the plate was incubated at 37°C and 5% CO_2 overnight.

On days 6-12, cells were pre-treated with B18R protein and transfected with mRNA reprogramming cocktail (same method as on days 2-4).

After completion of RNA transfections, the cells were maintained using conditioned Pluriton media for 1-3 extra days until the iPS colonies were large enough to be picked. The media was changed daily with NuFF-conditioned Pluriton media and Pluriton supplement, and cells maintained at 37°C and 5% CO_2.

On approximately day 15, the iPC colonies were picked, with each individual colony being transferred to a separate well (maintaining clonal lines). 12-well tissue culture plates were pre-coated with Matrigel® before starting. The iPS colonies were identified by morphology under the microscope and the position in the well marked. NuFF-conditioned Pluriton media with Pluriton supplement was added to the prepared 12-well plate, and cell media was replaced with fresh media. On the pre-marked colony, a sterile 10 µl pipette tip was used to gently separate the colony from the fibroblasts surrounding it, then the colony was broken into smaller pieces (most often into quarters, but depended on colony size). The colony pieces were removed with a sterile pipette tip and transferred to a single well of the prepared 12-well plate. The colonies were maintained at 37°C and 5% CO_2.

The colonies were maintained according to standard iPS cell culture protocol (described below) and immunocytochemistry and Sanger sequencing used to confirm the pluripotency and presence/absence of mtDNA mutations.

Karotyping iPSC

IPSC karotyping was carried out by TDL Genetics (London, W1T 4EU). The iPSCs were cultured on Geltrex® (ThermoFisher) coated T25 flasks and then prepared by TDL Genetics for analysis, beginning with a pretreatment of colcemid overnight before harvest and analysis. A 20 cell analysis was performed on all lines and all were found to have a normal karyotype and banding pattern.

Culturing IPSC

IPSC were maintained using Essential 8™ Medium (Gibco Life Technologies) on Geltrex® (ThermoFisher) coated 6-well tissue culture plates at 37°C and 5% CO_2. Media was changed everyday, except the day after a split.

The Essential 8™ Media (E8) was prepared by thawing the E8 supplement overnight at 4°C and adding to 500 mL E8 media which had been warmed to RT (not using a waterbath). To prevent degradation by repeated warming, the supplemented media was aliquoted into 50 ml falcons and stored at 4°C. For experiments involving mtDNA mutant cells, media was supplemented with 200 µM uridine (Sigma). Before use, an E8 aliquot was warmed (not artificially) to RT.

Stocks of Geltrex® were prepared by aliquoting 240 µl into sterile 15 mL falcons and storing at -20°C. When ready to use, 12 ml of DMEM media (Gibco) was added to a single 15 ml falcon aliquot, mixed well and 1 ml added to each well of two 6-well tissue culture plates. Plates were incubated for at least 1 hour at 37°C, and all excess Geltrex® removed before adding media or cells to the well.

IPSC grown to full confluency are likely to spontaneously differentiate, normally to fibroblasts, therefore it is important to

maintain cultures at no more than 70% confluency. At this point, cells were split using EDTA, most commonly at a ratio of 1:6.

To split cells, 6-well tissue culture plates were pre-coated with Geltrex® and media warmed to RT. The cell media was aspirated and cells washed briefly with 1 ml EDTA (Invitrogen). This EDTA was discarded, and 1 ml of fresh EDTA was added to the well for cell detachment. The plate was incubated with EDTA for 5 minutes at 37°C. Whilst incubating, the Geltrex® was aspirated from the new tissue culture plate and fresh E8 media added. Under the microscope, the appearance of small holes in the colonies was checked to indicate that the EDTA was ready to be removed. The EDTA was discarded and 1 ml of fresh media was added to the colonies, relatively harshly, to cause complete detachment from the plate surface, but not to break colonies up too much. Colonies will not attach well if in single cell suspension so it is important to break large colonies into smaller clumps, but not into single cells. The cells were then collected and distributed in a dropwise fashion to the new tissue culture plate. The plate was gently moved side to side and back and forth, to ensure even distribution of the colonies. The media was not changed the day after splitting.

Cortical neuron differentiation

Differentiation of iPSCs into cortical neurons was conducted using the protocol written by Shi *et al.,* IPSCs were cultured as described above for 2 weeks to establish a healthy culture before starting induction.(Shi et al. 2012). All media used in the protocol was supplemented with 200 µM uridine for maintenance of mtDNA mutations.

Differentiation took place in a 6-well tissue culture plate coated with Matrigel® on 100% confluent iPSCs. Therefore cells were first passaged 2:1 using EDTA, as described above, and plated into the Matrigel® coated wells in E8 media supplemented with 10 μM ROCK inhibitor (Sigma) to aid cell survival.

The following day (day 1), if the cells were 100% confluent, media was aspirated and cells washed briefly with PBS, then 2 ml of neural induction medium was added per well. Induction media was made by supplementing neural maintenance media with SB431542 (Tocris), a small-molecule inhibitor of TGF-β signalling, and Dorsomorphin (Tocris), a small-molecule SMAD inhibitor. By inhibiting TGF-β signalling, the activation of SMAD proteins mediated by TGF-β is inhibited, providing a 'dual SMAD inhibition' with these two compounds, which enables differentiation towards the anterior neuroectodermal lineage.

Neural maintenance media (referred to as N2B27 media) was prepared by adding supplemented Neurobasal media (Life Technologies) and supplemented DMEM F12 Glutamax media (Life Technologies) at a 1:1 ratio, which was stored at 4°C and used within 3 weeks. The components of N2B27 media were prepared as follows:

Reagent	**Supplier**	**Volume**
DMEM F12 +Glutamax	Gibco Life Technologies	500 ml
Insulin (10 mg/ml)	Sigma	0.25 ml
2-mercaptoethanol (50 mM)	Life Technologies	1 ml
Non essential amino acids (100x)	Life Technologies	5 ml
N2 supplement	Life Technologies	5 ml

Pen/Strep	Life Technologies	5 ml
Neurobasal	Gibco Life Technologies	500 ml
B27 supplement	Life Technologies	10 ml
L-Glutamine (200 mM)	Life Technologies	5 ml
Pen/Strep	Life Technologies	5 ml

Table 7 Neural maintenance media components

Neural induction media was prepared as follows:

Reagent	**Supplier**	**Volume**
N2B27 media	Prepared as above	10 ml
SB431542 (resuspended in DMSO to 10 mM stocks, stored at -20°C)	Tocris	10 µM
Dorsomorphin (resuspended in DMSO to 10 mM stocks, then diluted to 1 mM stock in H_2O, stored at -20°C)	Tocris	10 µM

Table 8 Neural induction media components

Neural induction media was changed daily for 10 days, by which point a neuroepithelial sheet should have appeared. The neuroepithelial cells were collected using dispase as follows: 200 µl dispase (Life Technologies) was added directly to the well (media was not removed) and incubated at 37°C for 10-15 minutes. Using a Gilson P1000 pipette, the cells were collected and added to 7 ml PBS in a sterile 15 ml falcon. The cells were left to settle to the bottom of the falcon, then the PBS was removed and replaced with fresh PBS, and this was repeated 3 times. Finally the cells were

resuspended in N2B27 media and plated at a 1:2 ratio onto laminin (Sigma) coated wells (plates were previously prepared by incubating with laminin overnight at 37°C). The cells were incubated overnight at 37°C and the following day the media changed to N2B27 supplemented with 20 ng/ml fibroblast growth factor 2 (FGF2, PeproTech), which promotes the expansion of neural stem cells. The media was then changed every other day.

After four days of N2B27 + FGF2, media was changed to just N2B27, again refreshing every other day for neural expansion and differentiation. Cells were split at a 1:2 ratio with dispase (as described above) when neural rosette structures began to expand and meet at the edges. Between days 20-30, cells were dissociated using accutase (Innovative Cell Technologies) at a ratio of 1:1. The cell media was aspirated and cells washed briefly with PBS, then 0.5 ml accutase was added per well and incubated for 5 minutes at 37°C. The cells were triturated with a Gilson P1000 pipette and returned to the incubator for a further 3 minutes. The cells were then collected in N2B27 media, centrifuged at 400 *g* for 5 minutes, resuspended in N2B27 media and plated in a pre-prepared laminin coated plate. The media was changed the day after plating and from then every other day. Accutase splitting was repeated at a 1:2 ratio when the cells reached 90% confluency. On days 27-31, the cells were split to a 1:4 ratio with accutase, and then passaged for the final time around day 35, as the cell the survival rate after this point has been found to be relatively low. The plates and coverslips for final experiments were prepared by coating first with poly-L-ornithine (Sigma) for at least 4 hours at 37°C, then with laminin as described previously. Cells were cultured for another 50-60 days after the last passage; using N2B27 media changed every other day.

Myogenic differentiation

Myogenic differentiation of iPSCs should take place on healthy, regularly passaged iPSCs and utilise fresh, non-freeze-thawed reagents. DMEM media was supplemented with 200 µM uridine throughout the myogenic differentiation protocol.

IPSCs were seeded onto Matrigel® coated plates (prepared at least 1 hour before seeding), by washing cells with PBS and adding 0.05% Trypsin/EDTA to detach the cells. To aid detachment, cells were incubated with Trypsin/EDTA at 37°C for 2-6 minutes, until the cells had separated into clumps of 3-4 cells (not single cells). The cell clumps were removed from the plate with DMEM 10% FBS and collected in a 15 ml sterile falcon. The falcon was centrifuged at 800 rpm for 4 minutes and the pellet resuspended in approximately 2 ml of media for cell counting, using a counting chamber. For each IPS line, 3 wells (of a Matrigel® coated 6-well tissue culture plate) of 1 x 10^5 cells were plated and another 3 wells at double density. The media used for cell plating was:

Reagent	Supplier	Conc	Volume	
DMEM F12	Gibco Life Technologies	1X	50 ml	F12 stands for Ham's Nutrient Mixture F12, which was developed for serum-free cell culture
CHIR	Tocris	3 µM	7.5 µl	Inhibitor of glycogen synthase kinase 3 (GSK-3). GSK3 is a negative modulator of myogenic differentiation

LDN	StemMACS Miltenyi Biotec	0.5 µM	5 µl	Inhibitor of bone morphogenetic protein (BMP) signalling. BMPs have a profound repressive effect on myogenic differentiation
Insulin-Transferrin-Selenium supplement (ITS)	Gibco Life Technologies	1X	500 µl (stock is 100X)	Aids cell culture in serum-free media
Rho-associated protein kinase (ROCK) inhibitor	Sigma	10 µM	50 µl	Boosts cell survival

Table 9 Myogenic differentiation media

The plated cells were incubated at 37°C and 5% CO_2 overnight. The following day (day 2), if cells had attached, the media was replaced with no ROCK inhibitor and half the concentration of CHIR (1.5 µM). On day 3, if enough cells were still attached, the media was aspirated off the cells and replaced with differentiation media:

DMEM F12	1X
CHIR	1.5 µM
LDN	0.5 µM
ITS	1X

Table 10 Day 3 Myogenic differentiation media

On day 4-6, cells underwent a full media change daily, with fibroblast growth factor-2 (FGF-2, R&D Systems), a key regulator of embryonic myogenesis (Świerczek et al. 2015):

DMEM F12	1X
CHIR	3 µM
LDN	0.5 µM
ITS	1X
FGF-2	10 ng/ml

Table 11 Day 4-6 Myogenic differentiation media

On day 7 and 8, cell media was changed to media containing human hepatocyte growth factor (HGF, R&D Systems) and human insulin-like growth factor I (IGF, R&D Systems), which plays an important role in muscle regeneration (Philippou et al. 2007). HGF has been shown to increase proliferation of quiescent satellite cells but also suppress the expression of late myogenic differentiation factors, thereby essentially delaying the process to enable proliferation of more cells for differentiation with the aim of generating a greater number of fibres at the end (Gal-Levi et al. 1998).

DMEM F12	1X
HGF	10 ng/ml
IGF	2 ng/ml
LDN	0.5 µM
FGF-2	20 ng/ml

Table 12 Day 7 Myogenic differentiation media

On day 9-12, cell media was changed daily to just DMEM-12, IGF-I (2 ng/ml) and 15% KnockOut™ Serum Replacement (KSR, Gibco Life Technologies). KSR is an FBS-free medium supplement used to support the growth of stem cells during *in vitro* differentiation; during this stage a lot of proliferation was expected so the KSR percentage could be reduced to 7.5% if necessary. From day 13, the media was changed every other day, this time containing the addition of 10 ng/ml HGF.

On day 35, the cells were plated for terminal differentiation. New 6-well tissue culture plates were prepared with Matrigel® coating prior to splitting. The media was aspirated from the well, cells washed briefly with PBS, and 1ml of collagenase (Life Technologies) and 100 µl of dispase (Life Technologies) added per well, then incubated at 37°C for approximately 30 minutes until cells had lifted in one clump. The cells were transferred to a 15 ml sterile falcon with DMEM F12 media and left to settle to the bottom (approximately 5 minutes), then the supernatant media was removed as close to the cells as possible with disturbing, discarded, and 5 ml of fresh DMEM F12 added. This was repeated twice more to thoroughly wash the cells, then finally 2 ml of plating media was added to the cell suspension:

DMEM F12	1X
KSR	15%
HGF	10 ng/ml
IGF	2 ng/ml
ROCK inhibitor	10 µM

Table 13 Terminal Myogenic differentiation media

The cells in plating media were triturated gently using a 5 ml stripette and then again with a p1000 pipette before seeding at a 1:6 ratio onto the pre-prepared culture plates. The cells were incubated at 37°C and 5% CO_2 overnight and the following day, the media was changed to remove the ROCK inhibitor.

For each line, cells in half the wells were matured using ITS media and the other half using KSR, since some lines mature better with one than the other but this is difficult to predict so both were used in parallel:

ITS maturation		KSR maturation	
DMEM F12	1X	DMEM F12	1X
ITS	1X	KSR	3%
HGF	10 ng/ml	HGF	10 ng/ml
IGF	2 ng/ml	IGF	2 ng/ml

Table 14 Myogenic maturation media

The media was then changed 3-4 times per week until day 45 when experiments were then performed.

Assessing mitophagy in differentiated cell types

To induce mitophagy, cells were depolarised with 10 µM carbonyl cyanide 4-(trifluoromthoxy)phenylhydrazone (CCCP, Sigma). In SH-SY5Y cell lines and fibroblasts, cells were exposed to CCCP for 12-24 hours, however in cortical neurons and myotubes the treatment was longer so CCCP was ‘refreshed’. This worked as follows: the cell media was changed 2 hours before inducing depolarisation, when 10 µM CCCP was added to the cell media. For myotubes, after 12 hours the media was discarded and fresh media containing 10 µM CCCP was added. This was repeated every 12 hours until a

total treatment time of 48 hours was reached. For cortical neurons, which are more prone to detachment, the same protocol applies however only half the media was removed at a time so as not to disturb the cells.

Chapter 1

Mechanistic insights into the mitophagy pathway

1.1 Introduction

1.1.1 Methods to induce mitophagy

To study the process of mitophagy, compounds can be used to cause global disruption to the mitochondrial network, or alternatively a more targeted approach can be taken. There are advantages and disadvantages to both, but since mitophagy in mammalian cells is a relatively infrequent process, artificial induction is required to study the pathway.

The mitochondrial stressor carbonyl cyanide *m*-chlorophenyl hydrazine (CCCP) causes uncoupling of the proton gradient and subsequent mitochondrial membrane depolarisation. As well as causing an increase in proton conductance, CCCP has many nonspecific effects. These include targeting autophagosome and lysosome degradation, and the stimulation of apoptotic processes (Kasianowicz et al. 1984; Padman et al. 2013; Cai et al. 2012). In addition to CCCP, the potassium ionophore valinomycin and the combination of oligomycin, an ATP synthase inhibitor, and antimycin A, a Complex III inhibitor, can be used to stimulate the mitophagy process. The use of these compounds enables simple and fast initiation of mitophagy that can be measured in numerous ways.

The global loss of membrane potential across the entire mitochondrial network is convenient for biochemical experiments, which often require a large mitophagy induction to detect the proteins involved in the process. However, this large area of mitochondrial damage is not particularly representative of physiological mitophagy in which subsets of mitochondria are more likely to be affected (Ashrafi & Schwarz 2013).

A technique that applies a more focused area of damage is the use of photobleaching, which has been demonstrated in neurons. This involves the use of neurons containing mitochondrial KillerRed and eliciting spatiotemporally controlled ROS-mediated damage (Ghazaleh Ashrafi et al. 2014). Whilst this technique is physiologically more relevant and fewer off-target effects will be produced, the analysis involves lower *n* numbers and therefore many more experiments would be required to identify significant effects. Furthermore, experimental approaches to analyse the effect of damage to sub-sets of mitochondria, through the use of microfluidics for example, will be mainly limited to imaging techniques.

1.1.2 Methods to study mitophagy

1.1.2.1 Detecting the autophagosome

A common technique used to confirm the induction of mitophagy is the engulfment of damaged mitochondria by autophagic machinery. However this timepoint of mitochondrion-autophagosome interaction is relatively short so for accurate assessment of mitophagy, lysosomal degradation is often inhibited (Klionsky et al. 2012).

The colocalisation of mitochondria and autophagosomes can be assessed in fixed cells by immunocytochemistry or in live cells

loaded with fluorescent dyes. For immunocytochemistry, mitophagy is induced in cells adhered to glass coverslips then after a certain timepoint of stimulation with a mitochondrial stressor, cells are fixed, for example with paraformaldehyde. After permeabilisation and blocking (described in detail in the methods section), cells are incubated with primary antibodies for a mitochondrial protein and an autophagic protein. Images of the prepared cells can be used to calculate colocalisation, whereby areas of overlap between the mitochondria channel and the autophagic channel are deduced. This requires comparable grey-level dynamics in each channel during image capture, and is highly sensitive to poor set-up of the image acquisition software. The benefit of immunocytochemistry is that if slides are properly stored, imaging can be repeated should it be required. Live cells loaded with dye however can only be imaged in one session and it is vitally important to be careful when preparing the settings. Cells used in these experiments are commonly transfected with GFP-LC3 and loaded with a membrane potential-independent mitochondrial dye, such as some MitoTracker dyes. However, the reported aggregation of LC3, which occurs separately from induced mitophagy, can result in false positives (Kuma et al. 2007).

1.1.2.2 Lysosomal delivery

Since the autophagosome-mitochondria interaction during mitophagy is transient and measurement of GFP-LC3 can be misleading, visualising the delivery of mitochondria to the lysosome provides an alternative method of mitophagy assessment.

The colocalisation of mitochondria and lysosomes can be performed using similar methods to that of the mitochondria and autophagic proteins. Lysosomal-associated membrane protein 1 (LAMP1) can be used in immunocytochemistry as a late endosome/lysosome

marker and colocalisation quantified between LAMP1 and a mitochondrial protein marker. For analysis of mitochondrial delivery to lysosomes in live cells, cells can be loaded with LysoTracker, which accumulates in the acidic environment of lysosomes. However this dye has been known to cause an increase in intracellular pH if cells are imaged over large timeframes, which can consequently quench the LysoTracker signal (Chen et al. 2015).

The acidic environment of lysosomes has been utilised in an alternative method of mitophagy assessment. The expression of a mitochondrial-targeted tandem mCherry-GFP tag enables a change in colour of fluorescence upon delivery of mitochondria to lysosomes (Allen et al. 2013). As described in the introduction, this has been used to detect mitophagy in systems not involving the overexpression of Parkin. Under basal conditions both tags will fluoresce, however in a low pH environment, protonation of the GFP fluorophore will occur and the signal will be quenched. This does not happen to the mCherry tag, since it has a lower pKa, which is the pH at which fluorescence is at 50% of its maximal signal. To determine mitophagy in this assay, the number of red mCherry puncta were counted, compared to yellow, which would be caused by the combined mCherry and GFP fluorescence.

Another lysosomal assay, which relies on its acidic environment, involves the use of a mitochondrial matrix-targeted mt-Keima. Mt-keima is a molecule that has a bimodal excitation spectrum, which represents neutral and acidic environments with a shift in excitation spectrum peak. This assay has been used in MEFs derived from a mt-Keima reporter mouse, using fluorescence-activated cell sorting (FAC) to distinguish the distribution of cells positive or negative for mitophagy (Sun, Yun, Liu, Malide, Liu, I. Rovira, et al. 2015).

1.1.2.3 Elimination of mitochondrial proteins

The measurement of mitochondrial proteins after mitophagy is stimulated enables quantification of the successful completion of the process. This is a convenient method which denotes the actual degradation of mitochondria. Most often this is achieved by immunoblotting and immunocytochemistry to quantify the amount of mitochondrial protein in control-treated cells compared to uncoupler-treated cells. In these experiments, the amount of protein is typically normalised to the expression of a housekeeping gene in Western blotting or by cell counting in imaging experiments.

A significant disadvantage of this method however is that the net change of mitochondrial mass is quantified, and not the amount of mitochondria degraded by mitophagy alone. This method therefore may falsely overestimate the amount of mitophagy by including, for example, proteasomal degradation, or falsely underestimate the amount of mitophagy by any stimulation of mitochondrial biogenesis, which may in fact be significantly upregulated in cases of widespread mitochondrial uncoupling.

1.1.3 Aims and hypothesis

In this chapter the aims were to investigate the triggers and methods of measuring mitophagy in different cell types. In particular, these experiments made use of the compound Rhodamine 6G in an attempt to study the mitophagy pathway without the use of the CCCP, which may be limiting our understanding of the ways mitophagy can be stimulated by simply causing loss of membrane potential.

Rhodamine 6G is a cationic dye, and therefore contains positively charged dye molecules which bind to the negatively charged region

of the mitochondrial membrane (Yaginuma et al. 1973). It was first proposed that Rhodamine 6G inhibited energy transduction in oxidative phosphorylation (OxPhos) by blocking adenine nucleotide translocase (ANT) (Gear & Gear 1974). The function of ANT is to export the ATP generated from the OxPhos mechanism to the cytosol. However, this proposed mechanism of inhibition by Rhodamine 6G was found to be incorrect and it is now believed that Rhodamine 6G targets two sites in the OxPhos mechanism (Higuti et al. 1980). The F_1F_0-ATPase comprises the F_1 head group, which combines P_i and ADP to form ATP, and the inner mitochondrial membrane embedded F_0 base which functions as a proton channel. The oligomycin-sensitivity conferring protein (OSCP) is required for the correct binding of F_1 to F_0. The ATPase activity of the purified F_1 region is not inhibited by oligomycin, nor by Rhodamine 6G, however Rhodamine 6G does inhibit ATP hydrolysis by purified oligomycin-sensitive ATPase, which suggests an inhibition site on F_0 (Higuti et al. 1980). In addition, unlike oligomycin and other uncoupling agents, Rhodamine 6G inhibition also occurs at sites related to H^+-ejection by redox components (Higuti et al. 1980).

As a consequence of inhibiting mitochondrial oxidative phosphorylation, Rhodamine 6G causes a profound reduction in the number of intact mitochondria in the cell. Rhodamine 6G has been used in the study of mitochondrial DNA diseases, through the generation of cytoplasmic hybrid cells, cybrids. A cybrid is produced by the fusion cell with a cytoplast, an enucleated cell generated by centrifugation and disruption of the cytoskeleton. Treatment of primary patient fibroblasts with Rhodamine 6G to eliminate mitochondria enables endogenous mtDNA to be replaced with an alternative mitochondrial genome through cytoplast fusion (Trounce & Pinkert 2007; Williams et al. 1999), (Ziegler & Davidson 1981). However, short term culture of human skin fibroblasts with Rhodamine 6G showed that whilst mtDNA remained present, mtDNA-encoded polypeptides were not synthesised or were

unstable, suggesting that mtDNA damage precedes mitochondrial elimination (Williams et al. 1999). The hypothesis for chapter one therefore was that Rhodamine 6G would trigger mitophagy using an alternative mechanism to CCCP, which would provide insight to the requirements of mitophagy. Understanding what is required to trigger mitophagy will contribute the main objective of this thesis, which is to identify whether the initiation of mitophagy is impaired in mtDNA disease.

1.2 Results

1.2.1 Rhodamine 6G causes PINK1 stabilisation, Parkin translocation, and triggers mitophagy

Using FLAG-Parkin overexpressing SH-SY5Y cells, Rhodamine 6G was found to cause significant PINK1 stabilisation in cell lysates at a dose of 2 μM for 1.5 hours (Figure 12 A,B). This was confirmed to occur at the mitochondria by the significant increase in PINK1 detected at the same dose in enriched mitochondrial fractions by immunoblot analysis (Figure 12 C, D). Translocation of FLAG-Parkin was identified by immunoblot analysis of enriched mitochondrial fractions and immunocytochemistry (Figure 13 A, B, E, G). Immunoblot analysis revealed striking degradation of mitofusin 1 occurring in Rhodamine 6G treated cells, to a similar extent as that seen in positive-control CCCP treated cells (Figure 13 C, D). Colocalisation was found to occur between FLAG-Parkin and mitochondrial respiratory chain protein Complex V after 3 hours of Rhodamine 6G treatment when assessed by immunocytochemistry (Figure 13 E, G). After 6 hours of Rhodamine 6G exposure, significant p62 colocalisation with mitochondria was observed and subsequent reduction in mitochondrial proteins was quantified (Figure 13 F, H; Figure 14 A, B). Analysis of outer and inner mitochondrial membrane proteins confirmed a significant loss of mitochondria by both immunocytochemistry and immunoblotting (Figure 14). Between 6 and 16 hours, there was an increased loss of mitochondria in CCCP treated cells, however in Rhodamine 6G treated cells the mitochondria were depleted to a greater extent at 6 hours compared to 16 hours. This finding suggests a different mechanism of action, by which Rhodamine 6G potentially possesses a shorter active timeframe or that the damage it exerts is more readily reversible compared to CCCP.

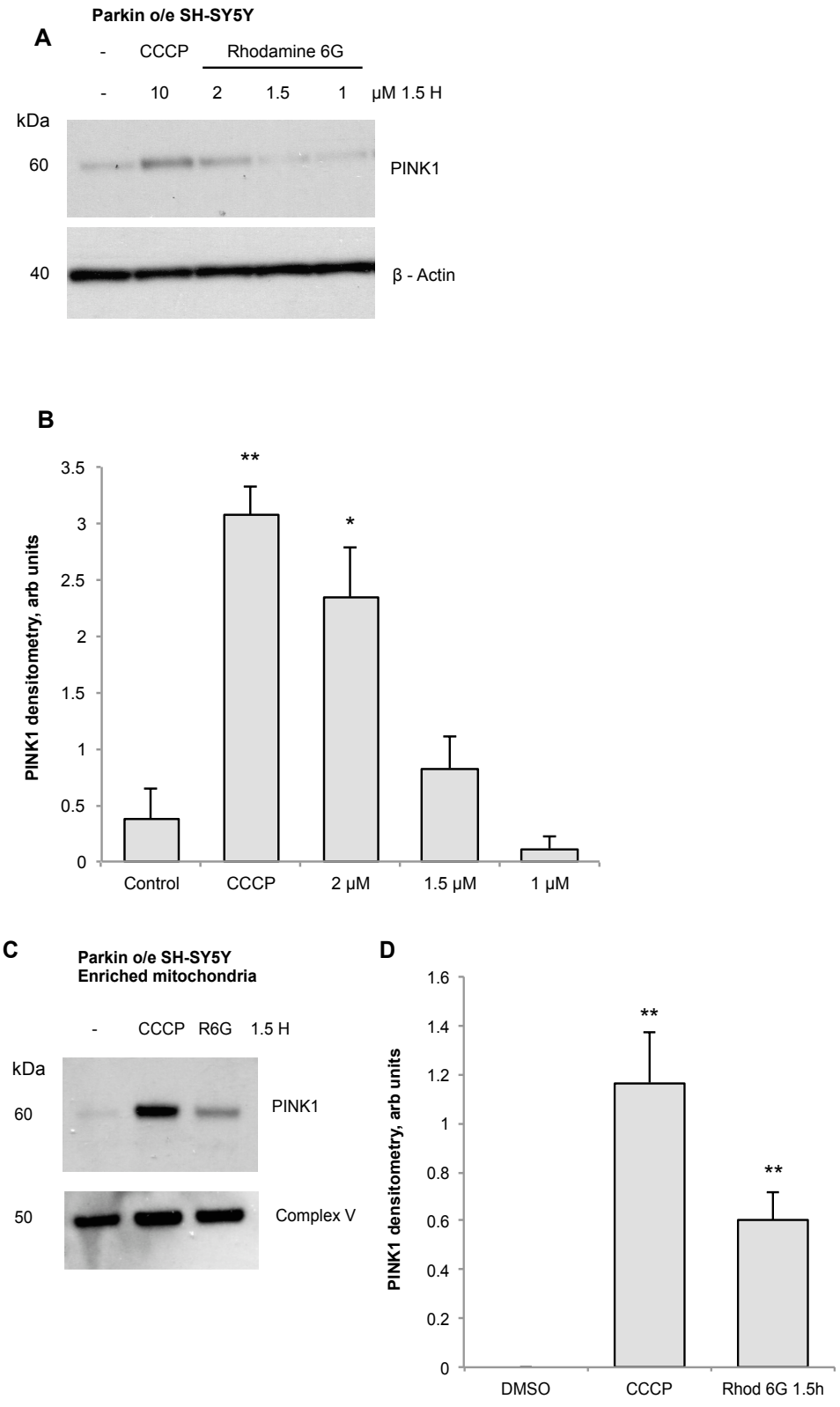

Figure 12: Rhodamine 6G induces PINK1 accumulation

A Representative immunoblot showing PINK1 protein levels in FLAG-Parkin-overexpressing SH-SY5Y cells. Cells were exposed to 2 µM, 1.5 µM or 1 µM Rhodamine 6G, or positive control 10 µM CCCP or negative control DMSO. B Histograms represent mean PINK1 protein levels, normalized to

loading control. Error bars represent SEM, two-tailed Student's *t*-test * $p < 0.05$, ** $p < 0.01$, $n = 3$. C Representative immunoblot showing the levels of PINK1 protein in enriched mitochondria from FLAG-Parkin-overexpressing SH-SY5Y cells. D Histogram to show quantification of PINK1 accumulation in enriched mitochondria. Error bars represent SEM, two-tailed Student *t*-test ** $p < 0.01$, $n = 3$.

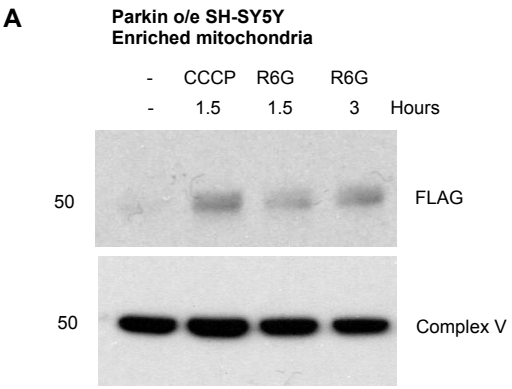

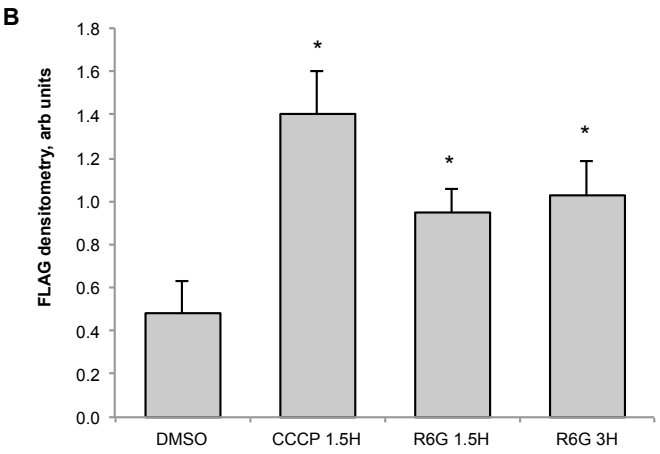

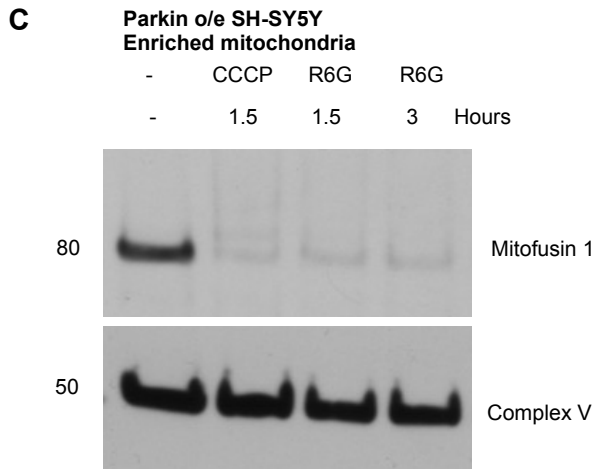

D

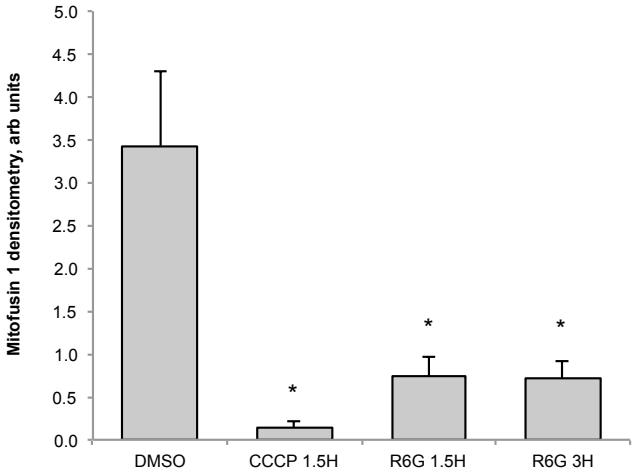
Mitofusin 1 densitometry, arb units
5.0
4.5
4.0
3.5
3.0
2.5
2.0
1.5
1.0
0.5
0.0
*
*
*
DMSO
CCCP 1.5H
R6G 1.5H
R6G 3H

E

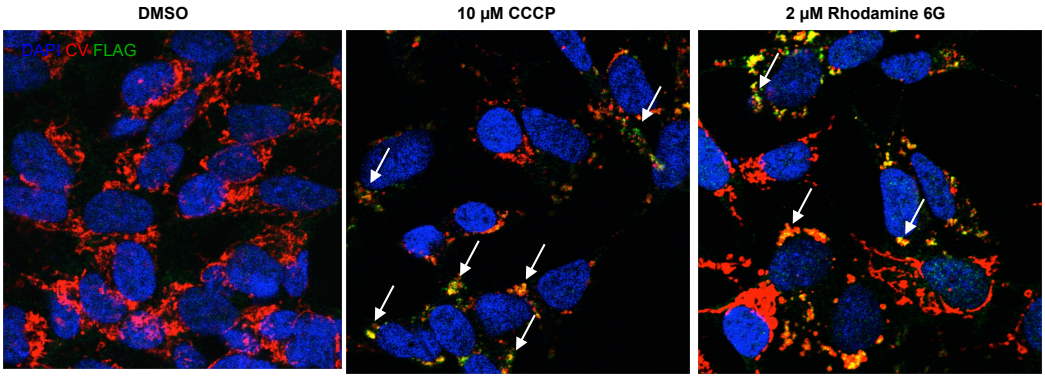
DMSO
10 µM CCCP
2 µM Rhodamine 6G
DAPI CV-FLAG

F

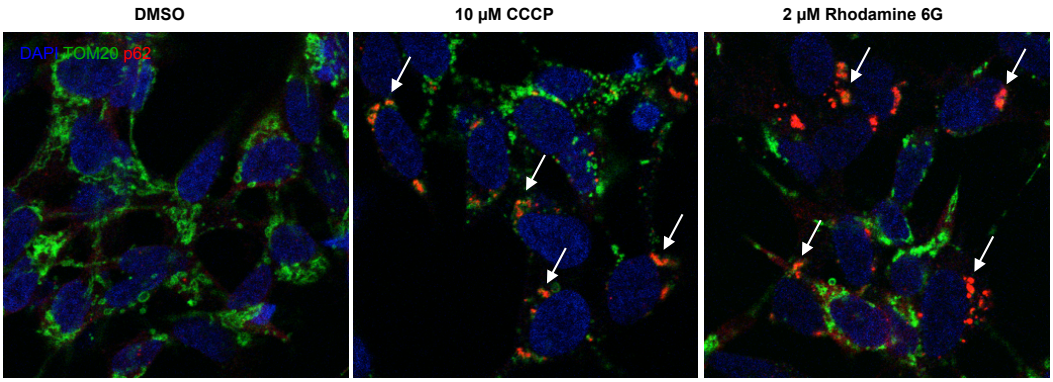
DMSO
10 µM CCCP
2 µM Rhodamine 6G
DAPI TOM20 p62

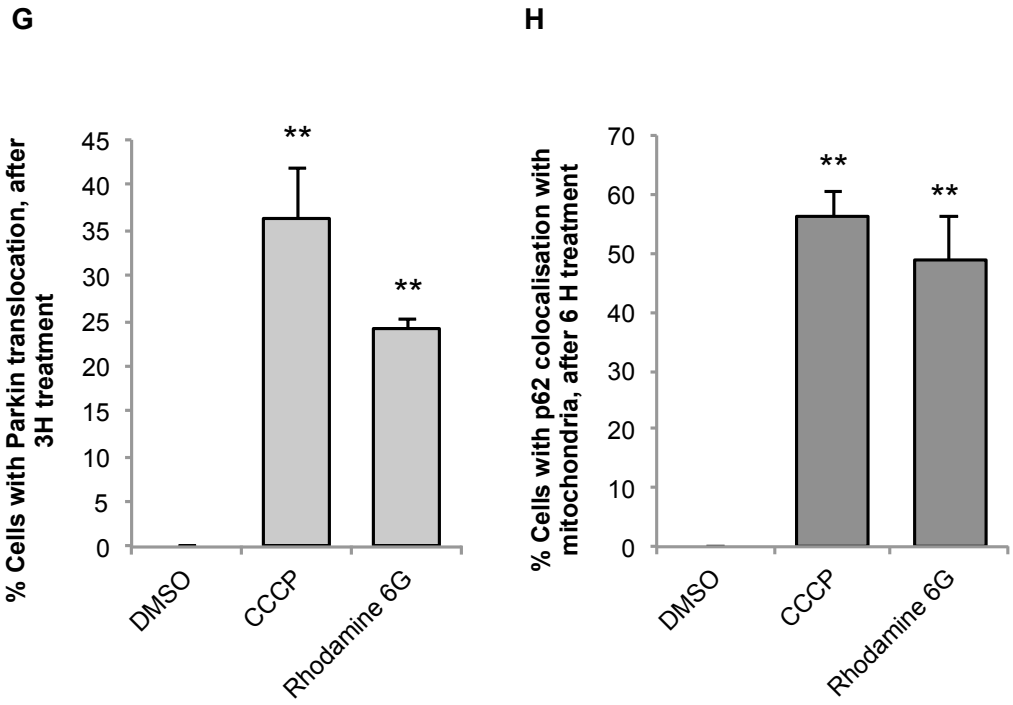

Figure 13: Rhodamine 6G stimulates Parkin translocation, p62 recruitment and the degradation of mitofusin 1

A Representative immunoblot of Parkin protein levels obtained from enriched mitochondria from FLAG-Parkin overexpressing SH-SY5Y cells treated with DMSO, 10 µM CCCP or 2 µM R6G. B Quantification of Parkin protein levels obtained by Western blotting, histograms represent mean protein levels normalized to loading control and error bars represent SEM; two-tailed Student's *t*-test * $p < 0.05$, $n = 3$. C Representative immunoblot showing mitofusin 1 levels in enriched mitochondria from FLAG-Parkin overexpressing SH-SY5Y cells treated with DMSO, 10 µM CCCP or 2 µM R6G. D Histogram indicates the mean protein levels of mitofusin 1, normalized to loading control. Error bars represent SEM, two-tailed Student's *t*-test * $p < 0.05$, $n = 3$. E Representative images of FLAG-Parkin translocation to mitochondria in FLAG-Parkin overexpressing SH-SY5Y cells, indicated by white arrows. Green: FLAG, red: Complex V, blue: DAPI. F Representative images of p62 translocation to mitochondria in FLAG-Parkin overexpressing SH-SY5Y cells, indicated by white arrows. Green: Tom20, red: p62, blue: DAPI. G Histogram represents the percentage of cells in which Parkin colocalises with mitochondria as determined by immunocytochemistry. Error bars represent SEM; two-tailed Student's *t*-test ** $p < 0.01$, $n = 3$ H Histogram represents the percentage of cells in which

p62 colocalises with mitochondria as determined by immunocytochemistry. Error bars represent SEM; two-tailed Student's *t*-test ** $p < 0.01$, $n = 3$.

A

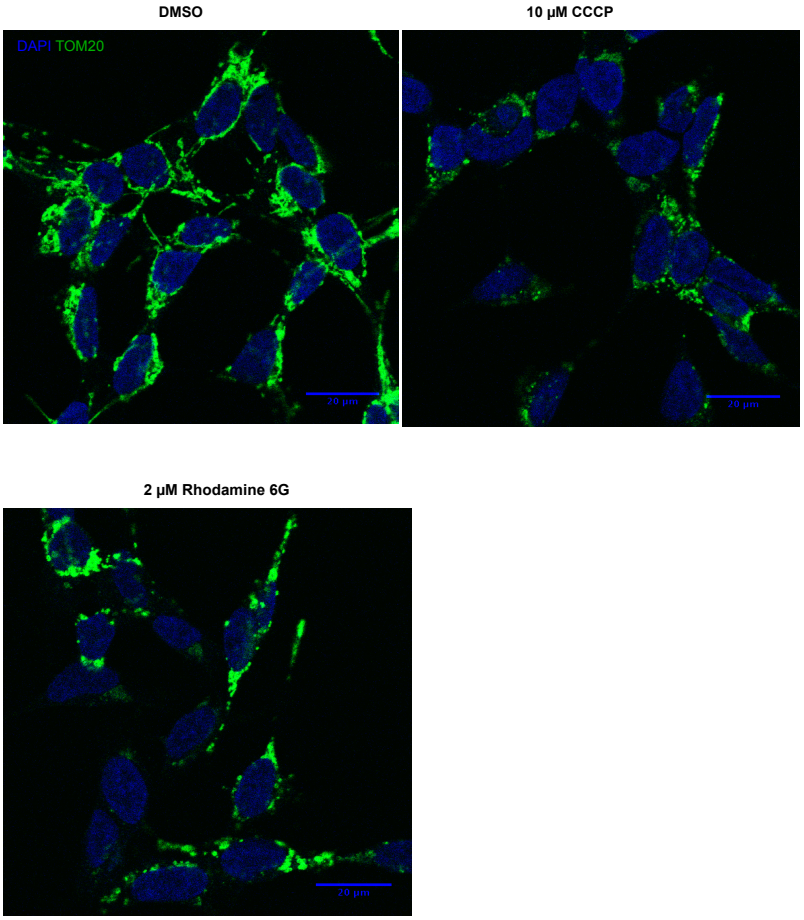

B

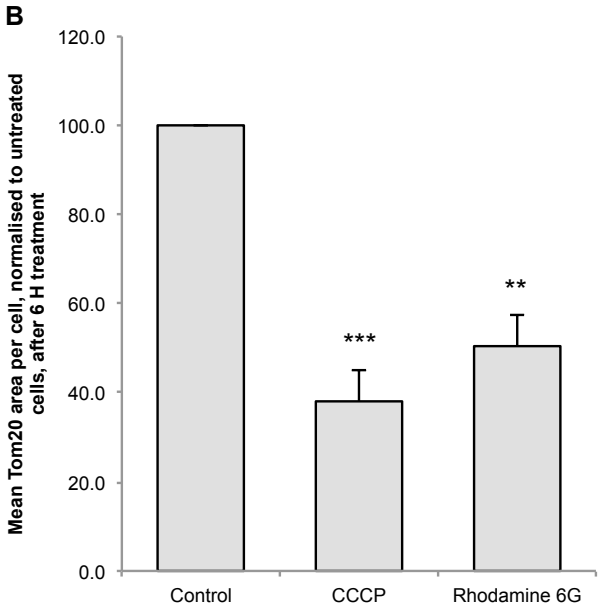

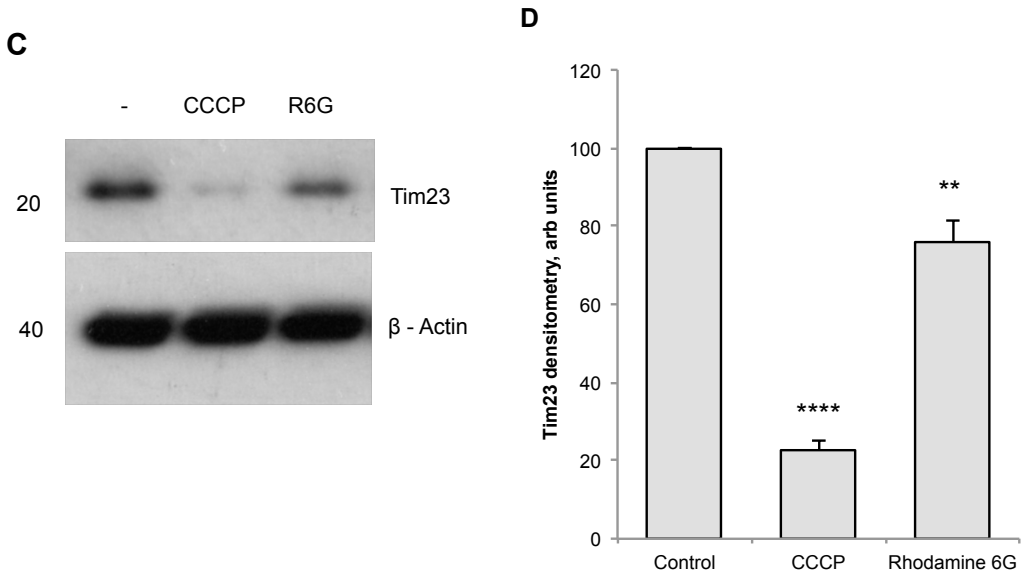

Figure 14: Rhodamine 6G induces mitophagy

A Representative images of Tom20 protein expression in FLAG-Parkin overexpressing SH-SY5Y cells, showing a reduction in protein levels after stimulation with CCCP or Rhodamine 6G for 6 H. Green: Tom20, blue: DAPI; scale bar represents 20 µm. B Quantification of the mean Tom20 area per cell as assessed by immunofluorescence. Error bars represent SEM; two-tailed Student's *t*-test ** $p < 0.01$, *** $p < 0.001$, $n = 3$. C Representative immunoblot showing the levels of Tim23 protein in FLAG-Parkin overexpressing SH-SY5Y cells after 16 hours of treatment with 10 µM CCCP or 2 µM R6G. D Quantification of Tim23 protein levels, normalized to loading controls after 16 hours of treatment with 10 µM CCCP or 2 µM R6G. Error bars represent SEM; two-tailed Student's *t*-test ** $p < 0.01$, **** $p < 0.0001$, $n = 4$.

1.2.2 Ubiquitination of mitofusin 1 is PINK1/Parkin dependent

Using human fibroblasts derived from Parkinson's disease patients, it was possible to assess the dependency upon PINK1 and Parkin for mitofusin 1 ubiquitination. The mutations in these fibroblasts were PINK1 c.261_276del16; p.T90LfsX12 (homozygous) and Parkin R275W. PINK1 and Parkin mutation fibroblasts have been used previously to demonstrate the requirement of these proteins

for mitofusin 1 ubiquitination when treated with mitochondrial uncouplers (Rakovic et al. 2011). The data here confirm those findings and also show that mitofusin 1 ubiquitination induced by Rhodamine 6G is also dependent upon the presence of PINK1 and Parkin (Figure 15).

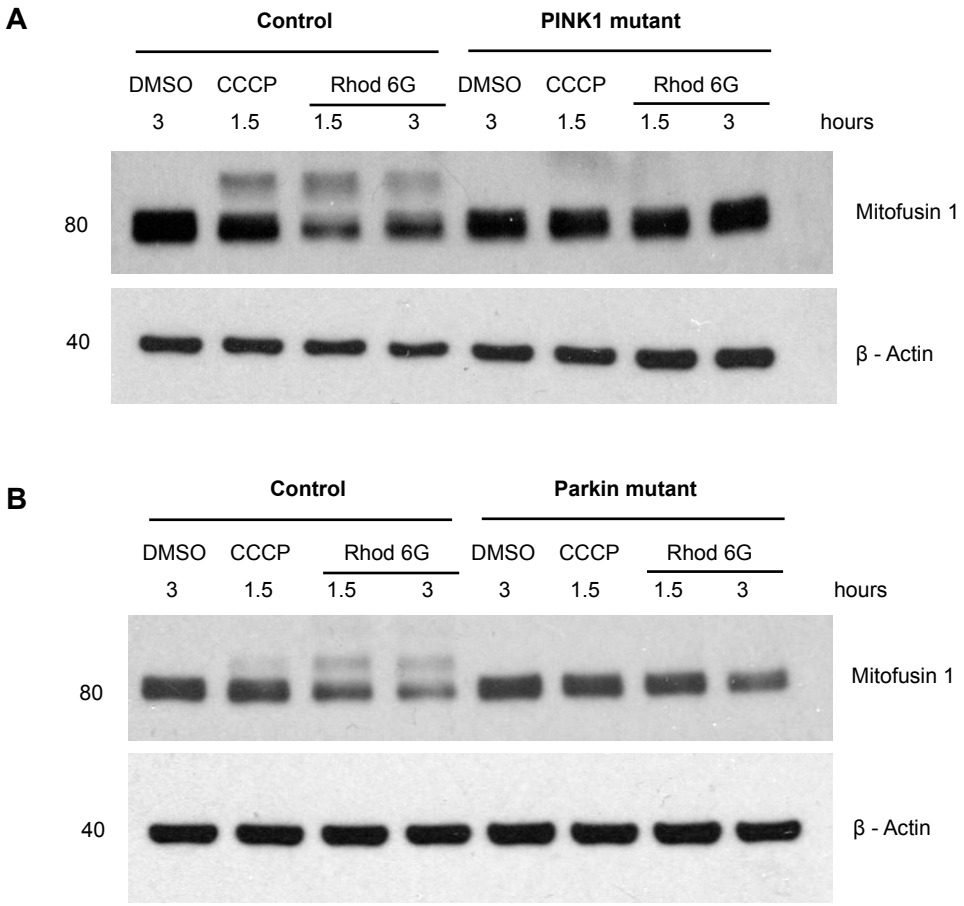

Figure 15: Mitofusin 1 ubiquitination stimulated by Rhodamine 6G is dependent upon PINK1 and Parkin

A Representative immunoblot showing mitofusin 1 protein and ubiquitinated mitofusin 1 protein in control and PINK1 homozygous mutant human fibroblasts (c.261_276del16) treated with DMSO, 10 µM CCCP or 2 µM R6G, for 1.5 or 3 hours. B Representative immunoblot showing mitofusin 1 protein and ubiquitinated mitofusin 1 protein in control and Parkin homozygous mutant human fibroblasts (R275W) treated with DMSO, 10 µM CCCP or 2 µM R6G, for 1.5 or 3 hours.

1.2.3 Rhodamine 6G does not induce membrane depolarisation, but PINK1 stabilisation is caused by oxidative stress

Since Rhodamine 6G is a red dye, to assess membrane depolarisation Rhodamine 123 (a green dye) was used instead of the commonly used TMRM dye. After 1.5 hours incubation of Parkin-overexpressing SH-SY5Y cells with Rhodamine 6G, the mitochondrial membrane potential was found to be hyperpolarised and could be subsequently depolarised with CCCP (Figure 16 A, B). This finding suggests that PINK1 accumulation in Rhodamine 6G treated cells is independent on membrane depolarisation.

Oxidative stress in cells is a balance between the production of reactive oxygen species and the presence of antioxidants. Reduced glutathione (GSH) is an abundant antioxidant, and levels can be measured using the dye monochlorobrimane (MCB). Using live cell imaging, Rhodamine 6G treated cells had a significantly lower MCB fluorescence, indication high oxidative stress, which could be restored by treatment in combination with N-acetyl-L-cysteine (NAC) (Figure 16 C). NAC is a precursor of GSH and therefore increases cellular levels of the antioxidant. Using the dose of NAC that restored MCB fluorescence, Western blot analysis showed that PINK1 accumulation induced by Rhodamine 6G was inhibited in the presence of NAC, suggesting that oxidative stress is the mechanism by which Rhodamine 6G stabilises PINK1 (Figure 16 D, E).

A

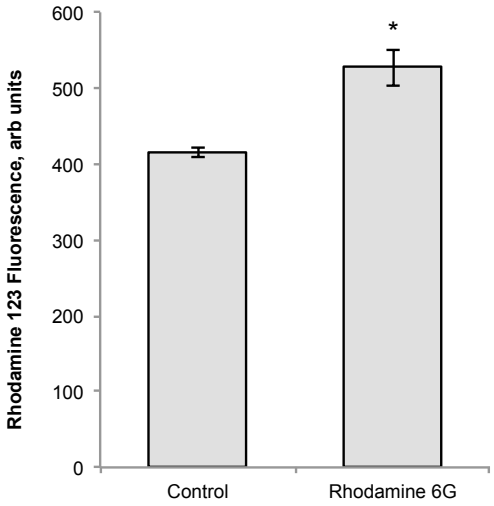
600
500
400
300
200
100
0
Rhodamine 123 Fluorescence, arb units
*
Control
Rhodamine 6G

B

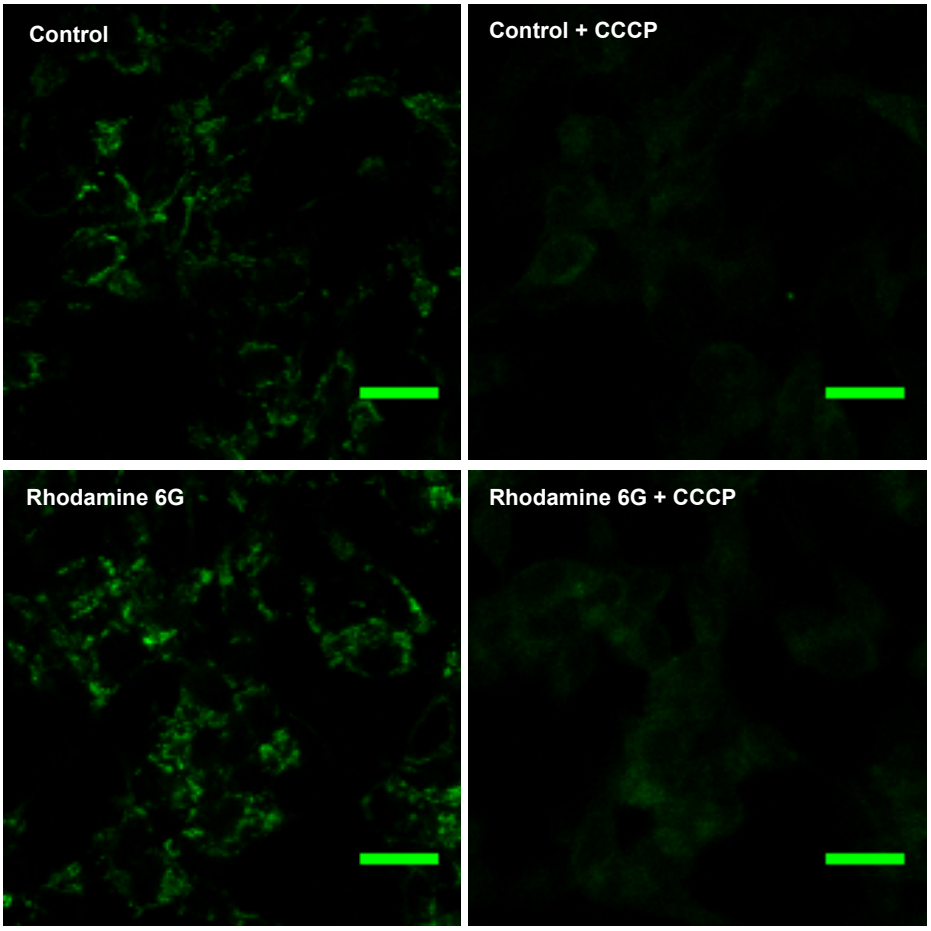
Control
Control + CCCP
Rhodamine 6G
Rhodamine 6G + CCCP

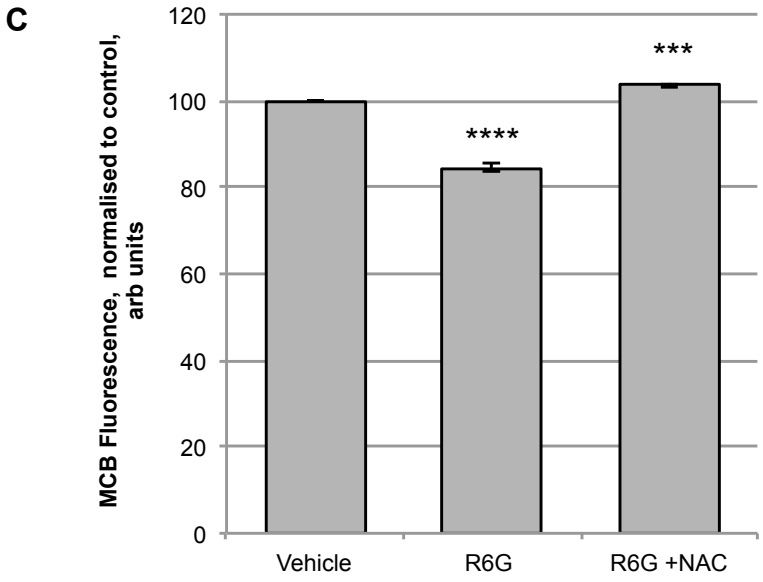
C
MCB Fluorescence, normalised to control, arb units
120
100
80
60
40
20
0
****
***
Vehicle
R6G
R6G +NAC

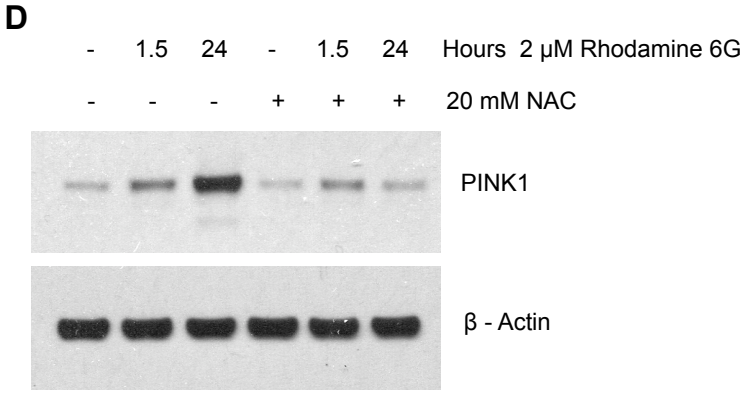
D
- 1.5 24 - 1.5 24 Hours 2 μM Rhodamine 6G
- - - + + + 20 mM NAC
PINK1
β - Actin

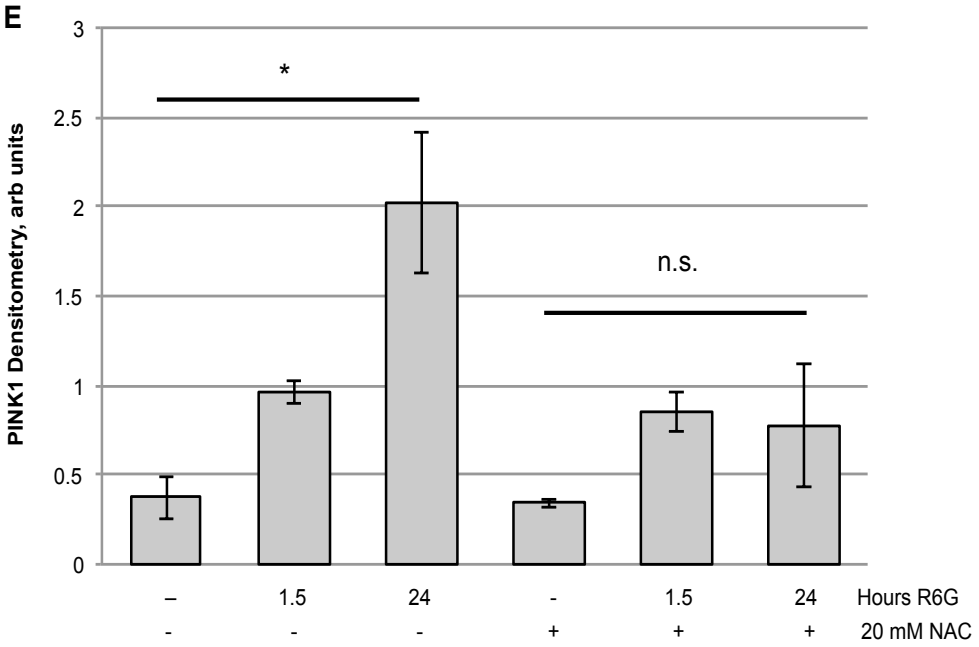
E
PINK1 Densitometry, arb units
3
2.5
2
1.5
1
0.5
0
*
n.s.
– 1.5 24 - 1.5 24 Hours R6G
- - - + + + 20 mM NAC

Figure 16: Rhodamine 6G does not depolarise the mitochondrial membrane but induces oxidative stress to cause PINK1 stabilisation

A Histogram represents mean basal mitochondrial membrane potential, measured in FLAG-Parkin overexpressing SH-SY5Y cells loaded with Rhodamine 123. Cells were pre-treated for 1.5 hours with vehicle or 2 µM Rhodamine 6G. Error bars represent SEM; two-tailed Student's *t*-test * $p < 0.05$, $n = 3$. B Representative images of FLAG-Parkin overexpressing SH-SY5Y cells loaded with Rhodamine 123 and treated as in A, then 10 µM CCCP was added to induce depolarization. Scale bars represent 20 µm. C Histogram to show the mean MCB fluorescence levels in live FLAG-Parkin overexpressing SH-SY5Y cells. Cells were pre-treated for 1.5 hours with vehicle or 2 µM Rhodamine 6G or 2 µM Rhodamine 6G with 20 mM NAC. Error bars represent SEM; two-tailed Student's *t*-test *** $p < 0.001$, **** $p < 0.0001$, $n = 3$. D Representative immunoblot of PINK1 protein levels in FLAG-Parkin overexpressing SH-SY5Y cells treated with just Rhodamine 6G for 1.5 or 24 hours, or in combination with 20 mM NAC. E Histogram to show quantification of PINK1 protein levels, normalized to loading control, in FLAG-Parkin overexpressing SH-SY5Y cells treated with just Rhodamine 6G for 1.5 or 24 hours, or in combination with 20 mM NAC. Error bars represent SEM; two-tailed Student's *t*-test * $p < 0.05$, $n = 3$.

1.2.4 Deep-sequencing reveals mitochondrial DNA mutations are caused by Rhodamine 6G

In order to identify whether Rhodamine 6G affected the mitochondrial genome, NGS was used to detect mutations caused by exposure to the compound. Parkin-overexpressing SH-SY5Y cells and human fibroblasts were treated with Rhodamine 6G, then the DNA extracted and sequenced to identify any changes in the mitochondrial genome. The sequences were aligned against the Cambridge Reference Sequence. Read-depth of the sequences varied between 200 and 10,000. After removing low quality reads, the variants were listed for each condition and the percentage of reads these variants occurred in calculated. After removing haplotype specific variants, homoplasmic variants that were present across cell types, the remaining variants were further sorted to

identify those that were not present in the untreated controls from each cell type. Figure 17 shows the gene in which a transition or deletion occurred under each condition caused by treatment with Rhodamine 6G (i.e. not showing those that occurred in control and Rhodamine-treated cells). The mutation frequency, i.e. the percentage of reads in which the mutation occurred, is represented by colour.

Deep-sequencing of the mitochondrial genome showed that variants were present in the DNA of cells treated with Rhodamine 6G. Of the SH-SY5Y cells, 80% of variants occurring within the D-loop were transitions, and the remaining 20 % were deletions. Variants that occurred elsewhere in SH-SY5Y cells were all deletions. Although these mutations occurred at a low frequency, the time scale at which these are found suggests that treatment with Rhodamine 6G increases the susceptibility of mtDNA to damage. The mechanism by which this occurs remains unknown.

Cell type	Parkin-o/e SH-SY5Y	Parkin-o/e SH-SY5Y	Fibroblast	Fibroblast
Length of treatment with Rhodamine 6G	1.5 hours	14 hours	24 hours	24 hours
Mutation frequency:	RNR2	ND2	DLOOP5	DLOOP5
	COX1	COX1	DLOOP5	ND2
		DLOOP3	COX1	TRNS1
		DLOOP3	ND3	ND4
< 2 %		DLOOP3	DLOOP5	DLOOP3
< 3 %		DLOOP3	DLOOP5	
< 4 %		DLOOP3		

Figure 17: Rhodamine 6G induces mutations in the mitochondrial genome

2 μM Rhodamine 6G was added to FLAG-Parkin overexpressing SH-SY5Y cells and control human fibroblasts for 1.5 H, 14 H or 24 H as stated. The DNA of cells was extracted and sequenced using NGS on the Illumina MiSeq. Here shows the position of mutations detected that were not present in control cells and the colour represents the mutation frequency in all the reads obtained (approximately 10,000 reads per base). Each lane corresponds to a different mutation, which are specified in the appendix.

1.2.5 PINK1-dependent mitofusin 1 ubiquitination can be detected in human fibroblasts, but not PINK1-dependent mitophagy

Treatment of healthy control fibroblasts for 16 hours with 10 μM CCCP revealed a striking loss of complex V signal, suggestive of mitophagy (Figure 18 A). However, performing this experiment in parallel with PINK1 mutant fibroblasts showed that this effect is not PINK1-dependent (Figure 18 A). This data suggests that PINK1-dependent mitophagy cannot be induced by 16 hours of 10 μM CCCP treatment. After 1.5 hours of 10 μM CCCP treatment however, PINK1-dependent mitofusin 1 ubiquitination can be identified (Figure 18 B). Whether the loss of mitochondria observed at 16 hours by immunocytochemistry is mitophagy or an artefact remains to be determined.

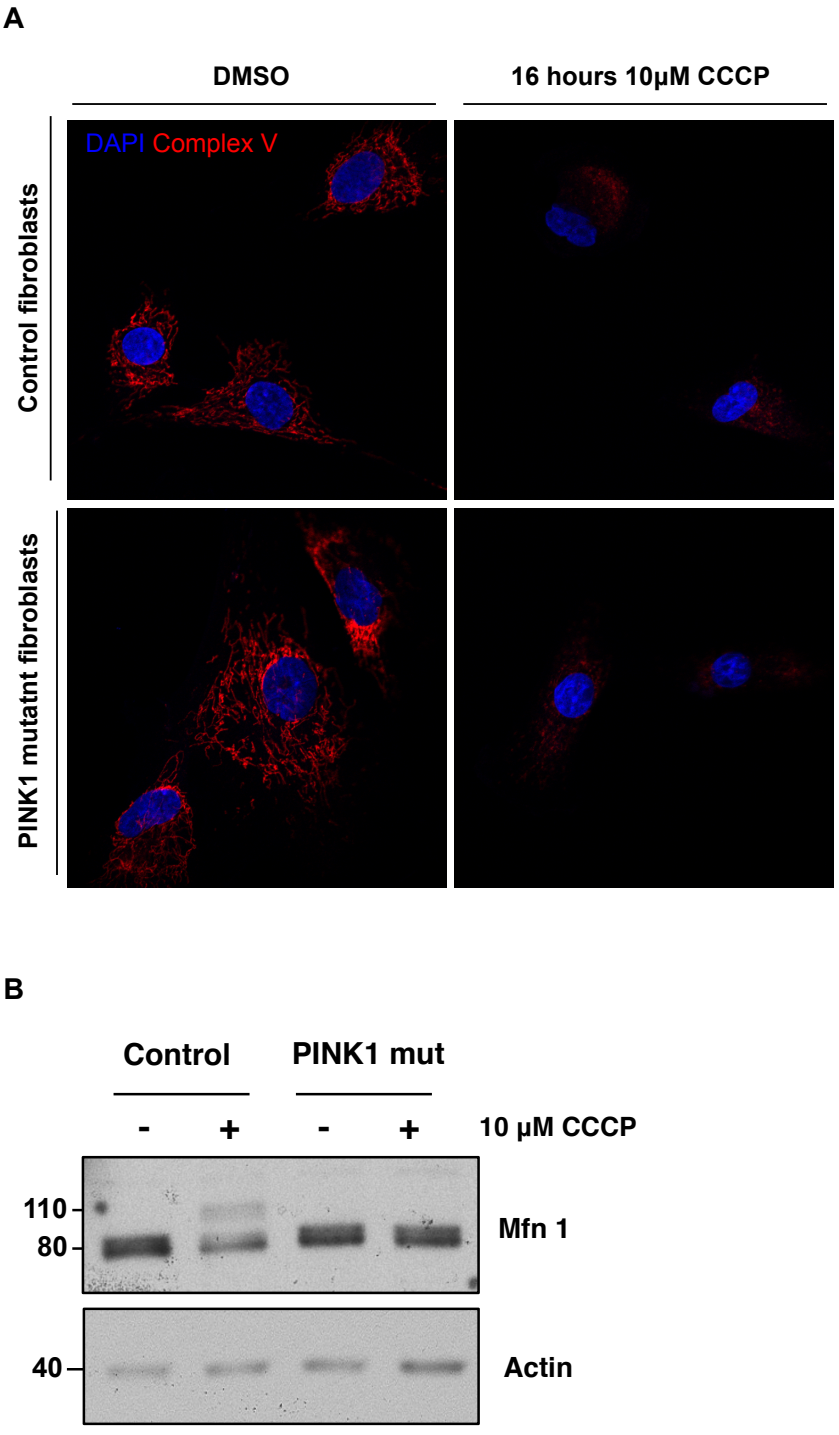

Figure 18: PINK1-dependent mitophagy cannot be detected in fibroblasts

A Representative images of fixed control and PINK1 mutant fibroblasts stained with Complex V and treated with DMSO or 10 µM CCCP for 16 H. Red: Complex V, blue: DAPI. B Representative immunoblot showing mitofusin 1 in control and PINK1 mutant fibroblasts treated with DMSO or 10 µM CCCP for 1.5 H.

1.2.6 Complex V mitochondrial staining is loss first upon induction of mitophagy in non Parkin-overexpressing cell systems

Identification of the loss of complex V signal in fibroblasts seen in figure 18 was particularly interesting since it has been reported that mitophagy cannot be detected in fibroblasts (Rakovic et al. 2013). This experiment was repeated in control fibroblasts but using several mitochondrial protein markers to measure mitophagy. It was found using analysis of Tom20 (OMM protein), Tim23 (IMM protein) and Hsp60 (matrix protein) that the loss of signal was limited to Complex V (Figure 19 A, B). Furthermore, the same effect was seen in control and PINK1 mutant fibroblasts (Figure 19 B). Immunoblot analysis revealed no loss of any mitochondrial proteins in the presence of CCCP, revealing discrepancies between results obtained from immunocytochemistry and Western blotting.

The fibroblasts used in these experiments contain only endogenous Parkin; therefore SH-SY5Y cells were employed to investigate any differences between systems containing endogenous and overexpressed Parkin. Treatment of Parkin-overexpressing SH-SY5Y cells with DMSO or 10 μM CCCP for 12 and 24 hours showed a decrease in both Complex V and Tom20 mitochondrial markers (as detected by immunocytochemistry) at a similar rate and at the 24 hour timepoint both were nearly completely lost (Figure 19 E). However, analysis by immunocytochemistry of wild-type SH-SY5Y cells treated with DMSO or 10 μM CCCP for 12 hours showed a loss of complex V signal but not Tom20, as had been observed in the fibroblasts (Figure 19 F).

A

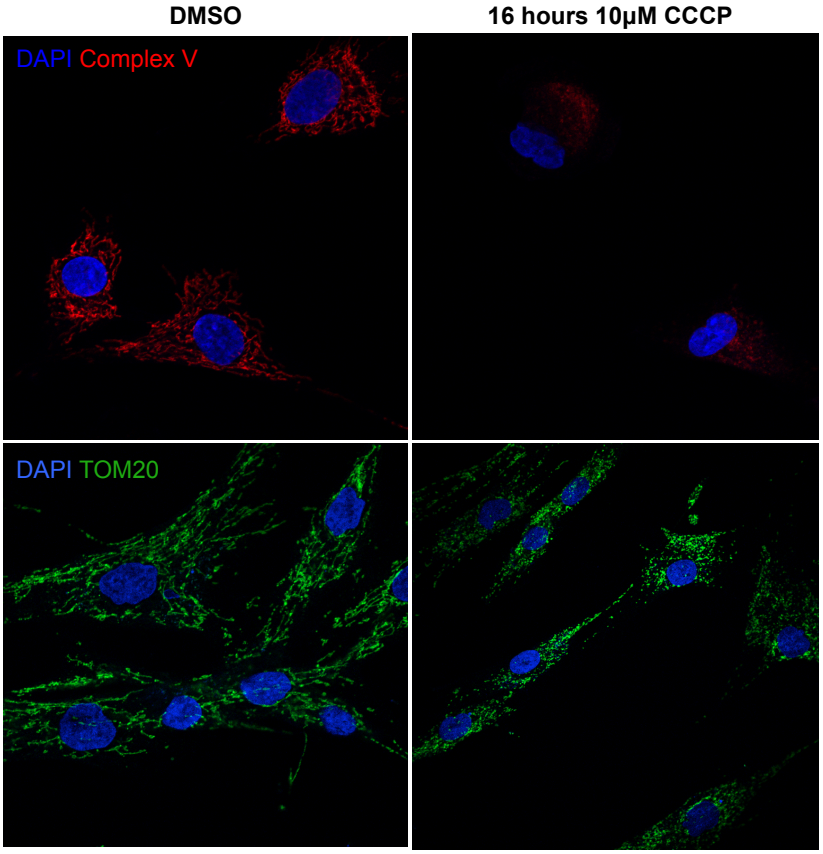
DMSO
16 hours 10μM CCCP
DAPI Complex V
DAPI TOM20

B

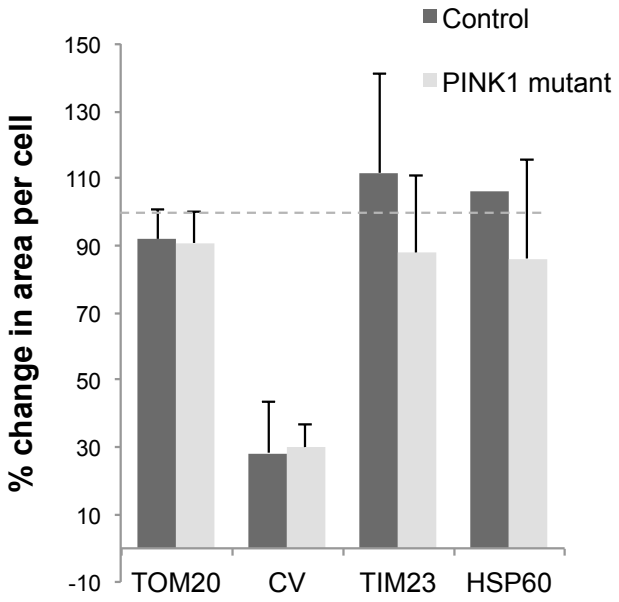
Control
PINK1 mutant
% change in area per cell
150
130
110
90
70
50
30
10
-10
TOM20
CV
TIM23
HSP60

C

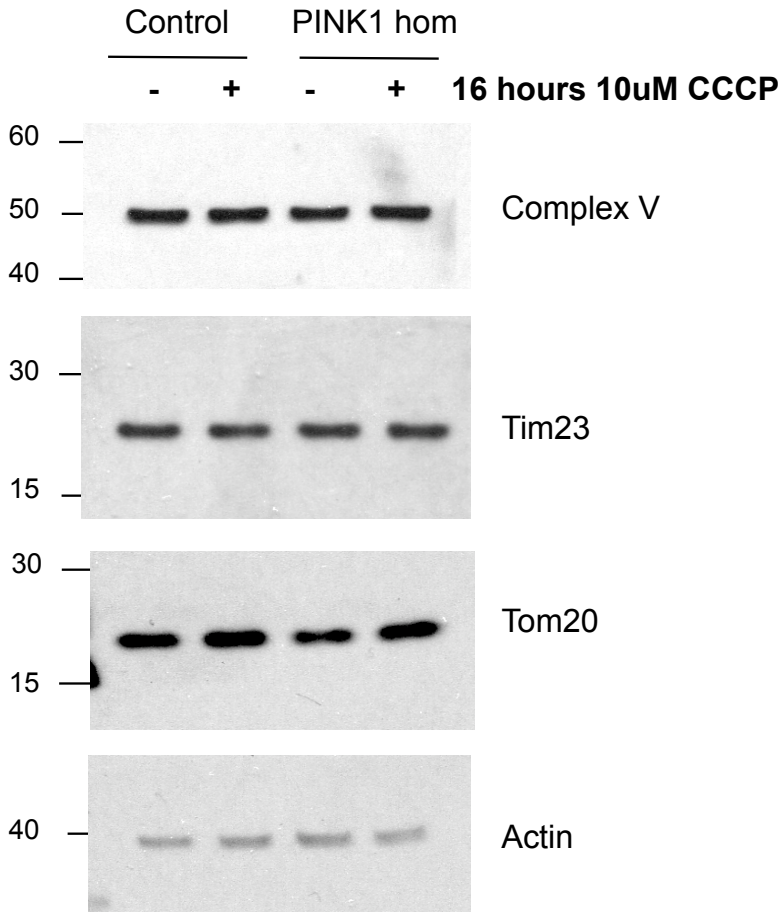
Control
PINK1 hom
- + - +
16 hours 10uM CCCP
60
50
40
Complex V
30
15
Tim23
30
15
Tom20
40
Actin

D

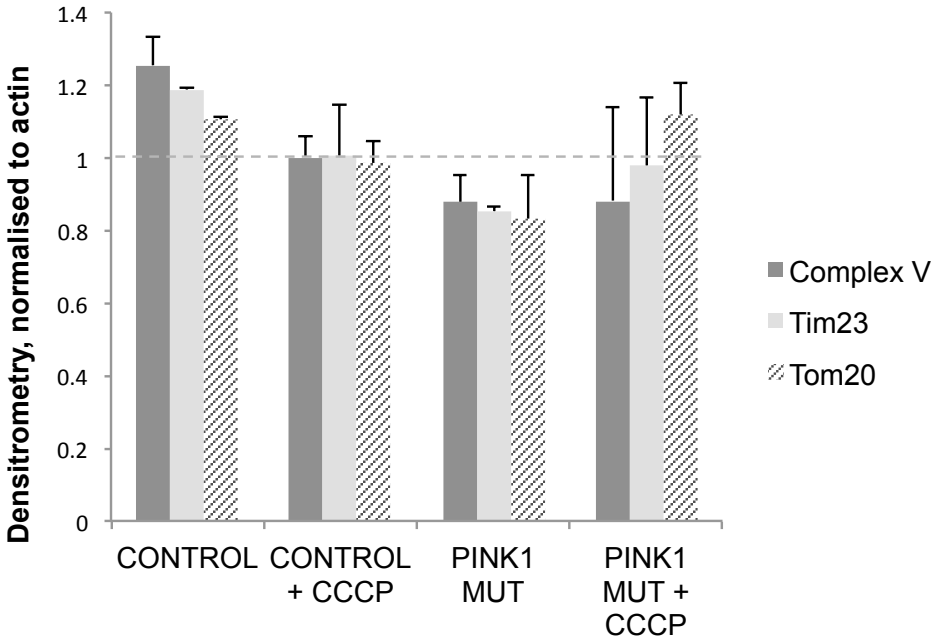
Densitrometry, normalised to actin
1.4
1.2
1
0.8
0.6
0.4
0.2
0
CONTROL
CONTROL + CCCP
PINK1 MUT
PINK1 MUT + CCCP
Complex V
Tim23
Tom20

E

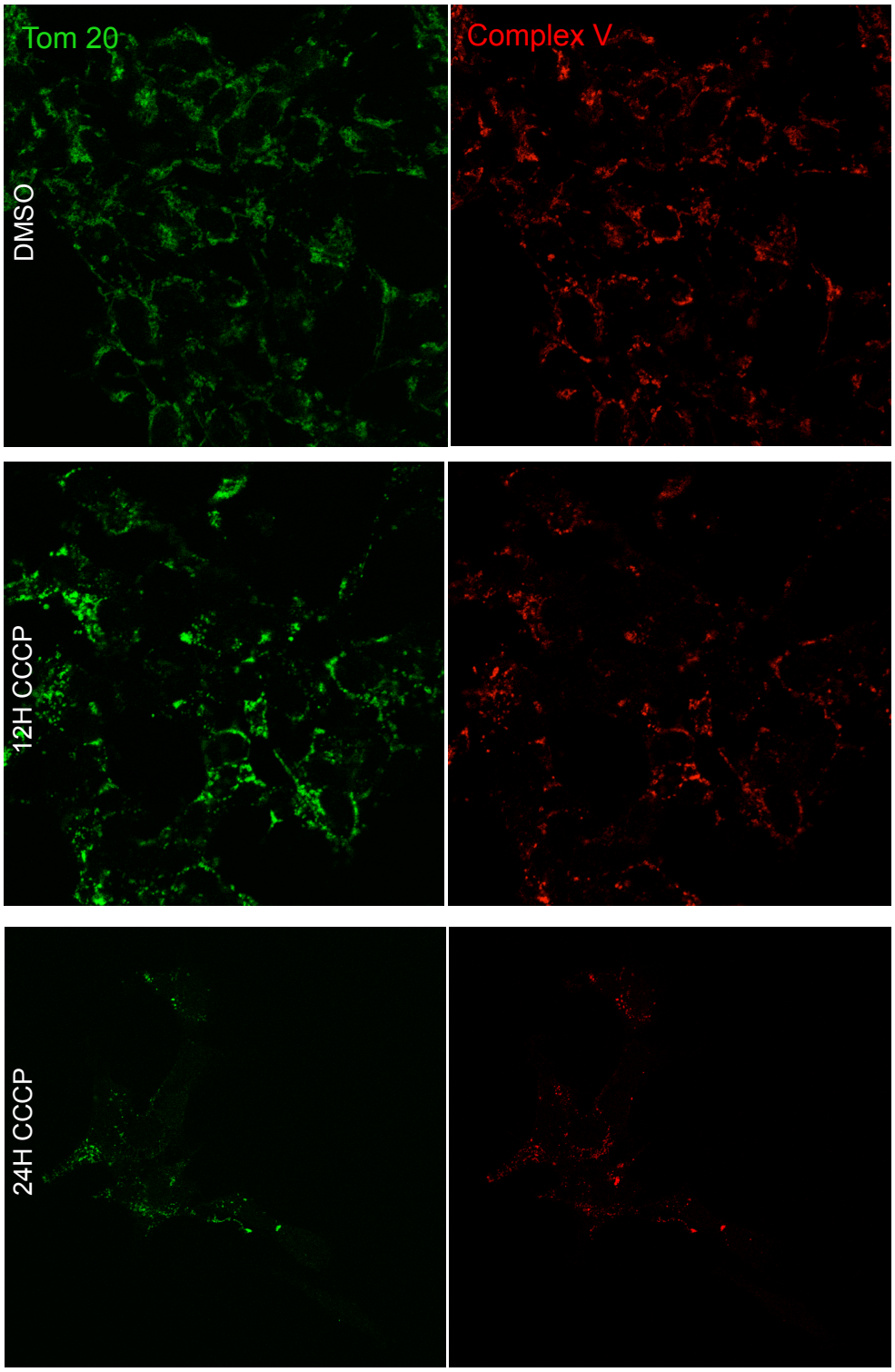

F

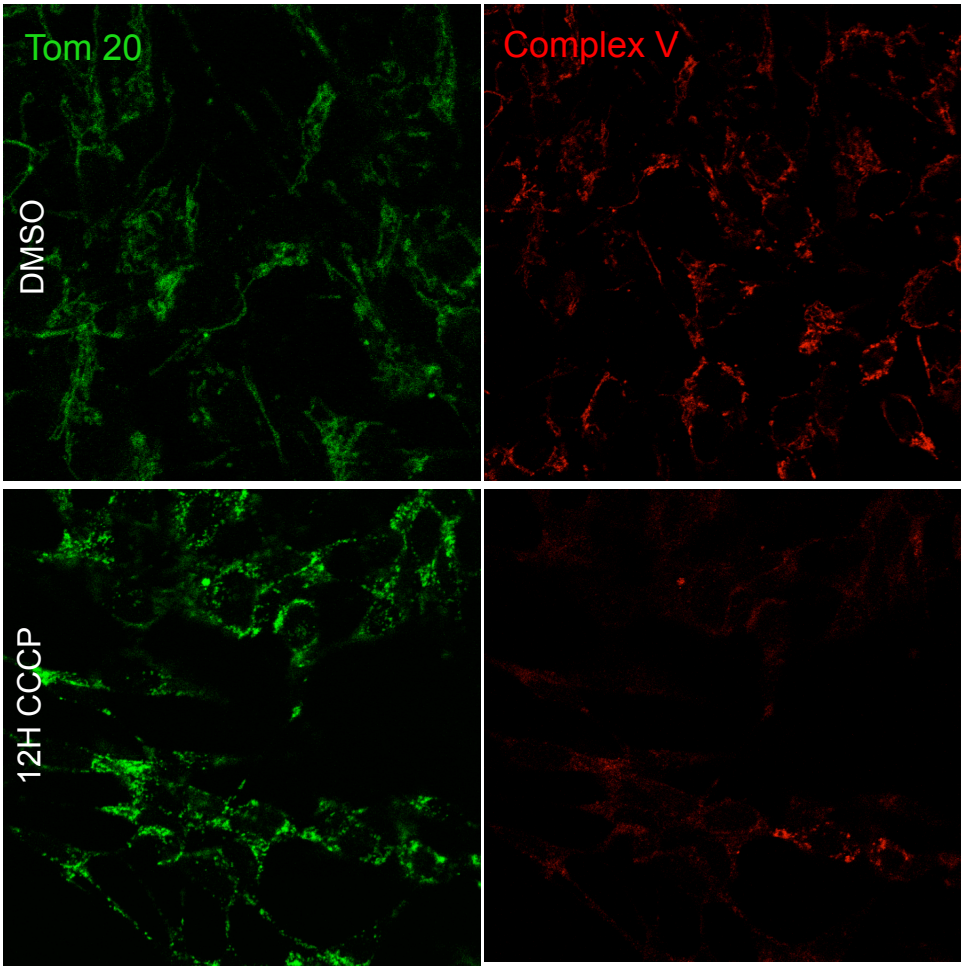

Figure 19: Differences in the loss of mitochondrial proteins in non over-expressing Parkin systems

A Representative images of fixed control fibroblasts treated with DMSO or 10 μM CCCP for 16 H. Red: Complex V, green: Tom20, blue: DAPI. B Quantification of mitochondrial protein area as determined by different mitochondrial markers (Tom20, Complex V, Tim23 and HSP60) in control and PINK1 mutant fibroblasts. Histograms represent the mean % change in area per cell between untreated control fibroblasts and control fibroblasts treated with 10 μM CCCP for 16 H. Dotted line indicates no change, error bars represent SEM, n = 3. C Representative immunoblots showing protein levels of mitochondrial proteins (Complex V, Tim23 and Tom20) of control or PINK1 mutant fibroblasts with and without 16 H of 10 μM CCCP. D Quantification of Western blots from E, normalised to loading control. Histograms represent mean densitometry, error bars represent SEM and dotted line indicates no change, n = 3. E Representative images of FLAG-Parkin overexpressing SH-SY5Y cells treated with DMSO, 12 H 10 μM CCCP or 24 H 10 μM CCCP. Fixed cells were stained with Tom 20 (green) or

Complex V (red). F Representative images of wild type SH-SY5Y cells (not Parkin overexpressing) treated with DMSO or 10 μM CCCP for 12 H. Fixed cells were stained with Tom20 (green) or Complex V (red).

1.3 Discussion

1.3.1 Key findings in the mitophagy pathway

As previously described, the short-term treatment of human fibroblasts with Rhodamine 6G causes inhibition of mtDNA-encoded polypeptides synthesis and reduces their stability (Williams et al. 1999). Treatment of Parkin-overexpressing SH-SY5Y cells, a commonly used system for the study of mitophagy, with Rhodamine 6G was found to cause the stabilisation of PINK1 and translocation of Parkin from the cytosol to the mitochondria. Downstream of this, p62 was found to colocalise with mitochondria indicating the recruitment of autophagic machinery and in line with this, a reduction in the area of mitochondria was observed.

Human fibroblasts obtained from patients with inherited Parkinson's disease caused by PINK1 and Parkin mutations were used in an assay to identify whether the effect of Rhodamine 6G is PINK1/Parkin-dependent. In the current model of the mitophagy pathway, the ubiquitination of outer mitochondrial proteins is understood to be caused by PINK1 and Parkin phosphorylation, therefore the presence of mitofusin 1 ubiquitination in PINK1 and Parkin mutant cells would indicate a PINK1/Parkin independent pathway (Lazarou et al. 2015). Here it was shown that Rhodamine 6G did not stimulate mitofusin ubiquitination in the PINK1 or Parkin mutant cells, suggesting that these proteins are necessary for Rhodamine 6G to exert it's effect.

The finding that Rhodamine 6G, like CCCP, required the presence of PINK1 and Parkin, suggested a similar mechanism of action between the two compounds. However, further investigation demonstrated that unlike CCCP, Rhodamine 6G did not induce the loss of mitochondrial membrane potential. Instead, the membrane was found to be hyperpolarised following treatment of Parkin-overexpressing cells with Rhodamine 6G.

Two subsequent findings suggested potential triggers of the mitophagy process caused by Rhodamine 6G. Firstly, Rhodamine 6G appeared to cause an increase in oxidative stress, which when inhibited with a precursor of reduced glutathione, did not cause long-term PINK1 stabilisation. In these experiments, the blue fluorescent dye monochlorobrimane was used to assess the cellular levels of GSH, and it was found that after the same dose of Rhodamine 6G that triggered the mitophagy process, levels of GSH were significantly reduced. Secondly, deep sequencing of the mitochondrial genome revealed that at this same timepoint low level mitochondrial DNA mutations were present in the Rhodamine 6G treated cells. With longer exposure these mutations increased in both location and frequency, and as expected, the D-loop was the most commonly affected area. The same effect was seen in two healthy control fibroblast lines treated with Rhodamine 6G.

These experiments using Rhodamine 6G demonstrate that PINK1-dependent mitophagy can be induced by oxidative stress independently of mitochondrial depolarisation. The mechanism of PINK1 stabilisation without loss of mitochondrial membrane potential is unknown but importantly it challenges the current model of mitophagy induction.

In addition to this, experiments using the known mitochondrial uncoupler CCCP in numerous cell lines, highlighted important

differences in the loss of mitochondrial proteins for the measurement of mitophagy. These experiments among others have shown that fibroblasts do not undergo complete mitophagy, however PINK1/Parkin-dependent ubiquitination of mitofusins can be induced (Rakovic et al. 2011; Rakovic, Shurkewitsch, Seibler, Grunewald, et al. 2013). Nevertheless, stimulation using CCCP caused the loss of mitochondrial protein Complex V (antibody against ATP-β) when assessed by immunocytochemistry. This effect appeared to be independent of PINK1, occurring in fibroblasts and wild-type SH-SY5Y cells, but not detectable in Parkin-overexpressing SH-SY5Y cells presumably because loss of other mitochondrial proteins also happens rapidly. Interestingly, the effect was only detectable by immunocytochemistry but not by Western blotting, which may suggest that the signal is lost due to a conformational change as opposed to the loss of mitochondrial protein. The effect was not seen in Tim23, another inner mitochondrial membrane protein, or the matrix protein HSP60.

1.3.2 Mitochondrial membrane depolarisation-independent mitophagy

As described in the mitophagy section of the introduction, under basal conditions PINK1 is understood to be imported from the cytosol into the mitochondria via the translocase of the outer mitochondrial membrane. PINK1 is undetectable under these conditions since it undergoes degradation by Rhomboid-7/Presenilin-associated rhomboid-like protein and Lon (Thomas et al. 2014; Whitworth et al. 2008; Jin et al. 2010). Loss of mitochondrial membrane potential has been shown to prevent the import of PINK1 through the translocase of the inner mitochondrial membrane, causing it to become stabilised on the outer membrane (Jin et al. 2010). Mitochondrial membrane potential is believed to be the critical element determining whether a daughter mitochondrion

re-joins the mitochondrial network or whether it is singularly left to be degraded by mitophagy (Twig, Elorza, Anthony J A Molina, et al. 2008a; Horbay & Bilyy 2016). The significant accumulation of PINK1 at the mitochondria, stimulated by Rhodamine 6G independently of membrane depolarisation, therefore suggests an alternative mechanism by which PINK1 import is prevented.

This data is not the first to question the standard model of membrane depolarisation causing PINK1 accumulation, which subsequently triggers mitophagy. Both carbonyl cyanide *m*-chlorophenyl hydrazine (CCCP) and carbonyl cyanide-p-trifluoromethoxyphenylhydrazone (FCCP) are known to cause uncoupling of the proton gradient established across the inner mitochondrial membrane and thereby cause membrane depolarisation (Heytler & Prichard 1962). Whilst a low concentration of FCCP can cause a complete loss of membrane potential, this does not cause the induction of mitophagy even in a Parkin-overexpressing system (Berezhnov et al. 2016). A dose of ten times the amount required to cause membrane depolarisation was sufficient to induce PINK1 stabilisation, Parkin translocation and downstream mitophagy. In this study, it was suggested that intracellular pH was the regulator of mitophagy, stimulated by FCCP through acidification of the cytosol (Berezhnov et al. 2016).

Alternatively to the use of CCCP, the combination of oligomycin and antimycin A has been shown to stimulate loss of membrane potential and trigger significant Parkin translocation from the cytosol to the mitochondria (Vives-Bauza, Zhou, Huang, Cui, Rosa L A de Vries, et al. 2010). However, whilst treatment with antimycin A alone causes inhibition of complex III and subsequent loss of membrane potential, it is unable to stimulate the mitophagy pathway (Rego et al. 2001; Vives-Bauza, Zhou, Huang, Cui, Rosa L A de Vries, et al. 2010; Allen et al. 2013). This effect was studied in both a model of Parkin-independent mitophagy and Parkin-dependent mitophagy.

Interestingly, using the Parkin-independent system to study mitophagy, it was shown that treatment of cells with oligomycin alone caused a significant increase in the delivery of mitochondria to lysosomes, despite the absence of membrane potential depolarisation (Allen et al. 2013). However until the data produced here, mitophagy in the absence of membrane depolarisation had not been shown in a seemingly PINK1/Parkin-dependent system. Whilst it remains unknown whether PINK1 accumulates in the presence of Rhodamine 6G due to the prevention of PINK1 import across the IMM or if PINK1 is simply no longer degraded, these data raise the possibility of an alternative mechanism of PINK1-dependent mitophagy induction.

1.3.3 Oxidative stress and mitochondrial DNA mutations as an inducer of mitophagy

Using fluorescent dye to measurement intracellular reduced glutathione levels and cotreatment with NAC to restore antioxidant levels, it was found that Rhodamine 6G causes oxidative stress to cells. This amount of oxidative stress was not sufficient to cause depolarisation of the mitochondrial membrane potential, however the use of NAC demonstrated that PINK1 accumulation was dependent upon depletion of reduced glutathione caused by Rhodamine 6G.

Interestingly, it has been shown previously that mitophagy can be stimulated through exposure to mild oxidative stress to a greater extent than through exposure to transient oxidative stress. This was demonstrated by the use of H_2O_2 to cause mild oxidative stress and starvation to simulate transient oxidative stress (Frank et al. 2012). Moreover, mild stress has also been associated with the formation of mitochondrial-derived vesicles (MDVs), the mechanism by which impaired mitochondrial components are transported to endosomes

or peroxisomes for degradation (Soubannier, G.-L. McLelland, et al. 2012). Study of the content of MDVs revealed a, enrichment of oxidised protein, suggesting a triggering of this quality control process upon exposure to oxidative stress.

Mitochondrial DNA mutations have also been associated with mitophagy in a study whereby mtDNA mutations appeared to be selectively removed upon overexpression of Parkin in heteroplasmic cybrid cells, suggesting that mitochondrial DNA mutations stimulated the mitophagy process (Suen et al. 2010). It has been suggested that under mild oxidative stress, or indeed the presence of low level mtDNA mutations, mitophagy may be triggered as a mechanism of damage limitation to prevent unnecessary stimulation of autophagy (Scherz-Shouval & Elazar 2011). The data shown here through the use of Rhodamine 6G presents an example of mitochondrial damage caused by mild oxidative stress and mtDNA mutations, that is sufficient to cause PINK1 accumulation and downstream processes, but does not cause uncoupling of the IMM proton gradient.

1.3.4 Detecting mitophagy: what causes loss of Complex V signal in immunocytochemistry?

Finding reliable and sensitive methods to measure mitophagic levels are critically important for the understanding of mitophagy and also for use in drug screens.

Mitophagy is commonly quantified by the loss of mitochondrial protein expression, either by immunocytochemistry or immunoblotting. Whilst this technique cannot distinguish between mitophagy and other degradation processes or the stimulation of biogenesis, it is often used in combination with the assessment of mitophagy-associated proteins such as PINK1 and Parkin.

Furthermore, in Parkin-overexpression systems, the complete loss of mitochondrial proteins can be detected within 24 hours of mitochondrial uncoupling; therefore it is believed that mitophagy occurs rapidly enough for the lack of distinction from other processes to not be a problem. Nevertheless, it is of particular importance that the levels of numerous mitochondrial proteins are measured as highlighted in the results shown in this chapter.

It is known that different mitochondrial proteins, even proteins that make up the same respiratory complex, can be degraded at different rates (Hare & Hodges 1982). Furthermore, mitochondrial proteins in the intermembrane space have been shown to be released following permeability transition, and therefore should not be measured alone in assessment of mitophagy (Scarlett & Murphy 1997). In these experiments it was found that Complex V signal was rapidly lost in CCCP-treated fibroblasts and SH-SY5Y cells independently of PINK1 as measured by immunocytochemistry.

These experiments gave rise to four important findings: 1. Of the mitochondrial proteins measured, from four different compartments in the mitochondria, Complex V signal only was lost following mitochondrial uncoupling 2. This finding was not emulated in experiments using immunoblotting 3. The finding was the same in control and PINK1 mutant fibroblasts, suggesting it is a PINK1-independent mechanism 4. The finding was undetectable in Parkin-overexpressing cells.

The discrepancies between immunostaining and immunoblotting are suggestive of a conformational change being the cause of signal loss, since this would not be detectable in the Western blot results. The antibody used was an Abcam monoclonal mouse antibody to the complex V beta subunit (ATPβ). If was of particular interest to find another antibody to this subunit at a different epitope to see whether the same effect was found, however upon contacting the

manufacturer, we were informed that the epitope had not been mapped.

The observation that loss of Complex V staining was not detectable in Parkin-overexpressing cells adds to the growing hypothesis that Parkin acts as an amplifier of the mitophagy process (Lazarou et al. 2015). It is likely that the substantial overexpression of Parkin in the SH-SY5Y cells caused rapid loss of all mitochondrial proteins, so all mitochondrial protein signals were lost together.

1.3.5 Future perspectives

The experiments in this chapter aimed to aid understanding of the requirements for mitophagy induction and to investigate the assessment of mitophagy in several cell types.

It has been demonstrated here that PINK1-dependent mitophagy can be induced independently of membrane depolarisation, however the mechanism of this remains unknown. Of particular interest would be to identify whether PINK1 is imported across the inner mitochondrial membrane in Rhodamine 6G, as PINK1 was thought to accumulation due to lack of import through TIM after loss of membrane potential.

These experiments have highlighted discrepancies in commonly performed experiments which can lead to false mitophagy data if not verified with more than one technique. For future experiments it would be particularly interesting to assess the timecourse of Complex V immunostaining to see when it is lost and also whether it returns after mitochondrial turnover. Further analysis is required to confirm whether this indeed is a conformational change.

Chapter 2

Fibroblast models of mtDNA disease and novel phenotypic findings

2.1 Introduction

2.1.1 Models of primary mtDNA disease

Creating suitable models of mtDNA disease is challenging, particularly due to the clinical variability a single mutation can cause.

Cytoplasmic hybrid (cybrid) cell models have been used in mitochondrial disease research for the characterisation of unsequenced mtDNA mutations, studying different heteroplasmic burdens of known mtDNA mutations, or for studying bigenomic (nuclear and mitochondrial DNA) compatibility (Khan et al. 2007). The cybrid technique utilises ρ0 cell lines, which are generated by first causing termination of mtDNA replication (Wilkins et al. 2014). Through subsequent rounds of cell division, the mtDNA pool will become 'diluted' until some cells contain no mtDNA, termed ρ0 cells. These cells can then be isolated and for use in creating ρ0 cell lines. To create a cybrid, ρ0 cells are fused with cytoplasts, which are enucleated cells derived from patient cell lines (King & Attardi 1989).

Cybrids cell lines have been of valuable use for studies investigating interactions between the nucleus and mitochondria, as well as the effect of mutant load on cellular function (figure 20). However, cybrid models have limitations to their use; for example, the generation of cybrids most often involves tumour cells, which are known to be glycolytic (depend on glycolysis for ATP production) and therefore are not metabolically similar to those cell types most often affected in mtDNA disorders. This may account for discrepancies reported between cybrid models and clinical phenotypes; for example a homoplasmic *MTTV* mutation that causes fatal metabolic defects in cardiac and skeletal muscle lacked any respiratory defect in the cybrid model (Rorbach et al. 2008).

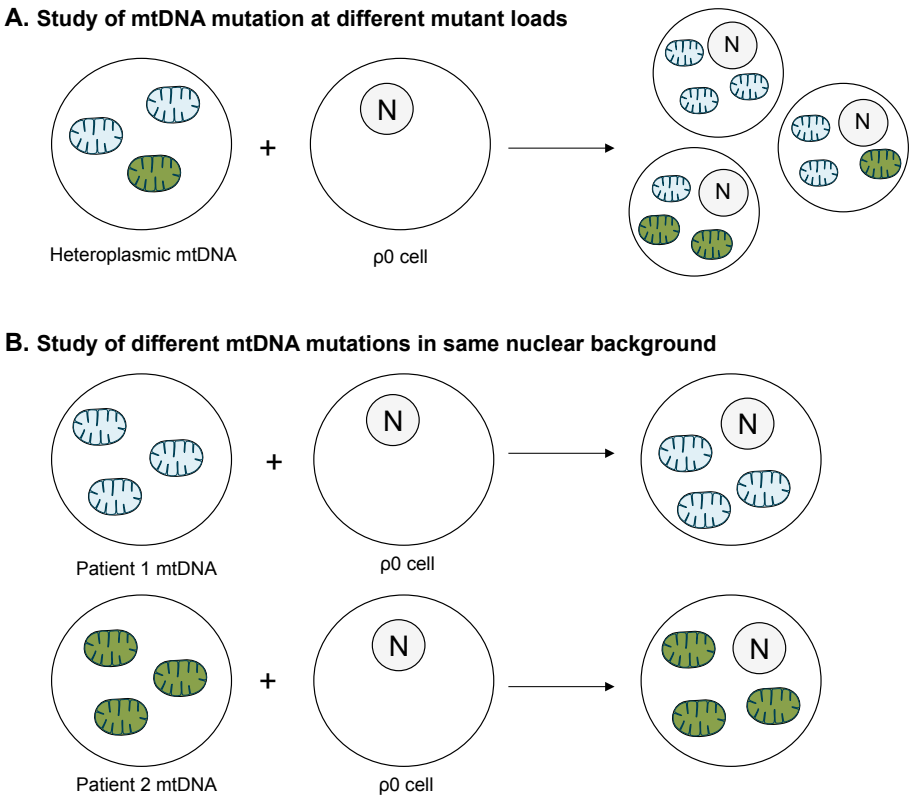

Figure 20 Schematic of the generation and use of cybrids for modelling mtDNA disease

A. Blue mitochondria represent mitochondria containing wild-type mtDNA, green mitochondria represent mitochondria containing mutant mtDNA, N = nucleus. B Blue mitochondria represent mitochondria belonging to patient

1, green mitochondria represent mitochondria belonging to patient 2, N = nucleus. Adapted from Wilkins *et al.,* 2014.

A naturally occurring animal model was identified in golden retriever dogs, which presents as a sensory ataxic neuropathy and is maternally inherited (Baranowska et al. 2009). The causative mutation was found to be a single base pair deletion in the mitochondrial tRNA tyrosine gene at position 5304. Similarly to human pathology, affected dogs exhibited reduced ATP production and respiratory chain enzyme function, and muscle biopsy indicated lowered cytochrome c oxidase (COX) activity, although no 'ragged red fibers' were found. The corresponding mutation site in the human mtDNA genome has not currently been associated with a mitochondrial disorder in humans, nor have similar phenotypes to those reported in dogs been reported in other mutations occurring in the human tRNA tyrosine gene. Nevertheless, a naturally occurring animal model would enable the inheritance of the pathogenic mutation to be studied and therefore may be of use in the development of treatments for the disease.

Patient fibroblasts as models of disease have many advantages. Fibroblasts are obtained by carrying out a simple skin biopsy, which is a safe procedure that does not require stitches. Experimentally, fibroblasts are simple to culture and have been extensively used for studying mitochondria, especially in the field of Parkinson's disease (Burbulla & Krüger 2012). Fibroblasts can be used in biochemistry experiments, immunocytochemistry and live cell imaging, making them a suitable cell type for many experiments.

However, fibroblasts do have some limitations; for example, experimentally fibroblasts are difficult to transfect using common transfection reagents, and their protein content is low, meaning

biochemistry experiments require large quantities of cells. Furthermore, unlike cell types most affected in mtDNA disease, fibroblasts are glycolytic, therefore the phenotypic effect of the mutation may not be detected (Ghesquière et al. 2014). Nevertheless, fibroblast models have been of use in pharmacological screens, as described in section 2.1.2.

2.1.2 Examples of uses of mtDNA disease fibroblast models

Mitochondrial encephalo-myopathy, lactic acidosis and stroke-like symptoms (MELAS) syndrome is a common mitochondrial disorder, most often associated with point mutations in tRNA genes. Fibroblasts derived from patients harbouring the m.3243A>G were previously characterised as having decreased mitochondrial membrane potential and significantly impaired coenzyme Q_{10} levels and respiratory chain enzyme activity (Cotán et al. 2011). These fibroblasts were subsequently used in a pharmacological screen to identify that supplementation with coenzyme Q_{10} or riboflavin could improve the phenotype of the MELAS fibroblasts (Garrido-Maraver et al. 2012). There have been reports of both these compounds being of benefit to some patients, though not all and rigorous conclusive trials have not been conducted, however coenzyme Q_{10} is very commonly used due to its good safety report, even at high doses (DiMauro & Rustin 2009; Haack et al. 2010; Ghezzi et al. 2010).

Studies into the effect of dietary manipulations on mtDNA disease has been investigated using fibroblasts with complex I deficiency derived from patients harbouring *NDUFS1* mutations. In this study, a high fat diet was found to increase respiratory chain activity in the patient fibroblasts, and subsequent experiments found that disease

progression was significantly slowed in the complex I deficient Harlequin mice (Schiff et al. 2011).

These examples, among others, show that fibroblast models can be good indicators before use of *in vivo* models (Viscomi et al. 2015).

2.1.3 Therapeutic strategies for mtDNA disease and targeting heteroplasmy

One of the many challenges of mitochondrial disease is the significant variation in clinical phenotype. Patients can present with a vast range of features, involving different organs types with varying severity. From a treatment point of view, therapy is currently limited to addressing the various symptoms of the disease but there is no cure for the cause of the disease. Patient heterogeneity causes difficulty not just in treatment itself, but also the ability to conduct clinical trials (Pfeffer et al. 2012). Mitochondrial diseases are rare in general, but together finding sufficient numbers of available patients who present with similar phenotypes or genotypes can be difficult. As a result, approaches in developing treatments for these diseases are focused on more general interventions that may alleviate a range of symptoms as opposed to targeting a particular genotype/phenotype (Lightowlers et al. 2015).

Among others, potential therapeutic avenues for mtDNA diseases include restoration of metabolic function, mitochondrial replacement, scavenging excessive reactive oxygen species, and eliminating pathogenic mtDNA (Lightowlers et al. 2015). MtDNA disease can cause mitochondrial dysfunction that may be relieved by increasing mitochondrial mass, i.e. a greater number of partially functioning mitochondria may be the equivalent of fewer functioning mitochondria. As a result, targeting mitochondrial biogenesis is a potential therapeutic strategy. Mitochondrial replacement

approaches aim to prevent the transmission of maternal transmission of mtDNA mutations to offspring. It has been shown *in vitro* that transferring patient zygote, with male and female pronuclei, into a donor fertilised oocyte, with male and female pronculei removed, can successfully develop into a blastocyte, enabling no transfer of disease from mother to child (Craven et al. 2010). In an iPSC model of Leber's hereditary optic neuropathy, cybrid technology was used to generate isogenic iPSC controls by replacing mutant mtDNA with wild-type mtDNA (Wong et al. 2017). However, replacement therapy is limited in its use for all mtDNA disease cases, and is not widely available.

Common to all mtDNA diseases is the occurrence of heteroplasmy: the coexistence of mutated mtDNA with wild-type mtDNA. As the mutant load increases, so does the biogenetic defect, leading to more severe phenotypes. In cases of heteroplasmy, the mutation is most often recessive, meaning that below a certain threshold (normally around 60% mutant load) the patient will experience no apparent dysfunction. Whilst different tissues will have different thresholds and varying clinical impact, it stands to reason that lowering heteroplasmy to below the threshold level may be as effective as elimination of mutant mtDNA altogether.

Numerous methods to reduce mutant load have been explored, such as engineered transcription activator-like effector nucleases (TALENs), which have been used to reduce the abundance of mtDNA containing a common deletion, by cleaving the breakpoint region of mutant mtDNA (Bacman et al. 2013). However, whilst targeting mutant mtDNA amongst the wild-type mtDNA to reduce mutant load appears a promising potential therapy, it remains unknown as to why high mutant loads can be maintained when the mitochondrial network constantly undergoes quality assurance processes such as mitochondrial dynamics (fission and fusion) and mitophagy.

Mitophagy selectively targets energetically compromised mitochondria for degradation, and it has been shown that Parkin is a modulator of heteroplasmy in models using heteroplasmic cybrid cells and *C. elegans* (Suen et al. 2010; Valenci et al. 2015). Consequently, in cases of heteroplasmic mtDNA disease, it remains unknown whether under physiological conditions, selective mitophagy is ineffective at controlling mutant load, or whether this process is impaired. Either way, correction or enhancement of this process presents as a potential therapeutic strategy for these diseases.

2.1.4 Mitophagy in mtDNA disease

MtDNA diseases are maternally inherited, and whilst the mechanism is not completely understood, studies in *C. elegans* have shown that the removal of paternal mtDNA is thought to occur via mitophagy in the early embryo (Al Rawi et al. 2011; Sato & Sato 2011). A recent study in mouse fibroblasts showed that paternal mitochondria loses mitochondrial membrane potential and that when embryos were injected with lentivirus expressing shRNA against *PINK1* there was a significant increase in the persistence of paternal mtDNA (Rojansky et al. 2016). This data suggests that mitochondrial membrane depolarisation triggers PINK1-dependent mitophagy to eliminate paternal mtDNA. When shRNA against *Parkin* alone was injected into the embryos, the increase in paternal mtDNA was modest and not found to be significant, which corresponds with more recent mitophagy research suggesting that Parkin is an amplifier of the process but not essential (Lazarou et al. 2015; Rojansky et al. 2016).

Elimination of paternal mtDNA is stable, and therefore utilising mitophagy for the removal of pathogenic mitochondria for therapy in several disease areas is an appealing target. As described briefly in

section 2.1.3, studies in heteroplasmic cybrid cells showed that overexpression of Parkin could stably maintain a favourable wild-type to mutant mitochondrial genome ratio (Suen et al. 2010). In these experiments, a mutation in the cytochrome *c* oxidase subunit I gene (COXICA65) caused a reduction in mitochondrial membrane potential but interestingly, there was no significant difference in the percentage of cells with Parkin located on the mitochondria between the COXICA65 mutant and wild-type cell lines (Suen et al. 2010). Overexpression of Parkin for several weeks caused a reduction in the presence of mutant mtDNA, suggesting that those mitochondria containing high levels of COXI mutant were selectively eliminated via mitophagy. Together with a favourable change in mutant load, activity of cytochrome *c* oxidase which had been on average 4.6% of wild-type cell lines, was restored to 96.9% (Suen et al. 2010).

Mitophagy in fibroblasts harbouring the m.3243A>G mutation has previously been studied using an IN Cell 1000 analyser (Diot et al. 2015). This technique was used to report the colocalisation of LC3-II positive autophagosomes with mitochondria, which was found to be increased in the heteroplasmic m.3243A>G patient compared to control, suggesting increased basal mitophagy (Diot et al. 2015). However, it was not reported whether the colocalisation observed was specific to mutant mitochondria, i.e. whether this effect was caused by a recruitment of autophagic machinery or if PINK1/Parkin machinery is selectively stimulating mitophagy in these mutants. If the latter is true, it is surprising that the presence of pathogenic mitochondria is maintained in cells over-stimulating the selective process of mitophagy. Whilst mitophagy is of interest in mtDNA disease research, the selective nature of this process is seldom investigated in great depth, and it remains unknown whether in patient cells PINK1/Parkin machinery is capable of selectively removing the pathogenic mitochondria.

2.1.5 Aims and hypothesis

In this chapter the aim was to investigate characteristics of patient fibroblasts harbouring several different mtDNA mutations, affecting respiratory complexes or tRNA genes. In particular, the objective was to investigate the mitophagic machinery in these patient lines, studying endogenous expression of PINK1 and Parkin, ubiquitination of mitofusins and biogenesis. The hypothesis was that for mtDNA mutants to persist at a pathogenic load, selective mitophagy might be impaired in these patient cells. The studies that demonstrate that Parkin can positively regulate heteroplasmy give evidence to suggest that selective mitophagy should be able to remove mitochondria when a high mutant load is causing a pathogenic phenotype (Suen et al. 2010; Valenci et al. 2015).

2.2 Results

2.2.1 Clinical description of patients with primary mitochondrial disease

Patient 1 (P1): ND5 mutation

Patient 1 had an A>G missense mutation in the complex I *ND5* gene, which presented as a MELAS (mitochondrial encephalopathy, lactic acidosis, stroke-like episodes) phenotype.

Patient 2 (P2): tRNA leucine mutation

Patient 2 had a heteroplasmic A>G point mutation in the mt-tRNA leucine gene. This m.3243A>G substitution in a highly conserved region of the tRNA(Leu) gene is the most common pathogenic mitochondrial DNA mutation, and is invariably heteroplasmic (de Laat et al. 2013; (Ng et al. 2015). It has been shown that this mutation causes a severe impairment of 16S rRNA transcription termination, which results in highly variable phenotypic characteristics (Tuppen et al. 2010; Hess et al. 1991). In this case the patient presented with a mixed MELAS/MERFF (myoclonic epilepsy with ragged-red fibers).

Patient 3 (P3): tRNA lysine mutation

Another common pathogenic mitochondrial DNA mutation is the A>G missense mutation found in the mt-tRNA lysine gene. This patient had a reported mutant load of 82% and presented as a MERFF phenotype, which is atypical for this genotype (Mancuso et al. 2014).

Patient 4 (P4): tRNA lysine mutation

Patient 4 was a relative of patient 3, and also had the A>G missense mutation in the mt-tRNA lysine gene. Patient 4 had a

mutant load of 44% which did not appear to cause a pathogenic phenotype.

Patient 5 (P5): tRNA serine mutation

Patient 5 presented with a phenotype of ataxia, myoclonus and deafness, caused by an insertion in the mt-tRNA serine gene. This m.7472insC mutation has been reported in several families to be a significant cause of hearing loss, and in some individuals with high mutation load levels neurological features, such as ataxia and myoclonus, are also reported (Hutchin et al. 2001; Jaksch et al. 1998; Tiranti et al. 1995)

Patient 6 (P6): tRNA serine mutation

Patient 6 was a relative of patient 5, who also harboured the m.7472insC and presented with a phenotype of ataxia, myoclonus and deafness.

Patient 7 (P7): ATP6 mutation

Patient 7 had a mutation affecting a specific respiratory chain complex, caused by a homoplasmic missense mutation in mt-ATP6 encoding the ATP6 subunit of the mitochondrial ATP synthase (OXPHOS complex V). This patient is part of an extended family, which was published reporting mt-ATP6 mutations as a previously unrecognised cause of isolated Charcot-Marie-Tooth (CMT) disease and distal hereditary motor neuropathy (dHMN) (Pitceathly et al. 2012).

Patient	Mutation	Gene	Heteroplasmy	Main clinical phenotype	Phenotype in detail	EMG/NCS	Muscle biopsy	Respiratory chain analysis (showed reduced complex)	Brain MRI/CT
1	m.13528A>G	MT-ND5	100% m, 99.9% b	MELAS	Epilepsy, stroke-like episodes, myopathy, peripheral neuropathy,hearing loss	n/a	COX-fibres/ragged red fibers	n/a	Right occipital infarction
2	m.3243A>G	MT-TL1	17% b, 85% u	MELAS/MERRF syndrome	Myoclonic epilepsy, stroke-like episodes, mild ataxia	n/a	n/a	n/a	Left occipital lobe stroke-like lesion, progressive atrophy and signal changes in the left hippocampal head
3	m.8344A>G	MT-TK	93%m,87% b	MERRF	Delay in motor development, cerebellar ataxia, myoclonic epilepsy, sensory>motor axonal peripheral neuropathy, amenhorrea	sensory>motor axonal peripheral neuropathy	1 ragged red fiber, denervation and reinnervation features	IV*	Cerebellar atrophy/atrophic mesencephalon
4	m.8344A>G	MT-TK	53%b	Pauci/asymptomatic	Mild balance problem	normal	n/a	n/a	n/a
5	m.7472insC	MT-TS1	n/a	Ataxia, myoclonus, deafness	Ataxia, myoclonus, deafness	normal	n/a	n/a	normal
6	m.7472insC	MT-TS1	n/a	Ataxia, myoclonus, deafness	Ataxia, myoclonus, deafness, fatigue	normal	n/a	n/a	n/a
7	m.9185T>C	MT-ATP6	100% b	CMT2	hereditary neuropathy,migraine, cerebellar atrophy, diabetes	sensory>motor axonal neuropathy	Features of denervation. Increased lipid stains	V	Mild cerebellar athrophy

Table 15 Clinical Information reported on mtDNA disease patients whose fibroblasts were used in this study.

The information in the tables shows clinical data obtained at the National Hospital for Neurology and Neurosurgery UCL, and Queen Square Centre

for Neuromuscular Diseases. M = muscle, b = blood and u = urine. n/a indicates where data was not collected or not present in patient notes.

*** Mild reduction complex IV (0.013 n.v. 0.014-o.034)**

2.2.2 Maintenance of mitochondrial membrane potential in cultured mtDNA disease fibroblasts

The charge across the inner mitochondrial membrane (IMM) is generated by the reductive transfer of electrons across the electron transport chain (ETC). This charge gradient provides the energy for protons to cross the IMM against their concentration gradient, causing a net accumulation of protons to occur on the outer side of the IMM. Both the electrical gradient and mitochondrial pH gradient that has been created can then then drive protons back across the IMM (into the mitochondrial cytoplasm) through the ATP synthase (complex V of the ETC) to generate ATP. Mitochondrial membrane potential ($\Delta\Psi_m$) therefore relates to a cells' ability to generate ATP by oxidative phosphorylation.

Tetramethylrhodamine methyl ester (TMRM) is a fluorescent probe, which accumulates in mitochondria with intact membrane potentials. Here we show that under basal conditions, fibroblasts containing the *ND5* mutation (P1) exhibited a reduced $\Delta\Psi_m$ to approximately 90% of healthy controls, consistent with other reports of reduced $\Delta\Psi_m$ in fibroblasts containing the m.13528A>G mutation (McKenzie et al. 2007) (Figure 21). A decrease in $\Delta\Psi_m$ was also observed in the common m.3243A>G mutation (P2) present in the tRNA leucine gene, as has been also reported previously in the literature (Garrido-Maraver et al. 2012) (Figure 21). However, despite the impairments tRNA genes have on respiratory chain complexes, a significantly reduced $\Delta\Psi_m$ was not observed in the tRNA lysine (P3, P4) or tRNA serine (P5, P6) mutated lines, which was consistent

between multiple patients containing the same mutation (Figure 21). Finally, also contradictory to reports in the literature, measurement at basal levels showed the ATP synthase mutant fibroblasts (P7) to have a significantly reduced $\Delta\Psi_m$ (Figure 21). In general it is thought that mutations in the tRNA genes and respiratory chain proteins causes a decrease in $\Delta\Psi_m$ but cells with mutations for the ATP synthase subunits result in hyperpolarised $\Delta\Psi_m$ (Lorenz et al. 2017; Szczepanowska et al. 2012). Interestingly, this mutation presents as a CMT2 phenotype in the patient (previously described (Pitceathly et al. 2012)) and other CMT causing mutations have also been associated with a reduced $\Delta\Psi_m$ (Loiseau et al. 2007; Noack et al. 2012).

To further investigate the maintenance of the $\Delta\Psi_m$, we applied two inhibitors of the respiratory chain complexes to cells loaded with TMRM. Firstly, oligomycin was applied to cells to block the ATP synthase. Any loss of $\Delta\Psi_m$ would indicate that the gradient across the IMM was in part maintained by the movement of protons across the ATP synthase out of the mitochondrial cytoplasm. Secondly, rotenone was applied to cells to inhibit complex I, to identify how much of the $\Delta\Psi_m$ is maintained by complex I.

The reduced $\Delta\Psi_m$ observed in the *ND5* mutant fibroblasts (P1) was not reduced any further following the addition of oligomycin, suggesting no compensation from the ATP synthase to maintain a 89.3% $\Delta\Psi_m$ (Figure 22A). In addition, the decrease in $\Delta\Psi_m$ upon addition of rotenone did not vary from control cells, suggesting that the functioning of complex I to maintain the $\Delta\Psi_m$ is not affected by the mutation in these fibroblasts.

In the tRNA leucine mutant fibroblasts (P2) an increase in $\Delta\Psi_m$ occurred after inhibition of the ATP synthase (Figure 22B). Upon repeating this three times, the extent of the increase was found to vary from a modest increase to a very large increase (depicted in

the large error bars) therefore did not reach statistical significance. Considering the significantly lower $\Delta\Psi_m$ under basal conditions, one possible hypothesis for seeing an increase at all in $\Delta\Psi_m$ with oligomycin could be an overactive ATP synthase, causing a greater influx of protons which lowers the $\Delta\Psi_m$ but causes it to polarize when the ATP synthase is inhibited. Moreover, an increase in $\Delta\Psi_m$ after inhibition of the ATP synthase can also occur due to an increased efflux of protons across the respiratory chain. Application of rotenone to the patient cells had the same effect as seen in control cells.

The $\Delta\Psi_m$ of tRNA lysine mutant fibroblasts (P3, P4) showed a tendency to lower slightly upon inhibition of the ATP synthase (Figure 22C, 22D). Both lines containing the same mutation exhibited a rapid loss of $\Delta\Psi_m$ compared to control upon addition of rotenone, which could suggest a greater dependency on complex I for maintenance of $\Delta\Psi_m$, however this data alone is not enough to confirm this. The tRNA serine mutants (P5, P6) showed no difference to control upon addition of oligomycin, or in the loss of $\Delta\Psi_m$ in response to rotenone (Figure 22E, 22F). In these four tRNA mutants, it was encouraging to see similar responses to these compounds between different lines containing the same tRNA mutation.

Upon addition of oligomycin to the ATP6 mutant fibroblast line (P7), the $\Delta\Psi_m$ showed no increase, which suggests a small compensation from the movement of protons out of the mitochondrial matrix via the ATP synthase (Figure 22G).

The data shown in Figures 21 and 22 is an indication of the heterogeneity of these patient cases, and it is particularly interesting that despite significantly a reduced membrane potential being observed in several of the patient lines, the mutant mtDNA is maintained.

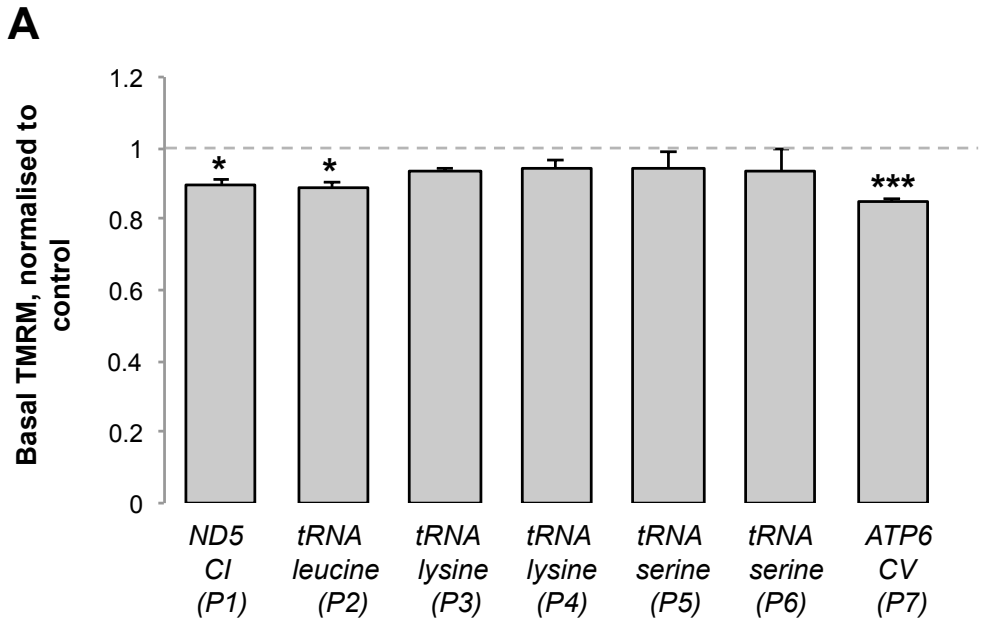

Figure 21: Mitochondrial membrane potential basal measurement in mtDNA disease patient fibroblasts

Histograms represent mean TMRM intensity measured by live cell imaging as an indicator of mitochondrial membrane potential. Data was averaged across three independent experiments and normalized to the average results from two healthy control fibroblasts. Error bars represent SEM, *n* = 3, two-tailed Student *t*-test * $p < 0.05$, *** $p < 0.005$.

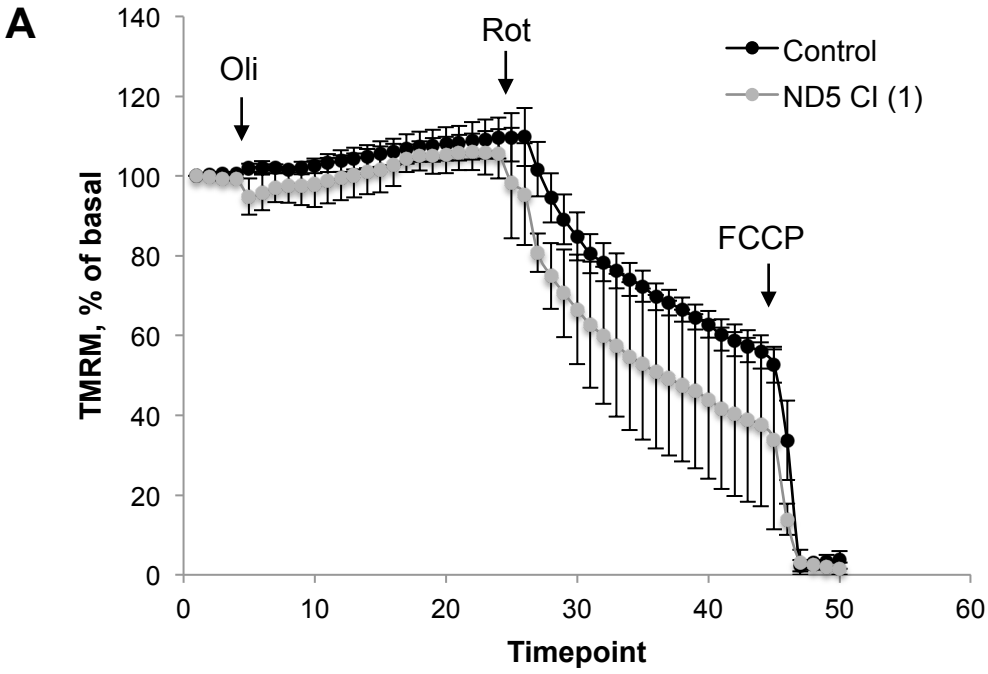

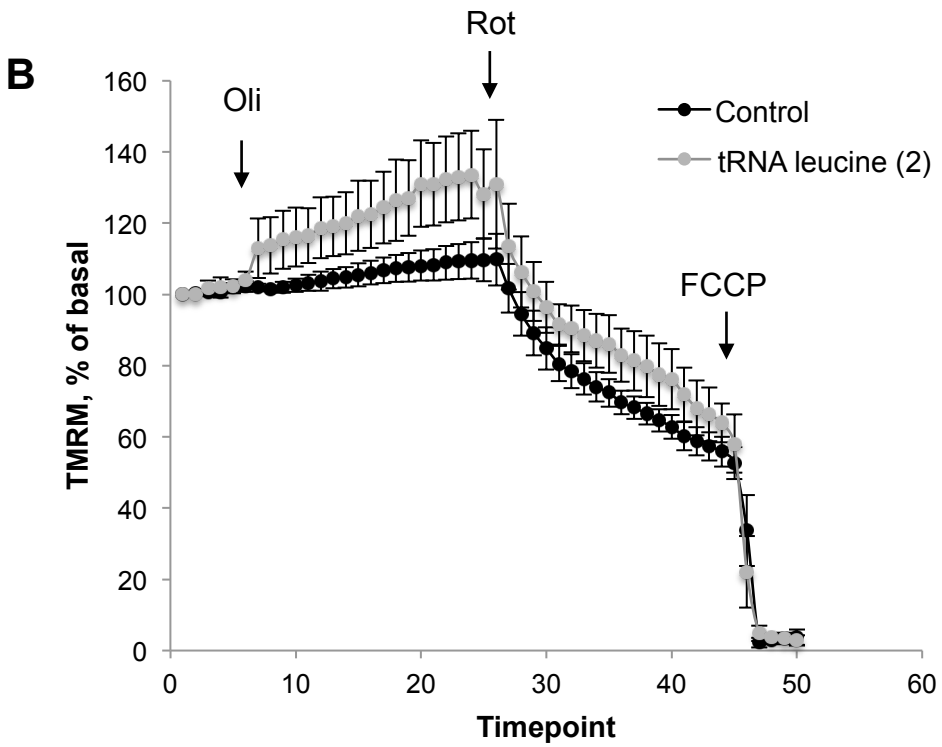
B
Rot
Oli
Control
tRNA leucine (2)
FCCP
TMRM, % of basal
160
140
120
100
80
60
40
20
0
0
10
20
30
40
50
60
Timepoint

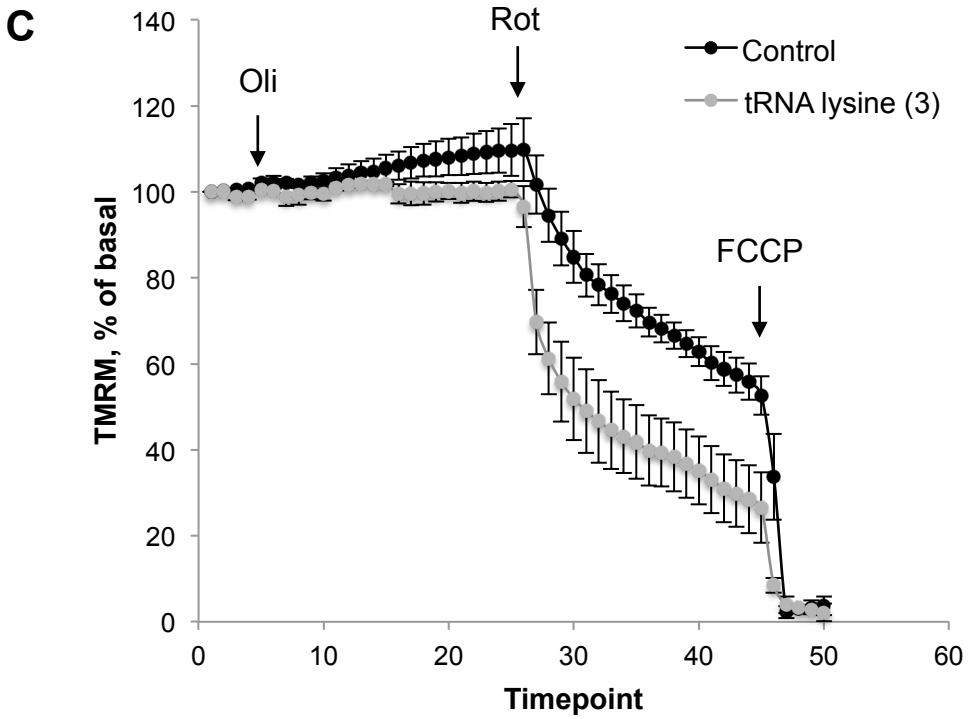
C
Oli
Rot
FCCP
Control
tRNA lysine (3)
TMRM, % of basal
Timepoint
0
20
40
60
80
100
120
140
0
10
20
30
40
50
60

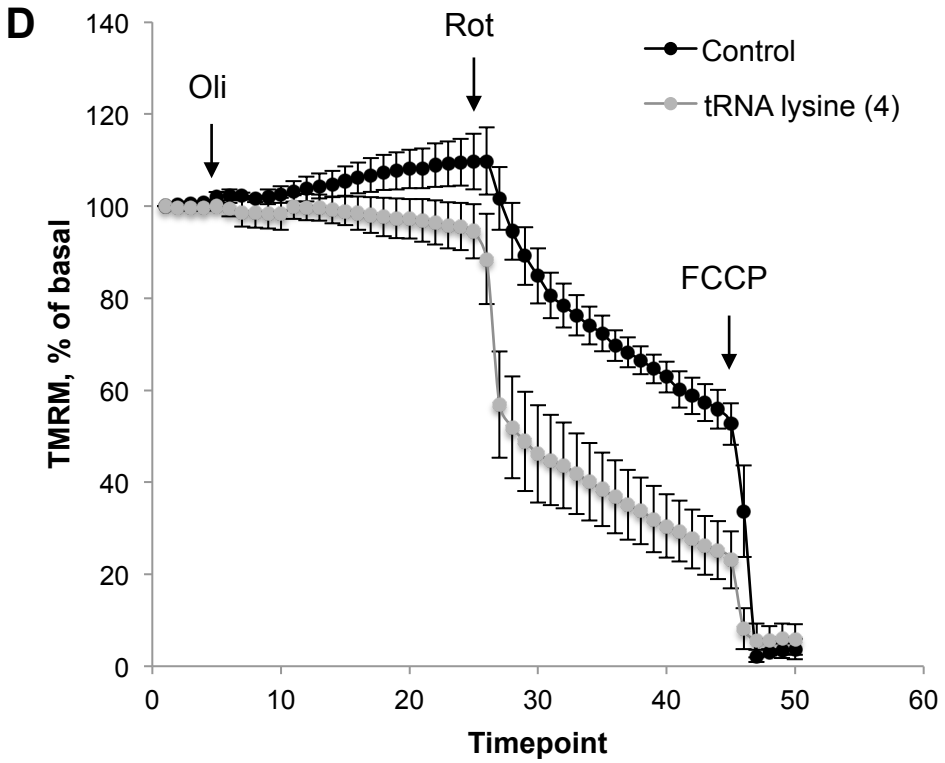
D
Oli
Rot
FCCP
Control
tRNA lysine (4)
TMRM, % of basal
Timepoint
0
20
40
60
80
100
120
140
0
10
20
30
40
50
60

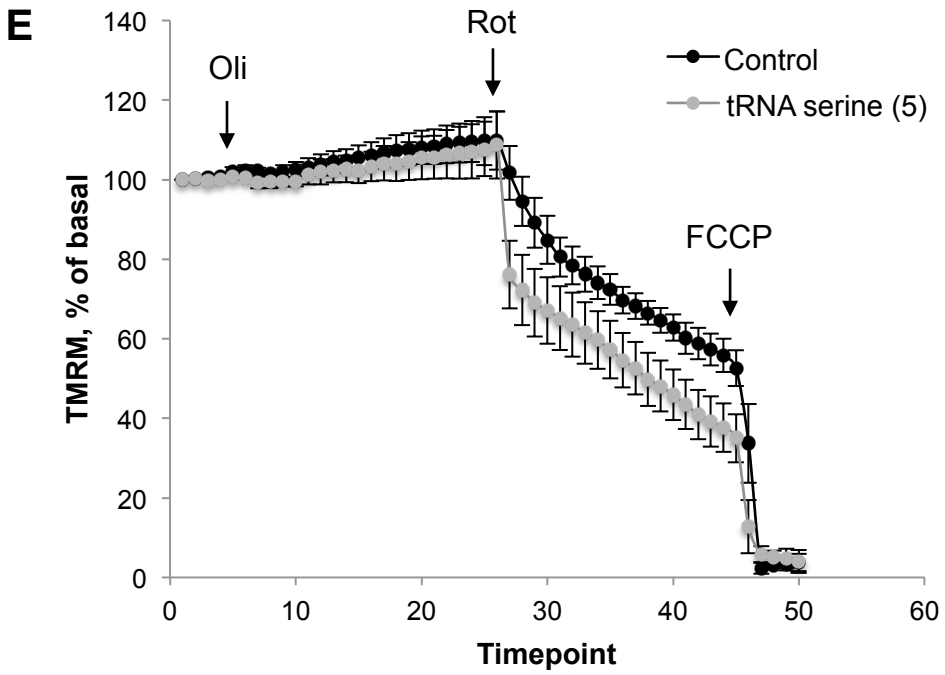
E
Oli
Rot
FCCP
Control
tRNA serine (5)
TMRM, % of basal
Timepoint
0
20
40
60
80
100
120
140
0
10
20
30
40
50
60

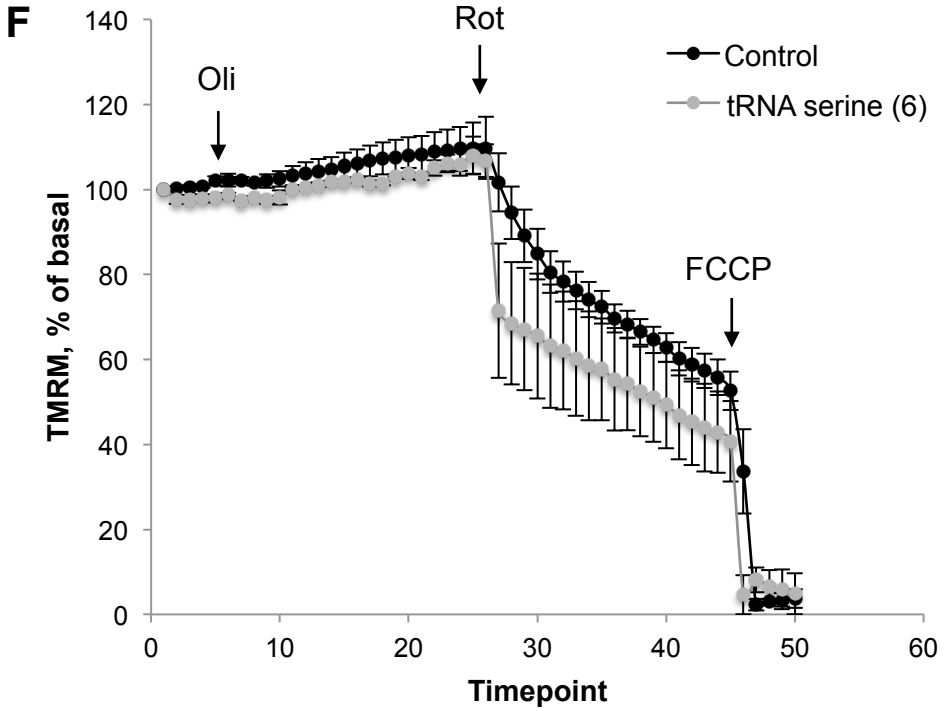
F
Oli
Rot
FCCP
Control
tRNA serine (6)
TMRM, % of basal
Timepoint
0
20
40
60
80
100
120
140
0
10
20
30
40
50
60

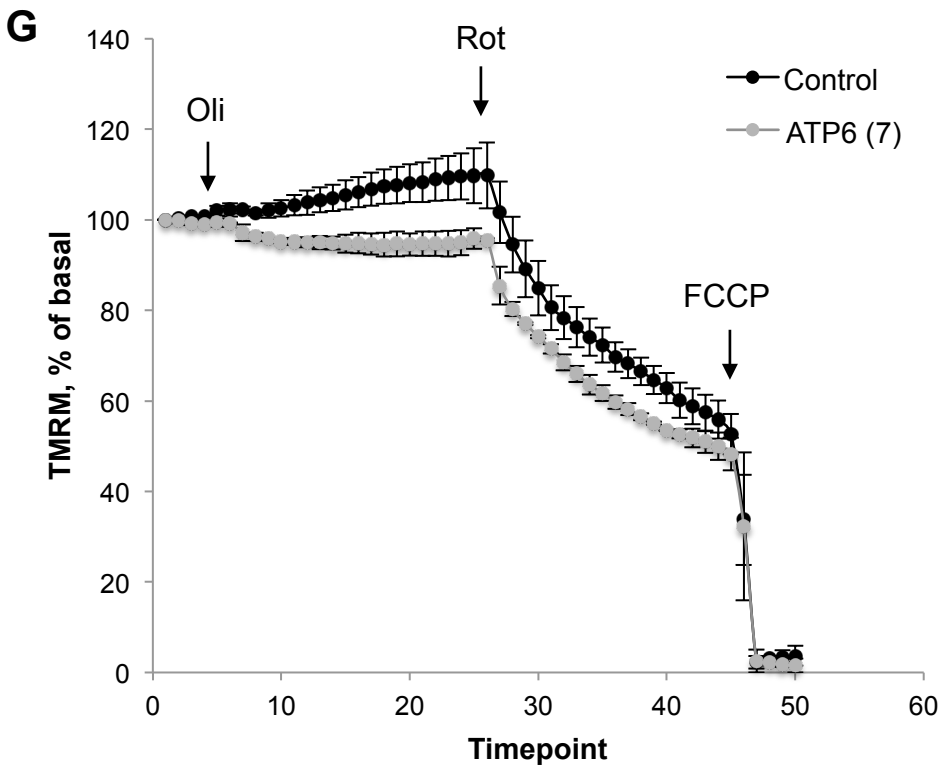

Figure 22: Maintenance of mitochondrial membrane potential

A-G Mitochondrial membrane potential, depicted as % of basal TMRM, in patient (*n*=3; grey) and control (*n*=4; black) fibroblasts. The gene in which each patient has the mtDNA mutation is stated in the key for each figure, along with the patient number (corresponding to table 15) in brackets. Data points represent mean TMRM intensity ± SEM. 2 µM Oligomycin was added to fibroblasts at timepoint 6, 2 µM Rotenone added at timepoint 26 and 5 µM FCCP added at timepoint 46.

2.2.3 Mitochondrial dynamics in cultured mtDNA disease patient fibroblasts

Mitochondria are highly dynamic organelles, continuously joining and dividing by processes of fusion and fission, respectively. These processes regulate the quality of the mitochondrial pool by enabling segregation of damaged mitochondria to be eliminated by mitophagy (Twig, Elorza, Anthony J A Molina, et al. 2008b). Mitofusins 1 and 2 (MFN1 and MFN2) are outer mitochondrial

membrane proteins that facilitate the process of fusion, and are ubiquitinated in a PINK1/Parkin-dependent manner upon loss of membrane potential to enable isolation of damaged mitochondria (Ishihara et al. 2004; Matthew E. Gegg et al. 2010).

On assessment of mitochondrial volume, it was found that the three patients which exhibited significantly lower $\Delta\Psi_m$ (P1, P2 and P7) all also had significantly lower mitochondrial volume in comparison to control fibroblasts Figure 23). This may suggest that the lower ΔΨm is triggering more mitophagy in these cells. However, identification of mitophagy in fibroblasts is particularly challenging and it has been suggested previously that overexpression of Parkin is required (Rakovic, Shurkewitsch, Seibler, Grünewald, et al. 2013). The method for data analysis of mitochondrial volume per cell is explained in the methods section under 'Mitochondrial network analysis'.

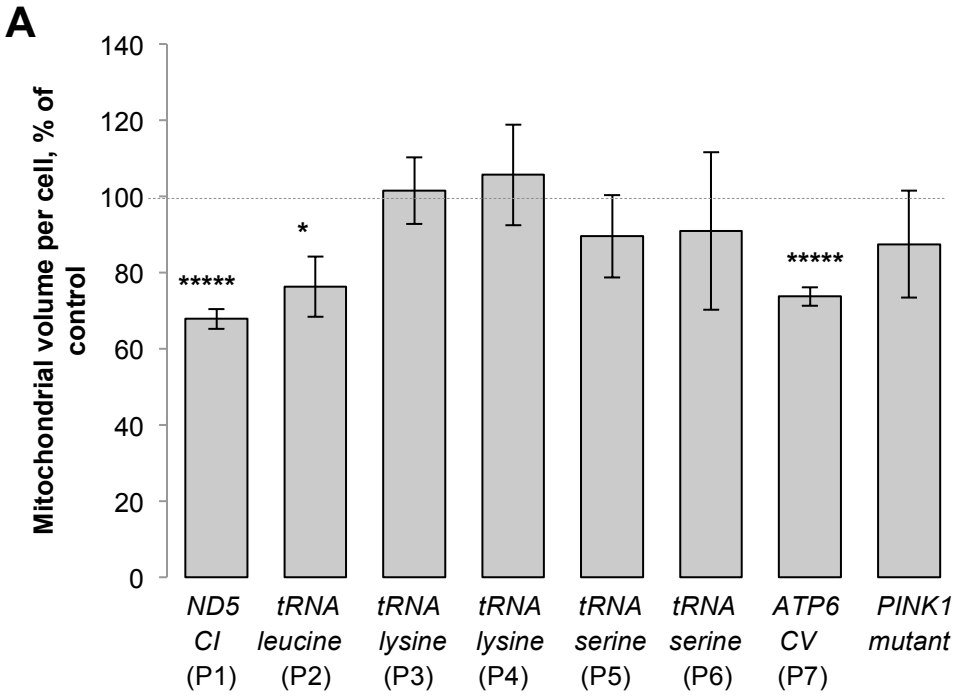

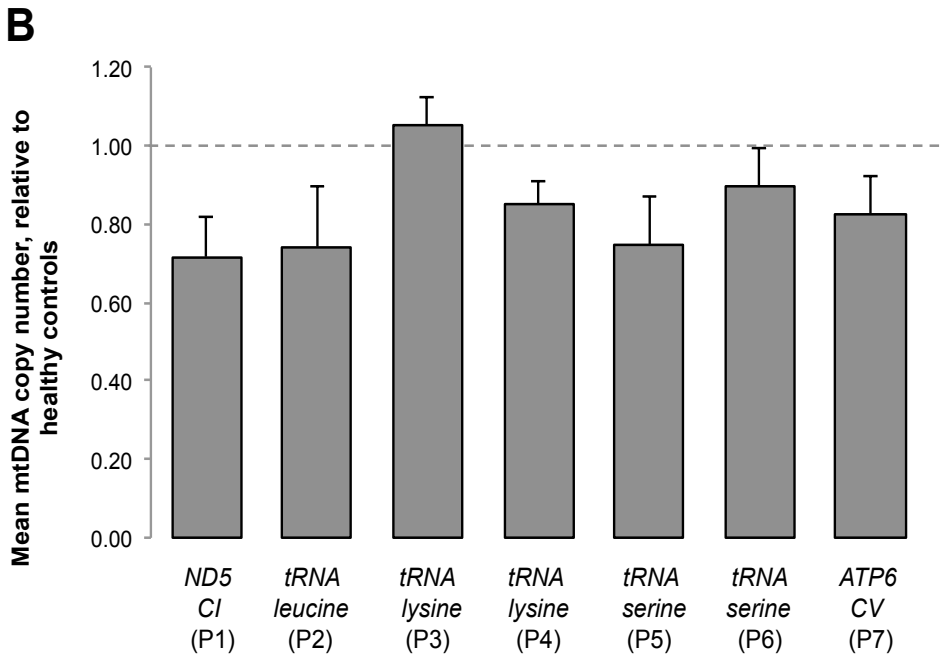

Figure 23: Mitochondrial volume and mtDNA copy number in mtDNA disease patient fibroblasts

A Histograms represent mean mitochondrial volume per cell, compared to control (dotted line), measured by z-stack imaging in live cells. Cells were loaded with MitoTracker and the area of mitochondrial signal calculated and summed across the depth of the z-stack. Mitochondrial volume was normalized to cell number by counting cell nuclei. Error bars represent SEM, *n*=3; two-tailed Student *t*-test * $p < 0.05$, ***** $p < 0.0005$. B Histograms represent mean mtDNA copy number relative to an average of two healthy controls (dotted line), measured by qPCR. The *ND1* gene was used for mtDNA and the *Human globulin* (HGB) was used for gDNA. Error bars represent SEM, *n*=3.

A PINK1/Parkin-dependent process indicative of mitophagy is the ubiquitination of mitofusins which is completely inhibited in PINK1 and Parkin mutant fibroblasts (Rakovic et al. 2011). MtDNA mutant fibroblasts were therefore stimulated with CCCP and ubiquitination of mitofusin 1 and mitofusin 2 quantified in order to identify impairments to this process. The most striking effect was found in the tRNA serine mutants (P5 and P6), whereby there was a highly significant reduction in the amount of ubiquitinated mitofusins found in both patients (Figure 24 A-D). This was particularly interesting,

as this effect has not been reported in fibroblasts other than PINK1 and Parkin mutants. These data suggest potential defects in the mitophagy process when stimulated with CCCP, but in this cell type do not appear to affect mitochondrial volume cell. However assessment of PINK1 homozygous mutant fibroblasts also did not have a significantly altered mitochondrial volume. Significant reductions in ubiquitinated mitofusins, compared to control fibroblasts, were found in all patient lines except for the *ATP6* mutant (P7), in which ubiquitination of mitofusin 1 and mitofusin 2 was consistently no different to controls (Figure 24 A-D).

Upon quantification of endogenous mitofusin protein levels, only the tRNA lysine mutants appeared to have any significantly lower levels compared to controls (Figure 24E).

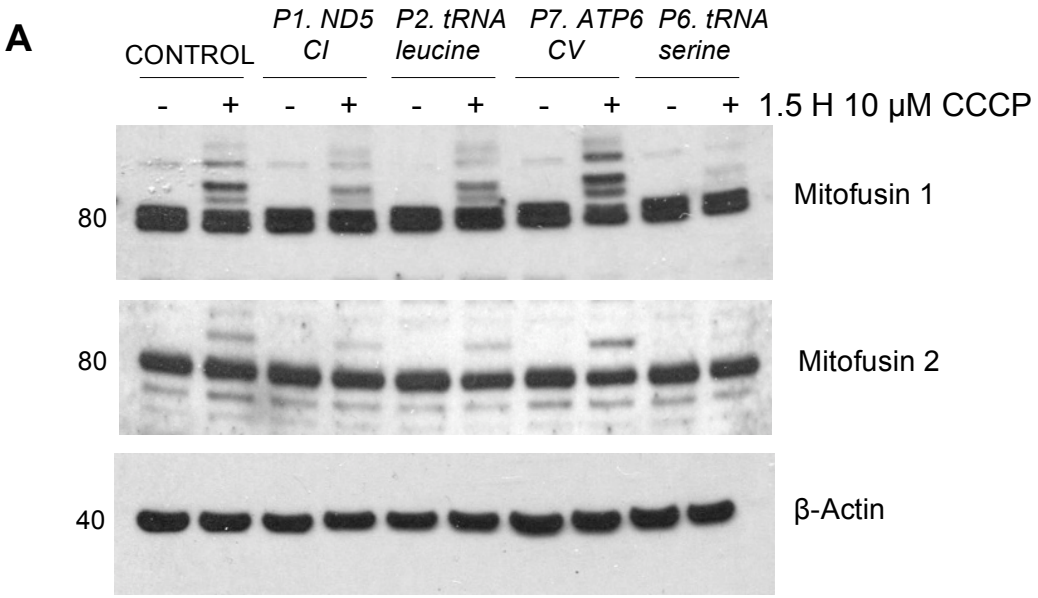

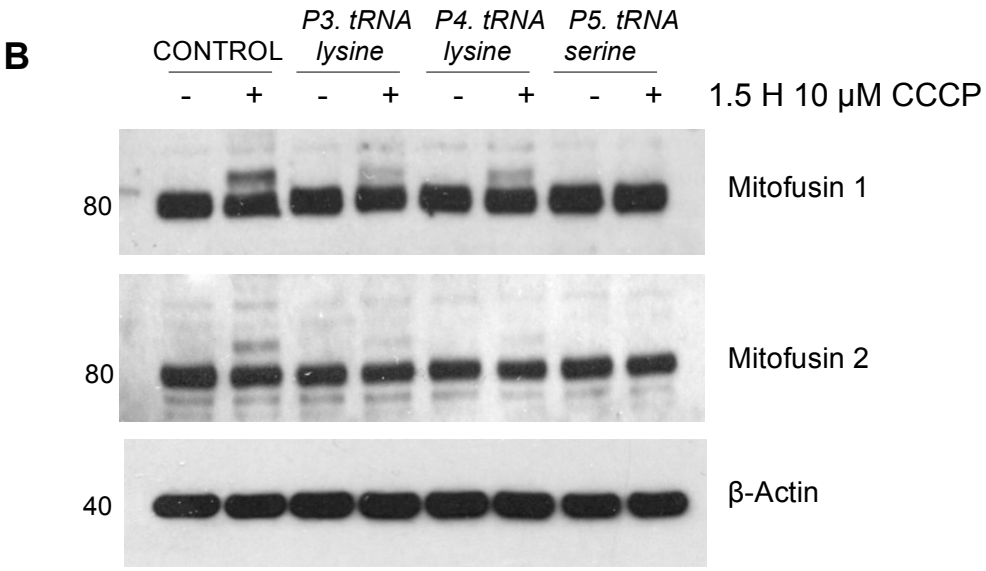
B
CONTROL
P3. tRNA lysine
P4. tRNA lysine
P5. tRNA serine
- + - + - + - +
1.5 H 10 μM CCCP
80
Mitofusin 1
80
Mitofusin 2
40
β-Actin

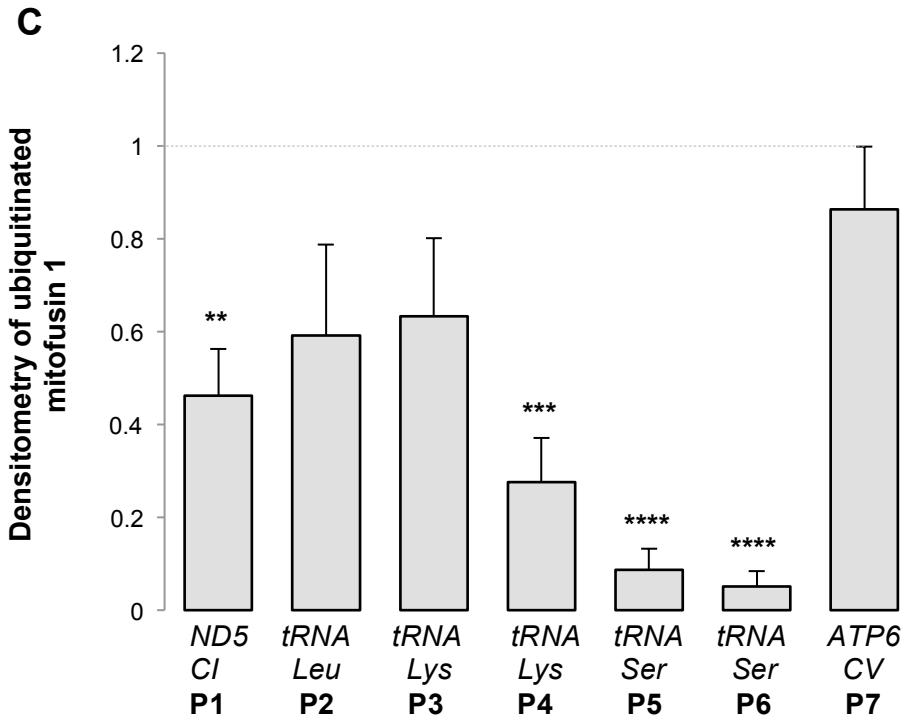
C
Densitometry of ubiquitinated mitofusin 1
1.2
1
0.8
0.6
0.4
0.2
0
**
***
****
****
ND5 CI P1
tRNA Leu P2
tRNA Lys P3
tRNA Lys P4
tRNA Ser P5
tRNA Ser P6
ATP6 CV P7

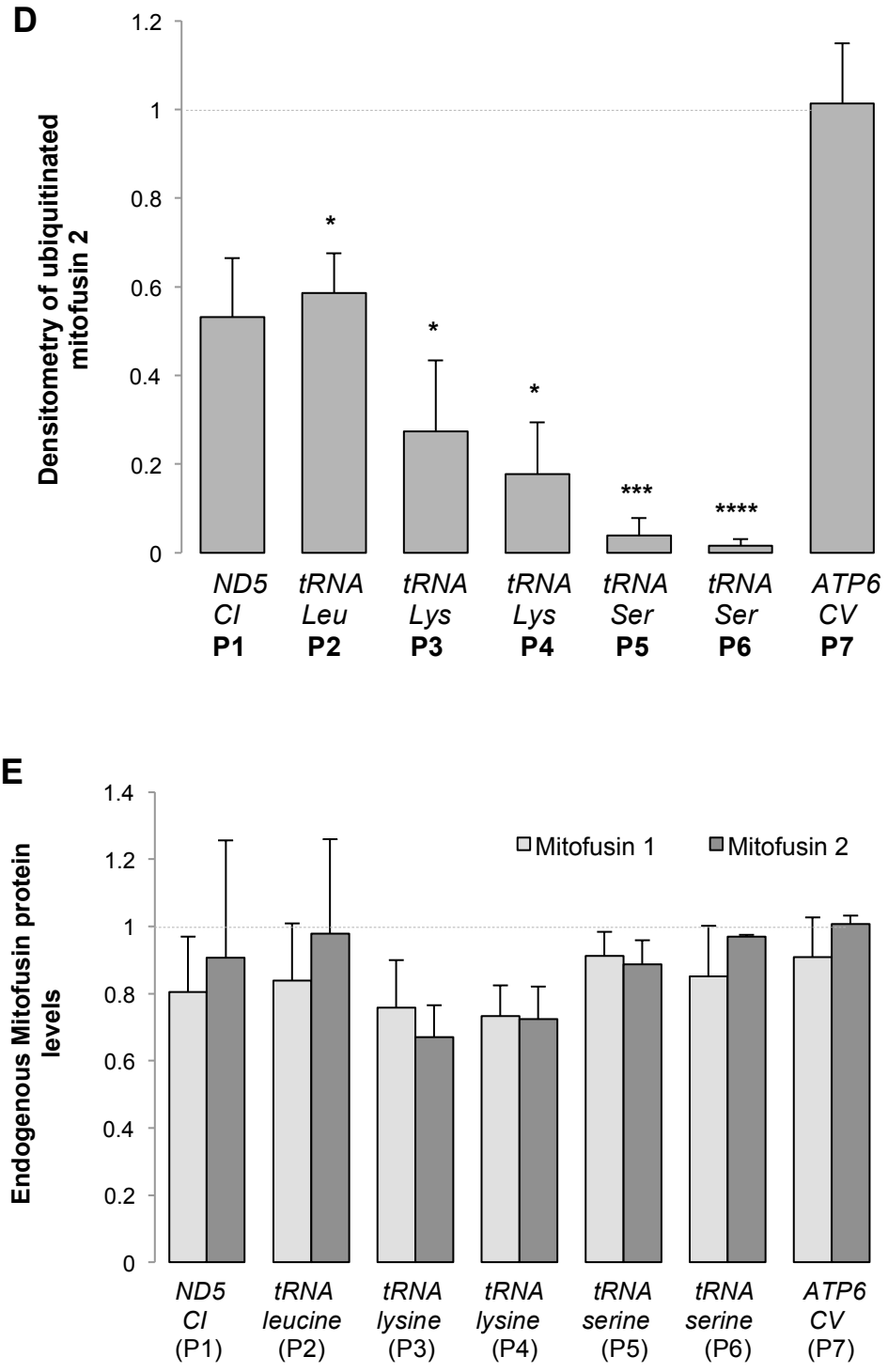

Figure 24: Ubiquitination of mitofusins in stressed mtDNA patient fibroblasts

A, B Representative immunoblots to show mitofusin1 and mitofusin2 ubiquitination following treatment with 10 μM CCCP for 1.5 hours. Loading control shown using housekeeping gene β-Actin. C, D Quantification of ubiquitinated mitofusin 1 and mitofusin 2 in response to 1.5 hours 10 μM CCCP, normalised to loading control (β-Actin) and presented relative to

healthy control (dotted line). Error bars represent SEM; mitofusin 1 (C): *n*=3; mitofusin 2 (D): *n*=2; two-tailed Student *t*-test * $p < 0.05$, ** $p < 0.01$, *** $p < 0.005$, **** $p < 0.001$. E Histograms represent the mean endogenous protein levels of mitofusin 1 and mitofusin 2 as assessed by immunoblot, normalised to loading control (β-Actin) and presented relative to healthy control. Error bars represent SEM, n = 3 (mitofusin 1), n = 2 (mitofusin 2).

2.2.4 Similarities in EM imaging and Complex I activity in tRNA Serine mutants and PINK1 mutant fibroblasts

The highly significant impairment of mitofusin ubiquitination in the tRNA serine mutants lead to further investigation into whether there were other similarities between these cells and PINK1 mutant fibroblasts.

Studies in PINK1 mutant drosophila have shown that defective mitochondria cause endoplasmic reticulum (ER) stress signalling and an increase in mitochondria-ER contact points is identified in PINK1 mutant flies and also PINK1 mutant fibroblasts (Celardo et al. 2016). Here it was found that mitochondrial-ER contact points were also increased in both tRNA serine mutant fibroblast lines, to the same significance as that seen in PINK1 mutant fibroblasts (Figure 25 A,B). Further analysis of mitochondrial morphology revealed a significant reduction in mitochondrial length, which was not observed in the PINK1 mutant fibroblasts but occurred in both tRNA serine mutant lines, suggesting greater fragmentation of the mitochondrial network (Figure 25C).

As well as its involvement in mitophagy, PINK1 has been implicated in the functioning of complex I activity. Complex I deficiency is implicated in Parkinson's Disease pathology and has been reported in PINK1 mutant models (Schapira et al. 1990; Morais et al. 2009; Deas et al. 2009). It is believed that the role of PINK1 in regulating complex I activity is independent of its role in the mitophagy pathway (Pogson et al. 2014). Using a complex I activity assay on

whole cell lysates, it was found that the tRNA serine mutant fibroblasts also exhibited a reduction in complex I activity, similar to PINK1 mutant fibroblasts (Figure 25D).

A

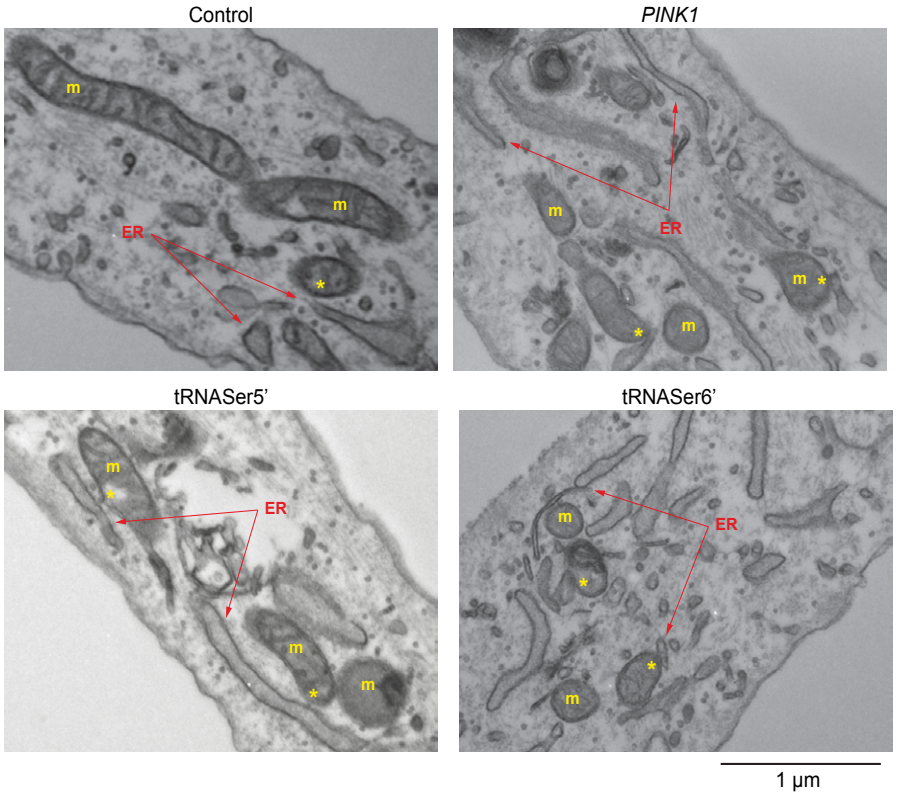

B

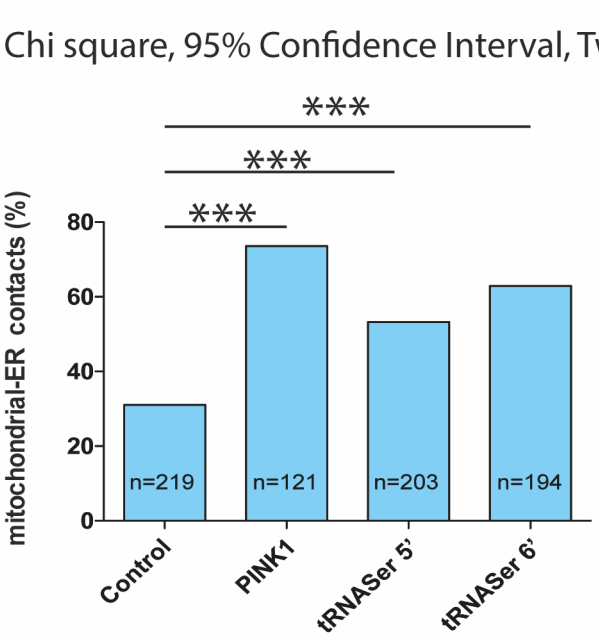

C

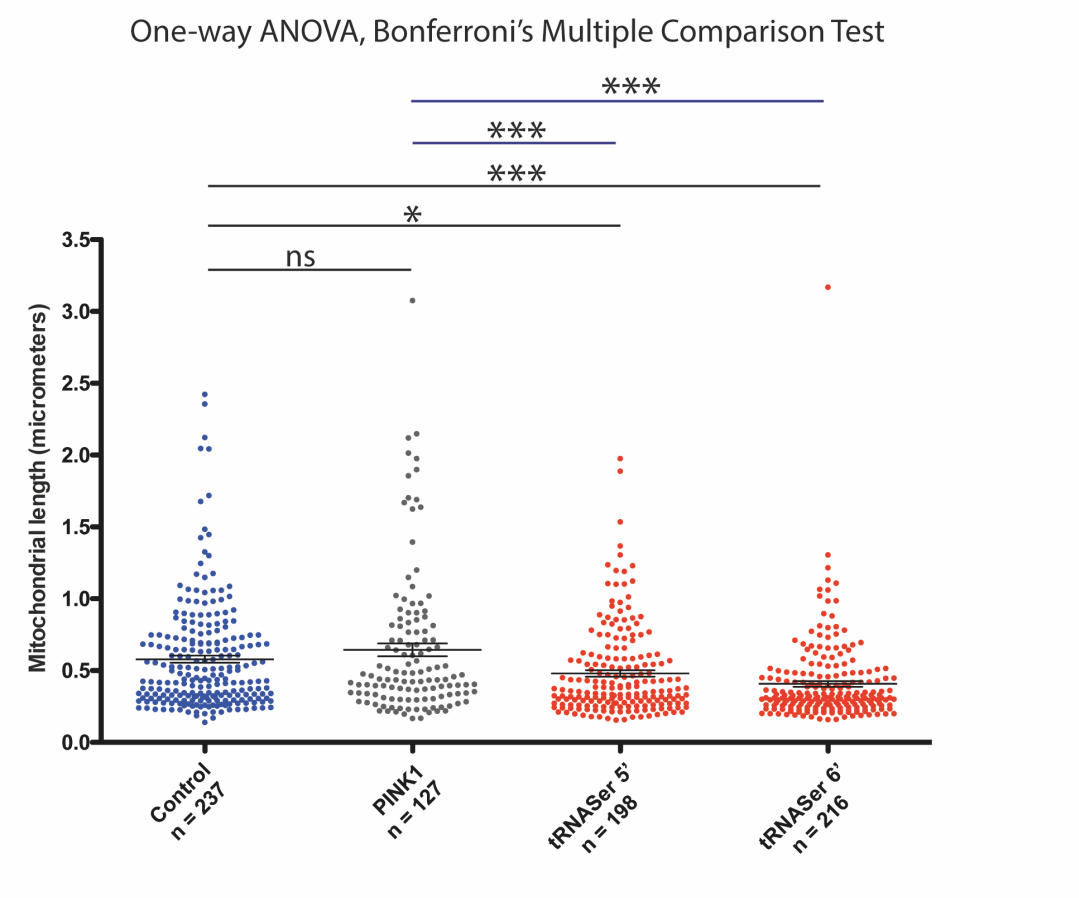

D

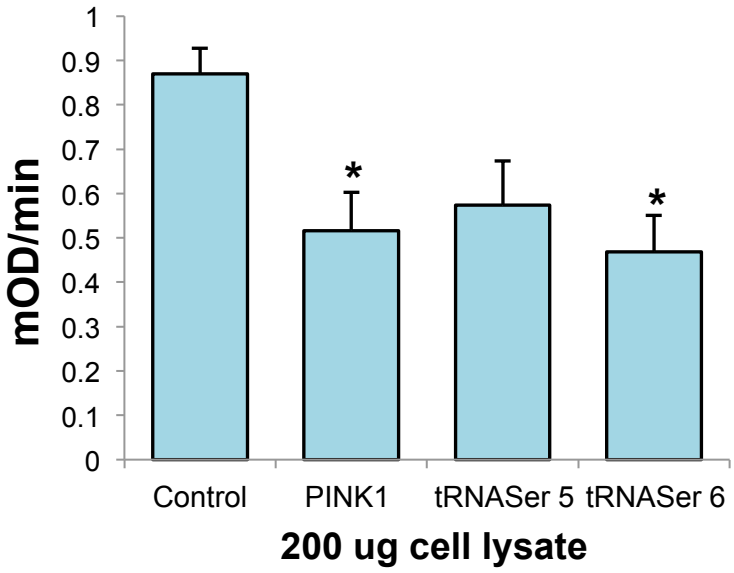

Figure 25: tRNA serine mutants and PINK1 homozygous mutant, comparison of morphology and function

A Representative EM images showing mitochondrial length and mitochondrial-ER contact. M in yellow indicates identified mitochondria, ER

in red indicates identified endoplasmic reticulum, and yellow stars indicate points of contact between mitochondria and ER. B Histogram showing the amount of mitochondria in contact with ER, represented as % of total mitochondria. Respective numbers of mitochondria are displayed on the histogram. C Scattergraph to show the respective lengths of mitochondria counted from EM images. D Histogram representing the Complex I activity measured from 200 ug of cell lysate. Error bars represent SEM, *n* = 3; two-tailed Student *t*-test * *p* < 0.05.

2.2.5 PINK1, Parkin and mitochondrial biogenesis in mtDNA disease patient fibroblasts

It has been suggested that activating mitophagy could have a therapeutic role in eliminating mitochondria containing the highest load of mutant mtDNA, especially in the modulation of heteroplasmy (Villanueva Paz et al. 2015). Overexpression of Parkin in a heteroplasmic cybrid model containing deleterious COXI mutations was found to stimulate the selective removal of mutant mitochondria, and functionally restore cytochrome *c* oxidase activity (Suen et al. 2010). Similarly, Parkin was identified as a modulator of heteroplasmy *in vivo* also, which lead us to postulate whether endogenous levels of Parkin were lower in the mutant fibroblasts which exhibited reduced mitofusin ubiquitination (Valenci et al. 2015). However, upon assessment of protein levels by immunoblotting, endogenous Parkin levels were found to be highly variable between mutant fibroblasts, as well as healthy controls (Figure 26). Significance of the patient data was not assessed due to the variation in the controls within the same experiment.

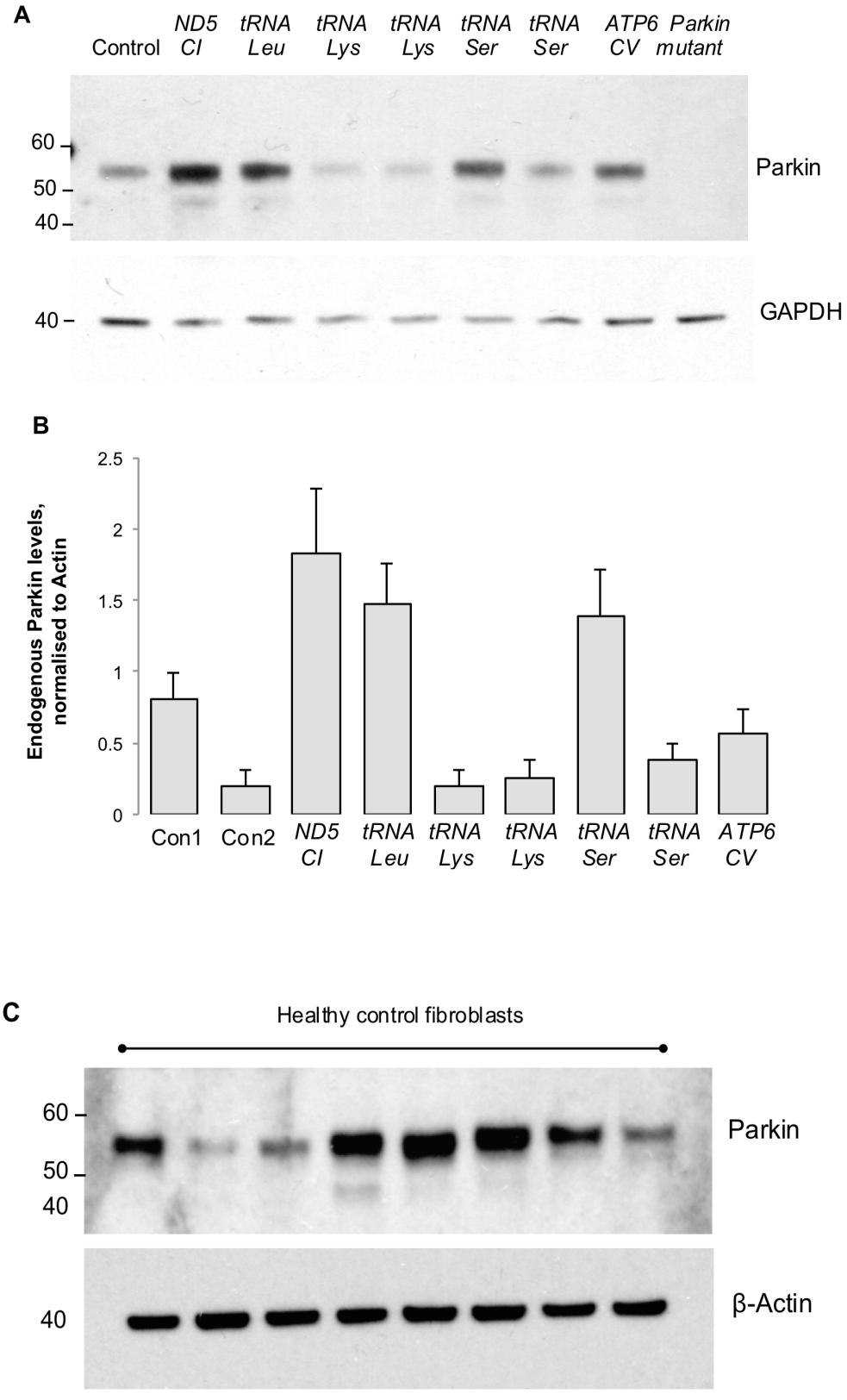

Figure 26: Endogenous Parkin levels in mtDNA patient fibroblasts and healthy controls

A Representative immunoblot showing endogenous Parkin protein expression. B Quantification of endogenous Parkin levels. Histograms represent mean Parkin normalised to β-Actin, error bars represent SEM, *n* = 3. C Representative immunoblot showing the endogenous Parkin levels in 8 control fibroblast lines

Mitophagy has been suggested as a potential therapeutic target for mitochondrial disease, however whether or not the quality control process is impaired in these diseases remains unknown. Due to unavailability of working antibodies for Western blotting or immunocytochemistry, PINK1 expression was assessed by RT-PCR and found under basal conditions that there was significantly lower expression in in three of the tRNA mutant fibroblast lines (P3, P4 and P5) (Figure 27A).

Since the pool of mitochondria present in cells is regulated by mitochondrial biogenesis as well as mitophagy, the expression of PGC-1α, an important regulator of biogenesis was investigated, upon depolarisation of mitochondria. MRNA analysis revealed a consistent decrease in PGC-1α expression upon depolarisation in healthy control fibroblasts compared to untreated cells, suggesting a down-regulation of biogenesis when mitophagy is stimulated. A decrease was consistently observed in the *ND5* (P1) and *ATP6* (P7) mutants; however in all fibroblasts containing a mutation in a tRNA gene (P2, P3, P4, P5, P6), biogenesis appeared to be upregulated (Figure 27B).

Whilst the extent of upregulation was variable, no decreases in PGC-1α expression were observed in the depolarised tRNA mutants (P2, P3, P4, P5, P6), suggesting an alternative response to depolarisation compared to healthy cells. Interestingly, significant upregulation of PGC-1α has been previously identified in PINK1-mutant IPSCs stimulated by depolarisation, believed to be a compensatory response to impaired degradation of depolarised

mitochondria (Seibler et al. 2011). Combined with the reduced mitofusin ubiquitination identified in the tRNA mutant fibroblasts in particular, these data implicate an impairment of mitophagy that is compensated for by stimulation of biogenesis upon depolarisation. It has been reported previously in studies using muscle, that PGC-1α has a role in buffering of oxidative stress, which in its absence can induce transcription of PINK1 and LC3 genes, and consequently stimulate mitophagy (Baldelli et al. 2014). *In vivo* studies have suggested that PGC-1α may have a protective role against excessive mitophagy; it has been shown using a mouse hindlimb immobilization and remobilization model that PGC-1α attenuated ubiquitination and degradation of mitofusin 2 (Kang & Ji 2016).

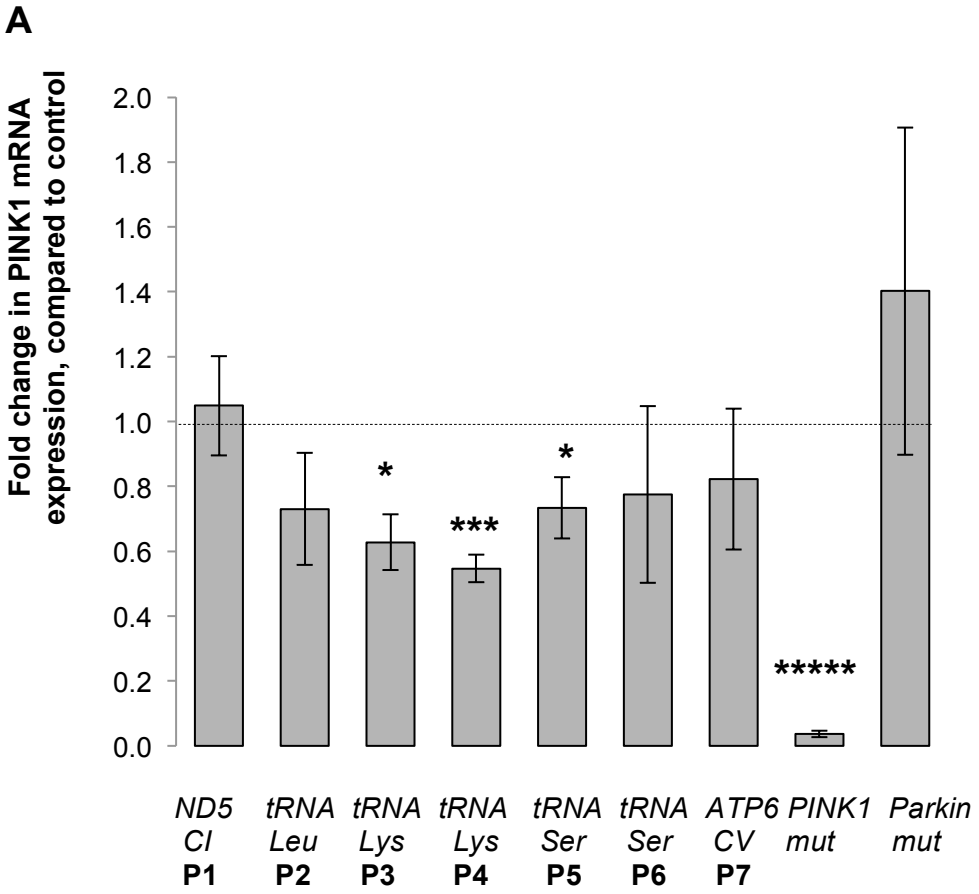

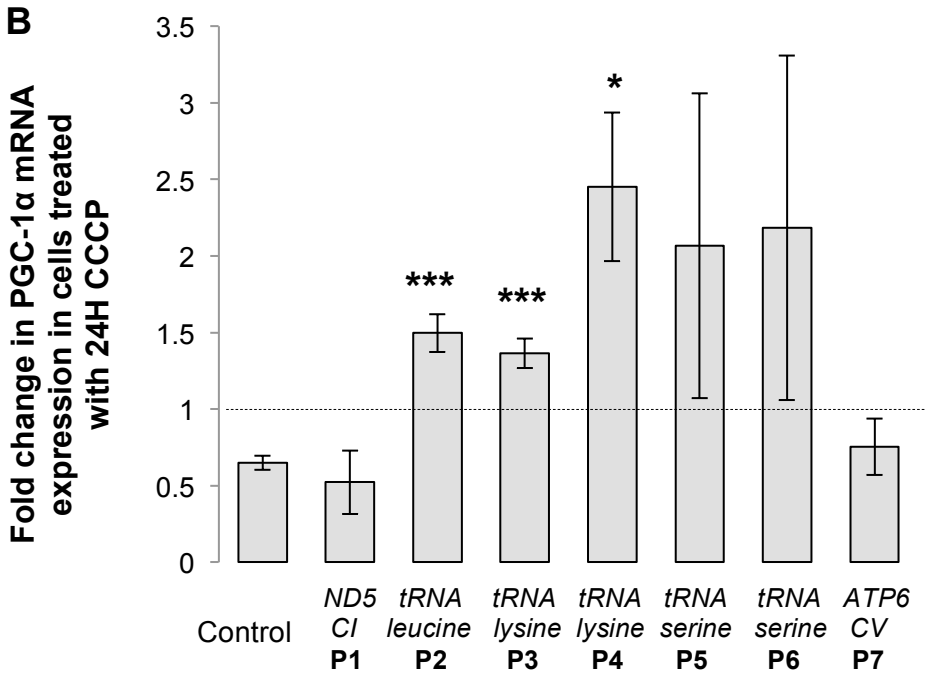

Figure 27: mRNA expression of PINK1 and PGC1α in mtDNA disease patient fibroblasts

A Histogram showing the mean fold change in mRNA expression of endogenous PINK1, compared to control. Dotted line represents control mRNA expression. Error bars represent SEM, *n* = 3; two-tailed Student *t*-test * $p < 0.05$, *** $p < 0.005$, ***** $p < 0.0005$. B Histogram showing the mean fold change in mRNA expression of PGC-1α after 12 hours 10 μM CCCP treatment, compared to DMSO treatment. Dotted line represents mRNA expression in untreated cells. Error bars represent SEM, *n* = 3; two-tailed Student *t*-test * $p < 0.05$, *** $p < 0.005$.

2.3 Discussion

2.3.1 Mitochondrial dynamics in mtDNA disease patient fibroblasts

Studying mitochondrial dynamics in fibroblasts derived from patients with primary mitochondrial diseases revealed only minor differences in some of the fibroblast lines, suggesting that under basal conditions mtDNA patient fibroblasts show only slight phenotype. Mitochondrial membrane potential was significantly reduced in three of the patient lines (Complex I mutant, tRNA leucine mutant and the ATP6 mutant) but, whilst consistent, to no less than 80% of the potential maintained in control fibroblasts. Furthermore the addition of oligomycin and rotenone did not reveal compensatory mechanisms being utilised by the cells to maintain membrane potential. In the same fibroblast lines that exhibited reduced mitochondrial membrane potential, a significant reduction in mitochondrial volume, as measured by live cell imaging, was observed. The tRNA lysine and tRNA serine mutants (of which there are two patients with each mutation) all displayed no significant loss of membrane potential, and the mitochondrial volume was found to be no different to control. Mitochondrial membrane potential and mitochondrial volume data was collected by confocal imaging and data analysed by taking an average measurement across the cells in the field of view when imaging. Therefore it could be speculated that the fibroblast lines with approximately 90% of the control membrane potential may contain some depolarised mitochondria, which would cause only a modest decrease in overall membrane potential in numerous cells, but those depolarised few would trigger mitophagy and cause the significantly lower mitochondrial volume.

Inducing mitochondrial stress to the fibroblasts enabled identification of mitofusin ubiquitination, a phenomenon thought to

occur due to the E3 ubiquitin ligase activity of Parkin. Upon loss of mitochondrial membrane potential caused by uncoupler CCCP, a reduction in ubiquitinated mitofusins was observed compared to control in all patient lines, except for the ATP6 mutant. The loss of ubiquitination in PINK1 and Parkin mutant fibroblasts is well-known, however has not been reported in other cells containing different mutations (Rakovic et al. 2011). The tRNA serine mutation appeared to cause the most significant loss of ubiquitinated mitofusin, in both patient lines, and therefore these cells were used to identify other similarities between PD-associated mutants.

In collaboration with the University of Leicester, EM imaging was used to identify an increase in mitochondria-endoplasmic reticulum contacts, believed to occur via mitofusin bridges activating enhanced ER stress (Celardo et al. 2016). Using PINK1 mutant fibroblasts as a positive control, it was found that tRNA serine mutant fibroblasts also contained increased mito-ER contacts suggesting activation of ER stress. Furthermore, tRNA serine mutants exhibited reduced complex I activity in a similar manner to PINK1 mutant fibroblasts. These experiments have revealed phenotypic similarities between tRNA serine mutants and PINK1 mutants in three areas: complex I activity, ER stress signalling and ubiquitination of mitofusins.

Although Parkin has been implicated as a modulator of heteroplasmy and therefore is of great interest in the mtDNA disease field, endogenous Parkin protein levels were found to be widely variable even in healthy controls. It was not possible to find specific Parkin primers to investigate mRNA expression by QPCR, however this technique was used to study the expression of PINK1 and PGC-1α. PINK1 mRNA expression was found to be significantly lower compared to controls in the two tRNA lysine fibroblast lines and one of the tRNA serine fibroblast lines. Most interesting was the change in mRNA expression of biogenesis regulator PGC-1α in

response to 12 hours CCCP treatment. Mitophagy and mitochondrial biogenesis are two tightly coordinated processes to enable efficient regulation of mitochondrial quality. Whilst the mechanism of their interaction remains largely unknown, it is thought that under physiological conditions, biogenesis is stimulated in response to mitophagy in order to maintain mitochondrial quantity, as well as quality (Palikaras & Tavernarakis 2014). In these experiments 10 μM CCCP was used to completely depolarise the entire mitochondrial network, causing a much greater level of mitochondrial stress than normal under physiological conditions. Interestingly, after 12 hours of CCCP treatment, mRNA expression of PGC-1α in control cells revealed a suppression of biogenesis in response to widespread activation of mitophagy. Presumably, under this great amount of mitochondrial stress the priority of the cell is to degrade the damaged mitochondria instead of producing more to prevent newly synthesised mitochondria being damaged by the production of ROS from the existing stressed mitochondria. This same response was seen in the complex I mutant fibroblasts and the ATP6 mutant fibroblasts, however none of the tRNA mutants appeared to trigger suppression of biogenesis but largely cause an upregulation in mRNA expression. If mitophagy were to be compromised in these lines, promoting biogenesis would be a likely compensatory mechanism in response to widespread mitochondrial damage. However, as will be discussed further in section 2.3.2, directly assessing mitophagy has proven difficult in mammalian cell cultures and measurement of mitochondrial volume/mass is often inconclusive, as shown in this data with PINK1 mutant fibroblasts which do not display increased quantities of mitochondria (figure 23A).

2.3.2 Assessing mitophagy in fibroblast models

2.3.2.1 Basal mitophagy or stress-induced mitophagy?

In these experiments, mtDNA disease patient derived fibroblasts displayed striking impairments to mitofusin ubiquitination upon exposure to mitochondrial uncoupler CCCP, but by comparison only modest variation in mitochondrial membrane potential or mitochondrial volume under basal conditions. A previous study, which utilised various mitochondrial disease cell lines, showed that contrary to reports in the literature, mitochondrial membrane potential was often not found to be reduced in mtDNA disease patient derived fibroblasts and that under basal conditions autophagy was increased in these lines but not mitophagy (Morán et al. 2014). However in another study by the same authors and same patients showed that OXPHOS deficiencies caused slower recovery of membrane potential compared to control cells upon induced mitochondrial depolarisation (Morán et al. 2010). These reports show that measurement of mitochondrial mass or detection of autophagic machinery is not sufficient to make conclusions about mitophagy, especially in unstressed cells.

The use of mitochondrial uncouplers enables easier detection of the response to damaged mitochondria, and is compatible with the use of biochemistry techniques such as Western blotting. Furthermore, fibroblasts are an unaffected cell type in these diseases, therefore whilst the mutation is present, cell stress may be required to assess its effect.

2.3.2.2 Can decreases in mitochondrial volume be detected?

In order to identify defects in selective PINK1/Parkin-mediated mitophagy, it is logical to look at PINK1 mutant and Parkin mutant fibroblasts derived from PD-patients as a positive control.

Data shown here and reported in the literature has shown that despite the lack of PINK1, either by the presence of a homozygous PINK1 PD-causing mutation or the generation of PINK1-KO of mouse embryonic fibroblast (MEF) lines, an increase in mitochondrial mass is not observed (Heeman et al. 2011). Therefore quantification of the basal mitochondrial network is not indicative of PINK1-dependent mitophagy impairments.

Studies in both mutant and control fibroblasts have shown however that cells containing endogenous protein levels of Parkin do not exhibit significant reductions in mitochondrial proteins upon depolarisation (Rakovic, Shurkewitsch, Seibler, Grünewald, et al. 2013). Despite it being difficult to find good commercial Parkin antibodies for Western blotting, this study used the separation of mitochondrial and cytosolic fractions to show translocation of Parkin to the mitochondria but found that from 3 hours post depolarisation, the presence of Parkin was reduced. Further investigation showed that in fibroblasts, endogenous Parkin is self-ubiquitinated and degraded so the loss of mitochondrial proteins cannot be detected despite the loss of membrane potential. When Parkin was overexpressed in primary fibroblasts, PINK1-dependent loss of mitochondrial proteins could be detected (Rakovic, Shurkewitsch, Seibler, Grünewald, et al. 2013).

Difficulties in identifying Parkin-mediated mitophagy in mammalian cell cultures is often blamed on the fact that most of our understanding of the mitophagy pathway comes from studies utilising potent mitochondrial uncouplers in Parkin overexpressed

non-neuronal immortalised cell lines. However, a study using both highly mitochondria-dependent cortical neurons and glycolytic HeLa cells, showed that overexpressing Parkin in neurons still does not cause translocation of Parkin to depolarised mitochondria, and that when normally glycolytic HeLa cells are forced to rely on mitochondrial respiration, Parkin translocation no longer occurs (Van Laar et al. 2011). These data show that manipulation of the mitophagy model may produce misleading and unhelpful data. Consequently, in these experiments, cells were not transfected with Parkin or cultured in galactose media to reduce their glycolytic nature.

2.3.2.3 What does mitofusin ubiquitination tell us?

In these experiments, a suitable Parkin antibody was obtained which was able to detect endogenous levels of protein in 30 µg protein lysates by Western blot. However this antibody was not sensitive enough to be able to detect translocation of Parkin to the mitochondria. Therefore to investigate PINK1/Parkin-dependent effects upon mitochondrial depolarisation in a non-over-expressed system, mitofusin ubiquitination was studied. Using PINK1 and Parkin mutant fibroblasts, both depolarisation of the mitochondrial membrane potential or exposure to H_2O_2 failed to induce ubiquitination of mitofusins in mutant fibroblasts unlike control fibroblasts (Rakovic et al. 2011). This provided a robust PINK1/Parkin-dependent assay to identify impairments in this process. Ubiquitination of outer mitochondrial membrane proteins mitofusins 1 and 2 is mediated by Parkin, which leads to enhanced turnover by proteasomal degradation (M. E. Gegg et al. 2010; Glauser et al. 2011). In addition to the use of fibroblasts with PINK1 and Parkin mutations, silencing of PINK1 or Parkin in SH-SY5Y cells was also found to cause significant reduction in the ubiquitination of mitofusins (M. E. Gegg et al. 2010). Ubiquitination

of mitofusins enables recruitment of ubiquitin-binding proteins, such as p62, to mediate elimination of damaged mitochondria via the autophagosome, and also prevents fusion of damaged mitochondria to the healthy mitochondrial network (Gegg & Schapira 2011).

The significant reduction of ubiquitinated mitofusins to almost completely absent in the tRNA serine mutant lines indicates impairment in an early event in the mitophagy process, and therefore is of interest as a previously undescribed phenotype in mtDNA diseases. Investigations into Parkinson's disease pathogenesis have hypothesised that the lack of mitofusin ubiquitination prevents clearance of mitochondria by the autophagosome system and enables damaged mitochondria to rejoin the mitochondrial network, causing persisting damage and a decline in mitochondria function (Abramov et al. 2011). It has been suggested that activation of mitophagy may play a therapeutic role in tissues such as muscle and neurons, which rely on efficient mitochondrial function (Abramov et al. 2011).

2.3.3 Similarities between tRNA serine mutants and PINK1 mutants

The observation of reduced mitofusin ubiquitination in several of the mtDNA disease patient fibroblast lines was unexpected, as this phenomenon has not been reported in mutations other than PINK1 and Parkin. Therefore investigating other phenotypes associated with PD pathogenesis was of interest. PINK1 deficiency has been reported to cause reduced complex I activity in PINK1(-/-) mice and pink(B9)-null mutant Drosophila (Morais et al. 2014). Furthermore, loss of complex I activity is a property of some Parkinson's disease model neurotoxins, e.g. rotenone (Dauer & Przedborski 2003). In addition to mtDNA disease caused by mutations in complex I, complex I deficiency has been associated with mutations in

ribosomal and transfer RNAs in the mitochondrial genome (Porcelli et al. 2016; Haack et al. 2012; Lax et al. 2013). The finding of reduced complex I activity, to similar levels seen in PINK1 mutants, in two fibroblast lines containing the same mutations that had a highly significant reduction in mitofusin ubiquitination, provides further evidence that PINK1 may not be functioning correctly in these lines. It has been reported that the complex I subunit NdufA10 is phosphorylated at Ser250 in a PINK1-dependent manner, and that phosphomimetic NdufA10 can rescue complex I activity but not mitophagy, suggesting that this function of PINK1 is independent of mitophagy (Morais et al. 2014; Pogson et al. 2014). Together, this data has shown impaired PINK1 function both under basal conditions and under stressed conditions, and impairments in two reportedly independent functions both dependent on PINK1.

In addition, the EM experiments in this chapter revealed similarities in the morphology of tRNA serine mutant cells to PINK1 mutant cells. Celardo et al., demonstrated by EM imaging that an increase in contact points between mitochondria and endoplasmic reticulum was a characteristic of PINK1 and Parkin mutant fibroblasts (Celardo et al. 2016). The contact between the endoplasmic reticulum and mitochondria is thought to be important for the function of the PINK1-Parkin pathway, with implications in neurodegeneration (Erpapazoglou & Corti 2015). Analysis of PARK2 mutations in fibroblasts derived from mice and PD patients revealed a closer mito-ER proximity compared to controls (Gautier et al. 2016). An increase in mito-ER contact was also identified by ultrastructural analysis of *pink1* and *parkin* mutant fly brains, and inhibition of PERK signalling was found to the neuroprotective even in the presence of damaged mitochondria (Celardo et al. 2016). This suggests that pharmacological intervention of PERK signalling may provide an alternative therapeutic target in mtDNA disease in which PINK1 activity is defective.

2.3.4 mtDNA disease and PD pathogenesis

The accumulation of deletions in the mitochondrial genome is a feature associated with aging, though studies in PD patients and age-matched controls found these to have a higher incidence in PD patients in various brain regions (Ikebe et al. 1990; Ozawa et al. 1990). The presence of parkinsonian features in mitochondrial disease however has only occasionally been observed, for example caused by a novel 12SrRNA point mutation or a cytochrome *b* gene deletion (Rana et al. 2000; Thyagarajan et al. 2000).
Parkinson's disease is considered the second most common neurodegenerative disease, and in an aging population, causes considerable strain on the health service. A substantial amount of research in academia and the pharmaceutical industry is focused on developing effective therapeutics for this disease. In contrast, as discussed in section 2.1.3, the heterogeneous nature of already rare mitochondrial diseases is a limiting factor in the development of disease therapeutics. As a result, the common features identified here between tRNA serine mutants and PD-causing PINK1 mutants may prove particularly beneficial in finding effective treatment for a subset of mtDNA disease patients more readily.

2.3.5 Biogenesis and mitophagy in mtDNA disease

A particularly interesting finding was the segregation of tRNA mutations and mutations in genes encoding for a subunit of a respiratory complex in the effect on biogenesis in response to mitochondrial stress. At the timepoint observed, when cells had been stressed with 10 μM CCCP, control fibroblasts and those with a mutation in a gene encoding a subunit of a respiratory complex repressed the expression of PGC-1α, a master regulator of mitochondrial biogenesis. In fibroblasts harbouring mutations in

tRNA genes, repression did not occur, and a significant upregulation of PGC-1α mRNA expression was activated.

A mouse model containing a proof-reading deficient form of mitochondrial DNA polymerase gamma, which causes mtDNA deletions in various tissues was found to exhibit activated mitochondrial biogenesis, thought to be a compensatory mechanism (Perier et al. 2013). More recently, mitochondrial biogenesis was found to be protective against neuronal degeneration through the overexpression of necdin, a stabiliser of endogenous PGC-1α (Hasegawa et al. 2016). As well as activating transcription for mitochondrial biogenesis, PGC-1α has been shown to promote the expression of antioxidant enzymes during differentiation to buffer oxidative stress, strengthening the hypothesis that activation of PGC-1α may be a compensatory mechanism utilised in stressed cells (Baldelli et al. 2014).

Interestingly, a study performed in atrophied muscle, a tissue type most commonly affected in mitochondrial disorders, showed that PGC-1α overexpression attenuated the ubiquitination and degradation of mitofusin 2, inhibiting the activation of mitophagy (Kang & Ji 2016). Moreover, in PINK1-mutant IPSC, after 12 hours of valinomycin, mRNA expression of PGC-1α was found to be significantly increased compared to untreated cells, despite there being no difference observed in the wild-type cells before and after valinomycin treatment (Seibler et al. 2011). These studies suggest that the activation of biogenesis observed in the tRNA mutant fibroblasts could be a compensatory mechanism, in line with the reduced ubiquitination of mitofusins upon stimulation of mitophagy. In cells with damaged mitochondria but defective mitophagy, expression of PGC-1α appears beneficial in order to attempt to maintain mitochondrial function by producing newly synthesised mitochondria and also for buffering of oxidative stress.

This effect was found to occur in the tRNA mutants but not the *ND5* or *ATP6* mutant fibroblasts, and it remains unknown as to why this occurred. A mutation in a mitochondrial tRNA gene is likely to affect the translation of all mitochondrial genes, and perhaps stimulation of PGC-1α is therefore more effective as a compensatory mechanism. The fibroblasts containing the *ATP6* mutation showed no impairment to mitofusin ubiquitination and as a result it is unsurprising that repression of PGC-1α occurred in the same manner as control fibroblasts. The *ND5* mutant fibroblasts showed significant reduction in mitofusin 1 to approximately 50% of control cells, but no significant reduction was observed in the ubiquitination of mitofusin 2. In contrast, two of the tRNA mutant lines showed significantly impaired ubiquitination of mitofusin 2, but not mitofusin1, and both of these displayed a highly significant increase in PGC-1α mRNA expression in response to CCCP, which could suggest a greater reliance of the ubiquitination of mitofusin 2 compared to mitofusin 1 in the mitophagy pathway. However, further investigation is required to understand these results.

2.3.6 Future perspectives

The data presented in this chapter have demonstrated novel phenotypic findings in mitochondrial DNA disease patient fibroblasts, such as impairment of mitofusin ubiquitination and increased mitochondrial-endoplasmic reticulum contacts. Two fibroblast lines containing the tRNA serine mutation m.7472insC were investigated in parallel with PINK1 mutant fibroblasts to reveal similarities in their characteristics. However due to experimental practicalities it was not possible to use all the patient lines with numerous age-matched controls to determine whether this effect would be found in some of the other patient lines too. In particular, considering the responses identified when analysing the mRNA

expression of PGC-1α, it would be interesting to determine whether these findings were limited to the tRNA mutant lines.

As well as repeating some of these experiments with all the patient lines available, it would be particularly interesting to further investigate the highly significant mitofusin ubiquitination defect. In order to test whether mitofusin ubiquitination was reduced due to the same mechanism as observed in the PINK1 and Parkin mutants, it would beneficial to attempt to overexpress these proteins. Whilst the facilities were not available at the time of these experiments, it would be particularly interesting to transfect these fibroblasts using electroporation to overexpress PINK1 or Parkin to see if ubiquitination could be rescued. In the literature it has been shown that ubiquitination of mitofusin 2 in PINK1 mutant fibroblasts could be rescued by overexpressing PINK1 but not Parkin, and Parkin mutant fibroblasts rescued by overexpressing Parkin but not PINK1 (Rakovic et al. 2011). If a rescue were to be obtained, it could suggest whether impairments in PINK1 or Parkin were the cause.

Chapter 3

Neuronal and Myogenic models of tRNA serine m.7472insC pathogenic mutation

3.1 Introduction

3.1.1 Induced Pluripotent Stem Cell models of mtDNA disease

Patients harbouring the same mtDNA mutation can often present with varying clinical phenotypes, affecting different tissues with differing severity. How the same mutation can have a different effect in separate tissues remains unknown. Furthermore, how mutant load is determined from tissue to tissue is also not understood. The generation of induced pluripotent stem cells (iPSCs) has enabled huge advancements in disease modelling across many disease areas. Cultured cells from patients, most commonly skin biopsies, enable the study of a pathogenic mutation within the nuclear background of the patient, which has been shown to be important in modulation of the mutation effect (D'Aurelio et al. 2010). However, cultured cells commonly do not exhibit a pathological phenotype or are limited in their experimental potential, as experienced in Chapter 2.

Generation of iPSCs is now a relatively simple process, with several techniques available that achieve good reprogramming efficiency,

such as mRNA transfection or the use of non-integration viruses (Malik & Rao 2013). In the experiments in this chapter, iPSCs were derived from patient and control fibroblasts and created by reprogramming to an embryonic stem cell–like state (epiblast stage), i.e. possessing the ability to self-renew and differentiate into cell types of all three embryonic germ layers (pluripotency). Since the use of transgenic technologies to modify the mitochondrial genome has been largely unsuccessful, the potential to study the same patient-derived mutation in various cell types using iPSCs is particularly useful for mtDNA diseases.

Previous studies have shown normal efficiency of reprogramming cells with point mutations, and subsequent differentiation towards all three embryonic germ layers (Cherry et al. 2013; Hamalainen et al. 2013; Fujikura et al. 2012). The generation of iPSCs from patients with Pearson's syndrome, a mtDNA disease caused by deletions, enabled differentiation to erythroid cells which possessed abnormal iron accumulation, a characteristic feature of the disease (Cherry et al. 2013). Differentiation of MELAS-iPSCs produced neurons with a significant Complex I deficiency, and in another study using MELAS-iPSC lines this deficiency was found only to occur when derived from iPSC with a high mutant load (Kodaira et al. 2015; Hamalainen et al. 2013). This indicates that these models produce a phenotype characteristic of the disease that presents in a load-dependent manner, replicative of the human disease.

In accordance with previous reports of Parkin modulating heteroplasmy in cybrid models and *C. elegans*, neuronal differentiated MELAS-iPSCs showed Parkin and Complex I colocalisation in neurons with high mutant load (Hamalainen et al. 2013). It was noted by the authors of this study that Complex I appeared to be enriched to a subset of mitochondria, which were degraded by mitophagy. It remains unclear as to why a mutation in

a tRNA gene, which is required for translation of all mitochondrial genes, causes impairment to Complex I specifically.

In these studies, variability in the degree of heteroplasmy was observed during reprogramming, extended culturing and differentiation (Folmes et al. 2013; Cherry et al. 2013; Hamalainen et al. 2013; Kodaira et al. 2015). Whilst this effect poses a problem for reliably generating iPSC models of mtDNA disease, it may also be a useful tool in the creation of isogenic controls and the study of disease in the same cell type with different mutant loads. During the process of reprogramming, the load of mtDNA mutation appears to segregate in a bimodal fashion, generating iPS clones with no mutant mtDNA or a load of over 50% (Folmes et al. 2013; Cherry et al. 2013; Hamalainen et al. 2013; Fujikura et al. 2012). This segregation pattern is reflective of a mitochondrial bottleneck, which is observed in germ cells (Cao et al. 2009). It is unknown whether the mutant load level in iPS clones is dependent on the mtDNA load in the parental fibroblasts.

3.1.2 Reprogramming to iPSC – mtDNA bottleneck theory

The bottleneck mechanism is poorly understood, however its effect causes wide variation in the proportion of two genotypes within oocytes, leading to dramatic changes in heteroplasmy levels between generations. A small bottleneck size results in greater variation of heteroplasmy between mother and child, enabling reduction of mutant load to non-pathogenic levels or facilitating a more severe effect in the child than the mother.

The concept of the bottleneck was developed following early observations in cows of rapid switching in levels of heteroplasmy even within a single generation (Ashley et al. 1989). During germline development, the large number of mtDNA molecules from

the maternal mtDNA pool is segregated into relatively small units which are transferred to the developing oocyte (Figure 28) (Cao et al. 2007). It is unclear when the bottleneck occurs exactly during development, with several groups concluding different results (Wai et al. 2008; Cao et al. 2007; Samuels et al. 2010). A recent study utilising a large number of human pedigrees showed that different mtDNA mutations segregate at different rates, relating to different size bottlenecks (Wilson et al. 2016).

The bimodal segregation reported in the reprogramming process of several studies suggests a similar mitochondrial bottleneck (Cherry et al. 2013; Folmes et al. 2013; Fujikura et al. 2012; Hamalainen et al. 2013). The study of mouse germ cells has shown that mtDNA nonsynonymous mutations were underrepresented compared to synonymous mutations in protein-coding genes, and interestingly a similar phenomenon has been reported in iPSC with the reduction of *ND5* mutations that was not observed with tRNA-leucine mutations (Stewart et al. 2008; Folmes et al. 2013; Hamalainen et al. 2013).

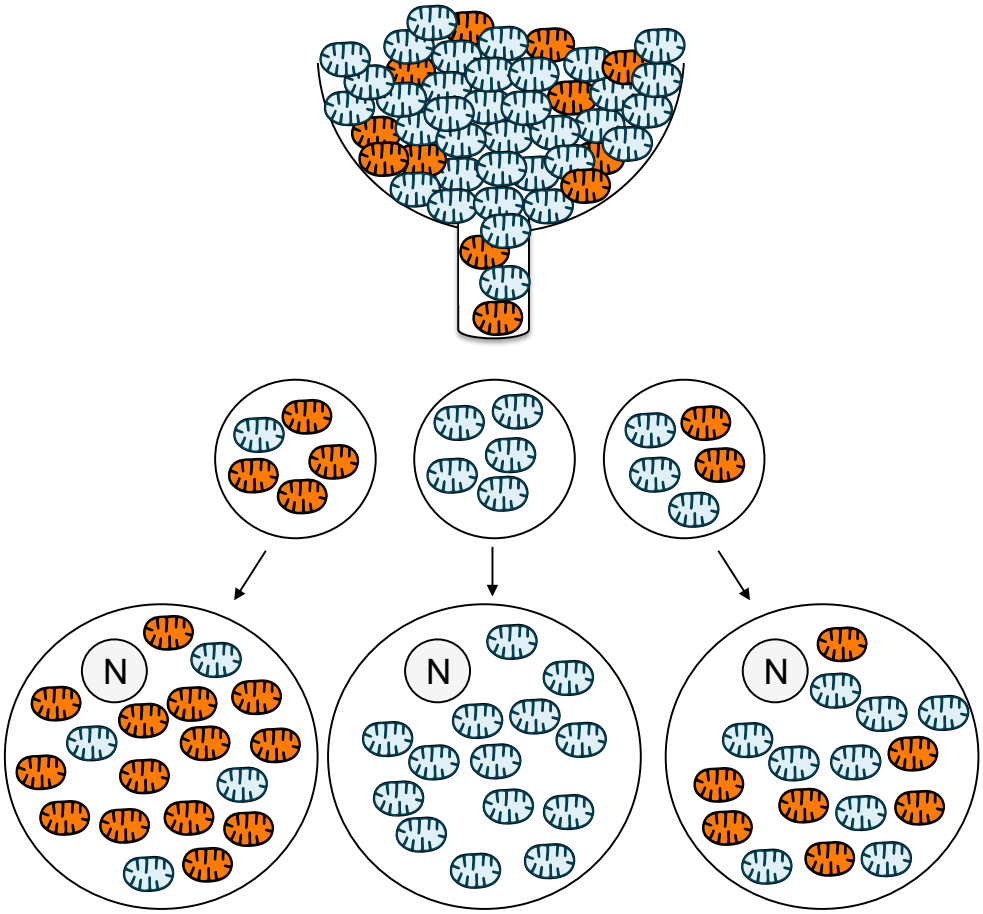

Figure 28: Mitochondrial DNA Germline Bottleneck

Schematic of the segregated units caused by the bottleneck from the large pool of maternal mtDNA. Blue mitochondria represent wild-type mtDNA containing mitochondria; red mitochondria represent mutant mtDNA containing mitochondria. N = nucleus. Beneath the bottleneck shape, which represents the maternal mtDNA pool, are the relatively small units that are transferred to the developing oocyte, demonstrating the variability of transfer and how mutant load can drastically increase or decrease.

3.1.3 Neuronal and muscle cell types in mtDNA disease

It is well known that mitochondrial disease phenotypes can be widely heterogeneous, however the involvement of both muscle and nerve is particularly common. Being diseases characterised by

impaired mitochondrial energy output, it stands to reason that tissues highly dependent on efficient energy production have more serious consequences due to the presence of the mutation. Even in healthy individuals, it has been shown that mitochondrial point heteroplasmy is most common in muscle, followed by liver and brain (Naue et al. 2015). For this reason, studying mitochondrial disease in patient fibroblasts may limit our understanding of pathomechanisms. The clinical phenotypes experienced in the patients involved in this study were MELAS, MERFF, ataxia, myoclonus, deafness and CMT2. No patients therefore experienced dermatological complications but all patients had affected muscle tissue and four patients also had neurological symptoms.

3.1.4 Aims and hypothesis

In this chapter the first aim was to reprogram patient and control fibroblasts to induced pluripotent stem cells using mRNA transfection, in order to create lines from which various cell models could be obtained by differentiation. Processes such as reprogramming fibroblasts, maintenance of iPSC cultures and differentiation are incredibly expensive and time-consuming, therefore it was not expected that all patient lines would be able to be used in these experiments.

From the iPSC cultures obtained, the second aim was to differentiate these towards cortical neurons using an established protocol (Shi et al. 2012). The objective was to characterise the neurons derived from patient cells in a more energy demanding cell type, compared to fibroblasts. In addition, since mitophagy was not detected in the fibroblasts, this process was to be triggered in the neurons in attempt to identify any defects in the patient cells.

In addition to neurons, the third aim was to differentiate the iPSC to myotubes, since this was the most commonly affected tissue in the patient cohort used in this study. Like in the neurons, the objective was to characterise the patient cells and to attempt to induce mitophagy.

The objective of generating iPSC possessing mtDNA mutations was to enable the comparison of mitochondrial phenotypes between fibroblasts, cortical neurons and myotubes. The hypothesis of this chapter was that, similar to the disease characteristics, generation of different cell types containing mutant mitochondrial DNA would result in some cell types possessing a phenotype and others not. This would benefit the study of mitochondrial DNA diseases, since it is poorly understood why some tissues present with clinical defects and others remain functioning despite the presence of the mutation.

3.2 Results

3.2.1 Characterisation of induced Pluripotent Stem Cells (iPSCs)

The seven mtDNA disease patient fibroblast lines used in chapter 2 underwent reprogramming to induced Pluripotent Stem cells (iPSCs) using the Stemgent mRNA Reprogramming Kit, the Stemgent microRNA Booster Kit and Stemgent Stemfect RNA Transfection Kit, as described in the methods section. Wild-type fibroblasts and one of the tRNA serine mutants (patient 6) underwent reprogramming first and iPSC colonies were obtained. Several clones for each line were picked but only two each were used in the following experiments. In the following experiments WT Clone 1 and Clone 2, and Mutant Clone 11 and Clone 12 are used (WT Cl.1, WT Cl.2, Mutant Cl.11 and Mutant Cl.12). DNA was extracted from these lines and the Illumina Nextera^{TM} library preparation kit was used to prepare for Next Generation Sequencing (NGS). Mutant Clone 11 and Mutant Clone 12 were both found to contain the tRNA serine m.7472insC mutation at a mutant load of greater than 80% (NGS data not shown).

Subsequent reprogramming attempts with the other mutant lines proved to be very difficult. It was found that either iPSC colonies did not form or that picked colonies no longer contained the mitochondrial DNA mutation. Repeating attempts at reprogramming is a very expensive and time-consuming, especially when it is unknown as to why it failed the first time, therefore experiments were pursued with wild-type and the tRNA serine mutant clones alone.

The iPSCs were first characterised before differentiated into other cell types to confirm their pluripotency. Nanog is a homeobox

transcription factor expressed in embryonic stem (ES) cells and was found to be strongly expressed in both wild-type and m.7472insC mutant clones when analysed by immunocytochemistry (Figure 29). Similarly, expression of Octamer-binding transcription factor 4 (Oct4) a transcription factor essential for maintenance of pluripotency and self-renewal of ES cells, was identified in all iPSC lines (Wu & Schöler 2014). Finally, SRY (sex determining region Y)-box 2 (SOX2), is a transcription factor which together with OCT4 forms a trimeric complex on DNA, controlling gene expression during embryogenesis and acting as a gene repressor of neuronal differentiation (Liu et al. 2014). Expression of hSOX2 was identified in both wild-type and m.7472insC mutant clones when analysed by immunocytochemistry (Figure 30).

Analysis of mRNA expression from RNA extracted from the four iPSC lines and a wild-type and mutant fibroblast cell line revealed increased expression of DNMT3 in the iPSCs compared to negligible expression in the fibroblasts (Figure 31). DNMT3 is a DNA methyltransferase, which during development, is essential for de novo DNA methylation, and therefore indicates similarities of the iPSCs to embryonic stem cells.

C-Myc and Kruppel-like factor 4 (KLF4) are transcription factors, and both present in the mRNA cocktail used during reprogramming. It is known that the endogenous loci of several reprogramming factors, including c-Myc and KLF4, are expressed in some somatic cells, and here it was found that the mRNA expression of c-Myc and KLF4 was greater in the fibroblasts than in the iPSCs (Figure 31). In the generation of iPSCs from fibroblasts via retroviral transduction with human reprogramming factors, it was found that gene expression of c-Myc and KLF4 were unexpressed in established iPSCs and that differentiation was more efficient from the colonies with transient acitivation of c-Myc expression (Takayama et al. 2010).

Finally, Rex1 (zfp42) is a zinc finger protein expressed primarily in undifferentiated stem cells in the embryo and adults, and therefore as expected its mRNA expression was greatly increased from unexpressed to highly expressed in the iPSCs compared to fibroblasts (Figure 31) (Scotland et al. 2009).

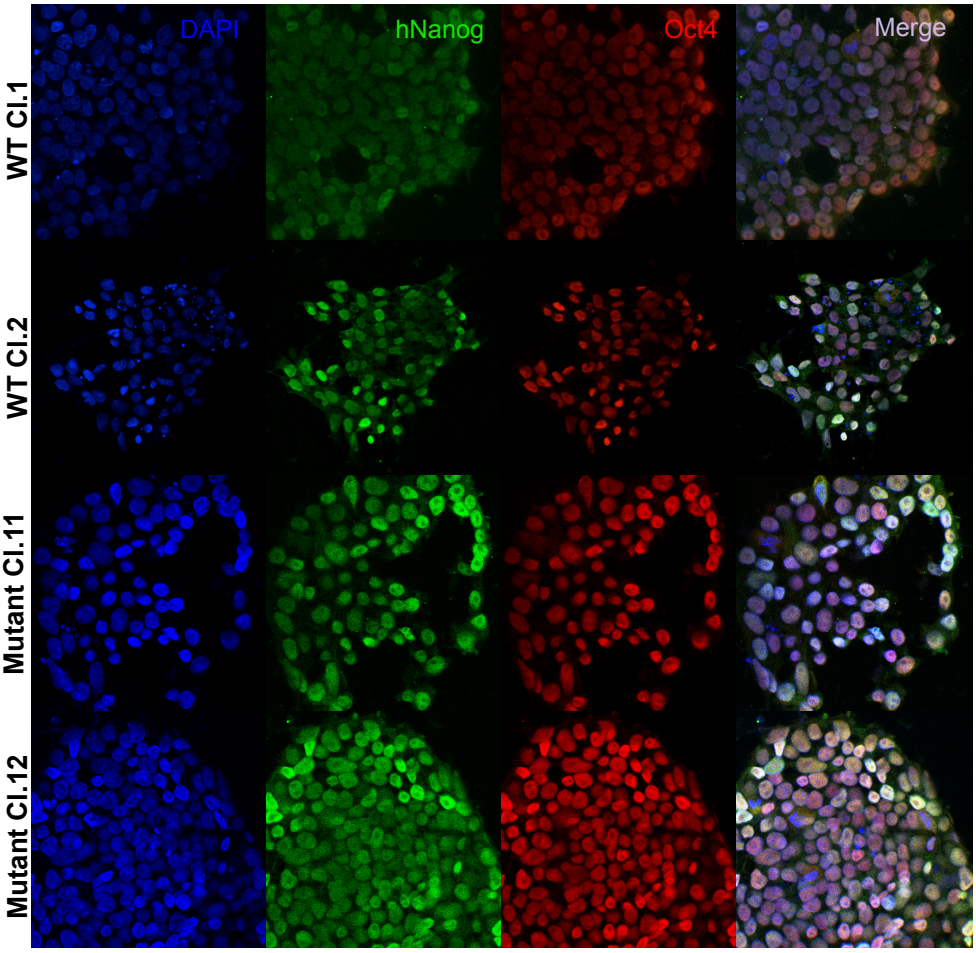

Figure 29: Characterisation of induced Pluripotent Stem cells

Representative images of iPSCs prepared by immunocytochemistry for staining with pluripotency markers hNanog (green) and Oct4 (red). DAPI staining labels cell nuclei.

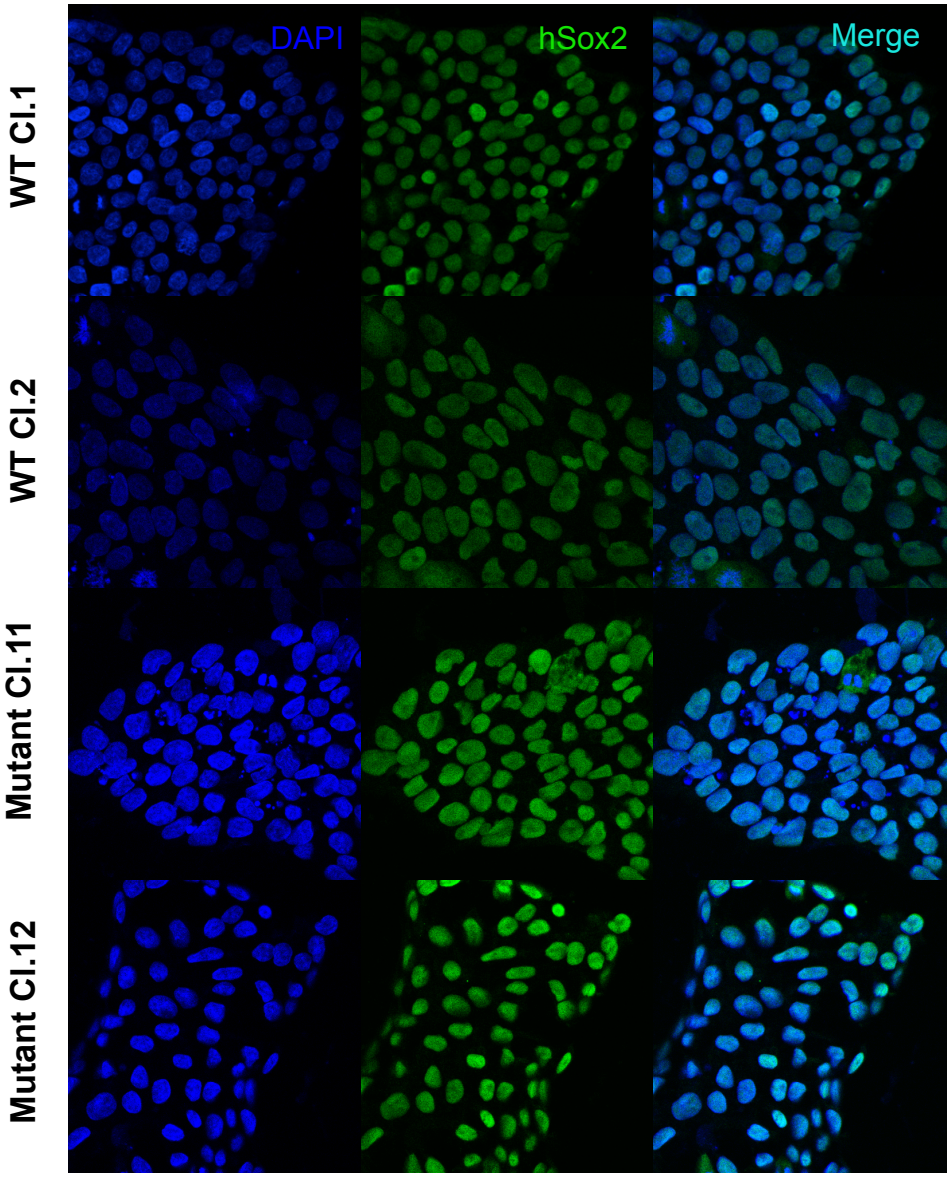

Figure 30: Characterisation of induced Pluripotent Stem cells

Representative images of iPSCs prepared by immunocytochemistry for staining with pluripotency marker hSox2 (green). DAPI staining labels cell nuclei.

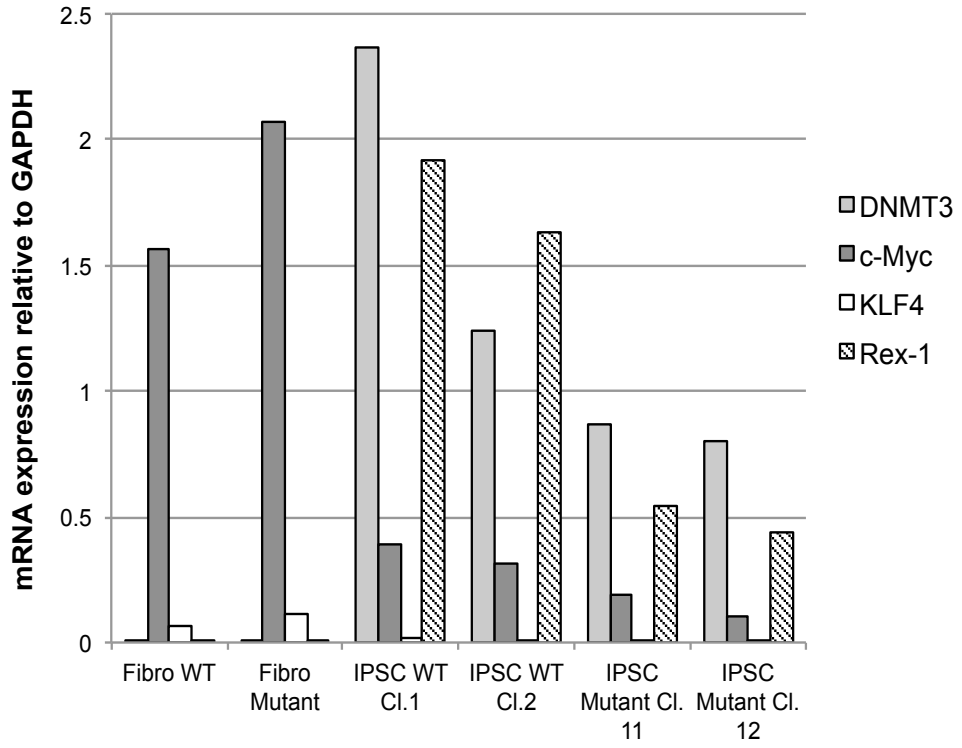

Figure 31: Characterisation of induced Pluripotent Stem cells by qPCR

Histogram to show the relative mRNA expression of markers DNMT3, c-Myc, KLF4 and Rex-1, relative to housekeeping gene GAPDH, in fibroblasts and iPSCs derived from control and patient skin biopsies.

3.2.2 Characterisation of iPSC-derived cortical neurons

IPSCs were differentiated to cortical neurons using the protocol written by Shi *et al,* described in the methods section. This protocol took 95 days before cells were characterised, and unfortunately the m.7472insC mutant clone 12 did not survive the differentiation by around day 50. In the interest of time, it was decided to proceed with the WT Cl.1, WT Cl.2 and Mutant Cl.11.

At day 95, cells were characterised by immunostaining and DNA extracted for Sanger sequencing to confirm the presence of the mutation in Mutant Cl.11. Whilst it is not possible to estimate mutant load when using Sanger Sequencing, this is a significantly cheaper and quicker way to confirm the presence of the mutation. An

inserted ‘C’ was identified at the correct position in the mutant line that was not present in the wild-type (Figure 32).

Neocortical markers Ctip2 and Tbr1 were used to assess the cortical properties of differentiated iPSCs by immunostaining. Pyramidal neurons in the neocortex are classified as deep-layer or upper-layer neurons, of which deep-layer are the first to be made during neurogenesis. Tbr1, a transcription factor, is expressed mainly in the neocortex by postmitotic pyramidal neurons, and is involved in the postmitotic regulation of layer VI and subplate (Hevner et al. 2001).

Ctip2 is a transcription factor expressed by postmitotic neocortical subtypes, and is involved in the directing of pyramidal neurons to a deep-layer fate, and the formation of the corticospinal tract. Immunostaining of WT Cl.1, WT Cl.2 and Mutant Cl.11 cells that were day 95 post neuronal induction, revealed Ctip2 and Tbr1 positive staining, indicating neocortical neurons (Figure 33). As expected, colocalisation of Ctip2 and Tbr1 was identified.

Satb2 is a marker of callosal projection neurons in layers II-V. Loss of *Satb2* expression causes upper-layer neurons to lose their upper-layer identity, suggesting that *Satb2* is involved in the regulation of upper-layer specification (Britanova et al. 2008). As expected, since deep-layer are the first to be generated during neurogenesis, fewer Satb2 positive cells were identified in the iPSC-derived neurons (Figure 33).

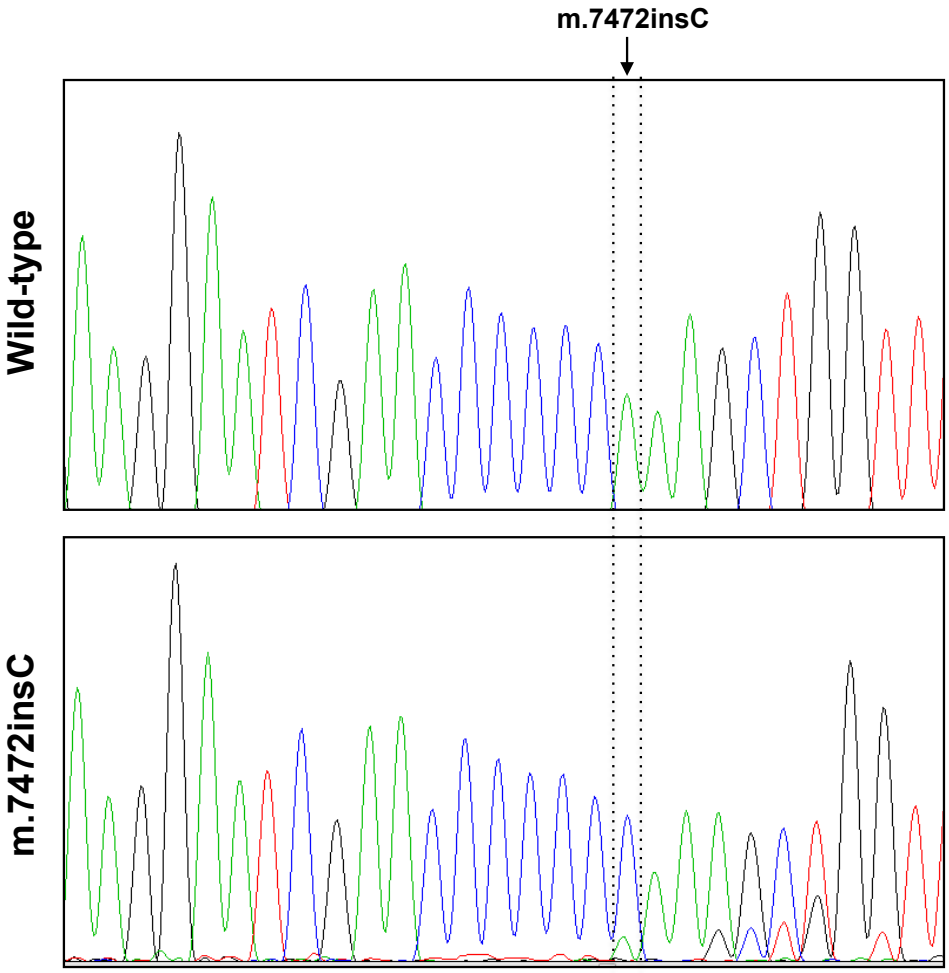

Figure 32: Sanger sequencing chromatogram of the m.7472insC mutation in iPSC-derived cortical neurons

Representative chromatogram showing the 7472bp position where the inserted C (blue) is found in the mutant neurons (Mutant Cl.11) and not the wild-type neurons (WT Cl. 1) obtained by Sanger sequencing. DNA was extracted from neurons at day 95.

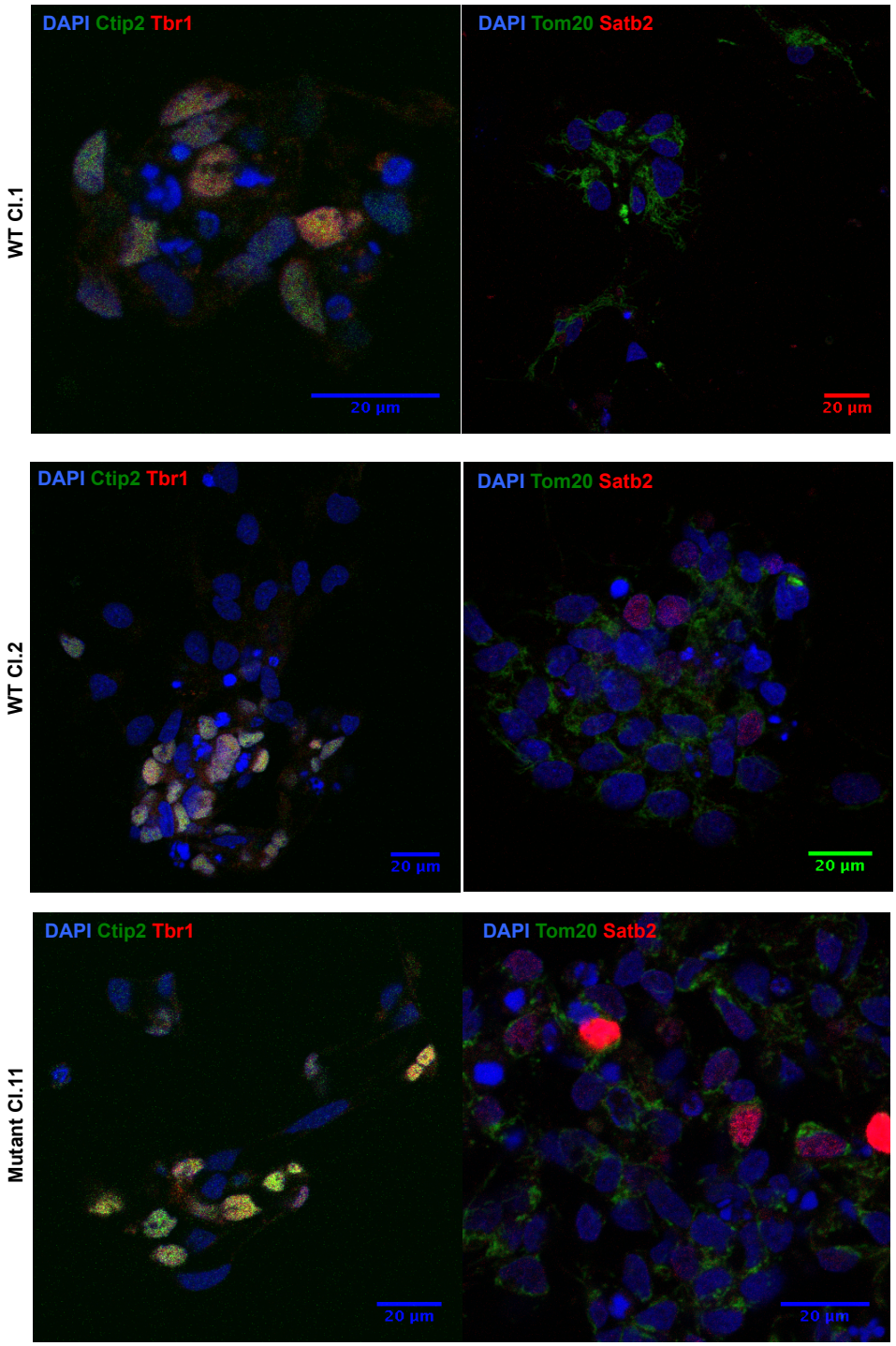

Figure 33: Characterisation of iPSC-derived cortical neurons

Representative images of iPSC-derived cortical neurons prepared by immunocytochemistry for staining with neuronal markers Ctip2 (green, left), Tbr1 (red, left), Tom20 (mitochondrial marker; green, right) and Satb2 (red, right). DAPI staining labels cell nuclei. Scale bar represents 20 µM distance.

3.2.3 Mitochondrial physiology and function in mtDNA disease derived cortical neurons

Analysis of basal mitochondrial membrane potential in live cells revealed no significant differences between wild-type neuronal lines and neurons containing the m.7472insC mutation (Figure 34A). In the analysis of TMRM intensity, both wild-type lines (WT Cl.1 and WT Cl.2), which were derived from different iPS colonies from the same fibroblast control line, had similar mean values; however analysis of cell lysates for the complex I activity assay proved quite different.

In untreated cell lysates, complex I activity was found to vary greatly between WT Cl.1 and WT Cl.2, although there was relatively little variation on subsequent repeats for each line suggesting that the differences between neuronal lines was real (Figure 34B). The complex I activity of the Mutant Cl. 11 line was found to be slightly lower than the WT Cl.2, however with the large variation between controls, statistical significance was not measured.

Previous experiments using PINK1 KD neuroblastoma cells have shown that growing cells for 24 hours in 300 μM folic acid (FA) could restore mitochondrial dysfunction (Tufi et al. 2014). Therefore taking into consideration the previous reduction in complex I activity observed in the mutant fibroblasts, the complex I assay was performed in parallel with lysates from cells that had been grown with folic acid for 24 hours. However, no differences in complex I activity were observed in any of the lines between the control and folic acid lysates (Figure 34B).

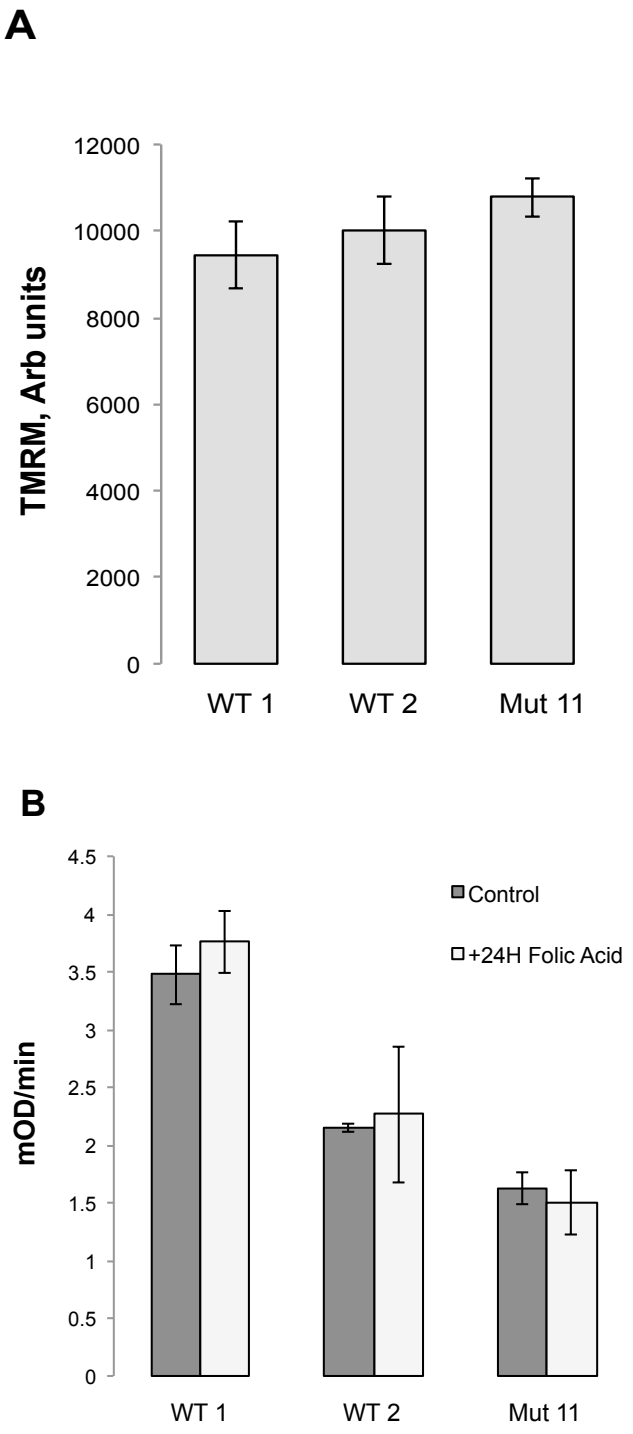

Figure 34: Quantification of mitochondrial membrane potential and complex I activity in cortical neurons

A Histogram represents mean TMRM intensity measured by live cell imaging as an indicator of mitochondrial membrane potential. Error bars represent SEM, *n* = 3. B Histogram representing the Complex I activity measured from 200 ug of cell lysate with and without 24 H pre-treatment with folic acid. Error bars represent SEM, *n* = 3.

Assessing mitophagy in neurons has been of great interest in the field of mitophagy and, in particular, Parkinson's disease research, however there have been several hurdles identified in the literature into the practicalities of doing so (as discussed in section 2.3.2).

Our lab has studying this in depth and it has been found that iPSC-derived cortical neurons treated with 10 μM CCCP for 48 H, 'refreshing' the CCCP every 12 H (as described in the methods section) caused loss of mitochondrial proteins (data unpublished). This protocol was applied to WT Cl.1, WT Cl.2 and Mutant Cl.11, however only degradation of mitofusin 1 and the accumulation of PINK1 in CCCP treated cells could be identified (Figure 35 A-C). No loss of inner mitochondrial membrane marker Tim23 or outer mitochondrial membrane marker Tom20 could be identified in any of the lines (Figure 35 A,D). Comparing the results in WT Cl.1 and WT Cl.2, both exhibited substantial degradation of mitofusin 1 after 48 H CCCP treatment, more PINK1 accumulation was identified in WT Cl.1 than WT Cl.2, but similarly in both lines, no loss of mitochondrial proteins was observed. The m.7472insC mutant neurons revealed no differences to controls in the change in protein levels upon exposure to CCCP. No ubiquitination of mitofusin 1 was observed after 48 hours CCCP treatment, so a shorter timepoint was next observed.

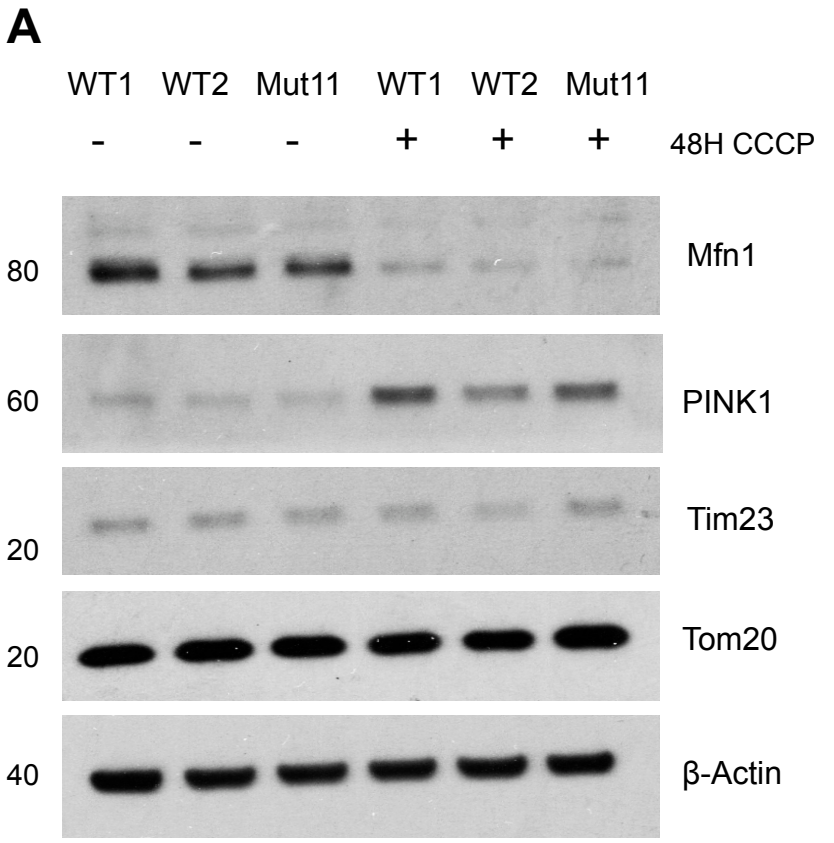
A
WT1
WT2
Mut11
WT1
WT2
Mut11
-
-
-
+
+
+
48H CCCP
80
Mfn1
60
PINK1
20
Tim23
20
Tom20
40
β-Actin

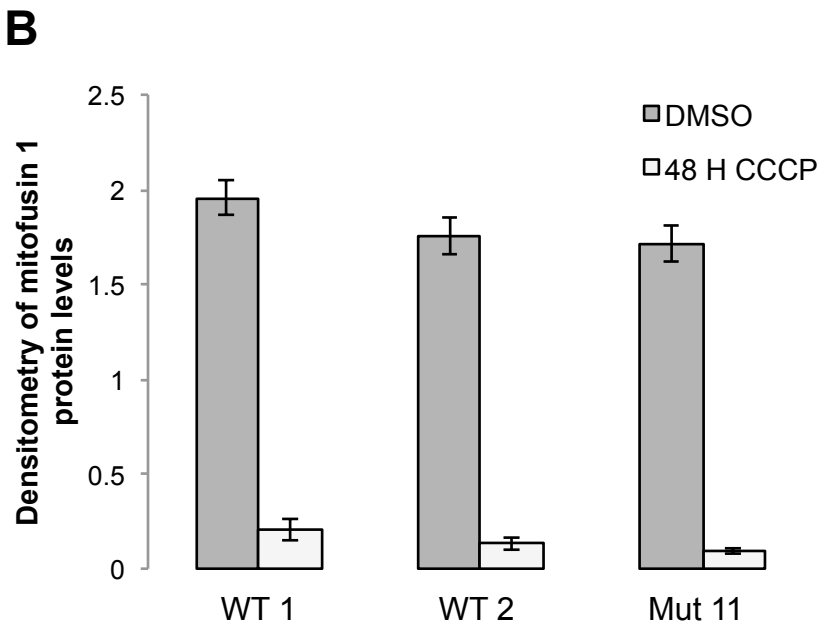
B
Densitometry of mitofusin 1 protein levels
2.5
2
1.5
1
0.5
0
DMSO
48 H CCCP
WT 1
WT 2
Mut 11

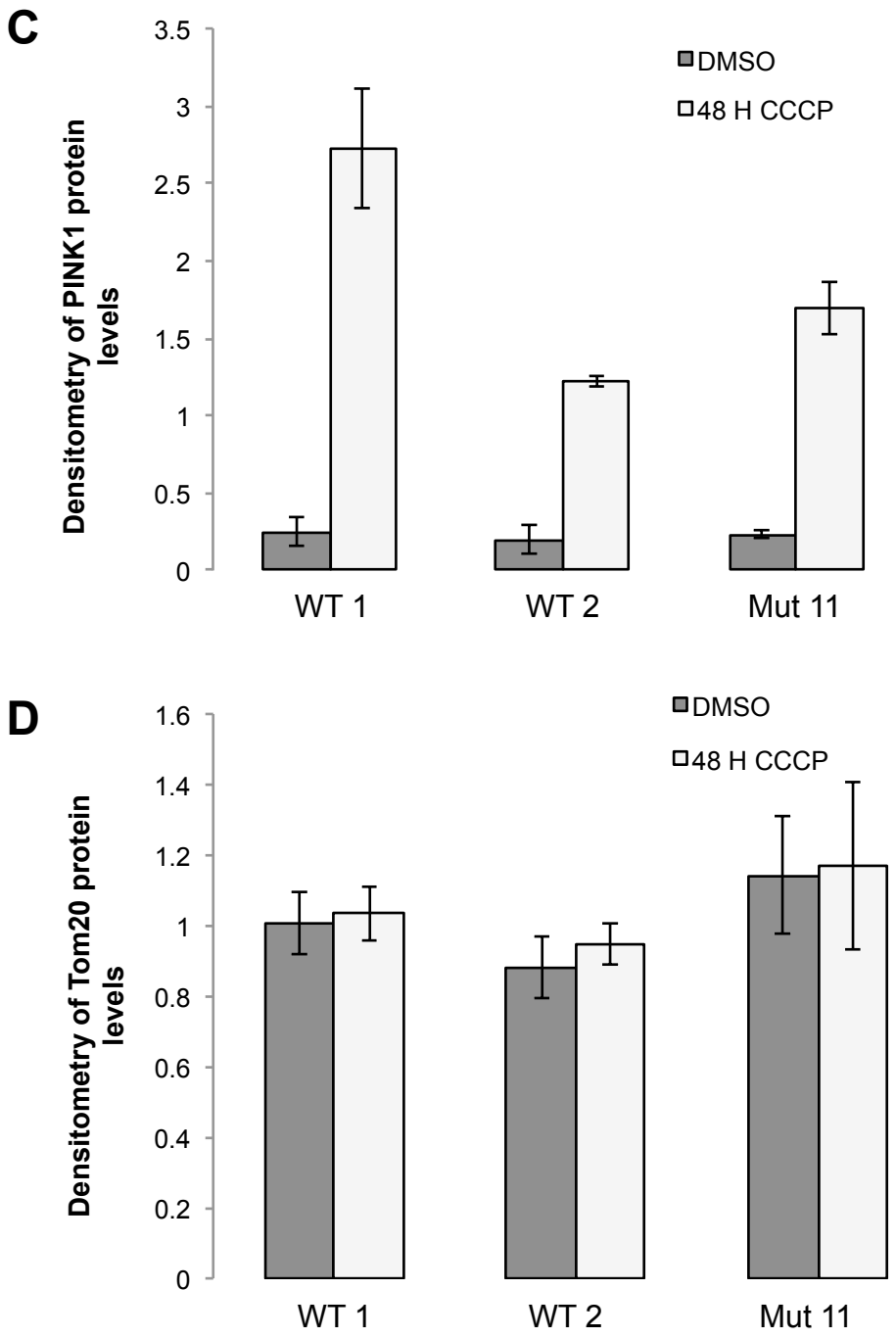

Figure 35: Stimulation of cortical neurons with CCCP and quantification of mitochondrial protein levels

A Representative immunoblot of mitophagy-associated protein levels in two wild-type cortical neuron lines and an m.7472insC mutant cortical neuron line, with and without 48H 10 µM CCCP treatment. B-D Histogram represents quantification of mitofusin 1 (B), PINK1 (C) and Tom20 (D) protein levels (normalised to β-actin protein levels) in the three lines (two WT and one mutant) with and without 48H 10 µM CCCP treatment. Error bars represent SEM.

WT Cl.1, WT Cl.2 and Mutant Cl.11 cortical neurons were treated with or without 10 µM CCCP for 24 hours, refreshing CCCP once after 12 hours (as described in the methods section). This experiment was also performed with CCCP alone or pretreatment (1 H) and co-treatment with 10 µM MG132 (proteasome inhibitor). At the 24 hour timepoint, degradation of mitofusin 1 was observed in all three lines, but no mitofusin 1 ubiquitination (Figure 36). In the cells treated with both CCCP and MG132, degradation of mitofusin 1 did not appear to be reduced but the appearance of ubiquitinated bands could be seen. If more neurons were available, it would have been preferable to perform a dose-response of MG132 in control cells to know if the most effective dose and treatment time had been used, in order to better draw conclusions from this effect.

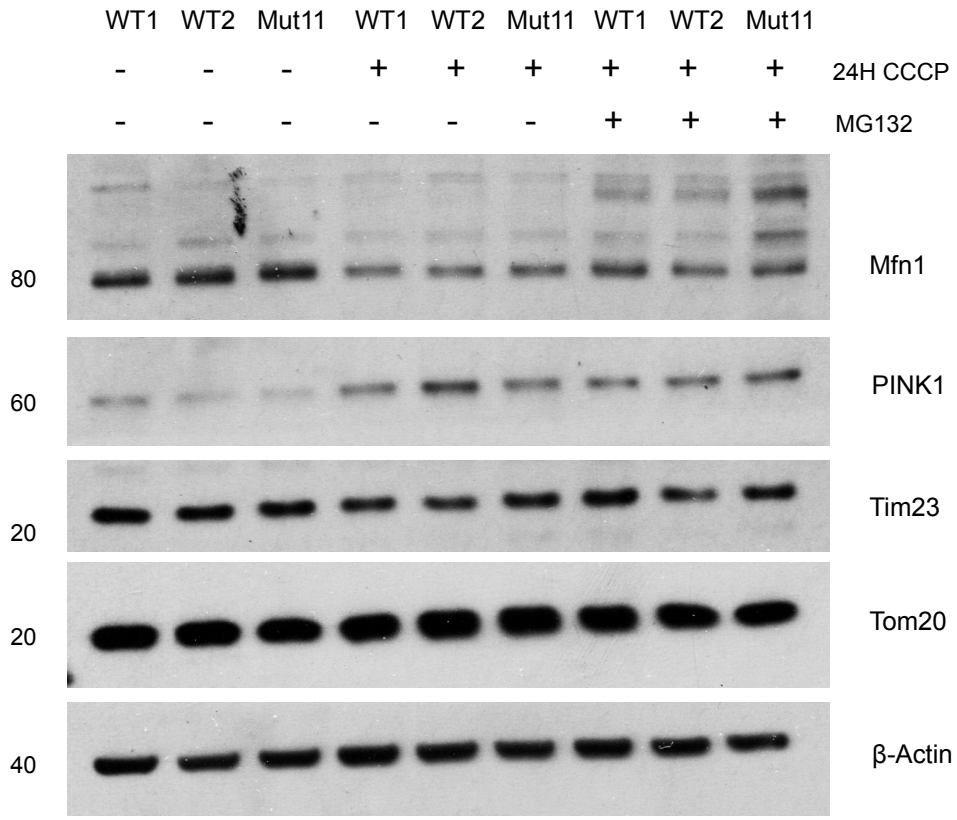

Figure 36: Stimulation with CCCP in the presence of proteasome inhibitor MG132 in iPSC-derived cortical neurons

Representative immunoblot to show the levels of mitophagy-associated proteins in two wild-type cortical neuron lines and an m.7472insC mutant cortical neuron line, with and without 24H 10 μM CCCP treatment, with and without proteasome inhibitor MG132.

3.2.4 Characterisation of iPSC-derived myotubes

IPSCs underwent myogenic differentiation following the protocol described in the methods section. For the first differentiation, WT Cl.1, WT Cl.2, Mutant Cl.11 and Mutant Cl.12 iPSCs were used and plated at p10 at a density of 1.2 $x10^5$ per well (in a 6-well tissue culture plate). Cells were treated as per the protocol described and split on day 25, however on examination of the cells on day 26, they had developed a neuronal-like morphology and it was clear that spontaneous differentiation had occurred. It was suspected that the cells had become too confluent prior to this spilt.

A new frozen vial of iPSC was thawed and cultured ready for a second attempt. Unfortunately the WT Cl.2 did not survive the thawing process so in the interest of time it was decided to continue just with WT Cl.1, Mutant Cl.11 and Mutant Cl.12. This time, cells were plated at p12 and at a density of 1 $x10^5$. As it had not been determined why the first attempt at myogenic differentiation had failed, for the second attempt all new reagents were used and freshly aliquoted stocks were made. The second attempt was successful in all three lines and twitching myotubes were observed around day 35.

Sanger sequencing of WT Cl.1, Mutant Cl.11 and Mutant Cl.12 confirmed the presence of the m.7472insC mutation in the two mutant lines but not in the wild-type (Figure 37A).

MyoD is a master regulator of skeletal muscle cell differentiation, and has a central role myogenesis (Tapscott 2005). Whilst immunostaining was not particularly strong, expression of MyoD was identified in all three lines and found to colocalise with DAPI nuclei stain (Figure 37B). Myosin heavy chain is a protein found in muscle thick filaments and positive fibres were identified by immunostaining in all three lines (Figure 37B).

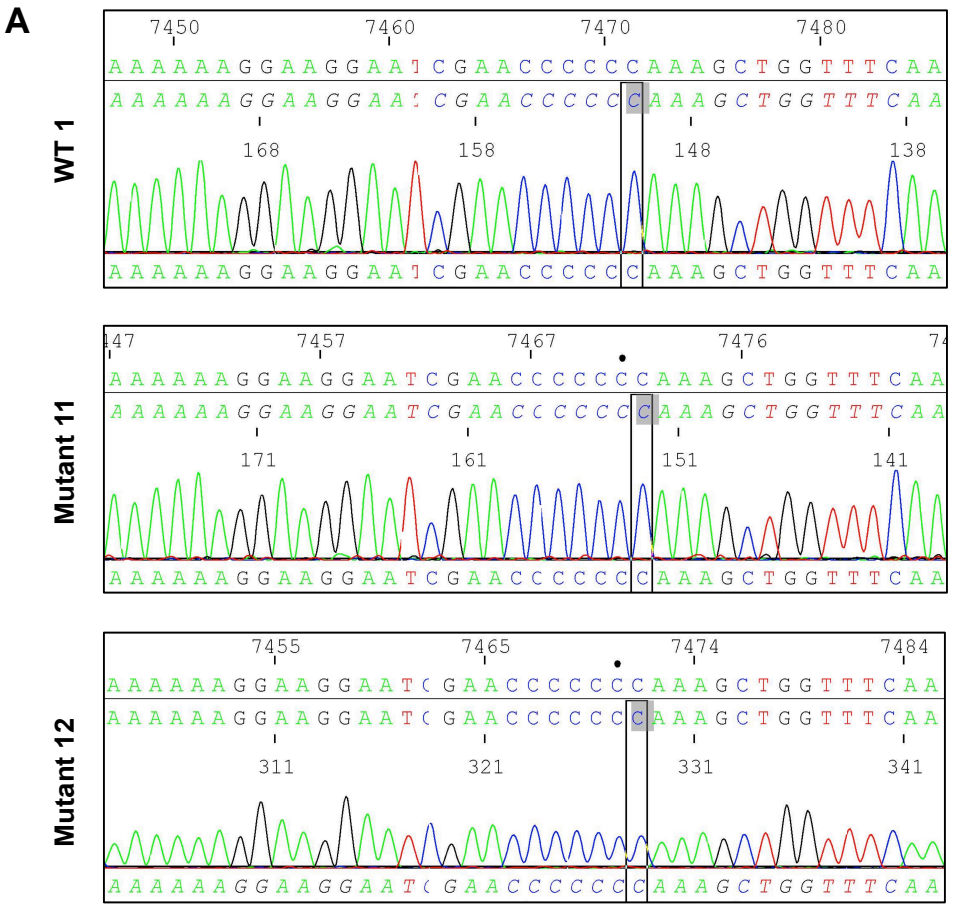

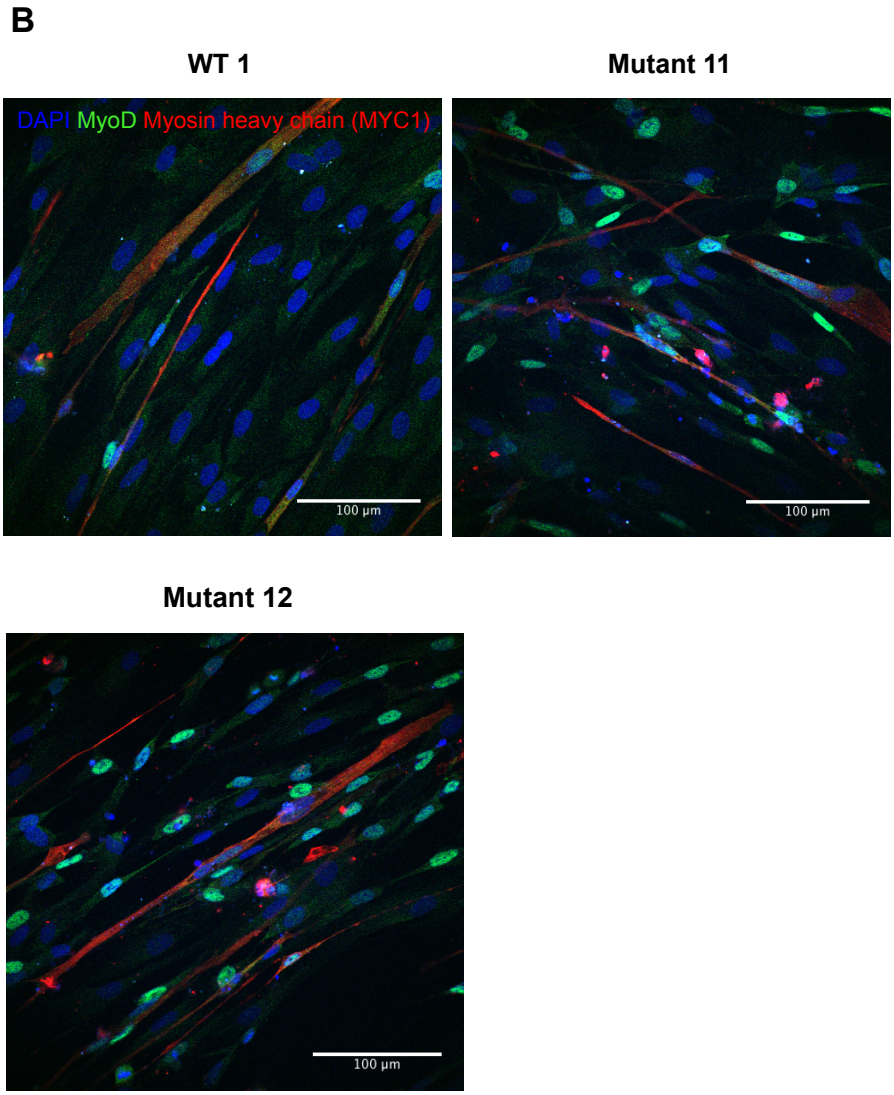

Figure 37: Confirmation of presence of m.7472insC mutation and characterisation of iPSC-derived myotubes

A Representative chromatogram of the 7472bp position where the inserted C (blue) is positioned in iPSC-derived myotubes. In the wild-type line (clone 1) at the site shown, there is a row of 6 'C's, but in the two mutant lines there are 7. B Representative images of iPSC-derived myotubes prepared by immunocytochemistry using MyoD and MYC1 myogenic markers. DAPI staining labels cell nuclei. Scale bars represent 100 µM.

3.2.5 Mitochondrial physiology and function in mtDNA disease derived myotubes

Basal mitochondrial membrane potential obtained from experiments in live cells revealed no significant loss of membrane potential in either Mutant Cl.11 or Mutant Cl.12 compared to WT Cl.1 (Figure 38A). Although unfortunately only one wild-type myotube line was available for these experiments, the data here suggests a large reduction in complex I activity in the Mutant Cl.11 and Mutant Cl.12 compare to wild-type (Figure 38B). This difference was found to be of statistical significance between Mutant Cl.12 and WT Cl.1.

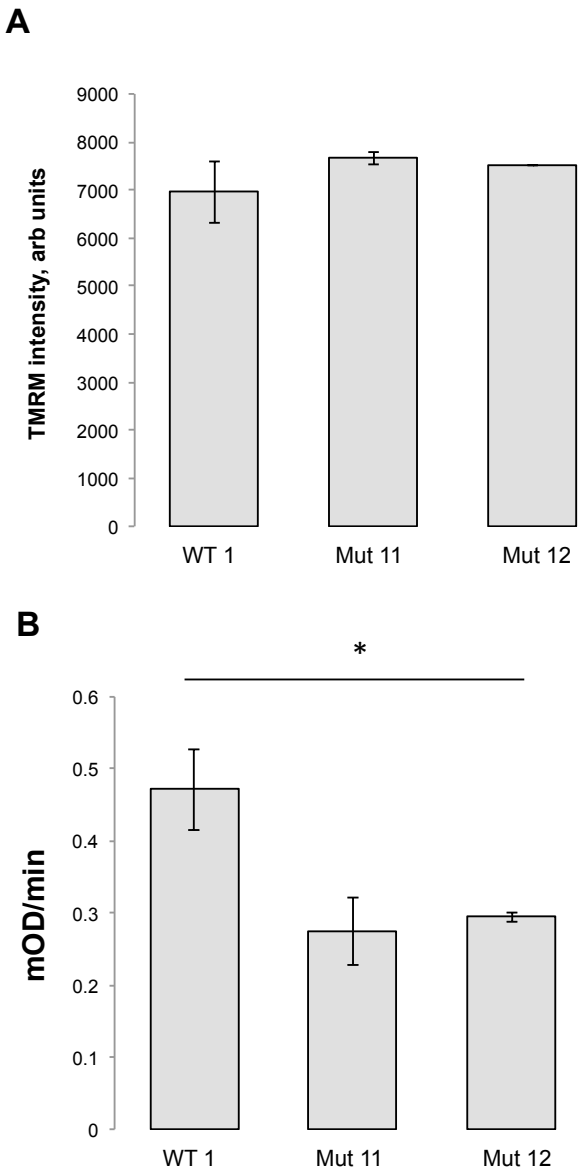

Figure 38: Quantification of mitochondrial membrane potential and complex I activity in iPSC-derived myotubes

A Histogram represents mean TMRM intensity measured by live cell imaging as an indicator of mitochondrial membrane potential. Error bars represent SEM, *n* = 3. B Histogram representing the Complex I activity measured from 200 ug of cell lysate with and without 24 H pre-treatment with folic acid. Error bars represent SEM, *n* = 3; two-tailed Student *t*-test * *p* < 0.05

The same protocol was used in the muscle cells for mitophagy as that which was used in the neurons, involving 48 hours of 10 μM CCCP treatment that was refreshed every 12 hours. Interestingly in the WT Cl.1 line, similar to the observations in the neurons, after 48 hours of CCCP treatment, significant PINK1 accumulation and mitofusin 1 degradation was seen (Figure 39 A-D).

However, both PINK1 accumulation and mitofusin 1 degradation was not significant in both Mutant Cl.11 and Mutant Cl.12 (Figure 39 A-D). When analysing PINK1 protein levels a modest increase was observed in the mutants but not enough to reach significance like in the wild-type line. For the mitofusin 1 levels, the degradation observed was more variable, as depicted in the large error bars of the histogram, which is likely the reason for a non-significant difference.

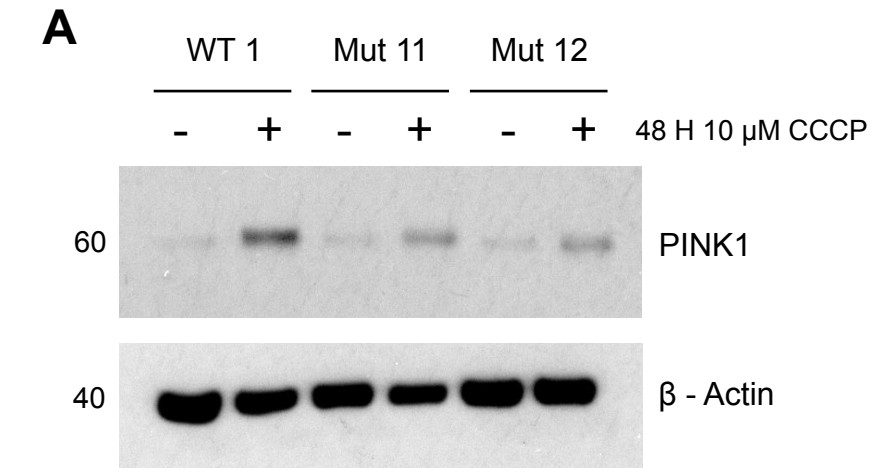
A
WT 1
Mut 11
Mut 12
- + - + - +
48 H 10 µM CCCP
60
PINK1
40
β - Actin

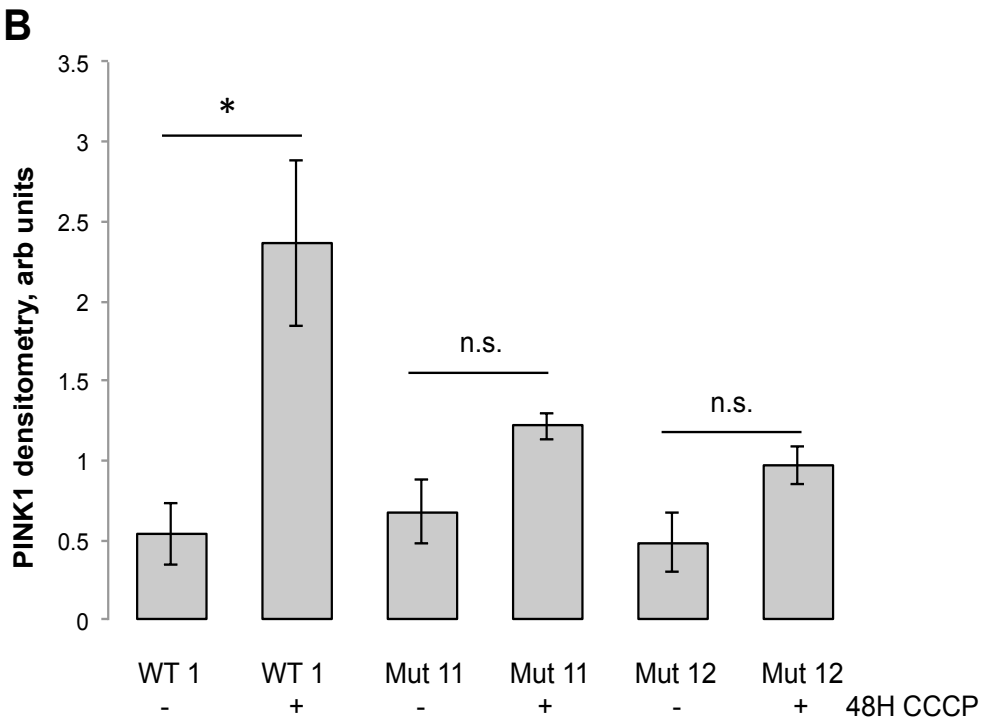
B
PINK1 densitometry, arb units
3.5
3
2.5
2
1.5
1
0.5
0
*
n.s.
n.s.
WT 1 - WT 1 + Mut 11 - Mut 11 + Mut 12 - Mut 12 +
48H CCCP

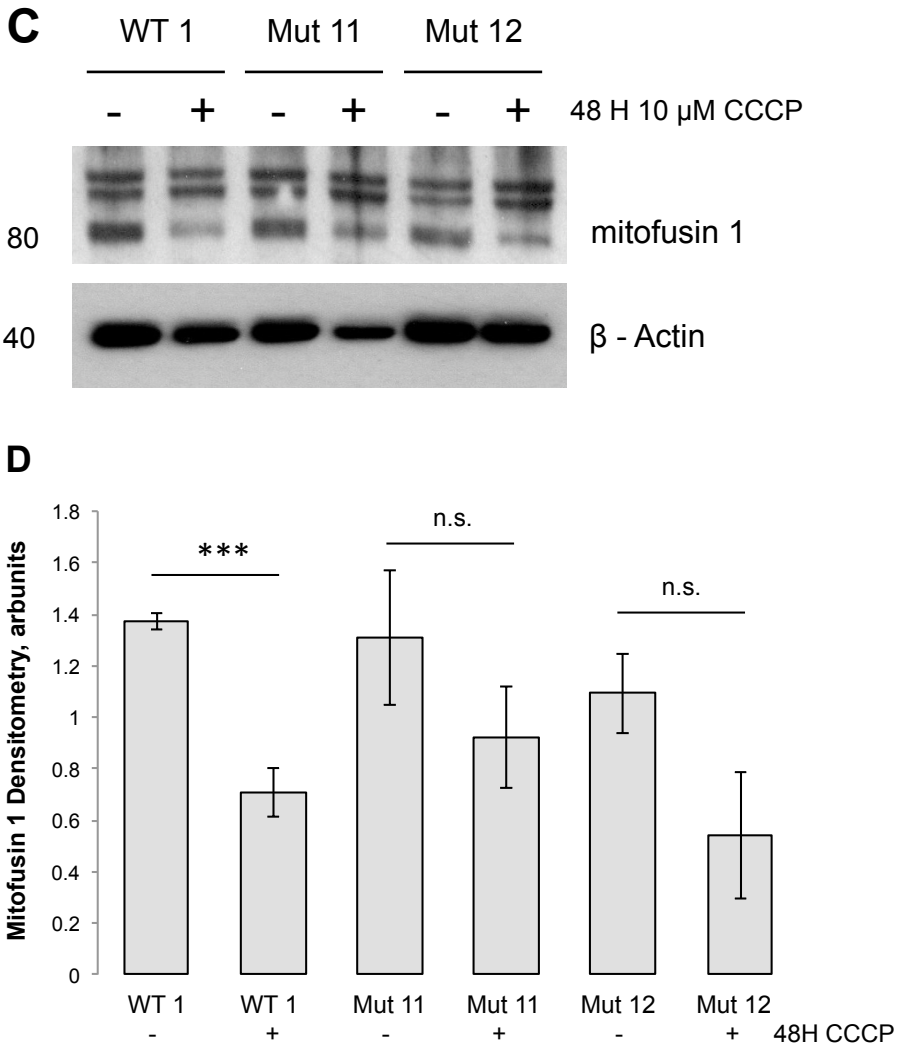

Figure 39: Quantification of PINK1 levels in myotubes stimulated with mitochondrial uncoupler CCCP

A Representative immunoblot showing PINK1 protein levels in wild-type and m.7472insC mutant (two clones) iPSC-derived myotubes with and without 48 H of 10 µM CCCP treatment. B Histogram to show the quantification of PINK1 protein levels, normalised to β-Actin protein levels. Error bars represent SEM, *n* = 3; two-tailed Student *t*-test * *p* < 0.05 C Representative immunoblot showing mitofusin 1 protein levels in wild-type and m.7472insC mutant (two clones) iPSC-derived myotubes with and without 48 H of 10 µM CCCP treatment. D Histogram to show the quantification of mitofusin 1 protein levels, normalised to β-Actin protein levels. Error bars represent SEM, *n* = 3; two-tailed Student *t*-test * *p* < 0.005**

Measurement of mitochondrial proteins by immunoblotting revealed that CCCP treatment after 48 hours stimulated biogenesis instead of mitophagy. Like in neurons, no loss of mitochondrial proteins was observed in wild-type muscle cells, however quantification of Tom20 revealed a significant increase in protein levels after 48 hours of CCCP (Figure 40). This increase was found to be significant also in both Mutant Cl.11 and Mutant Cl.12 (Figure 40).

On analysis of another mitochondrial protein, Tim23, no significant increase or decrease was observed in WT Cl.1 after 48 hours of CCCP, and there was little difference in the mean values between untreated and treated (Figure 40). However an increase in Tim23 protein levels was identified in both the Mutant Cl.11 and Mutant Cl.12, the latter of which reached statistical significance (Figure 40). Interestingly, under basal conditions (i.e. in the untreated samples) the protein levels of Tim23 were found to be significantly lower in Mutant Cl.12 that WT Cl.1 (Figure 40).

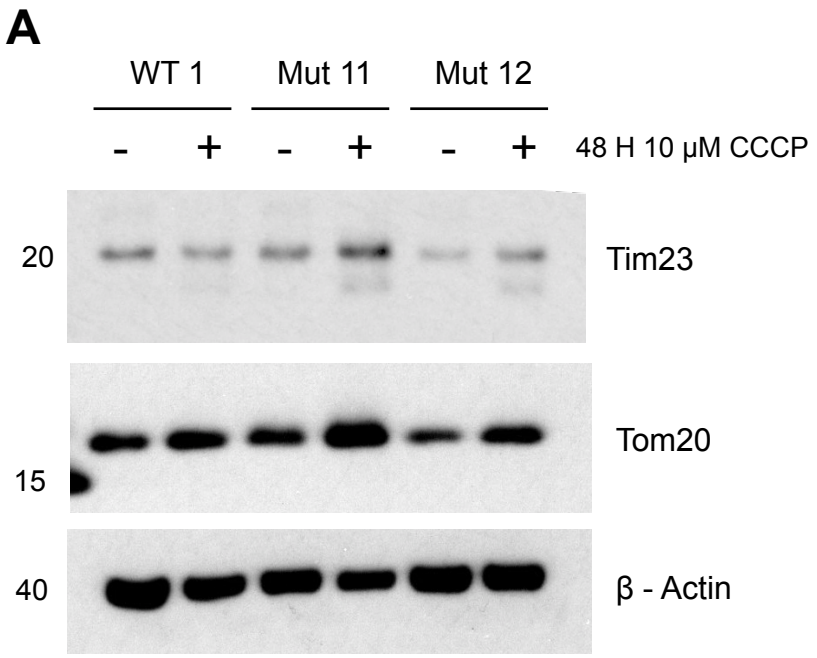

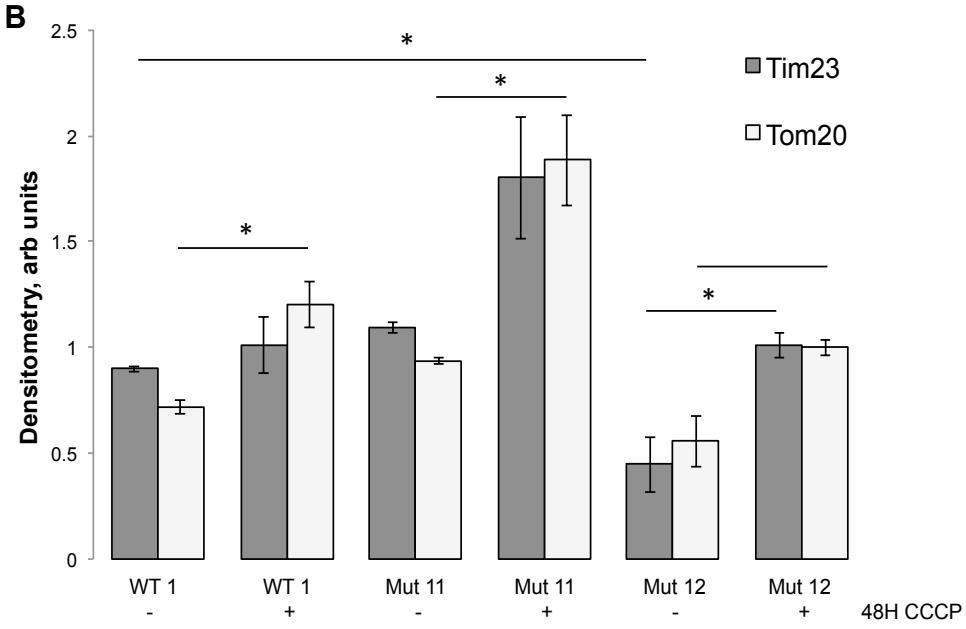

Figure 40: Quantification of mitochondrial protein levels in myotubes stimulated with 48 H CCCP

A Representative immunoblot showing the protein levels of mitochondrial markers Tim23 and Tom20 in iPSC-derived myotubes treated with and without 10 µM CCCP for 48 H. B Histogram shows the quantification of Tim23 (dark grey) and Tom20 (light grey) protein levels, normalised to β-actin protein levels. Error bars represent SEM, *n* = 3; two-tailed Student *t*-test * *p* < 0.05

3.3 Discussion

3.3.1 Limitations of iPSC derived mitochondrial disease models

The differentiation of iPSCs expressing multiple pluripotency markers towards neuronal or myogenic cell fates did not cause a loss of mutation; on successful attempts, a high mutant load was obtained.

Unfortunately, two major limitations were experienced during the experiments in this chapter, which would have required a significant amount of time to overcome which was not available. First, each differentiation into myotubes and neurons was only carried out once. All experiments performed in neurons or myotubes were carried out in triplicate, however it would have been beneficial to repeat these experiments from a separate induction. The process of differentiation involves long term exposure to many growth factors and can result in mixed cell populations; therefore it would be unsurprising if slightly variable results were observed on different inductions. To ensure results deemed significant were dependent on the presence of the mutation, it would be best to show this occurring in cells derived from a separate induction. Furthermore, multiple reprogramming and differentiation experiments may have enabled the generation of an isogenic control, which would have been particularly advantageous for determining the mutation dependent phenotype.

Secondly, iPSCs and differentiated cell types in culture are particularly sensitive especially compared to immortalised cell lines and fibroblasts, therefore experiments in muscle and neurons could only be conducted on three lines due to cell survival problems. In the differentiation of iPSCs towards cortical neurons, mutant clone

12 did not survive beyond day 50, at which point the cells had completely detached from the tissue culture plate. During the later stages of neuronal differentiation, half-media changes are performed so as not to disturb the extremely delicate neurons in culture, therefore cell detachment could have been caused by a disturbance during the differentiation protocol. However more likely this was due to iPSC culture itself since duplicate wells of the same line are cultured during a single induction and all of these were lost originating from only one iPS clone. It was hypothesised at the time that the death of neurons could have been a phenotypic effect of a high mutant load, however once the differentiation protocol was completed and the surviving mutant clone was sequenced, this appeared to have a high mutant load itself, therefore would have been unlikely to survive if this was the reason for the loss of clone 12. It is well known that iPSC cultures are characteristically heterogeneous, even among those derived from healthy controls, and differentiation capacity has been found to be influenced by factors prior to the differentiation process, such as passage number of the iPSC (Koehler et al. 2011; Hu et al. 2010). Whilst it is impossible to identify the reason for the loss of mutant clone 12, the heterogeneous nature of iPSCs is likely to be a factor and it is probable that a different induction with a different population of mutant clone 12 iPSCs would result in a successful differentiation.

For the differentiation of iPSCs towards myogenic cell fates, one of the wild-type iPSC clones did not survive the thawing process. The iPSCs should be thawed and maintained in culture for at least two weeks before switching to mTeSR™ media for a few days before plating to begin muscle differentiation. Since the first differentiation failed at 26 days after cell plating, believed to be due to the importance of cell density being not too high, it was decided in the interest of time to continue with one wild-type clone and two mutant clones.

It was unfortunate that in both the neuronal and muscle experiments that the same three clones weren't utilised, in particular because of the noticeable differences observed between the two neuronal wild-type clones in complex I activity and PINK1 accumulation – two characteristics that appeared to be affected in the myotubes containing the m.7472insC mutation. It is not unusual to obtain different results from various healthy controls, for example the endogenous Parkin levels measured in 8 fibroblasts derived from healthy subjects from chapter 2, however it is more surprising to see different results from two clones obtained from the same fibroblast line.

3.3.2 Phenotypes in cortical neurons containing tRNAserine mtDNA mutation

In the iPSC-derived cortical neurons, fewer Satb2 positive nuclei were identified than Ctip2 and Tbr1, suggesting fewer more mature neurons were present in the cell population and it is likely that these cells were relatively glycolytic at the time of experiments (Agostini et al. 2016). Analysis of mitochondrial membrane potential in live cells using the TMRM dye, showed no significant differences in the maintenance of membrane potential suggesting an energised inner membrane that can sufficiently balance the movement of protons in order to generate ATP.

The assessment of complex I activity showed considerable variation between the two wild-type clones. The activity of complex I was measured in cell lysates from neurons and also neurons cultured in folic acid for 24 hours prior to cell lysis. This was in anticipation of any significant decreases in complex I activity, like the results seen in fibroblasts. It has been shown previously that enhancing nucleotide pools through the use of folic acid, which adds 1-carbon units in the biosynthesis of nucleotides can alleviate mitochondrial

dysfunction caused by PINK1 deficiency (Tufi et al. 2014). Therefore it was hypothesised that had there been a significant decrease in the mutant neurons compared to controls that if it could be alleviated in the presence of folic acid it might suggest that this phenotype was linked to PINK1 deficiency. However, for these experiments there was no positive control, such as iPSC-derived neurons containing the PINK1 mutation use in the fibroblast experiments, therefore it was not possible to perform a dose-response of folic acid treatment beforehand. In reality however, it was found that discrepancies between wild-type clone 1 and clone 2, with the complex I activity measured from clone 2 cell lysates being approximately 60% of that measured in clone 1 lysates, made it not possible to identify any reliable changes in the mutant cells. Compared to clone 1, the mutant cell complex I activity was approximately 46%; but compared to clone 2 the mutant activity was at approximately 73%.

When stimulating cells with the mitochondrial uncoupler CCCP, cortical neurons responded with a decrease in protein level of mitofusin 1, suggesting protein degradation however no ubiquitination was detected after 48 H. This effect was consistent between wild-type clones and the mutant neurons. The accumulation of PINK1 was detected at the 48 H timepoint, with a greater amount of protein detected in the wild-type clone 1 treated with CCCP than clone 2, however the accumulation in the mutant neurons appeared to be close to an average of both wild-type clones. These data suggest that the upstream processes of mitophagy, such as the accumulation of full-length PINK1 and the degradation of outer mitochondrial proteins, such as mitofusin1, were as expected in both wild-type and mutant neurons.

Nevertheless, quantification of mitochondrial proteins, such as Tom20, showed no activation of mitophagy at the same timepoint. In the current model of mitophagy, PINK1 accumulation on depolarised mitochondria occurs upstream of the ubiquitination of

outer mitochondrial membrane proteins by the E3 ubiquitin ligase Parkin, and this triggers the ubiquitin-binding adaptor p62 and autophagic machinery for elimination. Therefore it is unclear why one outer mitochondrial protein, mitofusin 1, is degraded but not another outer mitochondrial membrane protein, Tom20. There was no significant difference in the Tom20 levels in any of the cells treated with DMSO to those treated with CCCP for 48H, therefore it is not known whether mitophagy or even biogenesis had been stimulated. If biogenesis was stimulated in these cells as a result of the widespread loss of functioning mitochondria caused by CCCP, the levels of Tom20 may be maintained but so too would mitofusin 1 which would be also present on the newly synthesised mitochondria. The increase in PINK1 protein at this timepoint suggests that damaged mitochondria remain in the cells, but the near complete loss of mitofusin 1 suggests widespread mitochondrial clearance. These data, together with the findings in depolarised myotubes are discussed further in section 3.3.6.

3.3.3 Phenotypes in myogenic cells containing tRNAserine mtDNA mutation

In the iPSCs differentiated towards a myogenic cell fate, a high mutant load was determined in the two mutant clones and no insertion was detected in the one wild-type line used in these experiments. On analysis of mitochondrial membrane potential in live cells, the two mutant lines appeared to be polarised similarly to the wild-type myotubes. On repeat experiments it was found that nearly no noticeable difference was measured in the mutant lines, suggesting good reproducibility even in live cell imaging. Although only one wild-type line of differentiated myotubes was used, a significant decrease was found in complex I activity in the lysates of mutant clone 12, again with high reproducibility. Whilst it did not reach statistical significance, the complex I activity in mutant clone

11 cell lysates was also noticeably reduced. Since Sanger sequencing of mtDNA cannot be used to accurately quantify mutant load, the significant decrease achieved in clone 12 could not be attributed to a greater mutant load than in clone 11.

The wild-type and mutant myotubes were treated with mitochondrial uncoupler CCCP as was carried out in the cortical neurons. The accumulation of PINK1 was significant in wild-type myotubes at the 48 H timepoint, similarly to that seen in neurons. However the same exposure to CCCP in the two mutant clones caused no significant increase in PINK1 protein levels. The CCCP did appear to stimulate the stabilisation of full-length PINK1 in the mutants, but to a much more modest effect at this timepoint. No other timepoints were observed, so it is not to say that PINK1 did not accumulate at a different rate to that in the wild-type but it is interesting that the same reduction was identified in the two different mutant clones. Similarly, the significant degradation of mitofusin 1 was again observed in the wild-type myotubes, but this did not reach statistical significance in the two mutant clones. It should be noted that this was not a case of entirely no degradation of mitofusin 1 being caused in the mutant lines, but in both lines this degradation appeared to be variable across the triplicate experiments, in contrast to the very consistent effect of CCCP in the wild-type cells.

In myotubes differentiated from iPSC containing wild-type mtDNA, no change in the protein levels of inner mitochondrial membrane protein Tim23 was detected after 48 hours of CCCP. However, a significant increase in outer mitochondrial membrane protein Tom20 was identified, suggesting stimulation of mitochondrial biogenesis. As with the observations in the neurons, it is unclear why mitofusin 1 is degraded when Tom20 protein levels are higher, in the case of myotubes, significantly. Looking at the effect of the mutation, a significant increase in Tom20 was also identified in both mutant clone lines, and in mutant clone 12 there was also a significant

increase in Tim23 protein levels; suggesting that biogenesis is stimulated in the mutants, and to a greater extent in particular in mutant clone 12. Interestingly, the basal protein levels of Tim23 were found to be significantly reduced in mutant clone 12 compared to wild-type.

Encouragingly, despite not having more than one wild-type line, phenotypic characteristics seemed to be consistent in both mutant clones. These myotubes exhibited reduced basal complex I activity, and under depolarised conditions, reduced PINK1 accumulation, reduced mitofusin 1 degradation and increased mitochondrial biogenesis.

3.3.4 Differences in the effect of the same mutation in different cell types – fibroblasts, cortical neurons and myotubes

It is commonly found in heterogeneous mitochondrial DNA diseases that high-energy demanding tissues are most often affected and to a greater severity. The reasoning behind this is that high-energy demanding tissues require a greater output from mitochondria and therefore the consequences of dysfunctional mitochondria are more apparent. In the phenotypic information provided for the patients harbouring the m.7472insC mutation, the observations were ataxia, myoclonus and deafness. Myoclonus can originate from numerous areas, defined for example as cortical myoclonus, spinal myoclonus or peripheral myoclonus; whilst cortical myoclonus is the most common presentation, the predicted origin of the m.7472insC patient's myoclonus was not stated (Kojovic et al. 2011).

In the three cell types studied containing the m.7472insC mutation, no significant changes in mitochondrial membrane potential were detected. In fibroblasts obtained from patients harbouring the

m.7472insC mutation, a significant reduction in Complex I activity was identified, however no dermatological symptoms were reported in the patients. In iPSC-derived neurons, Complex I activity appeared to be no different to one of the controls and in iPSC-derived myotubes a significant reduction was again identified. Interestingly, no phenotypes were detected in the iPSC-derived neurons but both the fibroblasts and iPSC-derived myotubes appeared to harbour defects in part of the mitophagy pathway in addition to Complex I activity impairment. In the fibroblasts, mitofusin ubiquitination was significantly reduced, a phenotype also associated with PINK1 and Parkin mutant patient-derived fibroblasts, and in the myotubes a reduction in PINK1 accumulation was observed and no significant mitofusin degradation.

A Complex I defect caused by the m.7472insC mutation has been reported in many patients harbouring this mutation and presenting with sensorineural deafness (Tiranti et al. 1995; Toompuu et al. 2002). It is unknown whether the absence of Complex I defect in the iPSC-derived neurons is a result of tissue-specific phenotypes commonly seen in mitochondrial diseases or whether the model is not effective in this cell type. If this occurred due to a tissue-specific phenotype, it is particularly interesting to have three cell types all expressing the m.7472insC mutation to what is believed to be a high mutant load, but with one cell type not displaying a phenotype and two cell types which do but one a high-energy demanding cell type and the other a low-energy demanding cell type. In this case, these models provide a great set-up for studying why the Complex I and mitophagy alterations occur in muscle and not cortical neurons, and also why fibroblasts in the patient appear to ‘cope’ with the molecular pathology but muscle is implicated in the presentation of the patient.

3.3.4.1 Why was a phenotype not detected in the iPSC-derived cortical neurons?

Studies in numerous patients harbouring the m.7472insC mutation have shown that neurological features of ataxia and myoclonus occur when mutant loads reach over 95% (Hutchin et al. 2001; Tiranti et al. 1995; Jaksch et al. 1998). Since the mutant load was not determined by NGS and therefore could not be accurately quantified, the absence of phenotype could be a result of a mutant load less than 95%. The other cell types, fibroblasts and myotubes, may not have a mutant load threshold so high and therefore a phenotype could be identified. Generation of numerous cell lines with various mutant loads would be required to identify if this was the cause. Unlike if iPSC-derived cardiomyocytes were generated and found to have no phenotype, it was surprising that the cortical neurons did not show any defects since they are a cell type likely to be involved in the myoclonus observed in the patient.

Alternatively, the isolated iPSC-derived cortical neurons may not be sufficient to emulate functional consequences of mitochondrial DNA mutations. A two-dimensional culture may not be adequate to model neural circuitry and functional output (Paşca et al. 2015). Furthermore, the differences in the two neuronal lines derived from two wild-type iPS clones may have prevented the detection of a significant phenotype if the result from one of the wild-type clones was due to an error. Moreover, without a positive control, such as an iPSC-derived PINK1 mutant, and an abundance of cells to confidently establish a mitophagy assay, it remains unknown whether the concentrations and timepoints used for investigating mitophagy in the neurons were correct. The occurrence of mitophagy in neurons is discussed further in section 3.3.6.

3.3.4.2 Why do patients not exhibit a phenotype in fibroblasts when the cell model shows impaired Complex I activity?

The m.7472insC fibroblasts and myotubes in these experiments revealed impairments in Complex I activity, which is a known consequence of some mitochondrial mutations, providing validity to this model. Furthermore, the presence of mitophagy-associated impairments in the cell types also exhibiting Complex I deficiencies suggests an involvement of mitophagy in the pathomechanism of this disease.

As shown in Chapter 2, m.7472insC fibroblasts also exhibited increased mitochondria-endoplasmic reticulum contacts, increased biogenesis upon depolarisation of the mitochondrial membrane, and decreased mitochondrial length; however patients had no dermatological symptoms. Although not all these effects could be assessed in muscle, similar phenotypes were observed in the iPSC-derived myotubes in Complex I activity and mitophagy-associated proteins, but the patient's muscle is implicated in their presentation. Fibroblasts grown under standard culture conditions are glycolytic, and therefore utilise mitochondrial oxidative phosphorylation to a lesser extent, meaning that defects in their mitochondria may not affect their function (Zheng 2012). It has been found too that cultured muscle cells can be highly glycolytic, however mature myotubes in the patient rely predominantly on oxidative phosphorylation (Aguer et al. 2011; Sin et al. 2016).

3.3.5 Working hypothesis for the effect of m.7472insC mutation on mitochondria in myotubes

The data obtained from experiments in iPSC-derived myotubes suggest that under stressed conditions, such as exposure to the mitochondrial uncoupler CCCP, the accumulation of full-length

PINK1 is triggered in wild-type cells. With this, degradation of outer mitochondrial membrane protein mitofusin 1 was observed, which based on the current model of mitophagy is likely to be caused by the recruitment of the E3 ubiquitin ligase Parkin. Furthermore, measurement of mitochondrial protein expression suggested a stimulation of biogenesis, since the total mitochondrial protein levels either remained the same or increased. The high respiratory demands of myogenic cell types for efficient function suggests that even under circumstances of widespread depolarisation of mitochondria, which is not particularly likely to occur under normal biological conditions, it would not be energetically worthwhile to solely remove all mitochondria (Moraes et al. 1992). Instead, proliferation is more likely to be stimulated in parallel with mitophagy.

In the myotubes containing the m.7472insC, stressed conditions did not cause an accumulation of PINK1, nor significant degradation of mitofusin 1, suggesting that PINK1 did not stimulate the translocation of Parkin. On assessment of total mitochondrial protein levels, a large increase in mitochondrial proteins was observed, suggesting that biogenesis had been stimulated. Experiments investigating the mRNA expression of PGC-1α in patient fibroblasts showed a large stimulation of biogenesis upon stress induced by CCCP, which was hypothesised as being compensatory since PGC-1α has been shown to buffer reactive oxygen species (Baldelli et al. 2014). Here it remains unknown whether stimulation of biogenesis occurs to the a greater extent in patient cells than wild-type, or whether larger increases in mitochondrial proteins are only due to the lack of mitophagy stimulated. If under widespread depolarisation the stimulation of mitophagy is impaired, it stands to reason that under basal conditions the quality control process is unable to regulate defective mitochondria and this is shown functionally in the impaired activity of Complex I.

3.3.6 Does mitophagy occur in neurons and myotubes?

As discussed previously, exposing cells to a mitochondrial uncoupler for 48 hours is energetically compromising in high-energy demanding tissues, and various studies in muscle have revealed the importance of repopulation of biogenesis with mitophagy, described as a 'cross-talk' between two contrasting processes (Sin et al. 2016; Vainshtein et al. 2015; Greene et al. 2015). Other studies *in vivo* have also shown that the pathway of mitophagy is likely to be cell-specific, therefore since our understanding of mitophagy so far has been largely dependent on artificial cell lines, we should be open to potential alternative mechanisms (McWilliams et al. 2016; Sun, Yun, Liu, Malide, Liu, I. I. Rovira, et al. 2015).

Recent studies in neurons have revealed alternative mechanisms to the traditional mitophagy model. In particular, the emergence of mitochondrial transfer, shown both in a Parkin-overexpressed system and *in vivo* (G. Ashrafi et al. 2014; Davis et al. 2014). This process involves the extrusion of damaged mitochondria for degradation by the lysosomes of neighbouring glia. It has been shown also that healthy mitochondria can be acquired from neighbouring glia following neuronal damage via neuro-glial mitochondrial transfer (Hayakawa et al. 2016).

These studies call into question further the validity of a two-dimensional neuronal cell model for mitophagy, since if damaged mitochondria are cleared by the transfer to neighbouring glia, this will not occur in isolated cell models. This may be why in these experiments, PINK1 accumulation is observed but no loss of mitochondrial membrane proteins Tom20 and Tim23.

3.3.7 Future perspectives

The next experiments to do in this section would be to repeat the differentiation into myotubes and neurons. Independent differentiation experiments would help validate the findings shown here. Furthermore it would enable the use of more controls and potentially generate mutant lines with different mutant loads, including an isogenic control.

The m.7472insC mutation has a similar molecular effect to the mitochondrial mutation A7445G, therefore it would be interesting if it were possible to obtain fibroblasts from these patients to assess the specificity of the phenotypes observed to the m.7472insC mutation (Toompuu et al. 2002).

The recent work on trans-mitophagy in neurons also suggests that neuronal three-dimensional cultures should be investigated for the study of mitophagy. This would be particularly effective in neurons as this cell-type is very network dependent and relies on connectivity for function.

Discussion

The main aim of this thesis involved testing the hypothesis that the process of selective mitophagy is impaired in mitochondrial DNA disease such that mutant mitochondrial DNA can persist.

To do this, the requirements for mitophagy induction were explored as well as the methods of detection in various cell types. In chapter one it was shown that PINK1-dependent mitophagy can be induced independently of mitochondrial membrane depolarisation. The study of the mitophagy pathway is largely limited by the repeated use of mitochondrial uncouplers to initiate the process. Using only this method restricts our understanding of the physiological role of mitophagy. Here, using an alternative compound Rhodamine 6G, it was shown that oxidative stress at an insufficient level to cause membrane depolarisation could however induce the accumulation of PINK1. It has been shown previously that loss of mitochondrial membrane potential prevents the import of PINK1 through the translocase of the inner mitochondrial membrane, causing it to become stabilised on the outer membrane, however these results suggest that there must be an alternative mechanism by which PINK1 accumulates (Jin et al. 2010). Using next generation sequencing, it was found that Rhodamine 6G also induced low levels mutations in SH-SY5Y cells and fibroblasts, indicating that damage to the mitochondrial genome may also contribute to the induction of mitophagy. This data contributes to other evidence in the literature, which show mitophagy occurring in polarised mitochondria, such as a reduction in activity of mitochondrial processing peptidase and the loss of mitochondrial protease LONP1, both causing the accumulation of PINK1 at the mitochondrial surface (Jin & Youle 2013; Greene et al. 2012). The

main hypothesis of this thesis is that mitophagy is not triggered in mtDNA disease patient cells containing high ratios of mutant mtDNA, therefore not only do the requirements of mitophagy induction need to be better understood, if the hypothesis is found to be true then therapies targeting stimulation of mitophagy would need to be explored.

The experiments in chapter one also highlighted a significant flaw in the field of mitophagy research. Using non-Parkin-overexpressing systems to assess the clearance of mitochondrial proteins, it was found by immunocytochemistry that the signal from one particular mitochondrial marker, an antibody against Complex V, was lost in a PINK1-independent manner, at a much earlier timepoint than other mitochondrial protein markers. This however was not found to be the case by Western blotting, and this phenomenon has not been reported in the literature. As discussed in section 1.1.2, there are several different methods that can be used to assess mitophagy and unfortunately each have their limitations. Without an approved and consensually agreed experimental method of defining mitophagy, the research in this field is hindered by non-comparable methods of assessing mitophagy between publications. The loss of mitochondrial proteins as assessed by immunocytochemistry is a common mitophagy indicator, however had Complex V been used to measure this in certain cell systems, the results would be misleading and false. In my opinion, it should be standard practice to show mitophagy by providing evidence of colocalisation of mitochondria with lysosomes in the presence of autophagy inhibitors, which would indicate ‘end-stage’ mitophagy, and not measuring ‘net’ change in mitochondria, which is heavily influenced by biogenesis as well as mitochondrial clearance.

In the second chapter of this thesis, a range of different patient fibroblast lines with mitochondrial DNA disease were used to explore mitochondrial dysfunction. All these patients harboured a

mutation in the mitochondrial genome, however the presentations were heterogeneous. These included two sets of relatives; one of the sets included a symptomatic and an asymptomatic case, and the other set included two patients both presenting with the same phenotype. Furthermore, one patient had a mutation in a subunit of the ATP synthase but was clinically diagnosed as having Charcot-Marie-Tooth hereditary neuropathy type 2 (CMT2).

The aim of this chapter was to use this range of fibroblast lines to identify common characteristics between the lines in this cell type and investigate the induction of mitophagy. In the context of the main thesis hypothesis, using a range of lines it was possible to show significant impairment of mitofusin ubiquitination affected all patient fibroblasts, except for the CMT2 patient. Moreover, biogenesis was stimulated upon mitochondrial depolarisation in a manner not observed in control cells in all the lines which possessed a mutation in a mitochondrial tRNA gene. In these experiments, mRNA analysis of PGC-1α was used to indicate an upregulation of biogenesis, however this data would benefit from showing an increase in mtDNA copy number, and also the activation of TFAM (mitochondrial transcription factor A) expression. Interestingly, upon closer examination of one particular mutation, m.7472insC, similarities in both function and morphology were observed between these lines and PINK1 mutant fibroblasts. These findings supported the hypothesis of an impaired mitophagy pathway, however the process of mitophagy appears to be incomplete in this cell type. Studies in control, PINK1 and Parkin mutant fibroblasts have demonstrated that complete removal of mitochondria does not occur following mitochondrial membrane depolarisation even in wild-type fibroblasts, however the ubiquitination of mitofusins is dependent upon PINK1 or Parkin. Therefore the striking reduction of mitofusin ubiquitination, particularly in the m.7472insC mutant fibroblasts, strongly implicated

a disturbance to the normal mitophagy pathway since this effect has only previously been reported in PINK1 and Parkin mutants.

The decision to study the m.7472insC mutation further was to enable more experiments to be performed in a shorter timeframe, since culturing large numbers of fibroblasts, which are slow growing and have a particularly low protein content, would limit the depth in which this hypothesis could be studied. Since fibroblasts are an unaffected tissue type in these diseases, the next experiments involved reprogramming fibroblasts to iPSCs and differentiating them into neurons and myotubes. As a result, only the m.7472insC fibroblasts were used since these processes are particularly time-consuming.

The objective of chapter three was to generate neuronal and myogenic cell models of mitochondrial DNA disease using the m.7472insC mutant fibroblasts. The mitophagy pathway has been most extensively characterised in immortalised cell lines, therefore how these known mechanisms translate in different cell types is not well understood. As a result, after generating mutation-containing iPSC-derived cell types, the aim was to attempt to induce mitophagy, using techniques used in SH-SY5Y cells, and assess whether defects could be observed in these cell types. Although complete mitophagy could not be detected in either cortical neurons or myoblasts, the accumulation of PINK1 and mitofusin degradation could be quantified.

The same experiments were performed in the iPSC-derived cortical neurons and iPSC-derived myoblasts, and interestingly only a mitophagy-associated defect was identified in the myoblasts. Mitochondrial diseases are well known to affect tissues differently despite the presence of the mutation in all cells, so this effect was particularly interesting in the development of a valid mitochondrial disease model. No significant differences were observed in the

mutant neurons compared to those derived from control iPSC, however in the myoblasts, significantly reduced Complex I activity was reported. Furthermore, upon depolarisation of the mitochondrial membrane potential, a significant reduction in both PINK1 accumulation and mitofusin 1 degradation was identified in the mutant myoblasts. Whilst these experiments were performed from only one induction, and more controls would be ideal for future experiments, it was particularly interesting to observe that in the neurons there was both no functional defect and no apparent mitophagy impairments, but in the myoblasts a functional defect was present with a seeming deficiency to the accumulation of PINK1 and downstream processes.

If these experiments were to be repeated after further inductions, it would be particularly interesting to monitor mutant load throughout the duration. In the experiments conducted using fibroblasts, cortical neurons and myoblasts, mutant load was only assessed once in each cell type. It is well known that in the human disease and in cultured cells that mutant load can change over time, however it is not usually monitored throughout experimental studies. It would be beneficial when repeating experiments in triplicate to know if the mutant load was the same each time, since changes in load may correlate with phenotype. Since Next Generation Sequencing is the most accurate method of measuring mutant load, but also very expensive, it would be useful to obtain a cell ‘sample’ for each experiment conducted, for example by plating an extra well of cells for each experiment preparation. Cells could then be harvested for DNA extraction at the timepoint of each experiment, and ultimately all samples loaded onto a sequencing run to provide a comparison of mutant load across all experiments.

Although more experiments are required, dysfunction in mitophagy-associated proteins has been observed in cell types with compromised mitochondrial function (fibroblasts and iPSC-derived

myotubes), but not in cell types in which the same functional impairment is not observed (iPSC-derived cortical neurons). Any reductions in mitochondrial membrane potential did not seem to correlate with mitochondrial dysfunction or mitophagy-related impairments, which was in accordance with the findings in chapter one, which showed that membrane depolarisation is not required to stimulate mitophagy. Together the findings in this thesis provide evidence that mitophagy impairments are implicated in mitochondrial DNA disease and that this pathway could be a target for developing therapeutic strategies towards the management of these diseases.

Appendix

Cell Type	Treatment time	Locus	Position	Change	% Reads
SH-SY5Y	1.5 H	RNR2	2456	TA > T (del)	1.05
		COX1	6691	GA > G (del)	1.03
SH-SY5Y	14 H	ND2	4604	CA > C (del)	1.01
		COX1	6691	GA > G (del)	1.03
		DLOOP3	16161	TA > T (del)	2.17
		DLOOP3	16186	C > T (ts)	2.67
		DLOOP3	16294	C > T (ts)	1.58
		DLOOP3	16304	T > C (ts)	2.17
		DLOOP3	16327	C > T (ts)	2.95
Fibroblast	24 H	DLOOP5	247	G > A (ts)	1.04
		DLOOP5	302	A > AC (ins)	2.49
		DLOOP5	309	C > CCT (ins)	3.63
		DLOOP5	564	G > A (ts)	1.26
		COX1	6691	GA > G (del)	1.01
		ND3	10348	T > C (ts)	1.16
Fibroblast	24 H	DLOOP5	312	C > CA (ins)	1.57
		ND2	4604	CA > C (del)	1.07
		TRNS1	7506	G > T (tv)	1.05
		ND4	10806	G > T (tv)	1.01
		DLOOP3	16419	C > A (tv)	1.01

Table shows the base changes observed by Next Generation Sequencing of different cell types (SH-SY5Y cells or fibroblasts) treated for different time periods (1.5 H – 24 H) with 2 µM

Rhodamine 6G, a summary of which is shown in Figure 17. Data shows mitochondrial genome base changes, the position and type of variant: tv = transversion, ts = transition, ins = insertion and del = deletion. The ‘Change’ shows the reference base and the change that occurred at that position. The ‘% reads’ is the percentage of reads (approx. 10,000 reads per base) containing the variant.

References

Abramov, A.Y. et al., 2011. Bioenergetic Consequences of PINK1 Mutations in Parkinson Disease M. P. Mattson, ed. *PLoS ONE*, 6(10), p.e25622. Available at: http://dx.plos.org/10.1371/journal.pone.0025622 [Accessed February 16, 2017].

Aerts, L. et al., 2015. PINK1 kinase catalytic activity is regulated by phosphorylation on serines 228 and 402. *The Journal of Biological Chemistry*, 290(5), pp.2798–2811.

Agostini, M. et al., 2016. Metabolic reprogramming during neuronal differentiation. *Cell death and differentiation*, 23(9), pp.1502–14. Available at: http://www.ncbi.nlm.nih.gov/pubmed/27058317 [Accessed June 13, 2017].

Aguer, C. et al., 2011. Galactose Enhances Oxidative Metabolism and Reveals Mitochondrial Dysfunction in Human Primary Muscle Cells R. M. Luque, ed. *PLoS ONE*, 6(12), p.e28536. Available at: http://dx.plos.org/10.1371/journal.pone.0028536 [Accessed June 21, 2017].

Alemi, M. et al., 2007. Mitochondrial DNA deletions inhibit proteasomal activity and stimulate an autophagic transcript. *Free radical biology & medicine*, 42(1), pp.32–43. Available at: http://www.ncbi.nlm.nih.gov/pubmed/17157191 [Accessed July 5, 2017].

Allen, G.F.G. et al., 2013. Loss of iron triggers PINK1/Parkin-independent mitophagy. *EMBO reports*, 14(12), pp.1127–1135. Available at: http://embor.embopress.org/cgi/doi/10.1038/embor.2013.168.

Antonicka, H. et al., 2013. The Mitochondrial RNA-Binding Protein GRSF1 Localizes to RNA Granules and Is Required for Posttranscriptional Mitochondrial Gene Expression. *Cell*

Metabolism, 17(3), pp.386–398. Available at: http://www.ncbi.nlm.nih.gov/pubmed/23473033 [Accessed June 28, 2017].

Ashley, M. V., Laipis, P.J. & Hauswirth, W.W., 1989. Rapid segregation of heteroplasmic bovine mitodiondria. *Nucleic Acids Research*, 17(18), pp.7325–7331. Available at: https://academic.oup.com/nar/article-lookup/doi/10.1093/nar/17.18.7325 [Accessed June 6, 2017].

Ashrafi, G. et al., 2014. Mitophagy of damaged mitochondria occurs locally in distal neuronal axons and requires PINK1 and Parkin. *The Journal of Cell Biology*, 206(5), pp.655–670.

Ashrafi, G. et al., 2014. Mitophagy of damaged mitochondria occurs locally in distal neuronal axons and requires PINK1 and Parkin. *The Journal of Cell Biology*, 206(5), pp.655–670. Available at: http://www.jcb.org/cgi/doi/10.1083/jcb.201401070.

Ashrafi, G. & Schwarz, T.L., 2013. The pathways of mitophagy for quality control and clearance of mitochondria. *Cell Death and Differentiation*, 20(1), pp.31–42. Available at: http://www.nature.com/doifinder/10.1038/cdd.2012.81.

Bacman, S.R. et al., 2013. Specific elimination of mutant mitochondrial genomes in patient-derived cells by mitoTALENs. *Nat Med*, 19(9), pp.1111–1113. Available at: http://dx.doi.org/10.1038/nm.3261.

Baldelli, S., Aquilano, K. & Ciriolo, M.R., 2014. PGC-1α buffers ROS-mediated removal of mitochondria during myogenesis. *Cell death & disease*, 5(11), p.e1515. Available at: http://dx.doi.org/10.1038/cddis.2014.458.

Baranowska, I. et al., 2009. Sensory Ataxic Neuropathy in Golden Retriever Dogs Is Caused by a Deletion in the Mitochondrial tRNATyr Gene M. Georges, ed. *PLoS Genetics*, 5(5), p.e1000499. Available at: http://dx.plos.org/10.1371/journal.pgen.1000499 [Accessed May 15, 2017].

Baughman, J.M. et al., 2011. Integrative genomics identifies MCU

as an essential component of the mitochondrial calcium uniporter. *Nature*, 476(7360), pp.341–345. Available at: http://www.ncbi.nlm.nih.gov/pubmed/21685886 [Accessed June 23, 2017].

Beckman, K.B. & Ames, B.N., 1996. Detection and quantification of oxidative adducts of mitochondrial DNA. *Methods in enzymology*, 264, pp.442–53. Available at: http://www.ncbi.nlm.nih.gov/pubmed/8965717 [Accessed June 28, 2017].

Behar, D.M. et al., 2008. A novel 154-bp deletion in the human mitochondrial DNA control region in healthy individuals. *Human mutation*, 29(12), pp.1387–91. Available at: http://www.ncbi.nlm.nih.gov/pubmed/18629826 [Accessed June 28, 2017].

Berezhnov, A. V. et al., 2016. Intracellular pH modulates autophagy and mitophagy. *Journal of Biological Chemistry*, 291(16), pp.8701–8708.

Bogenhagen, D.F., 2012. Mitochondrial DNA nucleoid structure. *Biochimica et Biophysica Acta (BBA) - Gene Regulatory Mechanisms*, 1819(9–10), pp.914–920. Available at: http://www.ncbi.nlm.nih.gov/pubmed/22142616 [Accessed June 28, 2017].

Britanova, O. et al., 2008. Satb2 Is a Postmitotic Determinant for Upper-Layer Neuron Specification in the Neocortex. *Neuron*, 57(3), pp.378–392. Available at: http://www.sciencedirect.com/science/article/pii/S0896627308000330 [Accessed May 31, 2017].

Burbulla, L.F. & Krüger, R., 2012. The use of primary human fibroblasts for monitoring mitochondrial phenotypes in the field of Parkinson's disease. *Journal of visualized experiments : JoVE*, (68). Available at: http://www.ncbi.nlm.nih.gov/pubmed/23070237 [Accessed May 15, 2017].

Burri, L. et al., 2006. Integral membrane proteins in the

mitochondrial outer membrane of Saccharomyces cerevisiae. *FEBS Journal*, 273(7), pp.1507–1515. Available at: http://www.ncbi.nlm.nih.gov/pubmed/16689936 [Accessed June 22, 2017].

Cai, Q. et al., 2012. Spatial Parkin Translocation and Degradation of Damaged Mitochondria via Mitophagy in Live Cortical Neurons. *Current Biology*, 22(6), pp.545–552. Available at: http://linkinghub.elsevier.com/retrieve/pii/S0960982212001224.

Cai, X. & Lytton, J., 2004. Molecular Cloning of a Sixth Member of the K+-dependent Na+/Ca2+ Exchanger Gene Family, NCKX6. *Journal of Biological Chemistry*, 279(7), pp.5867–5876. Available at: http://www.ncbi.nlm.nih.gov/pubmed/14625281 [Accessed June 23, 2017].

Cao, L. et al., 2009. New evidence confirms that the mitochondrial bottleneck is generated without reduction of mitochondrial DNA content in early primordial germ cells of mice. *PLoS genetics*, 5(12), p.e1000756. Available at: http://www.ncbi.nlm.nih.gov/pubmed/19997484 [Accessed June 5, 2017].

Cao, L. et al., 2007. The mitochondrial bottleneck occurs without reduction of mtDNA content in female mouse germ cells. *Nature Genetics*, 39(3), pp.386–390. Available at: http://www.nature.com/doifinder/10.1038/ng1970.

Celardo, I. et al., 2016. Mitofusin-mediated ER stress triggers neurodegeneration in pink1/parkin models of Parkinson's disease. *Cell Death and Disease*, 7(6), p.e2271. Available at: http://www.ncbi.nlm.nih.gov/pubmed/27336715 [Accessed February 16, 2017].

Chan, D.C., 2012. Fusion and Fission: Interlinked Processes Critical for Mitochondrial Health. *Annual Review of Genetics*, 46(1), pp.265–287. Available at: http://www.annualreviews.org/doi/10.1146/annurev-genet-110410-132529.

Chan, N.C. et al., 2011. Broad activation of the ubiquitin-

proteasome system by Parkin is critical for mitophagy. *Human Molecular Genetics*, 20(9), pp.1726–1737.

Chazotte, B., 2011. Labeling mitochondria with TMRM or TMRE. *Cold Spring Harbor Protocols*, 6(7), pp.895–897.

Chen, X. et al., 2015. Lysosomal targeting with stable and sensitive fluorescent probes (Superior LysoProbes): applications for lysosome labeling and tracking during apoptosis. *Scientific reports*, 5, p.9004. Available at: http://www.pubmedcentral.nih.gov/articlerender.fcgi?artid=4355733&tool=pmcentrez&rendertype=abstract [Accessed November 21, 2015].

Cherry, A.B.C. et al., 2013. Induced Pluripotent Stem Cells with a Mitochondrial DNA Deletion. *STEM CELLS*, 31(7), pp.1287–1297. Available at: http://www.ncbi.nlm.nih.gov/pubmed/23400930 [Accessed June 5, 2017].

Chinnery, P.F. et al., 2004. Risk of developing a mitochondrial DNA deletion disorder. *The Lancet*, 364(9434), pp.592–596. Available at: http://www.ncbi.nlm.nih.gov/pubmed/15313359 [Accessed July 5, 2017].

Chinnery, P.F. et al., 2000. The epidemiology of pathogenic mitochondrial DNA mutations. *Annals of neurology*, 48(2), pp.188–93. Available at: http://www.ncbi.nlm.nih.gov/pubmed/10939569 [Accessed July 4, 2017].

Clark, I.E. et al., 2006. Drosophila pink1 is required for mitochondrial function and interacts genetically with parkin. *Nature*, 441(7097), pp.1162–1166.

Clayton, D.A., 1982. Replication of animal mitochondrial DNA. *Cell*, 28(4), pp.693–705. Available at: http://www.ncbi.nlm.nih.gov/pubmed/6178513 [Accessed June 28, 2017].

Clayton, D.A., Doda, J.N. & Friedberg, E.C., 1974. The absence of a pyrimidine dimer repair mechanism in mammalian

mitochondria. *Proceedings of the National Academy of Sciences of the United States of America*, 71(7), pp.2777–81. Available at: http://www.ncbi.nlm.nih.gov/pubmed/4212385 [Accessed June 28, 2017].

Cotán, D. et al., 2011. Secondary coenzyme Q10 deficiency triggers mitochondria degradation by mitophagy in MELAS fibroblasts. *FASEB journal : official publication of the Federation of American Societies for Experimental Biology*, 25(8), pp.2669–87. Available at: http://www.fasebj.org/cgi/doi/10.1096/fj.10-165340 [Accessed May 15, 2017].

Craven, L. et al., 2010. Pronuclear transfer in human embryos to prevent transmission of mitochondrial DNA disease. *Nature*, 465(7294), pp.82–5. Available at: http://www.ncbi.nlm.nih.gov/pubmed/20393463 [Accessed May 12, 2017].

D'Aurelio, M. et al., 2010. Mitochondrial DNA background modifies the bioenergetics of NARP/MILS ATP6 mutant cells. *Human molecular genetics*, 19(2), pp.374–86. Available at: http://www.ncbi.nlm.nih.gov/pubmed/19875463 [Accessed June 5, 2017].

Dauer, W. & Przedborski, S., 2003. Parkinson's disease: mechanisms and models. *Neuron*, 39(6), pp.889–909.

Davis, C.O. et al., 2014. Transcellular degradation of axonal mitochondria. *Proceedings of the National Academy of Sciences of the United States of America*, 111(26), pp.9633–9638.

Deas, E., Plun-Favreau, H. & Wood, N.W., 2009. PINK1 function in health and disease. *EMBO molecular medicine*, 1(3), pp.152–165.

DeLuca, S.Z. & O'Farrell, P.H., 2012. Barriers to Male Transmission of Mitochondrial DNA in Sperm Development. *Developmental Cell*, 22(3), pp.660–668. Available at: http://www.ncbi.nlm.nih.gov/pubmed/22421049 [Accessed June 28, 2017].

DiMauro, S. & Davidzon, G., 2005. Mitochondrial DNA and disease. *Annals of Medicine*, 37(3), pp.222–232. Available at: http://www.ncbi.nlm.nih.gov/pubmed/16019721 [Accessed July 4, 2017].

DiMauro, S. & Rustin, P., 2009. A critical approach to the therapy of mitochondrial respiratory chain and oxidative phosphorylation diseases. *Biochimica et Biophysica Acta (BBA) - Molecular Basis of Disease*, 1792(12), pp.1159–1167. Available at: http://www.sciencedirect.com/science/article/pii/S0925443908002007 [Accessed May 15, 2017].

Diot, A. et al., 2015. A novel quantitative assay of mitophagy: Combining high content fluorescence microscopy and mitochondrial DNA load to quantify mitophagy and identify novel pharmacological tools against pathogenic heteroplasmic mtDNA. *Pharmacological Research*, 100, pp.24–35. Available at: http://linkinghub.elsevier.com/retrieve/pii/S1043661815001474.

Durcan, T.M. & Fon, E.A., 2015. The three “P”s of mitophagy: PARKIN, PINK1, and post-translational modifications. *Genes & Development*, 29(10), pp.989–999.

Erpapazoglou, Z. & Corti, O., 2015. The endoplasmic reticulum/mitochondria interface: a subcellular platform for the orchestration of the functions of the PINK1–Parkin pathway?: Figure 1. *Biochemical Society Transactions*, 43(2), pp.297–301. Available at: http://www.ncbi.nlm.nih.gov/pubmed/25849933 [Accessed September 14, 2017].

Esteban-Martínez, L. & Boya, P., 2017. BNIP3L/NIX-dependent mitophagy regulates cell differentiation via metabolic reprogramming. *Autophagy*, pp.00–00. Available at: http://www.ncbi.nlm.nih.gov/pubmed/28614042 [Accessed July 4, 2017].

Fedorowicz, M.A. et al., 2014. Cytosolic cleaved PINK1 represses Parkin translocation to mitochondria and mitophagy. *EMBO reports*, 15(1), pp.86–93.

Folmes, C.D.L. et al., 2013. Disease-Causing Mitochondrial Heteroplasmy Segregated Within Induced Pluripotent Stem Cell Clones Derived from a Patient with MELAS. *STEM CELLS*, 31(7), pp.1298–1308. Available at: http://www.ncbi.nlm.nih.gov/pubmed/23553816 [Accessed June 5, 2017].

Frank, M. et al., 2012. Mitophagy is triggered by mild oxidative stress in a mitochondrial fission dependent manner. *Biochimica et Biophysica Acta - Molecular Cell Research*, 1823(12), pp.2297–2310. Available at: http://dx.doi.org/10.1016/j.bbamcr.2012.08.007.

Fujikura, J. et al., 2012. Induced pluripotent stem cells generated from diabetic patients with mitochondrial DNA A3243G mutation. *Diabetologia*, 55(6), pp.1689–1698. Available at: http://www.ncbi.nlm.nih.gov/pubmed/22396012 [Accessed June 5, 2017].

Gal-Levi, R. et al., 1998. Hepatocyte growth factor plays a dual role in regulating skeletal muscle satellite cell proliferation and differentiation. *Biochimica et Biophysica Acta (BBA) - Molecular Cell Research*, 1402(1), pp.39–51. Available at: http://www.sciencedirect.com/science/article/pii/S0167488997001249 [Accessed May 4, 2017].

Gandhi, S. et al., 2006. PINK1 protein in normal human brain and Parkinson's disease. *Brain: A Journal of Neurology*, 129(Pt 7), pp.1720–1731.

Garrido-Maraver, J. et al., 2012. Screening of effective pharmacological treatments for MELAS syndrome using yeasts, fibroblasts and cybrid models of the disease. *British journal of pharmacology*, 167(6), pp.1311–28. Available at: http://www.ncbi.nlm.nih.gov/pubmed/22747838 [Accessed February 14, 2017].

Gautier, C.A. et al., 2016. The endoplasmic reticulum-mitochondria interface is perturbed in PARK2 knockout mice and patients with PARK2 mutations. *Human Molecular Genetics*, 25(14),

p.ddw148. Available at: http://www.ncbi.nlm.nih.gov/pubmed/27206984 [Accessed September 14, 2017].

Gautier, C.A., Kitada, T. & Shen, J., 2008. Loss of PINK1 causes mitochondrial functional defects and increased sensitivity to oxidative stress. *Proceedings of the National Academy of Sciences*, 105(32), pp.11364–11369. Available at: http://www.pubmedcentral.nih.gov/articlerender.fcgi?artid=2516271&tool=pmcentrez&rendertype=abstract [Accessed October 6, 2015].

Gear, A.R.L. & Gear, R.L., 1974. J. Biol. Chem. 1974, 249:3628-3637.

Gegg, M.E. et al., 2010. Mitofusin 1 and mitofusin 2 are ubiquitinated in a PINK1/parkin-dependent manner upon induction of mitophagy. *Human Molecular Genetics*, 19(24), pp.4861–4870.

Gegg, M.E. et al., 2010. Mitofusin 1 and mitofusin 2 are ubiquitinated in a PINK1/parkin-dependent manner upon induction of mitophagy. *Human Molecular Genetics*, 19(24), pp.4861–4870. Available at: http://www.ncbi.nlm.nih.gov/pubmed/20871098 [Accessed February 16, 2017].

Gegg, M.E. & Schapira, A.H. V, 2011. PINK1-parkin-dependent mitophagy involves ubiquitination of mitofusins 1 and 2: Implications for Parkinson disease pathogenesis. *Autophagy*, 7(2), pp.243–245.

Geisler, S. et al., 2010. PINK1/Parkin-mediated mitophagy is dependent on VDAC1 and p62/SQSTM1. *Nature Cell Biology*, 12(2), pp.119–131.

Ghesquière, B. et al., 2014. Metabolism of stromal and immune cells in health and disease. *Nature*, 511(7508), pp.167–176. Available at: http://www.ncbi.nlm.nih.gov/pubmed/25008522 [Accessed May 15, 2017].

Ghezzi, D. et al., 2010. Severe X-Linked Mitochondrial

Encephalomyopathy Associated with a Mutation in Apoptosis-Inducing Factor. *The American Journal of Human Genetics*, 86(4), pp.639–649. Available at: http://www.ncbi.nlm.nih.gov/pubmed/20362274 [Accessed May 15, 2017].

Giles, R.E. et al., 1980. Maternal inheritance of human mitochondrial DNA. *Proceedings of the National Academy of Sciences of the United States of America*, 77(11), pp.6715–6719. Available at: http://www.pubmedcentral.nih.gov/articlerender.fcgi?artid=350359&tool=pmcentrez&rendertype=abstract.

Glauser, L. et al., 2011. Parkin promotes the ubiquitination and degradation of the mitochondrial fusion factor mitofusin 1. *Journal of Neurochemistry*, 118(4), pp.636–645.

Gorman, G.S. et al., 2015. Prevalence of nuclear and mitochondrial DNA mutations related to adult mitochondrial disease. *Annals of neurology*, 77(5), pp.753–9. Available at: http://www.ncbi.nlm.nih.gov/pubmed/25652200 [Accessed July 4, 2017].

Greene, A.W. et al., 2012. Mitochondrial processing peptidase regulates PINK1 processing, import and Parkin recruitment. *EMBO reports*, 13(4), pp.378–385.

Greene, N.P. et al., 2015. Mitochondrial quality control, promoted by PGC?1 *?* , is dysregulated by Western diet?induced obesity and partially restored by moderate physical activity in mice. *Physiological Reports*, 3(7), p.e12470. Available at: http://www.ncbi.nlm.nih.gov/pubmed/26177961 [Accessed June 21, 2017].

Grigoriev, S.M. et al., 2004. Electrophysiological Approaches to the Study of Protein Translocation in Mitochondria. In pp. 227–274. Available at: http://linkinghub.elsevier.com/retrieve/pii/S0074769604380058 [Accessed June 22, 2017].

Haack, T.B. et al., 2010. Exome sequencing identifies ACAD9

mutations as a cause of complex I deficiency. *Nat Genet*, 42(12), pp.1131–1134. Available at: http://dx.doi.org/10.1038/ng.706.

Haack, T.B. et al., 2012. Mutation screening of 75 candidate genes in 152 complex I deficiency cases identifies pathogenic variants in 16 genes including *NDUFB9*. *Journal of Medical Genetics*, 49(2), pp.83–89. Available at: http://www.ncbi.nlm.nih.gov/pubmed/22200994 [Accessed May 19, 2017].

Hamalainen, R.H. et al., 2013. Tissue- and cell-type-specific manifestations of heteroplasmic mtDNA 3243A>G mutation in human induced pluripotent stem cell-derived disease model. *Proceedings of the National Academy of Sciences*, 110(38), pp.E3622–E3630. Available at: http://www.ncbi.nlm.nih.gov/pubmed/24003133 [Accessed June 5, 2017].

Hare, J.F. & Hodges, R., 1982. Turnover of mitochondrial inner membrane proteins in hepatoma monolayer cultures. *The Journal of biological chemistry*, 257(7), pp.3575–3580.

Hasegawa, K. et al., 2016. Promotion of mitochondrial biogenesis by necdin protects neurons against mitochondrial insults. *Nature Communications*, 7, p.10943. Available at: http://www.nature.com/doifinder/10.1038/ncomms10943.

Hayakawa, K. et al., 2016. Transfer of mitochondria from astrocytes to neurons after stroke. *Nature*, 535(7613), pp.551–555. Available at: http://dx.doi.org/10.1038/nature18928.

Hayakawa, M. et al., 1996. Age-related extensive fragmentation of mitochondrial DNA into minicircles. *Biochemical and biophysical research communications*, 226(2), pp.369–77. Available at: http://linkinghub.elsevier.com/retrieve/pii/S0006291X96913637 [Accessed June 28, 2017].

Heeman, B. et al., 2011. Depletion of PINK1 affects mitochondrial metabolism, calcium homeostasis and energy maintenance.

Journal of Cell Science, 124(7), pp.1115–1125. Available at: http://jcs.biologists.org/cgi/doi/10.1242/jcs.078303.

Hess, J.F. et al., 1991. Impairment of mitochondrial transcription termination by a point mutation associated with the MELAS subgroup of mitochondrial encephalomyopathies. *Nature*, 351(6323), pp.236–9. Available at: http://www.ncbi.nlm.nih.gov/pubmed/1755869 [Accessed March 20, 2016].

Hevner, R.F. et al., 2001. Tbr1 regulates differentiation of the preplate and layer 6. *Neuron*, 29(2), pp.353–66. Available at: http://www.ncbi.nlm.nih.gov/pubmed/11239428 [Accessed May 31, 2017].

Heytler, P.G. & Prichard, W.W., 1962. A new class of uncoupling agents — Carbonyl cyanide phenylhydrazones. *Biochemical and Biophysical Research Communications*, 7(4), pp.272–275. Available at: http://linkinghub.elsevier.com/retrieve/pii/0006291X62901894 [Accessed July 10, 2017].

Higuti, T. et al., 1980. Rhodamine 6G, inhibitor of both H+-ejections from mitochondria energized with ATP and with respiratory substrates. *Biochimica et Biophysica Acta (BBA) - Bioenergetics*, 593(2), pp.463–467. Available at: http://www.sciencedirect.com/science/article/pii/000527288090081X [Accessed January 5, 2016].

Holt, I.J., Harding, A.E. & Morgan-Hughes, J.A., 1988. Deletions of muscle mitochondrial DNA in patients with mitochondrial myopathies. *Nature*, 331(6158), pp.717–719. Available at: http://www.ncbi.nlm.nih.gov/pubmed/2830540 [Accessed July 4, 2017].

Holt, I.J. & Reyes, A., 2012. Human mitochondrial DNA replication. *Cold Spring Harbor perspectives in biology*, 4(12). Available at: http://www.ncbi.nlm.nih.gov/pubmed/23143808 [Accessed June 28, 2017].

Horbay, R. & Bilyy, R., 2016. Mitochondrial dynamics during cell

cycling. *Apoptosis*, 21(12), pp.1–9. Available at: http://dx.doi.org/10.1007/s10495-016-1295-5.

Hu, B.-Y. et al., 2010. Neural differentiation of human induced pluripotent stem cells follows developmental principles but with variable potency. *Proceedings of the National Academy of Sciences*, 107(9), pp.4335–4340. Available at: http://www.ncbi.nlm.nih.gov/pubmed/20160098 [Accessed June 13, 2017].

Hutchin, T.P. et al., 2001. Multiple origins of the mtDNA 7472insC mutation associated with hearing loss and neurological dysfunction. *European journal of human genetics : EJHG*, 9(5), pp.385–7. Available at: http://www.ncbi.nlm.nih.gov/pubmed/11378827.

Ikebe, S. et al., 1990. Increase of deleted mitochondrial DNA in the striatum in Parkinson's disease and senescence. *Biochemical and biophysical research communications*, 170(3), pp.1044–8. Available at: http://www.ncbi.nlm.nih.gov/pubmed/2390073 [Accessed May 22, 2017].

Ishihara, N. et al., 2009. Mitochondrial fission factor Drp1 is essential for embryonic development and synapse formation in mice. *Nature Cell Biology*, 11(8), pp.958–966. Available at: http://www.ncbi.nlm.nih.gov/pubmed/19578372 [Accessed June 29, 2017].

Ishihara, N., Eura, Y. & Mihara, K., 2004. Mitofusin 1 and 2 play distinct roles in mitochondrial fusion reactions via GTPase activity. *Journal of cell science*, 117(Pt 26), pp.6535–46. Available at: http://www.ncbi.nlm.nih.gov/pubmed/15572413 [Accessed March 20, 2016].

Jahangir Tafrechi, R.S. et al., 2005. Distinct nuclear gene expression profiles in cells with mtDNA depletion and homoplasmic A3243G mutation. *Mutation Research/Fundamental and Molecular Mechanisms of Mutagenesis*, 578(1–2), pp.43–52. Available at: http://www.ncbi.nlm.nih.gov/pubmed/16202796 [Accessed July

5, 2017].

Jaksch, M. et al., 1998. Progressive myoclonus epilepsy and mitochondrial myopathy associated with mutations in the tRNA(Ser(UCN)) gene. *Annals of neurology*, 44(4), pp.635–40. Available at: http://www.ncbi.nlm.nih.gov/pubmed/9778262 [Accessed March 20, 2016].

Jin, S.M. et al., 2010. Mitochondrial membrane potential regulates PINK1 import and proteolytic destabilization by PARL. *The Journal of Cell Biology*, 191(5), pp.933–942.

Jin, S.M. & Youle, R.J., 2013. The accumulation of misfolded proteins in the mitochondrial matrix is sensed by PINK1 to induce PARK2/Parkin-mediated mitophagy of polarized mitochondria. *Autophagy*, 9(11), pp.1750–1757.

Jourdain, A. et al., 2013. GRSF1 Regulates RNA Processing in Mitochondrial RNA Granules. *Cell Metabolism*, 17(3), pp.399–410. Available at: http://www.ncbi.nlm.nih.gov/pubmed/23473034 [Accessed June 28, 2017].

Kajander, O.A. et al., 2000. Human mtDNA sublimons resemble rearranged mitochondrial genoms found in pathological states. *Human molecular genetics*, 9(19), pp.2821–35. Available at: http://www.ncbi.nlm.nih.gov/pubmed/11092758 [Accessed June 28, 2017].

Kane, L.A. et al., 2014. PINK1 phosphorylates ubiquitin to activate Parkin E3 ubiquitin ligase activity. *The Journal of Cell Biology*, 205(2), pp.143–153. Available at: http://www.jcb.org/lookup/doi/10.1083/jcb.201402104 [Accessed November 29, 2016].

Kang, C. & Ji, L.L., 2016. PGC-1?? overexpression via local transfection attenuates mitophagy pathway in muscle disuse atrophy. *Free Radical Biology and Medicine*, 93, pp.32–40.

Kasamatsu, H. & Vinograd, J., 1974. Replication of Circular DNA in Eukaryotic Cells. *Annual Review of Biochemistry*, 43(1), pp.695–719. Available at:

http://www.ncbi.nlm.nih.gov/pubmed/4605048 [Accessed June 28, 2017].

Kasianowicz, J., Benz, R. & McLaughlin, S., 1984. The kinetic mechanism by which CCCP (carbonyl cyanide m-chlorophenylhydrazone) transports protons across membranes. *The Journal of membrane biology*, 82(2), pp.179–90. Available at: http://www.ncbi.nlm.nih.gov/pubmed/6096547 [Accessed November 17, 2015].

Kazlauskaite, A. et al., 2014. Parkin is activated by PINK1-dependent phosphorylation of ubiquitin at Ser65. *The Biochemical Journal*, 460(1), pp.127–139.

Keeney, P.M. et al., 2006. Parkinson's Disease Brain Mitochondrial Complex I Has Oxidatively Damaged Subunits and Is Functionally Impaired and Misassembled. *Journal of Neuroscience*, 26(19), pp.5256–5264. Available at: http://www.ncbi.nlm.nih.gov/pubmed/16687518 [Accessed July 3, 2017].

Khan, S.M., Smigrodzki, R.M. & Swerdlow, R.H., 2007. Cell and animal models of mtDNA biology: progress and prospects. *American journal of physiology. Cell physiology*, 292(2), pp.C658-69. Available at: http://www.ncbi.nlm.nih.gov/pubmed/16899549.

King, M. & Attardi, G., 1989. Human cells lacking mtDNA: repopulation with exogenous mitochondria by complementation. *Science*, 246(4929). Available at: http://science.sciencemag.org/content/246/4929/500.long [Accessed May 15, 2017].

King, M.P. et al., 1992. Defects in mitochondrial protein synthesis and respiratory chain activity segregate with the tRNA(Leu(UUR)) mutation associated with mitochondrial myopathy, encephalopathy, lactic acidosis, and strokelike episodes. *Molecular and cellular biology*, 12(2), pp.480–90. Available at: http://www.ncbi.nlm.nih.gov/pubmed/1732728 [Accessed July 5, 2017].

Klionsky, D.J. et al., 2012. Guidelines for the use and interpretation of assays for monitoring autophagy. *Autophagy*, 8(4), pp.445–544. Available at: http://www.pubmedcentral.nih.gov/articlerender.fcgi?artid=3404883&tool=pmcentrez&rendertype=abstract [Accessed July 10, 2014].

Kodaira, M. et al., 2015. Impaired respiratory function in MELAS-induced pluripotent stem cells with high heteroplasmy levels. *FEBS Open Bio*, 5(1), pp.219–225. Available at: http://doi.wiley.com/10.1016/j.fob.2015.03.008 [Accessed June 6, 2017].

Koehler, K.R. et al., 2011. Extended passaging increases the efficiency of neural differentiation from induced pluripotent stem cells. *BMC Neuroscience*, 12(1), p.82. Available at: http://bmcneurosci.biomedcentral.com/articles/10.1186/1471-2202-12-82 [Accessed June 13, 2017].

Kojovic, M., Cordivari, C. & Bhatia, K., 2011. Myoclonic disorders: a practical approach for diagnosis and treatment. *Therapeutic Advances in Neurological Disorders*, 4(1), pp.47–62. Available at: http://tan.sagepub.com/cgi/doi/10.1177/1756285610395653.

Kolesnikov, A.A., 2016. The mitochondrial genome. The nucleoid. *Biochemistry (Moscow)*, 81(10), pp.1057–1065. Available at: http://link.springer.com/10.1134/S0006297916100047.

Koshiba, T. et al., 2004. Structural Basis of Mitochondrial Tethering by Mitofusin Complexes. *Science*, 305(5685), pp.858–862. Available at: http://www.ncbi.nlm.nih.gov/pubmed/15297672 [Accessed June 29, 2017].

Koyano, F. et al., 2014. Ubiquitin is phosphorylated by PINK1 to activate parkin. *Nature*, 510(7503), pp.162–166.

Kühlbrandt, W., 2015. Structure and function of mitochondrial membrane protein complexes. *BMC biology*, 13, p.89. Available at: http://www.ncbi.nlm.nih.gov/pubmed/26515107 [Accessed June 22, 2017].

Kukat, C. et al., 2011. Super-resolution microscopy reveals that

mammalian mitochondrial nucleoids have a uniform size and frequently contain a single copy of mtDNA. *Proceedings of the National Academy of Sciences*, 108(33), pp.13534–13539. Available at: http://www.ncbi.nlm.nih.gov/pubmed/21808029 [Accessed June 28, 2017].

Kuma, A., Matsui, M. & Mizushima, N., 2007. LC3, an autophagosome marker, can be incorporated into protein aggregates independent of autophagy: caution in the interpretation of LC3 localization. *Autophagy*, 3(4), pp.323–8. Available at: http://www.ncbi.nlm.nih.gov/pubmed/17387262 [Accessed November 17, 2015].

Van Laar, V.S. et al., 2011. Bioenergetics of neurons inhibit the translocation response of Parkin following rapid mitochondrial depolarization. *Human Molecular Genetics*, 20(5), pp.927–940.

de Laat, P. et al., 2013. Inheritance of the m.3243A>G mutation. *JIMD reports*, 8, pp.47–50. Available at: http://www.pubmedcentral.nih.gov/articlerender.fcgi?artid=3565654&tool=pmcentrez&rendertype=abstract [Accessed March 20, 2016].

Lan, L. et al., 2004. In situ analysis of repair processes for oxidative DNA damage in mammalian cells. *Proceedings of the National Academy of Sciences*, 101(38), pp.13738–13743. Available at: http://www.ncbi.nlm.nih.gov/pubmed/15365186 [Accessed June 28, 2017].

Langer, T. et al., 2001. AAA proteases of mitochondria: quality control of membrane proteins and regulatory functions during mitochondrial biogenesis. *Biochemical Society transactions*, 29(Pt 4), pp.431–436.

Larsson, N.-G. et al., 1998. Mitochondrial transcription factor A is necessary for mtDNA maintance and embryogenesis in mice. *Nature Genetics*, 18(3), pp.231–236. Available at: http://www.ncbi.nlm.nih.gov/pubmed/9500544 [Accessed June 28, 2017].

Lax, N.Z. et al., 2013. Early-Onset Cataracts, Spastic Paraparesis,

and Ataxia Caused by a Novel Mitochondrial tRNA ^{Glu} (*MT - TE*) Gene Mutation Causing Severe Complex I Deficiency: A Clinical, Molecular, and Neuropathologic Study. *Journal of Neuropathology & Experimental Neurology*, 72(2), pp.164–175. Available at: http://www.ncbi.nlm.nih.gov/pubmed/23334599 [Accessed May 19, 2017].

Lazarou, M. et al., 2012. Role of PINK1 binding to the TOM complex and alternate intracellular membranes in recruitment and activation of the E3 ligase Parkin. *Developmental cell*, 22(2), pp.320–33. Available at: http://www.pubmedcentral.nih.gov/articlerender.fcgi?artid=3288275&tool=pmcentrez&rendertype=abstract [Accessed March 31, 2016].

Lazarou, M. et al., 2015. The ubiquitin kinase PINK1 recruits autophagy receptors to induce mitophagy. *Nature*, p.Accepted.

Lightowlers, R.N., Taylor, R.W. & Turnbull, D.M., 2015. Mutations causing mitochondrial disease: What is new and what challenges remain? *Science (New York, N.Y.)*, 349(6255), pp.1494–9. Available at: http://www.ncbi.nlm.nih.gov/pubmed/26404827.

Liu, Y.-R. et al., 2014. Sox2 acts as a transcriptional repressor in neural stem cells. *BMC Neuroscience*, 15(1), p.95. Available at: http://bmcneurosci.biomedcentral.com/articles/10.1186/1471-2202-15-95 [Accessed May 31, 2017].

Loiseau, D. et al., 2007. Mitochondrial coupling defect in Charcot-Marie-Tooth type 2A disease. *Annals of Neurology*, 61(4), pp.315–323. Available at: http://www.ncbi.nlm.nih.gov/pubmed/17444508 [Accessed February 15, 2017].

Lorenz, C. et al., 2017. Human iPSC-Derived Neural Progenitors Are an Effective Drug Discovery Model for Neurological mtDNA Disorders. *Cell Stem Cell*, 0(0). Available at: http://linkinghub.elsevier.com/retrieve/pii/S1934590916304696 [Accessed February 15, 2017].

Malik, N. & Rao, M.S., 2013. A review of the methods for human iPSC derivation. *Methods in molecular biology (Clifton, N.J.)*, 997, pp.23–33. Available at: http://www.ncbi.nlm.nih.gov/pubmed/23546745 [Accessed June 5, 2017].

Mancuso, M. et al., 2014. Myoclonus in mitochondrial disorders. *Movement Disorders*, 29(6), pp.722–728.

Maruyama, H. et al., 2010. Mutations of optineurin in amyotrophic lateral sclerosis. *Nature*, 465(7295), pp.223–226. Available at: http://www.ncbi.nlm.nih.gov/pubmed/20428114 [Accessed September 14, 2017].

McKenzie, M. et al., 2007. Mitochondrial ND5 Gene Variation Associated with Encephalomyopathy and Mitochondrial ATP Consumption. *Journal of Biological Chemistry*, 282(51), pp.36845–36852. Available at: http://www.ncbi.nlm.nih.gov/pubmed/17940288 [Accessed February 14, 2017].

McLelland, G.-L. et al., 2014. Parkin and PINK1 function in a vesicular trafficking pathway regulating mitochondrial quality control. *The EMBO journal*, 33(4), pp.282–295.

McWilliams, T.G. et al., 2016. mito-QC illuminates mitophagy and mitochondrial architecture in vivo. *The Journal of Cell Biology*, 214(3). Available at: http://jcb.rupress.org/content/214/3/333 [Accessed June 21, 2017].

McWilliams, T.G. & Muqit, M.M., 2017. PINK1 and Parkin: emerging themes in mitochondrial homeostasis. *Current Opinion in Cell Biology*, 45, pp.83–91. Available at: http://www.ncbi.nlm.nih.gov/pubmed/28437683 [Accessed June 29, 2017].

Meeusen, S., McCaffery, J.M. & Nunnari, J., 2004. Mitochondrial Fusion Intermediates Revealed in Vitro. *Science*, 305(5691), pp.1747–1752. Available at: http://www.ncbi.nlm.nih.gov/pubmed/15297626 [Accessed June 29, 2017].

Moraes, C.T. et al., 1992. The mitochondrial tRNA(Leu(UUR)) mutation in mitochondrial encephalomyopathy, lactic acidosis, and strokelike episodes (MELAS): genetic, biochemical, and morphological correlations in skeletal muscle. *American journal of human genetics*, 50(5), pp.934–49. Available at: http://www.ncbi.nlm.nih.gov/pubmed/1315123 [Accessed June 6, 2017].

Morais, V.A. et al., 2009. Parkinson's disease mutations in PINK1 result in decreased Complex I activity and deficient synaptic function. *EMBO molecular medicine*, 1(2), pp.99–111. Available at: http://www.pubmedcentral.nih.gov/articlerender.fcgi?artid=3378121&tool=pmcentrez&rendertype=abstract [Accessed October 6, 2015].

Morais, V.A. et al., 2014. PINK1 loss-of-function mutations affect mitochondrial complex I activity via NdufA10 ubiquinone uncoupling. *Science (New York, N.Y.)*, 344(6180), pp.203–207.

Morán, M. et al., 2014. Bulk autophagy, but not mitophagy, is increased in cellular model of mitochondrial disease. *Biochimica et Biophysica Acta - Molecular Basis of Disease*, 1842(7), pp.1059–1070. Available at: http://dx.doi.org/10.1016/j.bbadis.2014.03.013.

Morán, M. et al., 2010. Mitochondrial bioenergetics and dynamics interplay in complex I-deficient fibroblasts. *Biochimica et Biophysica Acta - Molecular Basis of Disease*, 1802(5), pp.443–453. Available at: http://dx.doi.org/10.1016/j.bbadis.2010.02.001.

Narendra, D. et al., 2008. Parkin is recruited selectively to impaired mitochondria and promotes their autophagy. *The Journal of cell biology*, 183(5), pp.795–803. Available at: http://jcb.rupress.org/content/183/5/795.full [Accessed March 31, 2015].

Narendra, D.P. et al., 2010. PINK1 is selectively stabilized on impaired mitochondria to activate Parkin. *PLoS biology*, 8(1),

p.e1000298.

Naue, J. et al., 2015. Evidence for frequent and tissue-specific sequence heteroplasmy in human mitochondrial DNA. *Mitochondrion*, 20, pp.82–94. Available at: http://www.ncbi.nlm.nih.gov/pubmed/25526677 [Accessed June 6, 2017].

Ney, P.A., 2015. Mitochondrial autophagy: Origins, significance, and role of BNIP3 and NIX. *Biochimica et Biophysica Acta (BBA) - Molecular Cell Research*, 1853(10), pp.2775–2783. Available at: http://www.ncbi.nlm.nih.gov/pubmed/25753537 [Accessed July 4, 2017].

Ng, Y.S. et al., 2015. Sudden adult death syndrome in m.3243A>G-related mitochondrial disease: an unrecognized clinical entity in young, asymptomatic adults. *European heart journal*. Available at: http://eurheartj.oxfordjournals.org/content/early/2015/07/16/eurheartj.ehv306.abstract [Accessed March 20, 2016].

Ngo, H.B., Kaiser, J.T. & Chan, D.C., 2011. The mitochondrial transcription and packaging factor Tfam imposes a U-turn on mitochondrial DNA. *Nature Structural & Molecular Biology*, 18(11), pp.1290–1296. Available at: http://www.ncbi.nlm.nih.gov/pubmed/22037171 [Accessed June 28, 2017].

Noack, R. et al., 2012. Charcot-Marie-Tooth disease CMT4A: GDAP1 increases cellular glutathione and the mitochondrial membrane potential. *Human Molecular Genetics*, 21(1), pp.150–162. Available at: http://www.ncbi.nlm.nih.gov/pubmed/21965300 [Accessed February 15, 2017].

Ojala, D., Montoya, J. & Attardi, G., 1981. tRNA punctuation model of RNA processing in human mitochondria. *Nature*, 290(5806), pp.470–4. Available at: http://www.ncbi.nlm.nih.gov/pubmed/7219536 [Accessed June 28, 2017].

Okatsu, K. et al., 2012. PINK1 autophosphorylation upon membrane potential dissipation is essential for Parkin recruitment to damaged mitochondria. *Nature Communications*, 3, p.1016.

Ordureau, A. et al., 2014. Quantitative proteomics reveal a feedforward mechanism for mitochondrial PARKIN translocation and ubiquitin chain synthesis. *Molecular Cell*, 56(3), pp.360–375.

Otera, H. et al., 2010. Mff is an essential factor for mitochondrial recruitment of Drp1 during mitochondrial fission in mammalian cells. *The Journal of Cell Biology*, 191(6), pp.1141–1158. Available at: http://www.ncbi.nlm.nih.gov/pubmed/21149567 [Accessed June 29, 2017].

Ozawa, T. et al., 1990. Quantitative determination of deleted mitochondrial DNA relative to normal DNA in parkinsonian striatum by a kinetic PCR analysis. *Biochemical and biophysical research communications*, 172(2), pp.483–9. Available at: http://www.ncbi.nlm.nih.gov/pubmed/2241948 [Accessed May 22, 2017].

Padman, B.S. et al., 2013. The protonophore CCCP interferes with lysosomal degradation of autophagic cargo in yeast and mammalian cells. *Autophagy*, 9(11), pp.1862–1875. Available at: http://www.tandfonline.com/doi/abs/10.4161/auto.26557.

Palikaras, K. & Tavernarakis, N., 2014. Mitochondrial homeostasis: The interplay between mitophagy and mitochondrial biogenesis. *Experimental Gerontology*, 56, pp.182–188. Available at: http://linkinghub.elsevier.com/retrieve/pii/S0531556514000333 [Accessed May 18, 2017].

Park, J. et al., 2006. Mitochondrial dysfunction in Drosophila PINK1 mutants is complemented by parkin. *Nature*, 441(7097), pp.1157–1161.

Paşca, A.M. et al., 2015. Functional cortical neurons and astrocytes from human pluripotent stem cells in 3D culture. *Nature Methods*, 12(7), pp.671–678. Available at:

http://www.nature.com/doifinder/10.1038/nmeth.3415.

Payne, B.A.I. et al., 2013. Universal heteroplasmy of human mitochondrial DNA. *Human molecular genetics*, 22(2), pp.384–90. Available at: http://www.ncbi.nlm.nih.gov/pubmed/23077218 [Accessed July 5, 2017].

Perier, C. et al., 2013. Accumulation of mitochondrial DNA deletions within dopaminergic neurons triggers neuroprotective mechanisms. *Brain : a journal of neurology*, 136(Pt 8), pp.2369–78. Available at: https://academic.oup.com/brain/article-lookup/doi/10.1093/brain/awt196 [Accessed May 22, 2017].

Perier, C. & Vila, M., 2012. Mitochondrial biology and Parkinson's disease. *Cold Spring Harbor perspectives in medicine*, 2(2), p.a009332. Available at: http://www.ncbi.nlm.nih.gov/pubmed/22355801 [Accessed July 3, 2017].

Pfeffer, G. et al., 2012. Treatment for mitochondrial disorders. In P. F. Chinnery, ed. *Cochrane Database of Systematic Reviews*. Chichester, UK: John Wiley & Sons, Ltd, p. CD004426. Available at: http://www.ncbi.nlm.nih.gov/pubmed/22513923 [Accessed May 12, 2017].

Philippou, A. et al., 2007. The role of the insulin-like growth factor 1 (IGF-1) in skeletal muscle physiology. *In vivo (Athens, Greece)*, 21(1), pp.45–54.

Pickrell, A.M. & Youle, R.J., 2015. The Roles of PINK1, Parkin, and Mitochondrial Fidelity in Parkinson's Disease. *Neuron*, 85(2), pp.257–273. Available at: http://linkinghub.elsevier.com/retrieve/pii/S0896627314010885.

Pitceathly, R.D.S. et al., 2012. Genetic dysfunction of MT-ATP6 causes axonal charcot-Marie-Tooth disease. *Neurology*, 79(11), pp.1145–1154.

Pogson, J.H. et al., 2014. The complex I subunit NDUFA10 selectively rescues Drosophila pink1 mutants through a mechanism independent of mitophagy. *PLoS genetics*, 10(11),

p.e1004815.

Porcelli, A.M. et al., 2016. A unique combination of rare mitochondrial ribosomal RNA variants affects the kinetics of complex I assembly. *International Journal of Biochemistry and Cell Biology*, 75, pp.117–122. Available at: http://dx.doi.org/10.1016/j.biocel.2016.04.007.

Rakovic, A. et al., 2011. Mutations in PINK1 and Parkin impair ubiquitination of Mitofusins in human fibroblasts. *PloS One*, 6(3), p.e16746.

Rakovic, A., Shurkewitsch, K., Seibler, P., Gr??newald, A., et al., 2013. Phosphatase and tensin homolog (PTEN)-induced Putative Kinase 1 (PINK1)-dependent ubiquitination of endogenous parkin attenuates mitophagy: Study in human primary fibroblasts and induced pluripotent stem cell-derived neurons. *Journal of Biological Chemistry*, 288(4), pp.2223–2237.

Rakovic, A., Shurkewitsch, K., Seibler, P., Grünewald, A., et al., 2013. Phosphatase and tensin homolog (PTEN)-induced putative kinase 1 (PINK1)-dependent ubiquitination of endogenous Parkin attenuates mitophagy: study in human primary fibroblasts and induced pluripotent stem cell-derived neurons. *The Journal of biological chemistry*, 288(4), pp.2223–37. Available at: http://www.pubmedcentral.nih.gov/articlerender.fcgi?artid=3554895&tool=pmcentrez&rendertype=abstract [Accessed November 1, 2015].

Rakovic, A., Seibler, P. & Klein, C., 2015. iPS models of Parkin and PINK1. *Biochemical Society Transactions*, 43(2), pp.302–307.

Rana, M. et al., 2000. An out-of-frame cytochrome b gene deletion from a patient with parkinsonism is associated with impaired complex III assembly and an increase in free radical production. *Annals of neurology*, 48(5), pp.774–81. Available at: http://www.ncbi.nlm.nih.gov/pubmed/11079541 [Accessed May 22, 2017].

Al Rawi, S. et al., 2011. Postfertilization Autophagy of Sperm Organelles Prevents Paternal Mitochondrial DNA Transmission. *Science*, 334(6059), pp.1144–1147. Available at: http://www.ncbi.nlm.nih.gov/pubmed/22033522 [Accessed May 16, 2017].

Rego, a C., Vesce, S. & Nicholls, D.G., 2001. The mechanism of mitochondrial membrane potential retention following release of cytochrome c in apoptotic GT1-7 neural cells. *Cell death and differentiation*, 8(10), pp.995–1003.

Rizzuto, R. et al., 1992. Rapid changes of mitochondrial Ca2+ revealed by specifically targeted recombinant aequorin. *Nature*, 358(6384), pp.325–327. Available at: http://www.ncbi.nlm.nih.gov/pubmed/1322496 [Accessed June 23, 2017].

Rojansky, R., Cha, M.-Y. & Chan, D.C., 2016. Elimination of paternal mitochondria in mouse embryos occurs through autophagic degradation dependent on PARKIN and MUL1. *eLife*, 5, p.e17896. Available at: http://elifesciences.org/lookup/doi/10.7554/eLife.17896.

Rorbach, J. et al., 2008. Overexpression of human mitochondrial valyl tRNA synthetase can partially restore levels of cognate mt-tRNAVal carrying the pathogenic C25U mutation. *Nucleic Acids Research*, 36(9), pp.3065–3074. Available at: https://academic.oup.com/nar/article-lookup/doi/10.1093/nar/gkn147 [Accessed May 15, 2017].

Rubio-Cosials, A. et al., 2011. Human mitochondrial transcription factor A induces a U-turn structure in the light strand promoter. *Nature Structural & Molecular Biology*, 18(11), pp.1281–1289. Available at: http://www.ncbi.nlm.nih.gov/pubmed/22037172 [Accessed June 28, 2017].

Samuels, D.C. et al., 2010. Reassessing evidence for a postnatal mitochondrial genetic bottleneck. *Nat Genet*, 42(6), pp.471–472. Available at: http://dx.doi.org/10.1038/ng0610-471.

Sarraf, S.A. et al., 2013. Landscape of the PARKIN-dependent

ubiquitylome in response to mitochondrial depolarization. *Nature*, 496(7445), pp.372–376.

Sato, M. & Sato, K., 2011. Degradation of Paternal Mitochondria by Fertilization-Triggered Autophagy in C. elegans Embryos. *Science*, 334(6059). Available at: http://science.sciencemag.org/content/334/6059/1141 [Accessed May 16, 2017].

Scaduto, R.C. & Grotyohann, L.W., 1999. Measurement of mitochondrial membrane potential using fluorescent rhodamine derivatives. *Biophysical journal*, 76(1 Pt 1), pp.469–77. Available at: http://www.ncbi.nlm.nih.gov/pubmed/9876159%5Cnhttp://www.pubmedcentral.nih.gov/articlerender.fcgi?artid=PMC1302536.

Scaglia, F. & Wong, L.-J.C., 2008. Human mitochondrial transfer RNAs: Role of pathogenic mutation in disease. *Muscle & Nerve*, 37(2), pp.150–171. Available at: http://www.ncbi.nlm.nih.gov/pubmed/17999409 [Accessed July 5, 2017].

Scarlett, J.L. & Murphy, M.P., 1997. Release Of Apoptogenic Proteins From the Mitochondrial Intermembrane Space During the Mitochondrial Permeability Transition. *FEBS Lett*, 418(3), pp.282–286. Available at: http://dx.doi.org/10.1016/S0014-5793(97)01391-4.

Schaefer, A.M. et al., 2008. Prevalence of mitochondrial DNA disease in adults. *Annals of Neurology*, 63(1), pp.35–39.

Schapira, A.H. et al., 1990. Mitochondrial complex I deficiency in Parkinson's disease. *Journal of Neurochemistry*, 54(3), pp.823–827.

Schatten, G. et al., 1999. Ubiquitin tag for sperm mitochondria. *Nature*, 402(6760), pp.371–372. Available at: http://www.ncbi.nlm.nih.gov/pubmed/10586873 [Accessed June 28, 2017].

Scherz-Shouval, R. & Elazar, Z., 2011. Regulation of autophagy by ROS: physiology and pathology. *Trends in Biochemical*

Sciences, 36(1), pp.30–38. Available at: http://www.ncbi.nlm.nih.gov/pubmed/20728362 [Accessed January 4, 2017].

Schiff, M. et al., 2011. Mouse Studies to Shape Clinical Trials for Mitochondrial Diseases: High Fat Diet in Harlequin Mice K. Maedler, ed. *PLoS ONE*, 6(12), p.e28823. Available at: http://dx.plos.org/10.1371/journal.pone.0028823 [Accessed May 15, 2017].

Schmitt, S. et al., 2006. Proteome analysis of mitochondrial outer membrane fromNeurospora crassa. *PROTEOMICS*, 6(1), pp.72–80. Available at: http://www.ncbi.nlm.nih.gov/pubmed/16294304 [Accessed June 22, 2017].

Scotland, K.B. et al., 2009. Analysis of Rex1 (zfp42) function in embryonic stem cell differentiation. *Developmental dynamics : an official publication of the American Association of Anatomists*, 238(8), pp.1863–77. Available at: http://www.ncbi.nlm.nih.gov/pubmed/19618472 [Accessed May 31, 2017].

Seibler, P. et al., 2011. Mitochondrial Parkin recruitment is impaired in neurons derived from mutant PINK1 induced pluripotent stem cells. *The Journal of Neuroscience: The Official Journal of the Society for Neuroscience*, 31(16), pp.5970–5976.

Shaltouki, A. et al., 2015. Mitochondrial Alterations by PARKIN in Dopaminergic Neurons Using PARK2 Patient-Specific and PARK2 Knockout Isogenic iPSC Lines. *Stem Cell Reports*, 4(5), pp.847–859.

Shi, Y., Kirwan, P. & Livesey, F.J., 2012. Directed differentiation of human pluripotent stem cells to cerebral cortex neurons and neural networks. *Nature Protocols*, 7(10), pp.1836–1846.

Silvestri, L. et al., 2005. Mitochondrial import and enzymatic activity of PINK1 mutants associated to recessive parkinsonism. *Human Molecular Genetics*, 14(22), pp.3477–3492.

Sin, J. et al., 2016. Mitophagy is required for mitochondrial

biogenesis and myogenic differentiation of C2C12 myoblasts. *Autophagy*, 12(2), pp.369–380. Available at: http://www.ncbi.nlm.nih.gov/pubmed/26566717 [Accessed June 21, 2017].

Song, Z. et al., 2009. Mitofusins and OPA1 mediate sequential steps in mitochondrial membrane fusion. *Molecular biology of the cell*, 20(15), pp.3525–32. Available at: http://www.ncbi.nlm.nih.gov/pubmed/19477917 [Accessed June 29, 2017].

Soubannier, V., McLelland, G.L., et al., 2012. A vesicular transport pathway shuttles cargo from mitochondria to lysosomes. *Current Biology*, 22(2), pp.135–141. Available at: http://dx.doi.org/10.1016/j.cub.2011.11.057.

Soubannier, V., McLelland, G.-L., et al., 2012. A vesicular transport pathway shuttles cargo from mitochondria to lysosomes. *Current biology: CB*, 22(2), pp.135–141.

De Stefani, D. et al., 2011. A forty-kilodalton protein of the inner membrane is the mitochondrial calcium uniporter. *Nature*, 476(7360), pp.336–340. Available at: http://www.ncbi.nlm.nih.gov/pubmed/21685888 [Accessed June 23, 2017].

Stewart, J.B. et al., 2008. Strong Purifying Selection in Transmission of Mammalian Mitochondrial DNA L. D. Hurst, ed. *PLoS Biology*, 6(1), p.e10. Available at: http://dx.plos.org/10.1371/journal.pbio.0060010 [Accessed June 6, 2017].

Stewart, J.B. & Chinnery, P.F., 2015. The dynamics of mitochondrial DNA heteroplasmy: implications for human health and disease. *Nature Reviews Genetics*, 16(9), pp.530–542. Available at: http://www.nature.com/doifinder/10.1038/nrg3966.

Stojanovski, D. et al., 2004. Levels of human Fis1 at the mitochondrial outer membrane regulate mitochondrial morphology. *Journal of cell science*, 117(Pt 7), pp.1201–10. Available at: http://jcs.biologists.org/cgi/doi/10.1242/jcs.01058

[Accessed June 29, 2017].

Strappazzon, F. et al., 2015. AMBRA1 is able to induce mitophagy via LC3 binding, regardless of PARKIN and p62/SQSTM1. *Cell death and differentiation*, 22(3), pp.419–32. Available at: http://dx.doi.org/10.1038/cdd.2014.139 [Accessed November 21, 2015].

Suen, D.-F. et al., 2010. Parkin overexpression selects against a deleterious mtDNA mutation in heteroplasmic cybrid cells. *Proceedings of the National Academy of Sciences of the United States of America*, 107(26), pp.11835–11840.

Sugiura, A. et al., 2014. A new pathway for mitochondrial quality control: mitochondrial-derived vesicles. *The EMBO journal*, 33(19), pp.2142–2156.

Sun, N., Yun, J., Liu, J., Malide, D., Liu, C., Rovira, I.I., et al., 2015. Measuring In Vivo Mitophagy. *Molecular Cell*, pp.1–12. Available at: http://linkinghub.elsevier.com/retrieve/pii/S1097276515007765.

Sun, N., Yun, J., Liu, J., Malide, D., Liu, C., Rovira, I., et al., 2015. Measuring In?Vivo Mitophagy. *Molecular Cell*, 60(4), pp.685–696. Available at: http://linkinghub.elsevier.com/retrieve/pii/S1097276515007765 [Accessed June 21, 2017].

Sutovsky, P. et al., 2000. Ubiquitinated sperm mitochondria, selective proteolysis, and the regulation of mitochondrial inheritance in mammalian embryos. *Biology of reproduction*, 63(2), pp.582–90. Available at: http://www.ncbi.nlm.nih.gov/pubmed/10906068 [Accessed June 28, 2017].

Świerczek, B., Ciemerych, M.A. & Archacka, K., 2015. From pluripotency to myogenesis: a multistep process in the dish. *Journal of muscle research and cell motility*, 36(6), pp.363–75. Available at: http://www.ncbi.nlm.nih.gov/pubmed/26715014 [Accessed May 4, 2017].

Szczepanowska, J. et al., 2012. Biochimica et Biophysica Acta

Effect of mtDNA point mutations on cellular bioenergetics ☆. *BBA - Bioenergetics*, 1817(10), pp.1740–1746. Available at: http://dx.doi.org/10.1016/j.bbabio.2012.02.028.

Takayama, N. et al., 2010. Transient activation of c-MYC expression is critical for efficient platelet generation from human induced pluripotent stem cells. *Journal of Experimental Medicine*, 207(13). Available at: http://jem.rupress.org/content/207/13/2817 [Accessed May 31, 2017].

Tapscott, S.J., 2005. The circuitry of a master switch: Myod and the regulation of skeletal muscle gene transcription. *Development*, 132(12). Available at: http://dev.biologists.org/content/132/12/2685 [Accessed May 31, 2017].

Taylor, R.W. & Turnbull, D.M., 2005. Mitochondrial DNA mutations in human disease. *Nature Reviews Genetics*, 6(5), pp.389–402. Available at: http://www.nature.com/doifinder/10.1038/nrg1606.

Thomas, R.E. et al., 2014. PINK1-Parkin Pathway Activity Is Regulated by Degradation of PINK1 in the Mitochondrial Matrix A. van der Bliek, ed. *PLoS Genetics*, 10(5), p.e1004279. Available at: http://dx.plos.org/10.1371/journal.pgen.1004279 [Accessed June 22, 2017].

Thyagarajan, D. et al., 2000. A novel mitochondrial 12SrRNA point mutation in parkinsonism, deafness, and neuropathy. *Annals of neurology*, 48(5), pp.730–6. Available at: http://www.ncbi.nlm.nih.gov/pubmed/11079536 [Accessed May 22, 2017].

Tiranti, V. et al., 1995. Maternally inherited hearing loss, ataxia and myoclonus associated with a novel point mutation in mitochondrial tRNASer(UCN) gene. *Human molecular genetics*, 4(8), pp.1421–7. Available at: http://www.ncbi.nlm.nih.gov/pubmed/7581383 [Accessed March 20, 2016].

Toompuu, M. et al., 2002. The 7472insC mitochondrial DNA

mutation impairs the synthesis and extent of aminoacylation of tRNASer(UCN) but not its structure or rate of turnover. *The Journal of biological chemistry*, 277(25), pp.22240–50. Available at: http://www.ncbi.nlm.nih.gov/pubmed/11919191 [Accessed June 20, 2017].

Trounce, I.A. & Pinkert, C.A., 2007. Cybrid models of mtDNA disease and transmission, from cells to mice. *Current topics in developmental biology*, 77, pp.157–83. Available at: http://www.ncbi.nlm.nih.gov/pubmed/17222703 [Accessed January 5, 2016].

Tufi, R. et al., 2014. Enhancing nucleotide metabolism protects against mitochondrial dysfunction and neurodegeneration in a PINK1 model of Parkinson's disease. *Nature cell biology*, 16(2), pp.157–66. Available at: http://www.ncbi.nlm.nih.gov/pubmed/24441527.

Tuppen, H.A.L. et al., 2010. Mitochondrial DNA mutations and human disease. *Biochimica et biophysica acta*, 1797(2), pp.113–28. Available at: http://www.sciencedirect.com/science/article/pii/S0005272809002618.

Turnbull, D.M. et al., 1999. Reanalysis and revision of the Cambridge reference sequence for human mitochondrial DNA. *Nature Genetics*, 23(2), pp.147–147. Available at: http://www.ncbi.nlm.nih.gov/pubmed/10508508 [Accessed June 28, 2017].

Twig, G., Elorza, A., Molina, A.J.A., et al., 2008. Fission and selective fusion govern mitochondrial segregation and elimination by autophagy. *The EMBO journal*, 27(2), pp.433–446.

Twig, G., Elorza, A., Molina, A.J.A., et al., 2008a. Fission and selective fusion govern mitochondrial segregation and elimination by autophagy. *The EMBO Journal*, 27(2), pp.433–446. Available at: http://emboj.embopress.org/cgi/doi/10.1038/sj.emboj.7601963

[Accessed November 29, 2016].

Twig, G., Elorza, A., Molina, A.J.A., et al., 2008b. Fission and selective fusion govern mitochondrial segregation and elimination by autophagy. *The EMBO journal*, 27(2), pp.433–46. Available at: http://www.ncbi.nlm.nih.gov/pubmed/18200046 [Accessed November 29, 2016].

Vainshtein, A. et al., 2015. PGC-1α modulates denervation-induced mitophagy in skeletal muscle. *Skeletal muscle*, 5, p.9. Available at: http://www.pubmedcentral.nih.gov/articlerender.fcgi?artid=4381453&tool=pmcentrez&rendertype=abstract [Accessed December 17, 2015].

Valenci, I. et al., 2015. Parkin modulates heteroplasmy of truncated mtDNA in Caenorhabditis elegans. *Mitochondrion*, 20, pp.64–70. Available at: http://www.sciencedirect.com/science/article/pii/S1567724914001639 [Accessed December 14, 2015].

Villanueva Paz, M. et al., 2015. Targeting autophagy and mitophagy for mitochondrial diseases treatment. *Expert Opinion on Therapeutic Targets*, 8222(November 2015), pp.1–14. Available at: http://www.tandfonline.com/doi/full/10.1517/14728222.2016.1101068.

Viscomi, C., Bottani, E. & Zeviani, M., 2015. Emerging concepts in the therapy of mitochondrial disease. *Biochimica et Biophysica Acta - Bioenergetics*, 1847(6–7), pp.544–557. Available at: http://dx.doi.org/10.1016/j.bbabio.2015.03.001.

Vives-Bauza, C., Zhou, C., Huang, Y., Cui, M., de Vries, R.L.A., et al., 2010. PINK1-dependent recruitment of Parkin to mitochondria in mitophagy. *Proceedings of the National Academy of Sciences of the United States of America*, 107(1), pp.378–383.

Vives-Bauza, C., Zhou, C., Huang, Y., Cui, M., de Vries, R.L.A., et al., 2010. PINK1-dependent recruitment of Parkin to

mitochondria in mitophagy. *Proceedings of the National Academy of Sciences of the United States of America*, 107(1), pp.378–83. Available at: http://www.ncbi.nlm.nih.gov/pubmed/19966284 [Accessed October 28, 2016].

Voos, W., 2013. Chaperone–protease networks in mitochondrial protein homeostasis. *Biochimica et Biophysica Acta (BBA) - Molecular Cell Research*, 1833(2), pp.388–399. Available at: http://www.sciencedirect.com/science/article/pii/S0167488912001607#s0035 [Accessed September 14, 2017].

Wai, T., Teoli, D. & Shoubridge, E.A., 2008. The mitochondrial DNA genetic bottleneck results from replication of a subpopulation of genomes. *Nature Genetics*, 40(12), pp.1484–1488. Available at: http://www.ncbi.nlm.nih.gov/pubmed/19029901 [Accessed June 6, 2017].

Wakabayashi, J. et al., 2009. The dynamin-related GTPase Drp1 is required for embryonic and brain development in mice. *The Journal of Cell Biology*, 186(6). Available at: http://jcb.rupress.org/content/186/6/805 [Accessed June 29, 2017].

Wallace, D.C. et al., 1988. Mitochondrial DNA mutation associated with Leber's hereditary optic neuropathy. *Science (New York, N.Y.)*, 242(4884), pp.1427–30. Available at: http://www.ncbi.nlm.nih.gov/pubmed/3201231 [Accessed July 4, 2017].

Walther, D.M. & Rapaport, D., 2009. Biogenesis of mitochondrial outer membrane proteins. *Biochimica et Biophysica Acta - Molecular Cell Research*, 1793(1), pp.42–51. Available at: http://dx.doi.org/10.1016/j.bbamcr.2008.04.013.

Wanrooij, S. et al., 2008. Human mitochondrial RNA polymerase primes lagging-strand DNA synthesis in vitro. *Proceedings of the National Academy of Sciences of the United States of America*, 105(32), pp.11122–11127. Available at: http://www.ncbi.nlm.nih.gov/pubmed/18685103%5Cnhttp://www

.ncbi.nlm.nih.gov/pmc/articles/PMC2516254/pdf/zpq11122.pdf.

Wanrooij, S. et al., 2012. In vivo mutagenesis reveals that OriL is essential for mitochondrial DNA replication. *EMBO reports*, 13(12), pp.1130–1137. Available at: http://www.ncbi.nlm.nih.gov/pubmed/23090476 [Accessed June 28, 2017].

Warren, L. et al., 2010. Highly efficient reprogramming to pluripotency and directed differentiation of human cells with synthetic modified mRNA. *Cell Stem Cell*, 7(5), pp.618–630.

Weihofen, A. et al., 2008. Pink1 Parkinson mutations, the Cdc37/Hsp90 chaperones and Parkin all influence the maturation or subcellular distribution of Pink1. *Human Molecular Genetics*, 17(4), pp.602–616.

Whitworth, A.J. et al., 2008. Rhomboid-7 and HtrA2/Omi act in a common pathway with the Parkinson's disease factors Pink1 and Parkin. *Disease Models & Mechanisms*, 1(2–3), p.168–174; discussion 173.

Wilkins, H.M., Carl, S.M. & Swerdlow, R.H., 2014. Cytoplasmic hybrid (cybrid) cell lines as a practical model for mitochondriopathies. *Redox Biology*, 2(1), pp.619–631. Available at: http://dx.doi.org/10.1016/j.redox.2014.03.006.

Williams, A.J. et al., 1999. A Novel System for Assigning the Mode of Inheritance in Mitochondrial Disorders Using Cybrids and Rhodamine 6G. *Human Molecular Genetics*, 8(9), pp.1691–1697. Available at: http://hmg.oxfordjournals.org/content/8/9/1691 [Accessed January 5, 2016].

Wilson, I.J. et al., 2016. Mitochondrial DNA sequence characteristics modulate the size of the genetic bottleneck. *Human Molecular Genetics*, 25(5), pp.1031–1041.

Wittenhagen, L. & Kelley, S.O., 2003. Impact of disease-related mitochondrial mutations on tRNA structure and function. *Trends in Biochemical Sciences*, 28(11), pp.605–611. Available at: http://www.ncbi.nlm.nih.gov/pubmed/14607091 [Accessed July

5, 2017].

Wong, L.-J.C., 2007. Diagnostic challenges of mitochondrial DNA disorders. *Mitochondrion*, 7(1–2), pp.45–52. Available at: http://www.ncbi.nlm.nih.gov/pubmed/17276740 [Accessed July 5, 2017].

Wong, R. et al., 2017. Mitochondrial replacement in an iPSC model of Leber Hereditary Optic Neuropathy. *bioRxiv*, 9(4), p.120659. Available at: http://www.biorxiv.org/content/early/2017/03/26/120659?%3Fcollection=.

Wu, G. & Schöler, H.R., 2014. Role of Oct4 in the early embryo development. *Cell regeneration (London, England)*, 3(1), p.7. Available at: http://www.ncbi.nlm.nih.gov/pubmed/25408886 [Accessed May 31, 2017].

Yaginuma, N., Hirose, S. & Inada, Y., 1973. Spectral change of rhodamine 6G caused by the energization of mitochondria, in relation to charge separation. *Journal of biochemistry*, 74(4), pp.811–5. Available at: http://www.ncbi.nlm.nih.gov/pubmed/4763664 [Accessed December 14, 2015].

Yang, Y. et al., 2006. Mitochondrial pathology and muscle and dopaminergic neuron degeneration caused by inactivation of Drosophila Pink1 is rescued by Parkin. *Proceedings of the National Academy of Sciences of the United States of America*, 103(28), pp.10793–10798.

Yoon, Y. et al., 2003. The mitochondrial protein hFis1 regulates mitochondrial fission in mammalian cells through an interaction with the dynamin-like protein DLP1. *Molecular and cellular biology*, 23(15), pp.5409–20. Available at: http://www.ncbi.nlm.nih.gov/pubmed/12861026 [Accessed June 29, 2017].

Yu, T. et al., 2005. Regulation of mitochondrial fission and apoptosis by the mitochondrial outer membrane protein hFis1. *Journal of Cell Science*, 118(18), pp.4141–4151. Available at:

http://www.ncbi.nlm.nih.gov/pubmed/16118244 [Accessed June 29, 2017].

Zahedi, R.P. et al., 2005. Proteomic Analysis of the Yeast Mitochondrial Outer Membrane Reveals Accumulation of a Subclass of Preproteins. *Molecular Biology of the Cell*, 17(3), pp.1436–1450. Available at: http://www.ncbi.nlm.nih.gov/pubmed/16407407 [Accessed June 22, 2017].

Zheng, J., 2012. Energy metabolism of cancer: Glycolysis versus oxidative phosphorylation (Review). *Oncology letters*, 4(6), pp.1151–1157. Available at: http://www.ncbi.nlm.nih.gov/pubmed/23226794 [Accessed June 21, 2017].

Zhou, C. et al., 2008. The kinase domain of mitochondrial PINK1 faces the cytoplasm. *Proceedings of the National Academy of Sciences of the United States of America*, 105(33), pp.12022–12027.

Ziegler, M.L. & Davidson, R.L., 1981. Elimination of mitochondrial elements and improved viability in hybrid cells. *Somatic Cell Genetics*, 7(1), pp.73–88. Available at: http://link.springer.com/10.1007/BF01544749 [Accessed January 5, 2016].

Zoratti, M. et al., 2009. Novel channels of the inner mitochondrial membrane. *Biochimica et Biophysica Acta (BBA) - Bioenergetics*, 1787(5), pp.351–363. Available at: http://linkinghub.elsevier.com/retrieve/pii/S0005272808007329 [Accessed June 22, 2017].

Züchner, S. et al., 2004. Mutations in the mitochondrial GTPase mitofusin 2 cause Charcot-Marie-Tooth neuropathy type 2A. *Nature Genetics*, 36(5), pp.449–451. Available at: http://www.nature.com/doifinder/10.1038/ng1341 [Accessed September 14, 2017].